TRANSPORTATION RESEARCH

RECORD

No. 1435

Pavement Design, Management, and Performance

Pavement and Traffic Monitoring and Evaluation

A peer-reviewed publication of the Transportation Research Board

TRANSPORTATION RESEARCH BOARD
NATIONAL RESEARCH COUNCIL

NATIONAL ACADEMY PRESS
WASHINGTON, D.C. 1994

Transportation Research Record 1435
ISSN 0361-1981
ISBN 0-309-05512-1
Price: $35.00

Subscriber Category
IIB pavement design, management, and performance

Printed in the United States of America

Sponsorship of Transportation Research Record 1435

GROUP 2—DESIGN AND CONSTRUCTION OF TRANSPORTATION FACILITIES
Chairman: Charles T. Edson, Greenman Pederson, Inc.

Pavement Management Section
Chairman: Joe P. Mahoney, University of Washington

Committee on Pavement Monitoring, Evaluation, and Data Storage
Chairman: Freddy L. Roberts, Louisiana Tech University
Secretary: Richard B. Rogers, Texas Department of Transportation
A. T. Bergan, Billy G. Connor, Brian E. Cox, Jerome F. Daleiden, Wade L. Gramling, Jerry J. Hajek, Scott A. Kutz, Kenneth J. Law, W. N. Lofroos, Edwin C. Novak, Jr., Dennis G. Richardson, Ivan F. Scázziga, Mohamed Y. Shahin, Roger E. Smith, Elson B. Spangler, John P. Zaniewski

Committee on Surface Properties–Vehicle Interaction
Chairman: John Jewett Henry, Pennsylvania State University
Secretary: James C. Wambold, CDRM Inc.
Roger Caignie, Robert A. Copp, Steven L. Cumbaa, Gaylord Cumberledge, Kathleen T. Diringer, Lawrence E. Hart, Carlton M. Hayden, Brian S. Heaton, Rudolph R. Hegmon, Walter B. Horne, David L. Huft, Michael S. Janoff, Khaled Ksaibati, Kenneth J. Law, Georg Magnusson, Kenneth H. McGhee, James E. McQuirt, Jr., William G. Miley, Robert L. Novak, William D. O. Paterson, Dennis G. Richardson, Richard B. Rogers, Elson B. Spangler, Roger S. Walker, Thomas J. Yager

Committee on Highway Traffic Monitoring
Chairman: Perry M. Kent, Federal Highway Administration
David Preston Albright, Shyamal Basu, Thomas F. Black, Harold R. Bosch, James Y. Campbell, Jr., Craig A. Copelan, Wiley D. Cunagin, Michael J. Dalgleish, Margaret E. Eidman, Edward K. Green, H. K. (Kris) Gupta, Barbara Mason Haines, John L. Hamrick, Lawrence E. Hart, Loyd R. Henion, David L. Huft, Bernard Jacob, Clyde E. Lee, D. Keith Maki, William A. Mickler, Thomas Papagiannakis, Peter Sebaaly, Herbert F. Southgate, Alex T. Visser

Transportation Research Board Staff
Robert E. Spicher, Director, Technical Activities
Daniel W. Dearasaugh, Jr., Engineer of Design
Nancy A. Ackerman, Director, Reports and Editorial Services
Naomi Kassabian, Associate Editor
Susan E. G. Brown, Assistant Editor

Sponsorship is indicated by a footnote at the end of each paper. The organizational units, officers, and members are as of December 31, 1993.

Transportation Research Record 1435

Contents

Foreword

The papers in this volume focus on current information on pavement and traffic monitoring and evaluation; most were presented at the 1994 TRB Annual Meeting in sessions sponsored by the TRB Committees on Pavement Monitoring, Evaluation, and Data Storage; on Surface Properties–Vehicle Interaction; and on Highway Traffic Monitoring. In addition, two papers on metric conversion, sponsored by the Pavement Management Section, appear at the end of the volume.

Hadley et al. present the quality assurance approach used to verify data being collected and input to the Strategic Highway Research Program–Long-Term Pavement Performance (SHRP-LTPP) Information Management System. Daleiden and Simpson take a close look at surface distress data being collected on SHRP-LTPP sites and evaluate the two data collection methods. Mohammad et al. report on a sophisticated data acquisition system developed for use with the accelerated loading device purchased by the Louisiana Transportation Research Center. Gulen et al. report on a study by the Indiana Department of Transportation to develop a correlation between pavement serviceability index (PSI) and international roughness index (IRI). Lu et al. present a comprehensive evaluation of the roughness subsystem of the automatic road analyzer including roughness correlation analysis and development of a new PSI model. Kalikiri et al. discuss current efforts at the University of Connecticut toward developing an image analysis and processing system compatible with the photolog system used by the Connecticut Department of Transportation for eventual automated distress evaluation. Grivas et al. present their current efforts toward developing and refining a morphology-based image analysis system for pavement surface distress assessment. Flintsch et al. evaluate several asphalt-rubber pavement treatments that have been used in Arizona for more than 25 years. Kim et al. describe a method to measure the spatial distribution and movement of moisture in a pavement section through the use of electrical resistance tomography imaging. Arora et al. report on several field test sites in Saudi Arabia paved with Sulfur-Extended Asphalt.

Yandell and Sawyer describe a device called the Yandell-Mee Texture Friction Meter for predicting friction between the tire and pavement surface by simulating a pneumatic tire sliding over a wet road surface texture. Tielking and Abraham discuss preliminary results of efforts to measure tire footprint pressures through the use of a triaxial load pin array. Streit et al. present a sensitivity analysis of the effect of variations in heavy vehicle parameters, speed, and pavement roughness on rear wheel loadings. Findley and Chen compare the effect of vehicle heat, represented by a catalytic converter, on bituminous pavement with that of solar radiation. Parcells and Hossain report on the smoothness of portland cement concrete pavement (PCCP) in Kansas and their experience that led toward eliminating the blanking bandwidth in profilograph trace reduction. Kalevela et al. discuss a study of the feasibility of using the K.J. Law profilometer to test PCCP smoothness, normally measured with the California profilograph. Al-Omari and Darter present and discuss the development of a non-linear model to express the relationship between IRI and PSR. Perera et al. describe a comparative testing experiment among the four K.J. Law profilometers being used to collect roughness data for the SHRP-LTPP program. Morrall and Talarico discuss the findings of a research project to determine the amount of side friction demanded and provided for a range of roadway curvatures, vehicle types and speeds, and pavement surface conditions.

Krukar and Evert present the findings on the basis of 5 years of operation from the automation of Oregon's Woodburn port of entry. Dahlin and Novak conducted an analysis of weigh-in-motion (WIM) data collected by continuously operating systems at three different sites along the same route. Hazen et al. provide the results of an extensive investigation of WIM data from 13 continuously operating WIM stations (some for as long as 20 years) throughout Florida to determine the optimal number of WIM sites to provide appropriate data for pavement management systems.

Turner and Lindly discuss the AASHTO *Guide to Metric Conversion*, and Lindly et al. describe the process of metric conversion and present a general conversion plan.

Strategic Highway Research Program–Long-Term Pavement Performance Information Management System

WILLIAM O. HADLEY, CHARLIE COPELAND, AND SHAHED ROWSHAN

A major impediment to past pavement research efforts was the lack of availability of and access to comprehensive diverse, yet consistent, traffic, materials, structural, and climatic data for various pavement types. One of the basic objectives or goals of the Strategic Highway Research Program (SHRP) was to establish a national pavement performance data base in which to store all of the data being collected or generated, or both, under the Long-Term Pavement Performance (LTPP) Program. Under this program researchers could pursue long-term pavement performance studies by accessing all sorts of data with confidence. The quality assurance approach used in the SHRP-LTPP Information Management System to verify the accuracy and correctness of the data it receives and stores before releasing the data to the public is presented. In addition, the levels of data release are presented and the information sources of benefit to the user are identified.

A major impediment to past pavement research efforts was the lack of availability of and access to comprehensive diverse, yet consistent, traffic, materials, structural, and climatic data for various pavement types. There is no doubt that data sets containing variable and inconsistent data make it extremely risky to develop inferential conclusions. Because of the historic problems with data comprehensiveness, quality, and consistency, it is of strategic importance to develop a national data base that can overcome these shortcomings and allow researchers to pursue long-term pavement performance (LTPP) studies by accessing all sorts of data sources with confidence.

LTPP AND INFORMATION MANAGEMENT SYSTEMS

One of the basic objectives or goals of the Strategic Highway Research Program (SHRP) was to establish a national pavement performance data base (NPPDB) in which to store all of the data being collected or generated, or both, under the LTPP Program (*1*). The type of data collected in the LTPP Program and stored in NPPDB include the following:

- Inventory (as built)
- Materials testing
- Profile
- Deflection [falling weight deflectometer (FWD)]
- Cross profile
- Distress
- Friction
- Maintenance
- Rehabilitation
- Climate
- Traffic

The Information Management System (IMS) developed in the SHRP-LTPP Program to service NPPDB is composed of five nodes—the central node and four regional nodes. The National Information Management System (NIMS) is the central node (*2*), which is composed of the hardware and software systems that were assembled to house NPPDB. This system is administered by and resides at TRB. The four regional nodes are represented by the Regional Information Management Systems (RIMS). The data generally are checked and entered at the RIMS by the four regional coordination office contractor personnel under the direction of a SHRP regional engineer. Periodic uploads are made from RIMS to NIMS at TRB.

A critical function of IMS is to verify and validate the accuracy and correctness of the data it receives and stores before releasing the data to the public for review, compilation, analysis and research. The NPPDB data must pass a number of quality assurance (QA) checks before being released to the public from NIMS. These checks verify the presence, reasonableness, and validity of the data. The procedures for data checks, as well as data uploads to NIMS, are critical elements in the SHRP-LTPP IMS. Data uploads include newly acquired data as well as updated or revised data that were previously submitted.

DESCRIPTION OF REGIONS

The four SHRP regions were selected primarily on the basis of climatic and jurisdictional considerations (*2*). The North Atlantic region corresponds to the wet-freeze AASHTO classification, whereas the southern region is situated in primarily a wet-nonfreeze zone. The north central region is predominantly wet-freeze, whereas the western region contains both dry-freeze and dry-nonfreeze. The regions were adjusted to correspond to state boundaries as illustrated in Figure 1 (*3*).

Four regional offices were established to coordinate and communicate SHRP-LTPP related activities across the United States and Canada. Each region includes a group of states or provinces, or both, in their jurisdiction, with test sections located throughout the defined boundaries. The regional centers then operate as central data collection and validation centers for pavement section data. Inventory, maintenance, rehabilitation, and traffic data are

W. O. Hadley, Hadley and Associates, 12402 Mercury Lane, Austin, Tex. 78727. C. Copeland, Texas Research and Development Foundation, 2602 Dellana Lane, Austin, Tex. 78746. S. Rowshan, FHWA, LTPP Division, 6300 Georgetown Pike, McLean, Va. 22101.

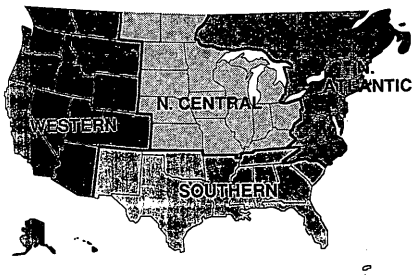

FIGURE 1 SHRP-LTPP regional boundaries.

collected at the state level and are then sent to the appropriate regional center. The regional centers receive these data from the states and collect test and monitoring data on the pavement sections. All data collected are entered in the RIMS through a menu-driven system or are loaded by programs reading data from machine-readable media. Quality checks are incorporated into all update programs, and reports are designed to provide additional checks. After verification, these data are transferred to NIMS.

The IMS functions performed at the regions involve primarily data collection, data validation, and data entry. This is an essential IMS element because the regional staff have a working relationship with all of the data providers and the technical expertise to judge data quality.

INFORMATION SOURCES

Several sources of information are available to describe in detail the data housed within the LTPP data base and how it was collected for the IMS. The SHRP-LTPP data collection guide (DCG) (*4*) is the main source of data collection sheets and instructions on data collection for the LTPP Program. Detailed DCGs for data gathered by SHRP contractors have been developed for the materials sampling and testing and some of the activities of the monitoring program. A schema report from IMS provides the data structure as it is implemented in the relational data base management system (ORACLE) and illustrates the data tables and the fields (or data elements) contained within those tables. The schema also identifies the key (index) fields and the data types associated with each field. The data dictionary report reference from IMS is a more thorough description of each of the fields (or data elements) and various items of interest about each of the fields.

DATA COLLECTION GUIDE

The primary purpose of the DCG (*4*) is to provide a uniform basis for data collection during long-term monitoring of the performance of pavement test sections under the LTPP study. Data items considered to be of high priority for achieving the goals of the LTPP Program are identified, but other data items that are desirable for inclusion in the NPPDB for other purposes are also included. Particular emphasis has been given to the collection of those data items considered essential to long-term pavement performance to ensure that crucial data will be available in NPPDB when it is utilized in the future for the development of pavement performance models.

The DCG was initially developed for use with the General Pavement Study (GPS) sections, but many of the DCG sheets are also used directly with the Specific Pavement Study (SPS) sections. Additional data sheets and tables have been designed and used to record data collected from the SPS project sections.

SCHEMA REPORT

The schema (*2*) is used in NIMS to define the various tables (categories of data) and fields (individual pieces of data) and to identify how they are to be stored in the IMS data base. Each of the data modules is composed of numerous tables (encompassing one or more data sheets) and represents a collection of information about a specific item, for example, the location of all LTPP pavement sections by state, elevation, and coordinates. Each table in turn is a collection of records that contain data about a specific pavement section. Each record is made up of individual fields that represent the smallest piece of information in the data base. The schema defines within the data base the fields that belong together as a record, the records that reside in a certain table, and the tables that compose a specific data module.

DATA DICTIONARY REPORT

The data dictionary is a supplemental report (*2*) that describes for the IMS users the various fields or data elements contained within each table. The data dictionary entry identifies the origin of the data (i.e., what data sheet and time) and presents a brief description of the field (data type), data ranges, and associated information.

The rules associated with the IMS data dictionary determine the amount and type of data that may be input in each field. For example, the data dictionary defines the length of a field, the type of data to be entered (e.g., numeric, alphabetic, date) and the acceptable ranges for the data (e.g., a positive number from 1 to100).

DATA TYPES, ELEMENTS, AND SOURCES

NIMS is the central repository for all LTPP data. All requests for LTPP information or data files from the user community are processed at NIMS, which consists of data uploaded from the four regional centers along with data entered directly at the national center. The data processed directly at NIMS includes the environmental data and all administrative data (e.g., information for new pavement sections, experiment assignments, and code tables). Each region is responsible only for the data on the SHRP pavement sections located within its assigned states; therefore, there is no overlap between states of the data collected. The procedures for the transfer of information are described in the SHRP Programmer's Reference Manual (*5*) and in the LTPP NIMS and RIMS User Manuals (*6,7*).

LTPP IMS

IMS QA Process

The QA concept of data checks is presented graphically in Figure 2. This QA process is necessary to provide researchers with con-

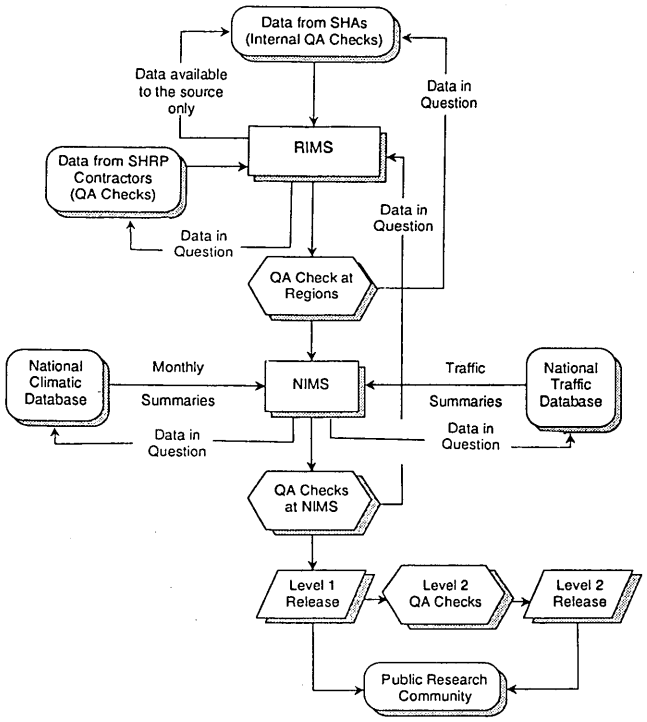

FIGURE 2 Data flow in the LTPP IMS.

fidence that the data are reliable and that their findings and recommendations are based on quality data.

The components of the IMS QA plan are performed in the following sequence:

1. Documentation of data collection procedures for each module in IMS to ensure that data are collected in similar format, types, and conditions, and so on;
2. Regional review of all input at RIMS to identify obvious data collection and data entry errors;
3. Internal checks at NIMS to identify data entry problems or errors; and
4. Execution of the format IMS QA software programs. This component involves nine categories of QA checks defined within two release levels.

IMS Data Entry Checks

Entry checks programming in the IMS include mandatory, logic, range, and data verification checks (*8*). The mandatory checks involve checks for non-null entries in all key fields and other designated fields. RIMS will require entry in these positions or will invoke an audible warning and message that data are required in the field.

Logic checks are also introduced in IMS and are included to ensure data compatibility across tables. The following is an example of a logic check: The "minimum data value $\leq$ mean $\leq$ maximum" for a given parameter.

Range checks are enforced to ensure that numeric field values fall within a defined value. Both absolute (i.e., theoretically possible range) and warning (i.e., practical range) limits are used.

Verification checks are instituted systemwide in IMS to verify that the SHRP-LTPP sections have been authorized for the LTPP Program before any data from that section can be entered in IMS.

Level 1: Section Release

The first release level is a section-by-section release process involving five individual QA/quality control (QC) checks defined as Checks A through E (*3*). It should be noted that the QA/QC checks are conducted on the individual tables within IMS and not on the SHRP sections as a whole. In this process, the Level 1 release could allow some data to be released for a section (e.g., friction results), whereas while other section data that fail to meet the checks would not achieve the release status (e.g., climate). Each table includes a large number of individual data elements.

These Level 1 data checks are structured to ensure quality data within a particular SHRP section but do not address QA/QC requirements between sections, states, and regions. These more sophisticated checks are required at the next release level. The Level 1 release QA/QC checks are presented in Figure 3 and involve the following activities:

- Check A: Random checks to ensure correct RIMS-NIMS upload exchange;
- Check B: Data dependency checks to ensure that basic, essential section information is recorded in NIMS (e.g., location and elevation);

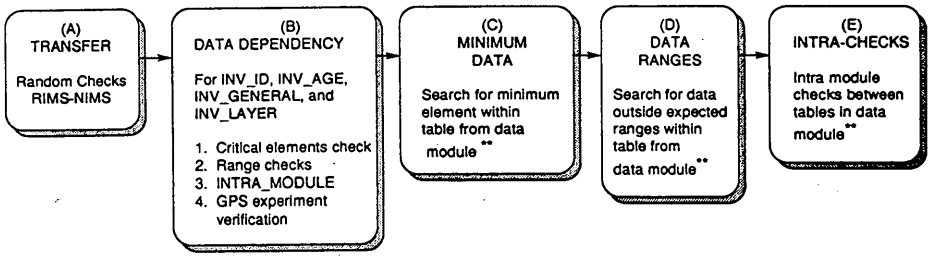

** Except INV_ID, INV_AGE, INV_GENERAL, and INV_LAYER tables in Inventory module

FIGURE 3 IMS Level 1 (section) release quality check.

- Check C: Minimum data search for critical elements (e.g., friction data should include skid number);
- Check D: Expanded range checks to identify data elements that fall outside an expected range; and
- Check E: Intramodular checks to verify the consistency of data within data modules.

The five checks (A through E) in the Level 1 release category are hierarchical in concept and must be conducted in succession, as indicated in Figures 3 and 4. Data elements that do not pass a particular QA check must be reviewed for confirmation or revision by SHRP regional personnel. In this concept, the data dependency checks (Check B) will not be processed until the RIMS-NIMS data check transfer (Check A) has been successfully completed. Similarly, Check E (intramodular) is not initiated until the range checks (Check D) have been successfully completed. After Check E has been conducted and the data within the particular IMS table have passed the check, that IMS table can be released for public use. Once records have passed through Check E, the data are available for a sectional release.

In May 1993 the Level 1 checks were defined and installed within NIMS. Four Level 1 data releases were completed using the checks. In the process the checks were reviewed, expanded, and revised as necessary.

Level 2: Experiment Release

A Level 2 IMS release is classified as an experimental release and includes QA checks across data modules (*9*), confirmation of GPS experiment and cell assignments (*10*), and statistical checks on the data and IMS tables within each designated GPS experiment (*11*). The successful completion of these checks means that the LTPP data would be available for a general experiment-by-experiment evaluation and analysis. The IMS Level 2 release QA/QC checks involve the following activities:

- Check F: Intermodular cross checks to verify existence and consistency of data for related categories;
- Check G: Experiment and cell assignment checks based on collected data;
- Check H: Various checks involving frequency distributions and bimodal and variance checks;
- Check I: Statistical checks for outliers, missing data, and completeness of experiment.

An example of the type of intermodular cross checks (QA/QC Check F) included in the QA program is presented in Figure 5. To assess FWD data at SHRP sites, it would be essential to have information on environment (temperature), materials (layer thicknesses and resilient modulus estimates), and depth to rigid layer. Similarly, an analysis of AASHTO performance (i.e., present serviceability index) would require information on roughness (profile), cracking and patching (distress), rutting, and surface material types. This check is in fact conducted for a specific SHRP-LTPP section but represents the type of checks that are performed across data modules. This check must be completed before being subjected to the experiment and cell assignment checks (or Check G).

The experiment and cell verification check (Check G) is essential for establishing the completeness of each GPS experiment matrix. As shown in Figure 6, the process is conducted for each SHRP section and involves

- Confirmation of the GPS experiment assignment,
- Confirmation of the cell assignment within the GPS experiment matrix, and
- Assessment of experiment completeness.

In essence, this IMS QA check is used to ensure appropriate GPS experiment assignment and to confirm that the distribution of LTPP sections within the experiment matrix is good enough to ensure unbiased data. This check must be successfully completed before Checks H and I are begun.

- The variation in data across regions, as well as within regions, will be analyzed as part of Check H to assess nonuniformity in variance distributions and to check for unusual occurrences or biases that may affect future analyses. Examples of this type of QA check are presented in Figure 7.

The final check before an IMS Level 2 release is shown in Figure 8 and involves statistical checks to identify missing and aberrant data and to confirm outliers. The process will include initial variance analyses at both the regional and national levels and preliminary regression analyses to investigate important factors and variability in materials, construction, or both.

Once the data and IMS tables have passed through Check I, the data are available for an experiment analysis release.

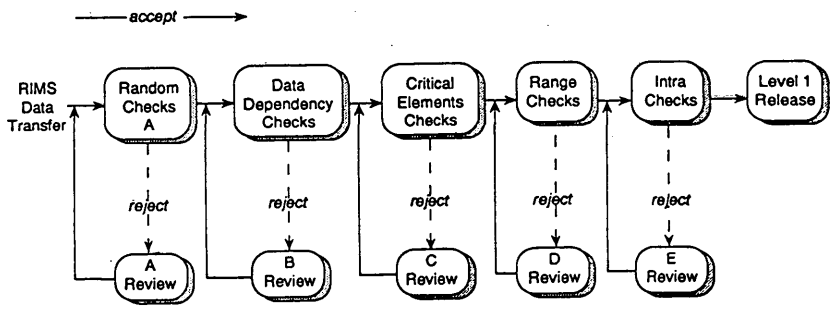

FIGURE 4 Data level advancement with quality control checks.

INTER-MODULAR CROSS CHECKS
Behavior Considerations

NDT - FWD	---	Load deflection
Environment	---	Mean monthly temperature
Materials	---	Layer thickness
Materials	---	Depth to rigid layer
Materials	---	Mr values

INTER-MODULAR CROSS CHECKS
Performance Considerations

Profile	---	IRI
Distress	---	Cracking & patching
Rutting	---	Rut depth
Materials/ Inventory	---	Surface type

FIGURE 5 IMS Level 2: F checks.

EXPERIMENT / CELL VERIFICATION

GPS Experiment Confirmation

Experiment Cell Confirmation

Completeness Of Experiment

GPS Experiment Definitions

GPS-1	Asphalt Concrete (AC) on Granular Base
GPS-2	AC on Bound Base
GPS-3	Jointed Plain Concrete
GPS-4	Jointed Reinforced Concrete
GPS-5	Continuously Reinforced Concrete
GPS-6A	Existing AC Overlay on AC
GPS-6B	New AC Overlay on AC
GPS-7A	Existing AC Overlay on Portland Cement Concrete (PCC) Pavements
GPS-7B	New AC Overlay on (PCC) Pavements
GPS-9	Unbound PCC Overlays of PCC Pavements

FIGURE 6 IMS Level 2: G checks.

DATA AVAILABILITY

Data generally are made available to the public from NIMS after appropriate QA and QC checks have been concluded. To obtain LTPP data from IMS, requests must be made to the TRB IMS administrator using a completed LTPP IMS data request form (*3*). All data requests are processed at TRB by the IMS administrator.

FREQUENCY - VARIANCE
DATA DISTRIBUTION CHECKS

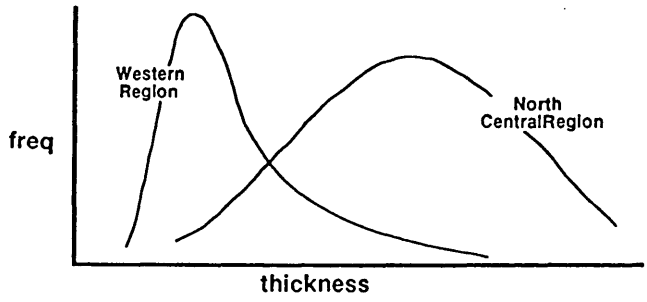

FREQUENCY - VARIANCE
BIMODAL DISTRIBUTION CHECKS

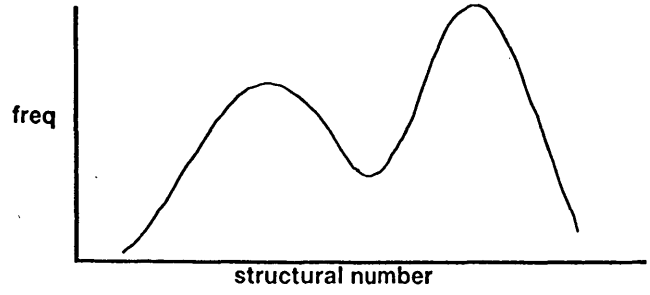

FIGURE 7 IMS Level 2: H checks.

STATISTICAL CHECKS / ANALYSES

Data Investigation
- Missing data
- Aberrant data
- Outliers

Initial Variance Analyses
- Regional
- National

Regression Analyses (Prelim)
- Important factors
- Materials/construction variability

FIGURE 8 IMS Level 2: I checks.

TABLE 1 Examples of Level 1 Releases

TABLE	RELEASE DATES JAN. 91	JULY 91	JAN 92	JULY 92
INV_ID	226	561	660	685
MON_SKID	95	416	560	744
MON_RUT_MASTER	-	2	355	902
REF_LAYER	-	118	296	495
MON_DEFL_MASTER	-	497	515	656
MNT_HIST	-	-	9	20
RHB_IMP	-	-	1	2
MON_PROFILE_MASTER	-	-	2860	3304
COMMENTS	-	913	2386	2800

In return, TRB will provide the requestor with a package containing the data on the requested media, a diskette containing significant portions of the Database Structure Manual (*12*) , and a notice describing major changes to the data base in the previous 6 months. The package will include a detailed LTPP schema and the LTPP data dictionary. The schema identifies the fields in each IMS table along with the columns where these data are available in flat ASCII files. The LTPP data dictionary contains a description of each field including the size, units, and expected ranges and identifies the table name where the field can be found.

The diskette also houses a report that indicates the codes used in the IMS and their associated descriptions. The use of codes provides more quality control by reducing the amount of data entry and storage. For example, comment codes were established for use in recording laboratory test results. Each numeric code corresponds to an individual comment relating to conditions that may affect the results (e.g., color, condition, insufficient size sample). The codes and their corresponding descriptions are provided on the diskette distribution with each completed request.

STATUS OF IMS RELEASES

By November 1992, four public data releases had been made, all at Level 1 involving only GPS data. The releases were completed at 6-month intervals because of the large volume of data inserted in RIMS during this start-up period. This can be seen in the amount of data that were released each time (Table 1). The table names (e.g., INV_ID) were selected to represent the status of the data module with which the table is associated.

The first data release was in January 1991 and was the initial trial of both the data release procedures and the QA/QC checking software. This initial release produced many expected anomalies involving missing inventory data. Because this information would never be available because it either was never collected originally or had been lost or destroyed over the years since the GPS section had been built, a comments table (*12*) was added to the IMS structure so that the regions could document what was missing and allow the data to pass through the QA/QC process without being permanently held at that level (and never being released). The initial release included 226 releasable sections (see INV_ID) and the only other module to successfully pass through Level 1 was friction (skid). For informational purposes, MON_RUT_MASTER is the table that contains the cross-profile data; REF_LAYER represents the materials and testing data module, which includes records for each pavement layer; MON_DEFL_MASTER represents the FWD data; MNT_HISTORY represents the maintenance data; RHB_IMP represents rehabilitation data; and MON_PROFILE_MASTER represents the profilometer data.

ACKNOWLEDGMENTS

The research in this paper was sponsored by SHRP, National Research Council, and appreciation is extended to the cooperative effort of the SHRP personnel.

REFERENCES

1. *Strategic Highway Research Program Research Plans.* Final Report. Strategic Highway Research Program, National Research Council, Washington, D.C., May 1986.
2. *Operations and Quality Assurance Manual.* Long-Term Pavement Performance Informational Management System, April 1990.
3. *Long-Term Pavement Performance Information Management Researchers' Guide.* Strategic Highway Research Program, National Research Council, Washington, D.C., July 1991.
4. *Data Collection Guide for Long-Term Pavement Performance Studies.* Operational Guide SHRP-LTPP-OG-001. Strategic Highway Research Program, National Research Council, Washington, D.C., Jan. 1990.
5. *Programmer's Reference Manual.* Long-Term Pavement Performance Information Management System, July 1989.
6. *NIMS Users Manual.* Long-Term Pavement Performance Information Management System, March 1990.
7. *RIMS Users Manual.* Long-Term Pavement Performance Information Management System, Jan. 1990.

8. *LTPP IMS Data Quality Assurance Checks.* Draft. Long-Term Pavement Performance Information Management System, May 1992.
9. Hadley, W. O. *IMS Level 2: F Checks—Intermodal.* Information Management System (IMS) Message TRDF-134. Texas Research and Development Foundation, Sept. 29, 1992.
10. Hadley, W. O. *IMS Level 2: G Checks—Experiment and Cell Verification.* Information Management Systems (IMS) Message TRDF-88. Texas Research and Development Foundation, Sept. 23, 1991.
11. High, R., and W. O. Hadley, *IMS Level 2: Statistical Quality Control and Assurance Procedures.* Information Management System (IMS) Message TRDF-134a. Texas Research and Development Foundation, Sept. 11, 1992.
12. *Database Structure Reference Manual.* Long-Term Pavement Performance Information Management System, Jan. 1990.
13. Copeland, C. *Comments Table Review and Usage Recommendations for SHRP-LTPP Regions.* Information Management System (IMS) Message TRDF-56. Texas Research and Development Foundation, May 3, 1991.

Publication of this paper sponsored by Committee on Pavement Monitoring, Evaluation, and Data Storage.

Evaluation of Strategic Highway Research Program–Long-Term Pavement Performance Surface Distress Data Collection Procedures

JEROME F. DALEIDEN AND AMY L. SIMPSON

Surface distress is commonly perceived to be one of the primary indicators of pavement performance. As such, the collection of these data for the Long-Term Pavement Performance (LTPP) program is a significant aspect of this overall effort—so significant in fact that there have been substantial efforts to develop a distress identification manual and guidelines for the measurement and recording of these distresses. Elaborate accreditation procedures also have been implemented to provide for the most uniform and consistent data possible. To further ensure that adequate observations of these data are obtained, two methods of data collection were utilized. The primary method of distress data collection for the LTPP program is from the digital analysis of 35-mm film taken of each test section on a routine basis. As a backup, manual surveys were conducted, as needed. From studies of the distress data collected to date, several observations were made. The first, and probably most significant, observation was that relatively few of these test sections have much distress. Second, some types of the distress occur more commonly than others. A variety of potential reasons for the limited occurrence of these distresses are considered in detail. The third observation is that there are distinct differences in the distress data collected from these two methods of distress data collection. Possible reasons for why these differences exist are discussed in detail. It is important to recognize these differences to ensure that the data are not misinterpreted. These limitations and distinctions are not intended to imply superiority of one methodology over the other. Instead, the studies should serve to document where additional research may be warranted to improve both methodologies. These studies also highlight the importance of not relying too heavily on either method of distress data collection alone.

Considerable quantities of surface distress data have been collected as part of the Long-Term Pavement Performance (LTPP) studies. Both manual and semiautomated procedures were utilized for the collection of these data. The objectives of this paper are twofold. The first objective is to review and summarize the distress data collected for the LTPP studies to date. The second objective is to compare and evaluate the differences between these two methods for collecting surface distress data on the basis of available data. This paper is not intended to prove that one method of distress data collection is superior to the other, but rather to highlight the differences and limitations of each to aid in the use and development of these data collection procedures in the future.

These studies were limited to distress data from the southern LTPP region, incorporating 261 general pavement study (GPS) test sections from New Mexico, Texas, Oklahoma, Arkansas, Louisiana, Mississippi, Tennessee, South Carolina, Alabama, Georgia, Florida, and the Commonwealth of Puerto Rico. These are standard sections of in-service highway. Of the 261 sections, 172 are asphalt concrete pavement (ACP), 52 are jointed concrete pavement (JCP), and 37 are continuously reinforced concrete pavement (CRCP).

Since the initiation of the LTPP studies in 1988, several rounds of both manual and semiautomated distress data have been collected in the southern region. Although limiting this study to the southern region introduces some biases in the types of distress observed, there is a sufficient distribution of the various pavement types and sufficient volumes of distress surveys to be reasonably representative of most distress manifestations. This study incorporates 586 surveys of ACP, 172 of JCP, and 122 of CRCP. These surveys represent multiple rounds of distress data collected at each of the test sections noted earlier.

To highlight the types of distress data being collected as part of the LTPP studies, a brief background will be provided on the guidelines for the collection of these distress data. Considerable effort has been made over the years to develop standard guidelines for collecting distress data. These guidelines serve an essential role in helping to provide greater consistency and uniformity to the observations made and the distress recorded.

DISTRESS IDENTIFICATION MANUAL

The guidelines for distress identification for the LTPP studies were first published in 1989 (*1*). These guidelines have gone through several iterations since that time, culminating with the most recent distress identification manual published in May 1993 (*2*). The LTPP Distress Identification Manual incorporates many of the guidelines provided in previous manuals of this type (*3–5*). Revisions to the manual are a direct reflection of areas identified in which inconsistencies in interpretation have resulted in problems in obtaining uniform and consistent distress data. The distress data types collected and their units of measurement are summarized in Tables 1 through 3 for ACP, JCP, and CRCP, respectively.

DATA COLLECTION PROCEDURES

The predominant methodology employed is classified as semiautomated distress data collection. The test sections were filmed by the PASCO Road Recon Unit. The camera was mounted on a boom in front of a vehicle so that it could photograph one full lane of pavement at a time while minimizing any potential dis-

Brent Rauhut Engineering, 8240 Mopac, Suite 200, Austin, Tex. 78759.

TABLE 1 Asphalt Concrete-Surfaced Pavement Distress Types

DISTRESS TYPE	UNIT OF MEASURE	DEFINED SEVERITY LEVELS?
Cracking		
1. Fatigue Cracking	Square Meters	Yes
2. Block Cracking	Square Meters	Yes
3. Edge Cracking	Meters	Yes
4a. Wheel Path Longitudinal Cracking	Meters	Yes
4b. Non-Wheel Path Longitudinal Cracking	Meters	Yes
5. Reflection Cracking at Joints		
Transverse Reflection Cracking	Number, Meters	Yes
Longitudinal Reflection Cracking	Meters	Yes
6. Transverse Cracking	Number, Meters	Yes
Patching and Potholes		
7. Patch/Patch Deterioration	Number, Square Meters	Yes
8. Potholes	Number, Square Meters	Yes
Surface Deformation		
9. Rutting	Millimeters	No
10. Shoving	Number, Square Meters	No
Surface Defects		
11. Bleeding	Square Meters	Yes
12. Polished Aggregate	Square Meters	No
13. Raveling	Square Meters	Yes
Miscellaneous Distresses		
14. Lane-to-Shoulder Dropoff	Millimeters	No
15. Water Bleeding and Pumping	Number, Meters	No

TABLE 2 Jointed Concrete-Surfaced Pavement Distress Types

DISTRESS TYPE	UNIT OF MEASURE	DEFINED SEVERITY LEVELS?
Cracking		
1. Corner Breaks	Number	Yes
2. Durability Cracking ("D" Cracking)	Number of Slabs, Square Meters	Yes
3. Longitudinal Cracking	Meters	Yes
4. Transverse Cracking	Number, Meters	Yes
Joint Deficiencies		
5a. Transverse Joint Seal Damage	Number	Yes
5b. Longitudinal Joint Seal Damage	Number, Meters	No
6. Spalling of Longitudinal Joints	Meters	Yes
7. Spalling of Transverse Joints	Number, Meters	Yes
Surface Defects		
8a. Map Cracking	Number, Square Meters	No
8b. Scaling	Number, Square Meters	No
9. Polished Aggregate	Square Meters	No
10. Popouts	Number/Square Meter	No
Miscellaneous Distress		
11. Blowups	Number	No
12. Faulting of Transverse Joints and Cracks	Millimeters	No
13. Lane-to-Shoulder Dropoff	Millimeters	No
14. Lane-to-Shoulder Separation	Millimeters	No
15. Patch/Patch Deterioration	Number, Square Meters	Yes
16. Water Bleeding and Pumping	Number, Meters	No

TABLE 3 CRCP-Surfaced Distress Types

DISTRESS TYPE	UNIT OF MEASURE	DEFINED SEVERITY LEVELS?
Cracking		
1. Durability Cracking ("D" Cracking)	Number, Square Meters Meters	Yes Yes
2. Longitudinal Cracking	Number, Meters	Yes
3. Transverse Cracking		
Surface Defects		
4a. Map Cracking	Number, Square Meters	No
4b. Scaling	Number, Square Meters	No
5. Polished Aggregate	Square Meters	No
6. Popouts	Number/Square Meters	No
Miscellaneous Distress		
7. Blowups	Number	No
8. Transverse Construction Joint Deterioration	Number	Yes
9. Lane-to-Shoulder Dropoff	Millimeters	No
10. Lane-to-Shoulder Separation	Millimeters	No
11. Patch/Patch Deterioration	Number, Square Meters	Yes
12. Punchouts	Number	Yes
13. Spalling of Longitudinal Joints	Meters	Yes
14. Water Bleeding and Pumping	Number, Meters	No
15. Longitudinal Joint Seal Damage	Number, Meters	No

tortion. Filming was conducted at night to control the lighting and potential for unwanted shadows. After the film was developed, it was then digitally analyzed by a technician to extract the distress data quantities. The film and distress quantities noted were then reviewed by the regional coordination offices as a quality control check. Discrepancies in the interpretation of the film were noted and edited as necessary.

This filming process provides several advantages. It allows the section to be reevaluated at any time should distress definitions change. Similarly, the film allows for the use of better technology for digital analysis as it becomes available. The filming process also minimizes the safety hazards of collecting distress data in the field.

As a backup to the filming procedure, personnel within the LTPP regional coordination offices were trained to collect these distress data through visual inspection, should the PASCO unit be unavailable. An accreditation program has been initiated (*6*) to provide greater consistency among the surveyors in the interpretation of the distress identification manual. Manual surveys allow for considerably greater freedom in reviewing a test section for the presence of distress.

DATA AVAILABILITY

The presence of distress data has numerous implications. To some analysts, this is an indication of which distresses are most or least common, or both. To others this information might reflect a bias in the types of sections being monitored, and perhaps an indication of adjustments or additional sections that need to be sought to represent equally all distress manifestations. A third possibility is that the magnitudes of data available for each distress type to some extent could indicate which distress manifestations are most readily identifiable by LTPP distress identification procedures and

perhaps highlight those distress manifestations for which better identification techniques are still warranted.

As one might expect, some of the distresses listed in Tables 1 through 3 are considerably more common than others. Some distresses, although known to be common, can be fairly difficult to discern. Distress manifestations, such as water bleeding and pumping, can be dependent on the timing of the distress survey. If the distress survey is conducted shortly after a heavy rain, pumping may be easily detected. If the timing is wrong, however, these types of distresses will likely go undocumented. Another good example of these timing-related distresses is a blowup in the concrete pavements. Several sections have been reported as having blowups. However, such a phenomenon is usually so catastrophic that it is typically patched immediately. By the time a distress survey is conducted at these locations, the surveyor can record only the location of the patch. Potholes typically fall into this same category.

Still other distress manifestations are uncommon by definition. One example would be edge cracking, which is defined to occur where paved shoulders do not exist. This type of distress is common in states where paved shoulders are not used; however, there are few states (at least in the southern region) where paved shoulders are not common practice. Similarly, reflective cracking over joints by definition is obviously limited to the asphalt overlays of concrete pavement. With these studies being limited to the test sections in the southern region, some of these distresses simply are not common to this area of the country (e.g., D-cracking in the concrete test sections).

For the 261 GPS test sections established in the southern region, several rounds of both manual and semiautomated distress data collection have been conducted, as previously noted. The results of these surveys have been tabulated and summarized to indicate the frequency of occurrence of each of the distress types on the applicable pavement types. These results are provided in Tables 4 through 6 for ACP, JCP, and CRCP, respectively. These results reflect the types of distresses recorded at these test sections over the past 5 years. The tables also have been highlighted to note those distresses considered timing dependent, uncommon by definition, and those uncommon to the Southeast, as noted earlier. The distresses indicated to be not available are primarily those requiring measurement of differences in vertical profile, which in most cases is being accommodated differently in the two methodologies. These distinctions will be discussed further under the heading of limitations.

Few of these results are particularly surprising. Some of these distresses for various reasons are not expected to be commonly noted. These tables have been further highlighted to distinguish those distress types that were actually noted on greater than 20 percent of the section. Those not highlighted are the distress types that are inexplicably minimal. One can only speculate whether these distresses will become more common with time or whether they are closely related to materials or construction deficiencies that may have been filtered out in the site nomination and selection process. Regardless of how such voids in the distress data occur, no meaningful analysis can be conducted for distresses of this type until they become more common.

LIMITATIONS OF DISTRESS DATA COLLECTION PROCEDURES

The authors are not aware of any foolproof method for the collection of distress data. All procedures currently in use have their

TABLE 4 Observations of ACP Distress

DISTRESS	L	%	M	%	H	%	TOT	%
CRACKING								
FATIGUE	118	20	48	8	10	2	133	23
BLOCK	16	3	8	1	0	0	19	3
EDGE	17	3	3	1	3	1	19	3
LONGITUDINAL	293	50	58	10	3	1	295	50
REFLECTIVE, LONG.	7	1	2	0	2	0	7	1
REFLECTIVE, TRAN.	10	2	4	1	3	1	10	2
TRANSVERSE	286	49	97	17	20	3	283	48
PATCHING AND POTHOLES								
PATCH DETERIORATION	41	7	15	3	7	1	49	8
POTHOLES	9	2	2	0	2	0	10	2
SURFACE DEFORMATION								
RUTTING	--	--	--	--	--	--	N/A	N/A
SHOVING	--	--	--	--	--	--	1	0
SURFACE DEFECTS								
BLEEDING	53	9	7	1	1	0	57	10
POLISHED AGGREGATE	--	--	--	--	--	--	0	0
RAVELING & WEATHERING	32	5	7	1	3	1	30	5
MISCELLANEOUS DISTRESSES								
LANE TO SHOULDER DROPOFF	--	--	--	--	--	--	N/A	N/A
WATER BLEEDING & PUMPING	--	--	--	--	--	--	15	3

TIMING DEPENDENT
UNCOMMON BY DEFINITION
NOT COMMON IN SOUTHEAST
COMMON DISTRESS

N/A - Not Available
-- - No Severity Levels
Observations noted are number of surveys (either manual or PASCO) for which the given distress was noted at the specified severity level.

TABLE 5 Observations of JCP Distress

DISTRESS	L	%	M	%	H	%	TOT	%
CRACKING								
CORNER BREAKS	13	8	6	3	4	2	20	12
DURABILITY "D"	0	0	0	0	0	0	0	0
LONGITUDINAL	18	10	0	0	0	0	18	10
TRANSVERSE	30	17	27	16	12	7	39	23
JOINT DEFICIENCIES								
JOINT SEAL DAMAGE	51	30	26	15	29	17	63	37
SPALLING OF LONG. JOINTS	25	15	9	5	0	0	24	14
SPALLING OF TRANS. JOINTS	77	45	11	6	7	4	85	49
SURFACE DEFECTS								
MAP CRACKING AND SCALING	--	--	--	--	--	--	11	6
POLISHED AGGREGATE	--	--	--	--	--	--	3	2
POP OUTS	--	--	--	--	--	--	17	10
MISCELLANEOUS DISTRESS								
BLOW UPS	--	--	--	--	--	--	0	0
FAULTING OF TRANS JTS &CRKS	--	--	--	--	--	--	N/A	N/A
LANE TO SHOULDER DROPOFF	--	--	--	--	--	--	N/A	N/A
LANE TO SHOULDER SEPARATION	--	--	--	--	--	--	16	9
AC PATCH DETERIORATION	7	4	7	4	1	1	12	7
PCC PATCH DETERIORATION	2	1	0	0	1	1	3	2
WATER BLEEDING & PUMPING	--	--	--	--	--	--	5	0

TIMING DEPENDENT
UNCOMMON BY DEFINITION
NOT COMMON IN SOUTHEAST
COMMON DISTRESS

N/A - Not Available
-- - No Severity Levels
Observations noted are number of surveys (either manual or PASCO) for which the given distress was noted at the specified severity level.

TABLE 6 Observations of CRCP Distress

DISTRESS	L	%	M	%	H	%	TOT	%
CRACKING								
DURABILITY "D"	0	0	0	0	0	0	0	0
LONGITUDINAL	9	7	2	2	0	0	9	7
TRANSVERSE	118	97	56	46	5	4	118	97
SURFACE DEFECTS								
'MAP CRACKING AND SCALING	--	--	--	--	--	--	6	5
POLISHED AGGREGATE	--	--	--	--	--	--	0	0
POP OUTS	--	--	--	--	--	--	11	13
MISCELLANEOUS DISTRESSES								
BLOW UPS	--	--	--	--	--	--	1	1
CONSTRUCTION JOINT DAMAGE	9	7	1	1	0	0	9	7
LANE TO SHOULDER DROPOFF	--	--	--	--	--	--	N/A	N/A
LANE TO SHOULDER SEPARATION	--	--	--	--	--	--	21	17
AC PATCH DETERIORATION	3	2	0	0	2	2	5	4
PCC PATCH DETERIORATION	3	2	0	0	0	0	3	2
PUNCHOUTS	5	4	0	0	1	1	6	5
SPALLING OF LONG. JOINTS	25	20	2	2	0	0	24	20
WATER BLEEDING & PUMPING	--	--	--	--	--	--	1	1
LONG. JOINT SEAL DAMAGE	--	--	--	--	--	--	N/A	N/A

TIMING DEPENDENT
UNCOMMON BY DEFINITION
NOT COMMON IN SOUTHEAST
COMMON DISTRESS

N/A - Not Available
-- - No Severity Levels
Observations noted are number of surveys (either manual or PASCO) for which the given distress was noted at the specified severity level.

own limitations. As the limitations of the procedures utilized for the LTPP studies are reviewed, it should be emphasized again that the objective here is not to minimize the value of these data (or the methods used to collect them) in any way. Rather, it is hoped that through the review of these limitations ideas for further refinement and development of these procedures might be spawned. In the meantime, users of these data can become more familiar with how to generate and make better use of these data.

Both data collection procedures utilize the same distress identification manual and ideally should generate the same distress data summary statistics for a given section at a given time. First one must recognize, however, that these sections are seldom surveyed by both procedures at the same time. Although this tends to make direct comparisons of the two methodologies difficult, it is not unreasonable to expect similar trends in the distress data for a given section: that is, if one methodology showed block cracking in 1991 and 1993, one might also expect the other methodology to also display block cracking in 1992. It also appears reasonable to expect the same relative order of magnitude for the quantities of distress noted (say within 25 percent). However, limitations make both procedures less than ideal. In the following paragraphs, the limitations of each methodology will be discussed to help explain some of the differences between the two methodologies and identify efforts that have been initiated to minimize these limitations. It is anticipated that as the limitations of each methodology are remedied, the results of the two methodologies will begin to provide more comparable results.

Reduction of Film

The three primary limitations of the semiautomated procedure are as follows:

1. Dependency on film resolution. With the distress quantities coming strictly from what is visible on the film, obviously the film resolution is fairly critical. Although improvements are being made in this area, the data available thus far still clearly indicate that the low severity levels for some distress types are simply not visible on the film. Distresses such as fatigue cracking in ACP and transverse cracking in CRCP are common examples of distresses that require higher film resolution.
2. Lack of depth perception. Distresses that require any depth perception or measurements of differences in surface elevations present problems during film reduction. Distress types such as faulting or lane-to-shoulder dropoff are virtually impossible to identify from the film. In some instances, establishing severity levels is also dependent on depth perception. Depths of potholes, settlement of corner breaks in JCP, or punchouts in CRCP are all dependent on depth perception.
3. Film contrast. Identification of some distress types where contrast is critical, such as joint seal damage in JCP, or surface distresses such as polished aggregate, bleeding or raveling and weathering, can prove difficult if not impossible.

Manual Distress Surveys

Two of the primary limitations of the manual distress surveys are as follows:

1. Potential for human error. Although it exists in both methodologies, the potential for human error is considerably more prevalent with manual distress surveys. One can tire of reviewing film but there are many means of remedying boredom. In the field, both physical and mental fatigue can hamper one's judgment, but taking a break is not always possible once traffic control has been established and traffic is backing up. Environmental conditions, such as excessive heat or cold or impending bad weather or personal safety from passing traffic, all serve to distract a surveyor in the field. Even the most experienced surveyors cannot help but be affected to some extent by the environment in which they are working. When vehicles weighing more than 80,000 lb rush by at speeds higher than 60 or 70 mph, a surveyor better take notice. Of course inadequately trained surveyors can also lead to other types of human error. This has not proven to be a significant concern thus far, however, with the training provided.
2. Discrepancies in distress identification associated with lighting. Unlike the filming process, where filming is conducted at night and lighting of the pavement surface is controlled, the manual surveyor must adjust to the lighting conditions for each site. If the surveyor is not positioned correctly to account for the position of the sun in the sky, low severity distresses can be completely overlooked.

Although there are other less significant deficiencies associated with each methodology, these limitations represent most of the distinctions between these methodologies and prevent directly interchangeable survey results. Recognizing the types of distress data being collected, how they are being collected, and the limitations associated with these procedures, one can now proceed with the comparisons of the survey results.

COMPARISON OF DATA FROM THE TWO METHODOLOGIES

After the availability of the various distress data elements for each of the three pavement types and the limitations associated with the two methodologies have been reviewed, the data may be studied to establish how the data from these two methodologies compare. To conduct comparisons of the distress data collected to date, all of the distress surveys were paired off (grouping one semiautomated distress survey with one manual distress survey for the same test section and comparable date). The surveys were sorted under the headings of manual and film. Averages of the quantities of distress for each distress type at each severity level were tabulated and have been summarized in Tables 7 through 9 for ACP, JCP, and CRCP, respectively. Standard *t*-tests were conducted on these data to establish where "significant" differences existed. Distress types exhibiting significant differences have been highlighted in these tables for discussion purposes.

As can be seen from these tables, for many if not all of the cracking distresses, low severity levels typically were significantly lower from the film than from the manual distress surveys. In some instances, this occurred even for the medium-severity distresses. Interestingly, however, the film reduction appears to overcompensate by noting slightly greater quantities of high-severity distress than those observed in the field. The most notable exception is the transverse cracking of ACP, where the trend is just the opposite. A logical explanation for this trend reversal for transverse cracking of ACP has not been identified.

TABLE 7 Comparisons for ACP

DISTRESS	UNITS	LOW		MED		HIGH		TOTAL	
		M	F	M	F	M	F	M	F
CRACKING									
FATIGUE	SQUARE METER	15.9	8.0	8.3	0.9	0.6	0.0	24.9	9.6
BLOCK	SQUARE METER	13.2	6.6	3.5	1.3	0.0	0.0	16.7	8.0
EDGE	METERS	4.2	0.4	0.0	0.0	0.0	0.0	4.2	0.4
LONGITUDINAL	METERS	34.4	32.4	1.7	1.5	0.2	0.0	36.3	33.9
REFLECTIVE, LONG.	METERS	1.1	0.7	0.0	0.0	0.0	0.0	1.2	0.7
REFLECTIVE, TRAN	METERS	0.1	0.7	0.0	0.1	0.0	0.2	0.2	1.0
TRANSVERSE	METERS	12.8	17.2	2.5	2.3	0.5	0.2	15.7	19.6
PATCHING AND POTHOLES									
PATCH DETERIORATION	SQUARE METER	2.3	0.5	0.1	0.2	0.0	0.0	2.5	0.7
POTHOLES	SQUARE METER	0.1	0.0	0.0	0.0	0.1	0.0	0.1	0.0
SURFACE DEFORMATION									
RUTTING	MILLIMETERS	--	--	--	--	--	--	N/A	N/A
SHOVING	SQUARE METER	--	--	--	--	--	--	0.2	0.0
SURFACE DEFECTS									
BLEEDING	SQUARE METER	30.0	3.1	7.5	2.4	0.0	0.0	37.5	5.4
POLISHED AGGREGATE	SQUARE METER	--	--	--	--	--	--	0.0	0.0
RAVELING & WEATHERING	SQUARE METER	10.5	0.5	3.0	0.0	0.0	0.0	13.2	0.5
MISCELLANEOUS DISTRESSES									
LANE TO SHOULDER DROPOFF	MILLIMETERS	--	--	--	--	--	--	N/A	N/A
WATER BLEEDING & PUMPING	METERS	--	--	--	--	--	--	0.7	0.0

SIGNIFICANTLY DIFFERENT
M : MANUAL
F : FILM

NOTE: 1METER = 3.3 FEET
1 SQUARE METER = 10.8 SQUARE FEET

N/A - Not Available
-- - No Severity Levels
Numbers noted are average quantities
for the given distress at the specified severity level.

TABLE 8 Comparisons for JCP

DISTRESS	UNITS	LOW		MED		HIGH		TOTAL	
		M	F	M	F	M	F	M	F
CRACKING									
CORNER BREAKS	NUMBER	0	0	0	0	0	0	0	0
DURABILITY "D"	SQUARE METERS	0	0	0	0	0	0	0	0
LONGITUDINAL	METERS	3.52	0.71	0	0	0	0	3.52	0.71
TRANSVERSE	METERS	3.53	1.41	2.16	2.7	0.7	1.24	6.4	5.34
JOINT DEFICIENCIES									
JOINT SEAL DAMAGE	METERS	50	0	6.92	0	9.94	0	66.8	0
SPALLING OF LONG. JOINTS	METERS	0.51	1.89	0.02	0.07	0	0	0.39	1.95
SPALLING OF TRANS. JOINTS	METERS	0.47	2.17	0.02	0.12	0.08	0.02	0.93	2.41
SURFACE DEFECTS									
MAP CRACKING AND SCALING	SQUARE METERS	--	--	--	--	--	--	285	4.63
POLISHED AGGREGATE	SQUARE METERS	--	--	--	--	--	--	12.6	0
POP OUTS	NUMBER/SQUARE ME	--	--	--	--	--	--	0.19	0.17
MISCELLANEOUS DISTRESS									
BLOW UPS	NUMBER	--	--	--	--	--	--	0	0
FAULTING OF TRANS JTS &CRKS	MILLIMETERS	--	--	--	--	--	--	N/A	N/A
LANE TO SHOULDER DROPOFF	MILLIMETERS	--	--	--	--	--	--	N/A	N/A
LANE TO SHOULDER SEPARATION	MILLIMETERS	--	--	--	--	--	--	0	0
AC PATCH DETERIORATION	SQUARE METERS	0.05	0.06	1.89	0.02	0.00	0	1.94	0.08
PCC PATCH DETERIORATION	SQUARE METERS	0	1.84	0	0	0	0	0	1.84
WATER BLEEDING & PUMPING	METERS	--	--	--	--	--	--	0.7	0

SIGNIFICANTLY DIFFERENT
M : MANUAL
F : FILM

NOTE: 1METER = 3.3 FEET
1 SQUARE METER = 10.8 SQUARE FEET

N/A - Not Available
-- - No Severity Levels
Numbers noted are average quantities
for the given distress at the specified severity level.

TABLE 9 Comparisons for CRCP

DISTRESS	UNITS	LOW		MED		HIGH		TOTAL	
		M	F	M	F	M	F	M	F
CRACKING									
DURABILITY "D"	SQUARE METERS	0.0	0.0	0.0	0.0	0.0	0.0	0.0	0.0
LONGITUDINAL	METERS	1.8	0.0	0.4	0.0	0.0	0.0	2.2	0.0
TRANSVERSE	METERS	449.6	247.0	11.2	89.0	0.0	5.6	483.4	341.6
SURFACE DEFECTS									
MAP CRACKING AND SCALING	SQUARE METERS	--	--	--	--	--	--	51.5	3.0
POLISHED AGGREGATE	SQUARE METERS	--	--	--	--	--	--	0.0	0.0
POP OUTS	NUMBER/SQUARE ME	--	--	--	--	--	--	0.6	0.3
MISCELLANEOUS DISTRESSES									
BLOW UPS	NUMBER	--	--	--	--	--	--	0.0	0.0
CONSTRUCTION JOINT DAMAGE	NUMBER	0.1	0.0	0.0	0.0	0.0	0.0	0.1	0.0
LANE TO SHOULDER DROPOFF	MILLIMETERS	--	--	--	--	--	--	N/A	N/A
LANE TO SHOULDER SEPARATION	MILLIMETERS	--	--	--	--	--	--	0.2	0.0
AC PATCH DETERIORATION	SQUARE METERS	0.0	0.0	0.0	0.0	0.0	0.0	0.0	0.0
PCC PATCH DETERIORATION	SQUARE METERS	0.0	0.0	0.0	0.0	0.0	0.0	0.0	0.0
PUNCHOUTS	NUMBER	0.6	0.0	0.0	0.0	0.0	0.0	0.6	0.0
SPALLING OF LONG. JOINTS	METERS	0.0	2.4	0.0	0.0	0.0	0.0	0.0	2.4
WATER BLEEDING & PUMPING	METERS	--	--	--	--	--	--	0.0	0.0
LONG. JOINT SEAL DAMAGE	METERS	--	--	--	--	--	--	N/A	N/A

SIGNIFICANTLY DIFFERENT
M : MANUAL
F : FILM

NOTE: 1METER = 3.3 FEET
1 SQUARE METER = 10.8 SQUARE FEET

N/A - Not Available
-- - No Severity Levels
Numbers noted are average quantities
for the given distress at the specified severity level.

As previously noted, measurements of faulting, lane to shoulder dropoff, or any distresses requiring measurement of a difference in vertical position cannot be accommodated by the film. These measurements are readily available from manual surveys, however. This creates a significant difference between the two methodologies. Procedures currently are being evaluated to capture some of these data in an automated fashion, but none have been implemented to date.

The distress quantities for most of the low-severity surface defects are considerably lower on the film than on the manual surveys. This finding tends to substantiate the concerns about the ability to discern minimal differences in color and contrast between the film and the field surveys. This limitation tends to become less dramatic as the severity levels of these surface defects increase. As seen from the differences in recording joint seal deterioration, however, these same limitations make it virtually impossible to get an accurate reading of this distress from the film. Like faulting, lane to shoulder dropoff, and the distresses discussed previously, joint seal deterioration is supposed to be recorded for all sections. As can be seen from Table 8, however, no observations of this distress have been made.

These limitations with perception of color and contrast also tend to create some differences in the interpretation of patches or their associated deterioration, or both. As shown in Table 8, in some instances patches were perceived on the film where none existed and in other instances no patch could be detected where one was known to exist. These are fairly extreme cases in this particular limitation, which occurred only in a few instances. The dimensions of patches typically are large enough that it takes only a couple of errant patches to distort these figures fairly significantly.

CONCLUSIONS

Surface distress is commonly perceived to be one of the primary indicators of pavement performance. As such, the collection of these data for the LTPP program is a fairly significant aspect of this overall effort—so significant in fact that substantial efforts have been made in the development of a distress identification manual and guidelines for the measurement and recording of these distresses, along with elaborate accreditation procedures to provide for the most uniform and consistent data possible.

To further ensure that adequate observations of these data are obtained, two methods of data collection are utilized. The primary method of distress data collection for the LTPP program is from the digital analysis of 35-mm film taken of each test section on a routine basis. As a backup, manual surveys are conducted as needed. The LTPP program places a high emphasis on the quality and consistency of the data collected on these test sections. Differences in data collected through other programs with lesser emphasis on quality may be considerably greater than those presented in this paper.

In reviewing the distress data collected to date, two primary conclusions can be drawn. Table 10 has been prepared to summarize all of the observations noted in this paper. The first and probably most significant observation is that few of these test sections have much distress. Some of the distresses occur more commonly than others. There are a variety of explanations for why some of these distresses may not exist, as discussed previously in greater detail. The conclusion, however, is that there still is not much distress on these sections to analyze.

The second conclusion that can be drawn from these data is that there are definitely distinct differences in the distress data collected by the two methods. Again, there are various reasons for why these differences exist. To ensure that the data are not misused, it is important to recognize these differences when using the data.

The limitations of and distinctions between the two methods of distress data collection noted in this paper are not intended to imply that one methodology is more appropriate than the other.

TABLE 10 Summary of Observations

ASPHALT	SEVERITY L	M	H	JOINTED	SEVERITY L	M	H	CONTINUOUSLY REINFORCED	SEVERITY L	M	H
CRACKING				CRACKING				CRACKING			
FATIGUE	F	F	F	CORNER BREAKS	B	B	B	DURABILITY "D"	ND	ND	ND
BLOCK	F	ND	ND	DURABILITY "D"	ND	ND	ND	LONGITUDINAL	F	F	ND
EDGE	F	ND	ND	LONGITUDINAL	F	ND	ND	TRANSVERSE	F	M	M
LONGITUDINAL	B	B	ND	TRANSVERSE	F	B	M	SURFACE DEFECTS			
REFLECTIVE	M	ND	ND	JOINT DEFICIENCIES				MAP CRACKING & SCALING	–	F	–
TRANSVERSE	M	B	B	JOINT SEAL DAMAGE	F	F	F	POLISHED AGGREGATE	–	ND	–
PATCHES AND POTHOLES				SPALLING OF LONG. JOINTS	M	B	ND	POPOUTS	–	B	–
PATCH DETERIORATION	F	B	ND	SPALLING OF TRANS. JOINTS	M	B	B	MISCELLANEOUS DISTRESS			
POTHOLES	B	ND	ND	SURFACE DEFECTS				BLOWUPS	–	ND	–
SURFACE DEFORMATIONS				MAP CRACKING & SCALING	–	F	–	CONSTRUCTION JOINT DAMAGE	B	ND	ND
RUTTING	–	ND	–	POLISHED AGGREGATE	–	F	–	LANE TO SHOULDER DROPOFF	–	ND	–
SHOVING	–	ND	–	POPOUTS	–	B	–	LANE TO SHOULDER SEPARATION	–	B	–
SURFACE DEFECTS				MISCELLANEOUS DISTRESS				PATCH DETERIORATION	B	ND	B
BLEEDING	F	ND	ND	BLOWUPS	–	ND	–	PUNCHOUTS	B	ND	ND
POLISHED AGGREGATE	–	ND	–	FAULTING OF TRANS JTS & CRKS	–	ND	–	SPALLING OF LONG. JOINTS	M	B	ND
RAVELING & WEATHERING	F	ND	ND	LANE TO SHOULDER DROPOFF	–	ND	–	WATER BLEEDING & PUMPING	–	ND	–
MISCELLANEOUS DISTRESS				LANE TO SHOULDER SEPARATION	–	B	–				
LANE TO SHOULDER DROPOFF	–	ND	–	PATCH DETERIORATION	M	F	B				
WATER BLEEDING & PUMPING	–	F	–	WATER BLEEDING & PUMPING	–	ND	–				

LEGEND:

B	IDENTIFIABLE FROM EITHER METHOD
F	MANUAL OK, FILM MARGINAL
M	FILM OK, MANUAL MARGINAL
F	UNIDENTIFIABLE FROM FILM SURVEYS
M	UNIDENTIFIABLE FROM MANUAL SURVEYS
ND	LESS THAN 2 % OF THE SECTIONS HAD THIS DISTRESS

Instead, the paper should serve to document those areas in which additional research and development may be warranted to improve on the methodologies employed. Most important, however, it is intended to highlight the importance of not relying too heavily on either method alone.

REFERENCES

1. *Distress Identification Manual for the Long-Term Pavement Performance Studies.* Report SHRP-LTPP-OG-002. Strategic Highway Research Program, National Research Council, Washington, D.C., June 1989.
2. *Distress Identification Manual for the Long-Term Pavement Performance Project.* Report SHRP-P-338. Strategic Highway Research Program, National Research Council, Washington, D.C., May 1993.
3. Shahin, M. Y., and S. D. Kohn. *Pavement Condition Index Field Manual.* APWA-PAVER, American Public Works Association, July 1984.
4. Smith, R. E., M. I. Darter, and S. M. Herrin. *Highway Pavement Distress Identification Manual for Highway Condition and Quality of Highway Construction Survey.* Report DOT-FH-11-9175/NCHRP 1-19. FHWA, U.S. Department of Transportation, March 1979.
5. Smith, K. D., M. I. Darter, J. B. Rauhut, and K. T. Hall. *Distress Identification Manual for the Long-Term Pavement Performance (LTPP) Studies.* FHWA, U.S. Department of Transportation, Dec. 1987.
6. Rada, G. R., J. S. Miller, and W. Y. Bellinger. Accreditation of SHRP-LTPP Pavement Distress Raters. Presented at the 72nd Annual Meeting of the Transportation Research Board, Washington, D.C., 1993.

This paper presents initial data from the LTPP Program, and the views and opinions expressed are those of the authors and do not necessarily represent the views or conclusions of the Federal Highway Administration or the LTPP Program.

Publication of this paper sponsored by Committee on Pavement Monitoring, Evaluation, and Data Storage.

Design and Reliability Assessment of Data Acquisition System for Louisiana Accelerated Loading Device

LOUAY N. MOHAMMAD, ANAND J. PUPPALA, AND SRINIVAS KATHAVATE

The Louisiana Transportation Research Center has purchased an accelerated loading device that is capable of conducting full-scale simulated and accelerated load testing of pavements. A sophisticated data acquisition system was developed for monitoring various types of sensors installed in pavements that help in understanding pavement materials responses associated with simulated traffic loading and environmental factors. In addition, this system is capable of performing such tasks as data management, data reduction, and graphical presentation. Performance validation tests were conducted on an instrumented pavement site to evaluate the developed system. Two types of sensors (H-gauge, T-type thermocouple) and three types of loading systems (passenger vehicle, falling weight deflectometer, and Dynaflect) were used in this study. Test results demonstrated the excellent capabilities of the data acquisition system. Results were highly repeatable and proved that the system was capable of monitoring traffic loading. The influences of loading mechanisms such as vehicle loading, impulsive loading, and other forms of loading on the longitudinal strains developed in pavement layers were compared.

The accelerated loading device (ALD) testing system provides a new era in evaluating pavement materials, construction practices, and performance. Results of a full-scale pavement testing can be used to verify mathematical models, develop new mechanistic design procedures on the basis of full-scale pavement response, and evaluate in situ material properties under various loading and environmental factors. The ALD also provides researchers with the capability to study the effect of loading on the behavior of the pavement system. Several comparative research studies of various types of construction materials (*1*) are scheduled at the newly developed Pavement Research Facility of Louisiana Transportation Research Center (LTRC). These studies involve performance evaluation, which requires instrumentation of those test sections. The purpose of this study was to develop a data acquisition system and to validate the performance of its features as it is subjected to various types of loading using different types of gauges.

Pavement instrumentation and the data acquisition system play an integral part in the evaluation of material responses. Generally, a variety of measurements are used to characterize the structural performance of full-scale pavement sections. This includes measurement from deflection and strain data, load data, and temperature data. Because of the dynamic effects, load, deflection, and strain data require a higher sampling rate than temperature data. Thus, the data acquisition system developed has all the capabilities to acquire data from various types of sensors at various sampling rates. In addition, the system should be able to perform other tasks, such as data storage and management in a computer file format to be accessed either in real time or later for analysis, and graphical presentation using a graphical user interface (GUI) environment.

A menu-driven, user-friendly software, accelerated loading device instrumentation software (ALDIS), was developed in C-language under LabWindows environment. ALDIS offers attractive GUI features to acquire data from most common types of sensors at various sampling rates, data management, and real-time graphical presentation of data.

Louisiana Transportation Research Center, Louisiana State University, 4101 Gourrier Lane, Baton Rouge, La. 70808.

OBJECTIVE

The main objective of this paper is to provide details on the development of the state-of-art data acquisition system, ALDIS. A second objective of this study is to validate the performance of the features of ALDIS. Several H-gauges and T-type thermocouples were placed at various depths in a pavement test section. Loading on this pavement section was applied by using nondestructive devices [falling weight deflectometer (FWD), Dynaflect, etc.) and by a passenger vehicle. Material responses associated with loading and temperature profile were recorded. These test results were used to assess the reliability of the developed data acquisition system.

BACKGROUND

The accelerated loading was used by AASHO in the late 1950s for conducting road tests. The results obtained in those tests were the basis for today's AASHTO pavement design procedures. The Accelerated Loading Facility (ALF) by the Australian Road Research Board has started a new innovative technique for evaluating pavement materials and construction practices. At present, there are two ALFs in the United States. FHWA owns the first one, which is located at Turner-Fairbank Highway Research Center in McLean, Virginia. LTRC owns the second one. This machine can test years of pavement wear in a few months and also provides real-time data on the performance of new and in-service pavement materials and designs. The results from the data col-

lected using ALDIS will help in the evaluation of materials, construction practices, and performances. In addition, these data will be used to verify mathematical models and evaluate in situ material properties. The details of the hardware and software features of the data acquisition system are described below.

DATA ACQUISITION AND CONTROL SYSTEM

The main functions in a data acquisition and control system are sensor signal conditioning, isolation, analog-to-digital conversion, digital-to-analog conversion, data reduction and analysis, control algorithms, and permanent data storage. The first four of these features are primary functions of the signal conditioning and data acquisition hardware. The last three are the functions of the software. A detailed description of the above features was described previously (*2,3*).

DESCRIPTION OF HARDWARE

Figure 1 shows a schematic diagram of the hardware architecture of the data acquisition system. In includes a 486 based personal computer (PC), plug-in distributed input/output board (I/O), interface circuit boards, and signal conditioning modules. The data acquisition board selected was a Microstar Laboratories model DAP 1200/4S. This 12-bit resolution board provides 16 single-ended analog input channels, or 8 differential-ended analog input channels with software selectable by channel and expansion to a maximum of 512 input channels through the use of a multiplexer scheme. The current configuration allows for 64 analog input channels. This board has 16 digital inputs that are synchronous and expandable to 64 inputs.

The material responses (i.e., load, deflection, strain, temperature) are fed into modulator signal conditioners (shown in Figure 1), which are used to translate a sensor's physical properties to either a digital value or a high-level analog output that can be digitized. In addition, these modules output a current loop in 0 to 20 mA/4 to 20 mA current standards. These current loop outputs are relatively immune to noise and can travel over several thousand feet without signal degradation.

The 0 to 20 mA loop current was carried to the DAP accessory board near the host computer for voltage conversion. A precision resistor was used to drop the current and the voltage across it. The voltage will be measured as analog input signal by the DAP. The PC was located in an instrumentation room about 70 ft (21.35 m) away from the test site.

SELECTION OF SOFTWARE DEVELOPMENT TOOL

Although the hardware used in data acquisition enables a computer to gather data from and control real-time events, it is the

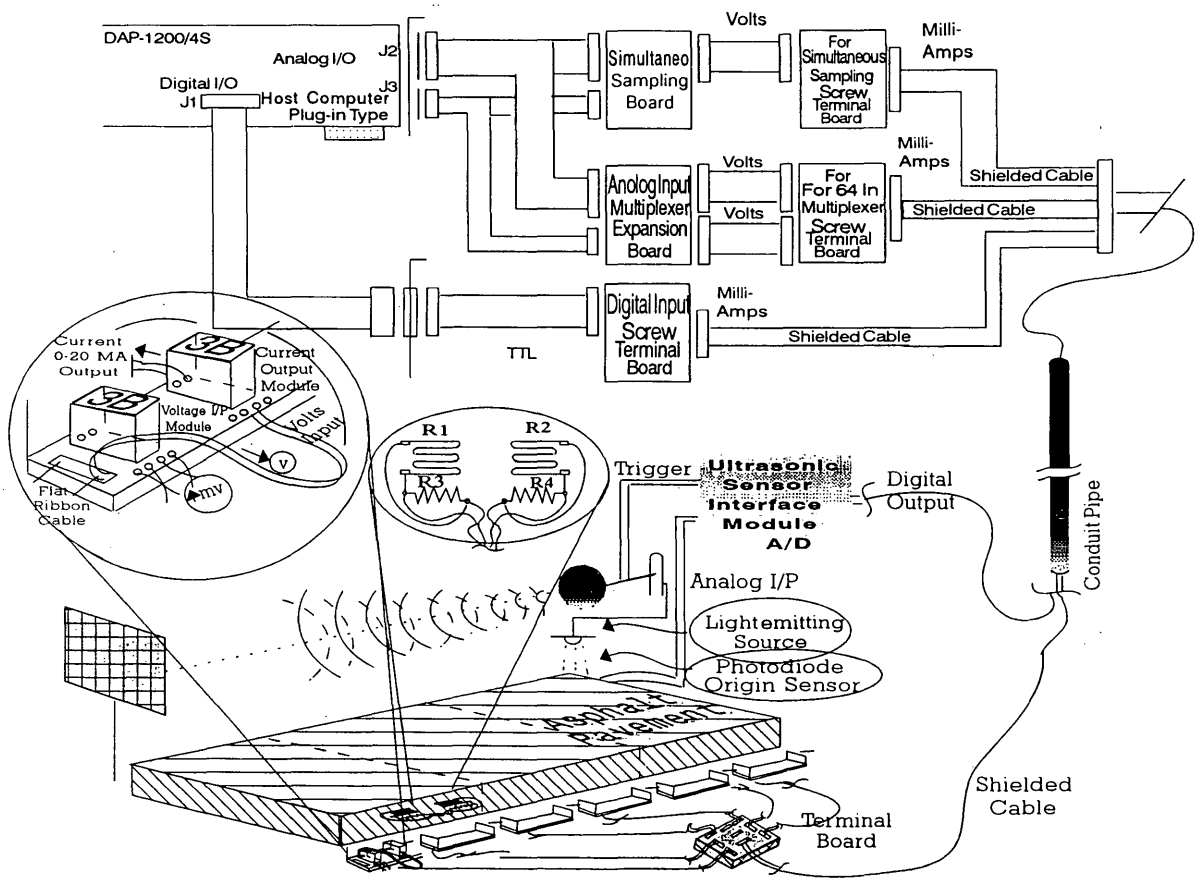

FIGURE 1 Data acquisition system hardware architecture.

software that provides the instructions. Software transforms the PC and data acquisition hardware into a complete data acquisition, analysis, and presentation system. The development of such software involves application of specific routines and interactive programs interfaced by system library functions.

The main criteria set for the selection of the development software was the ease of programming to take full advantage of the DAP board specifications in the GUI environment. Thus, National Instrument's LabWindows (*4*) development software was selected to meet this objective.

Included as part of the driver software were the instrument panel design routines. With usage of these routines one can develop and execute complex tasks with analog, digital, and counter/timer I/O monitoring routines under an attractive, user friendly, and menu-driven system. Instrumentation control panels can be integrated into data acquisition in designing multiple instrument panels. A detailed description of the hardware architecture and software features is described elsewhere (*3*).

DESCRIPTION OF SOFTWARE

The data acquisition software developed in this study was named ALDIS version 1.0. ALDIS is a state-of-the-art integrated tool for data acquisition, storage, and presentation. The GUI associated with ALDIS includes an attractive display feature with instrument panels such as strip charts, *xy*-graphs, digital panel meters, ring switch control, binary switch control, and pushbottom controls, as shown in Figure 2.

ALDIS supports individual and group channel operations with user programmable features such as individual channel sampling rate, single/differential input signal, channel type (analog input or digital input), scale factors and offset, and time delay factor. It also offers programmable data storage formats such as file format in ASCII/Binary, converted data in United States/Système International variation and data storage file name.

ALDIS is developed in C-language and runs on a personal computer under LabWindows environment. The user-friendly GUI takes the user through the software set-up features in three different screens effortlessly with the context help providing useful notes. These three scenes, (a) channel setup, (b) data storage and file format, and (c) data presentation formats, are shown in Figure 3. Calibration and zeroing of the various sensors can be performed in the individual channel mode. The organizational chart of ALDIS is presented in Figure 4.

RELIABILITY ASSESSMENT OF ALDIS

To access the performance of the features of ALDIS, a test strip was built and instrumented with two types of sensors (H-gauge and T-type thermocouple) (*3*). The test strip was then subjected to three types of loading (passenger vehicle, FWD, and Dynaflect). A detailed description of the test section, sensor selection, and sensor installation follows.

Test Site

The test site was a pavement strip located adjacent to the LTRC building. It consisted of a 3-in. (75-mm) asphaltic concrete layer and a 6-in. (150-mm) sand-clay-gravel base material and clay sub-

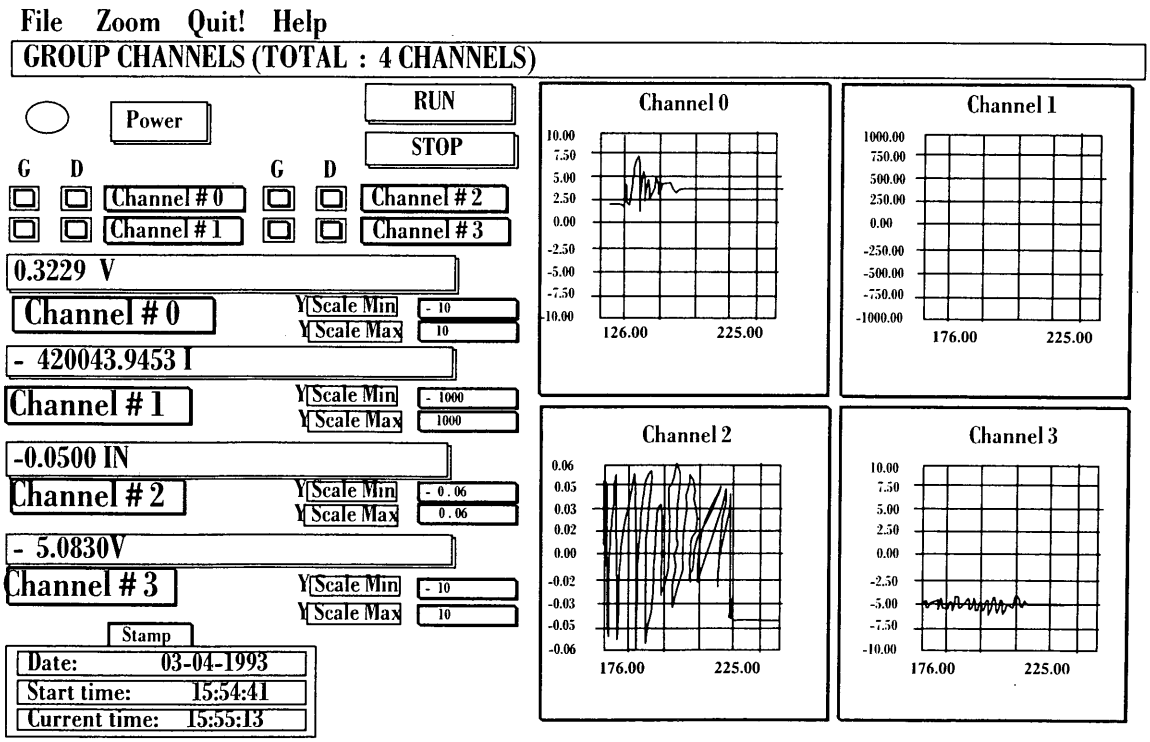

FIGURE 2 Typical display screen from ALDIS.

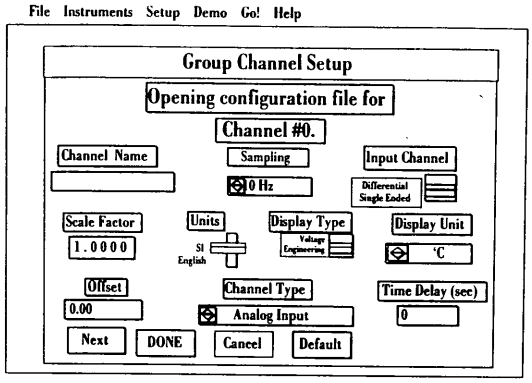

a) Channel Configuration

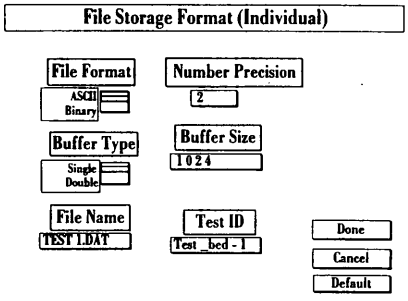

b) Data Storage and File Format

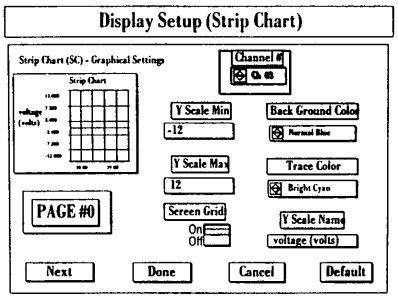

c) Data Presentation Attributes

FIGURE 3 Setup screens.

grade, as shown in Figure 5. In addition, a 2-in. concrete slab, on top of the surface layer, was used with FWD testing only.

Sensor Selection

Strain measurement in flexible pavements is usually performed by electrical resistance strain gauges. Strain gauges are generally selected on the basis of their gauge length. For pavement applications, this criterion is based on the maximum aggregate size of the paving mixture. The length is usually three to five times the maximum aggregate size (*5*). From the earlier research work experience with different types of strain gauge sensors, it was decided that embedded strain gauges with anchor support using metal bars that form the shape of the letter H were the appropriate type of strain gauges for strain measurement in an asphalt layer. Various types of thermocouples are available. The selection of a specific type of gauge is based on the environmental conditions under which it will be used. T-type thermocouples made of copper and constantan are usually used in pavements because they can be used from subzero temperatures to about 700°F (370°C) with an accuracy of ±1.8°F.

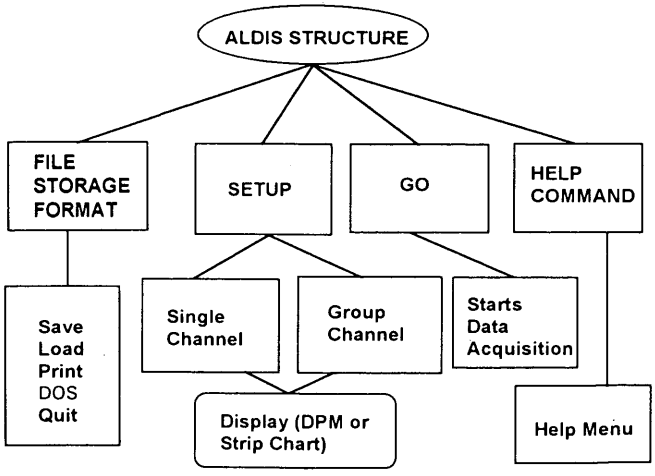

FIGURE 4 Organization of the ALDIS software.

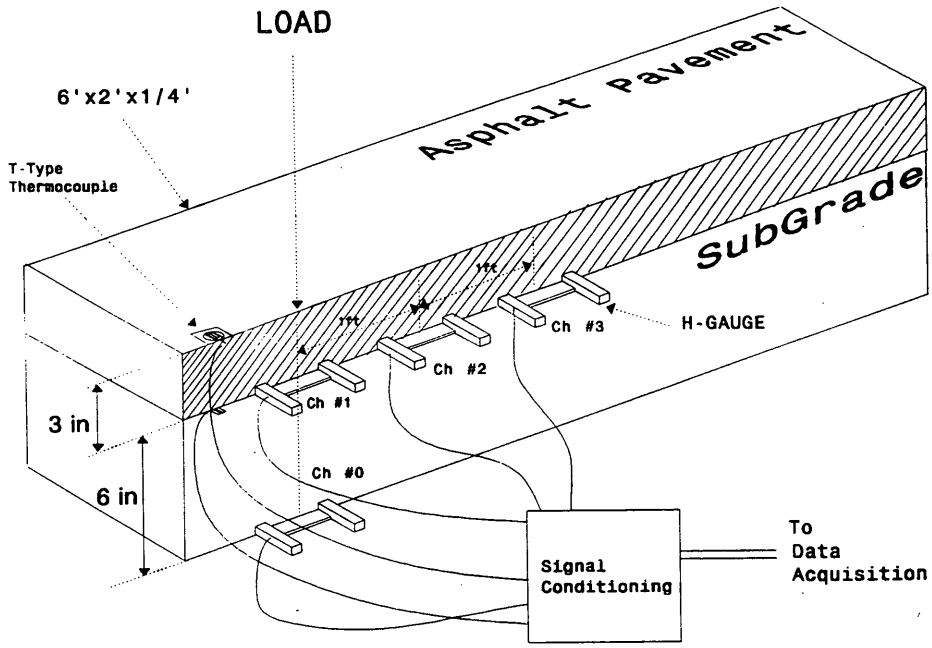

FIGURE 5 Instrumented pavement test section.

H-Gauge Construction and Specification

Figure 6 presents a typical H-gauge. It consists of two strips of aluminum/brass material that anchors the strain gauge firmly in pavement layers. The strain gauge type used was a KM-120-120-H2-11W1M3 from Kyowa Engineering, Inc. The dimensions were 4.68 × 0.58 × 0.17 in. (120 × 15 × 4.5 mm) (length × width × thickness) in matrix dimension with 120 Ω-gauge resistance, 2.0-gauge factor. Two aluminum bars, 2.92 × 0.46 × 0.39 in. (75 × 12 × 10 mm) anchor the embedment-type strain gauge to form the shape of the letter H. The strain gauge was flushed to the bottom of the anchor bars to give a good surface contact underneath it.

Sensor Installation Procedure

The location of the strain gauges and thermocouples in the test section is shown in Figure 5. The proper installation procedure is very important for precise data acquisition that otherwise would have resulted in either loss of data or improper data. Therefore, proper care should be taken while placing the sensors in the pave-

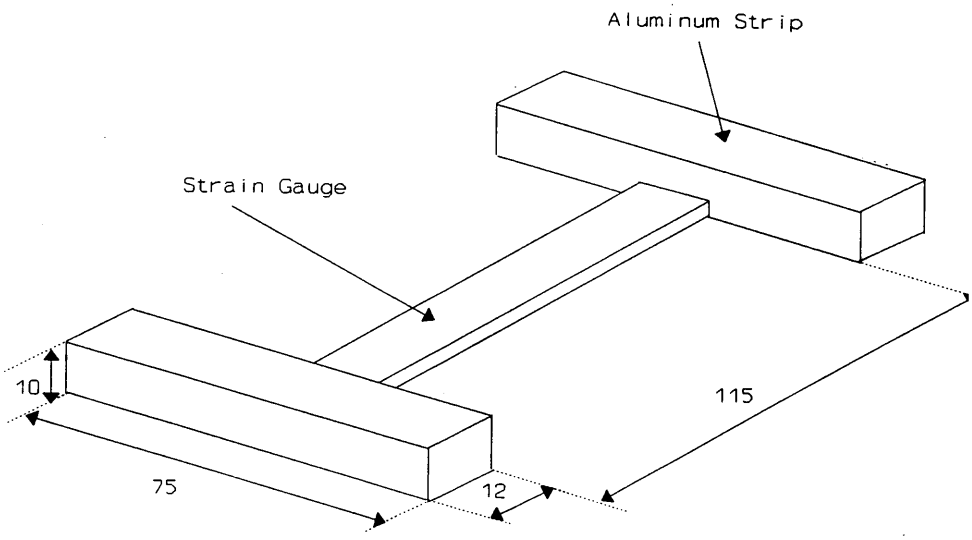

FIGURE 6 Schematic diagram of the H-gauge (embedded strain gauge); all dimensions are in millimeters.

ment. First, the existing pavement surface was removed up to a depth of the base layer, 3 in. (75 mm). Another 6 in. (150 mm) of the base layer was excavated and removed. The removed granular base material was used again as a replacement material. Six H-type strain gauges were placed in the test section. The first and the second gauges were on the same vertical axis, 9 and 3 in. below the surface, respectively, whereas the remaining four gauges were placed at the bottom of the asphalt layer 1 ft apart as shown in Figure 5. Two T-type thermocouples were used to measure the temperature at the surface and at the bottom of the asphalt layer. One was placed at the bottom of the asphalt layer, and the second one was on the surface. The sensors were carefully placed on top of the subgrade and base layers. Then, the replacement material was placed on the first sensor and cold mix was placed on top of the other sensors. Compaction was achieved by tamping with a 10-lb (44.4-N) hammer and subsequently passing a vehicle on top of it. Care was taken during compaction so that sensor wires were not disturbed and damaged.

Testing Procedure

The sampling rate plays an important role in the precision of test data results. Generally, higher sampling rates provide a better profile. However, storage of the data can be a problem because the data occupy a large space on a hard disk; thus, an optimum rate needs to be established. Three sampling rates of 10, 40, and 100 Hz were evaluated to examine changes in the precision of the response from the H-gauges.

Loading of the pavement section was performed in three phases. In the first phase, a passenger vehicle was passed. The second involved the loading of the pavement section by using an FWD. Tests were conducted by dropping the hammer of FWD directly on top of the pavement as well as on a concrete slab 2 in. (50 mm) thick placed on top of the test section. The third phase used a Dynaflect testing, which is of sinusoidal shape. The data acquisition system was used to monitor the sensors during all three phases of testing. Three types of sampling rates—10, 40, and 100 Hz—were used for storing the data.

DISCUSSION OF RESULTS

Phase 1

In Phase 1, a passenger vehicle traveling at a speed of 14 mph with a front axle load of 1,940 lb (8.62 kN) and a rear axle load of 1,160 lb (5.15 kN) was used. The measured data were recorded in volts and then converted to microstrain using the following formula:

$$\text{Strain} = \frac{\text{unstrained volt}}{\dfrac{\text{ch. gain} \times \text{excitation volt}}{\text{gauge factor}}} - \frac{\text{strained volt}}{\dfrac{\text{ch. gain} \times \text{excitation volt}}{\text{gauge factor}}} \times 10^6$$

The first set of strain readings was measured when the front wheel was on top of the pavement section, Figure 7 (top). The second set of peak strain readings was recorded when the rear wheel was on top of this section. Higher strains were measured under front wheel loading (shown as A in the figure) than those under rear wheel loading (shown as B). This difference is because the higher loading occurred under the front wheel that includes the engine load. The second set of strain readings, taken when the car was driven in reverse direction, was lower than the first set of peak readings. This difference can be the result of partial recovery of the viscoelastic component of the strains in the material during the reverse movement of the car. As expected, the strain varied from tension to compression as the loading approached and left the sensor, respectively.

Repeatability

Repeatability of the test results is an important aspect of this kind of testing. The repeatability was evaluated by passing the passenger vehicle on the pavement section several times and recording the strains in the gauge under each wheel. Five sets of readings were recorded in a span of 2 min by passing and reversing the vehicle over this section (B, Figure 7). The test results were examined in terms of the coefficient of variation (CV), and these results are presented in Table 1. The CV ranged between 1.7 and 4.7 for front wheel loadings and 3.7 and 8.1 for rear wheel loadings. The peak microstrains ranged from 64 to 74, and a standard deviation value of 3.5 was recorded under the front wheel. The peak microstrains under the rear wheel ranged from 62 to 66 with a standard deviation of 2.5, indicating the excellent repeatability of the responses measured with the data acquisition system.

Thermal Variations

Figure 8 presents a typical temperature measurement from the test site at the surface and at the bottom of the asphalt layer using a T-type thermocouple. The noon temperature measurements for the surface and the bottom of the asphalt layer were 115°F and 108°F, respectively. The surface temperature was validated with a digital temperature meter. Figure 8 demonstrates the capability of the data acquisition to measure the temperature profile.

Comparisons of H-Gauge Results

Figure 9 presents a comparison of the results between Gauges 0 through 2 as a result of the movement of the passenger vehicle. Gauge 0, which is located on the top of the subgrade, measured lower strains than Gauge 1, which is on top of the base layer. The magnitude of stress distribution, which decreases with the depth, produces lesser strains. Also, the confining stresses at these depths reduced the strains developed. These results were in agreement with those of theoretical models that show this strain trend with depth associated with stiffness variations of asphalt and soils. This is also the basis behind flexible pavement design, which provides lesser strain in the soil layers.

Numerical Simulations

A comparison of the measured longitudinal strains to the computed values was made. The numerical strains were obtained using

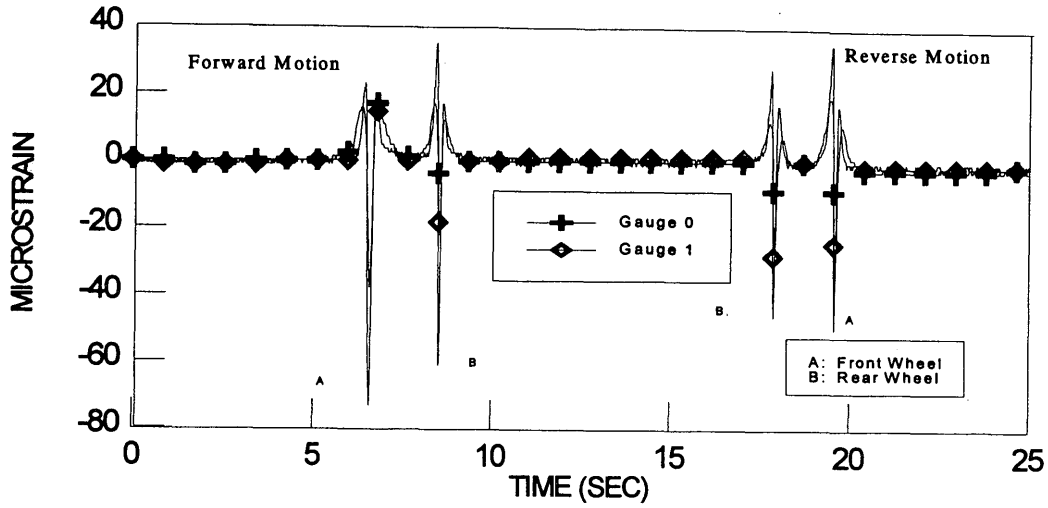

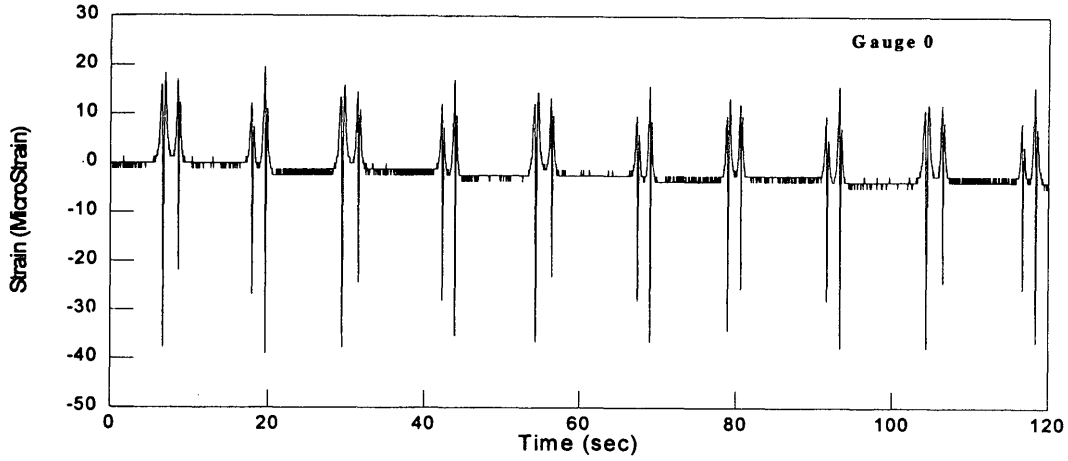

FIGURE 7 Typical response curve for longitudinal strain associated with passenger vehicle loading.

TABLE 1 Typical Peak Microstrains Under Passenger Vehicle Loading

No. of	Front Wheel				Rear Wheel			
Passes	Gauge 0	Gauge 1	Gauge 2	Gauge 3	Gauge 0	Gauge 1	Gauge 2	Gauge 3
1	-37.8	-73.2	-34.2	-37.8	-22.0	-58.6	-35.4	-31.7
2	-34.8	-68.4	-35.4	-36.6	-20.8	-63.5	-31.7	-30.5
3	-34.2	-64.7	-35.4	-36.6	-23.2	-64.7	-31.7	-31.7
4	-34.1	-64.7	-34.2	-35.4	-25.6	-61.0	-30.2	-28.1
5	-37.8	-63.5	-34.2	-34.2	-24.4	-64.7	-27.6	-30.5
Mean	-35.8	-66.9	-34.7	-36.1	-23.2	-62.5	-31.3	-30.5
S.D.	-1.7	-3.6	-0.6	-1.2	-1.7	-2.4	-2.5	-1.3
%C.V.	4.8	5.3	1.7	3.4	7.4	3.8	8.1	4.4

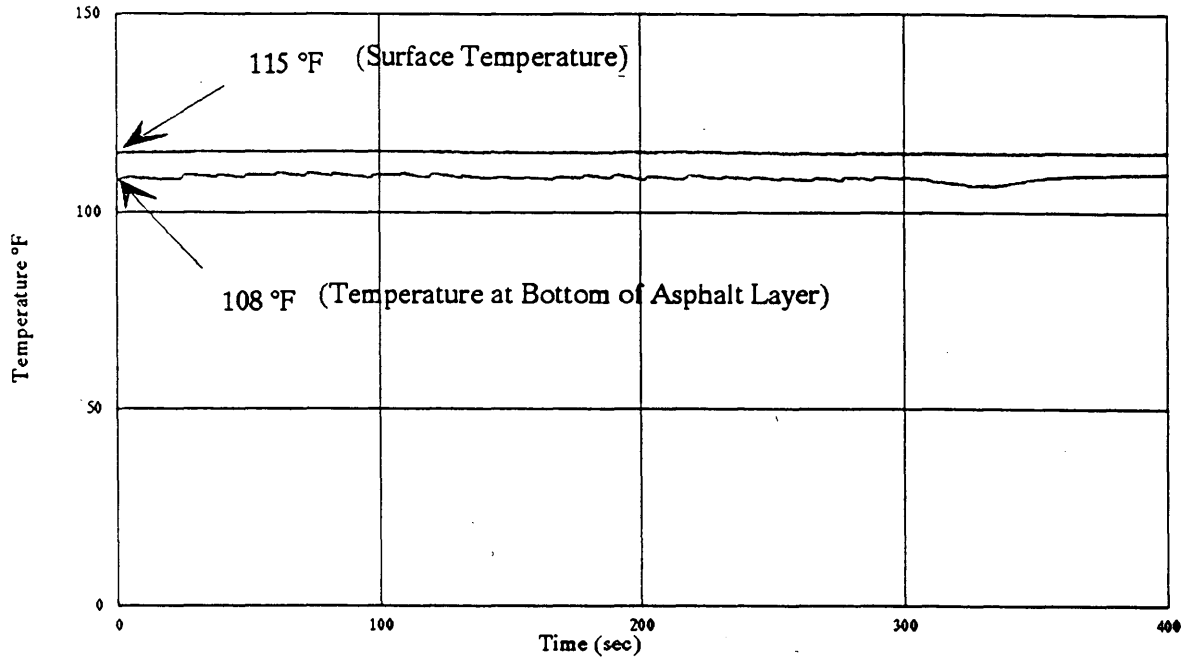

FIGURE 8 Typical temperature response from the test site.

a three-dimensional ideal elastic layered pavement system computer program, ELSYM5. Figure 10 presents the computed and measured longitudinal strains. The moduli and Poisson's ratio were estimated for each layer and a good agreement between the theoretical and measured values, as recorded and stored with ALDIS, was observed.

Phase 2

Loading in this phase was applied using the FWD. Loading is performed first on the original test section, then on the concrete slab 2 in. (50.08 mm) thick placed on top of the asphaltic concrete surface. This loading, which is an impulse type of loading, consists of dropping a known mass from a predetermined height. The falling weight strikes a plate placed on the pavement and thereby transmits a force to the pavement. Four sets of loads [3,431 lb (15.23 kN), 5,791 lb (25.71 kN), 8,934 lb (39.66 kN), and 13,176 lb (58.5 kN)] were applied. Figure 11 presents the strains of three different gauges developed because of these loads. H-gauges at Locations 0 and 1 show similar pattern of strains because they were located along the same vertical loading axis. However, Gauge 1, at the top of the base layer, produced lower strains than Gauge 0, located at the top of the subgrade. This difference is attributed to the dissipation of energy developed as a result of the impulse loading, which needs a longer time to dissipate than the energy from a typical traffic loading. Gauge 2, which was located away from the loading axis, as expected, yielded tensile strains as shown in Figure 11.

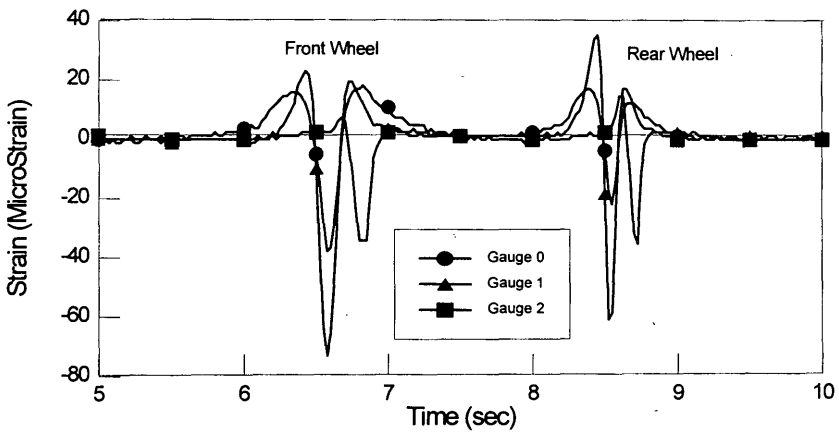

FIGURE 9 Comparison of longitudinal strain responses of gauges at different depths under passenger vehicle loading.

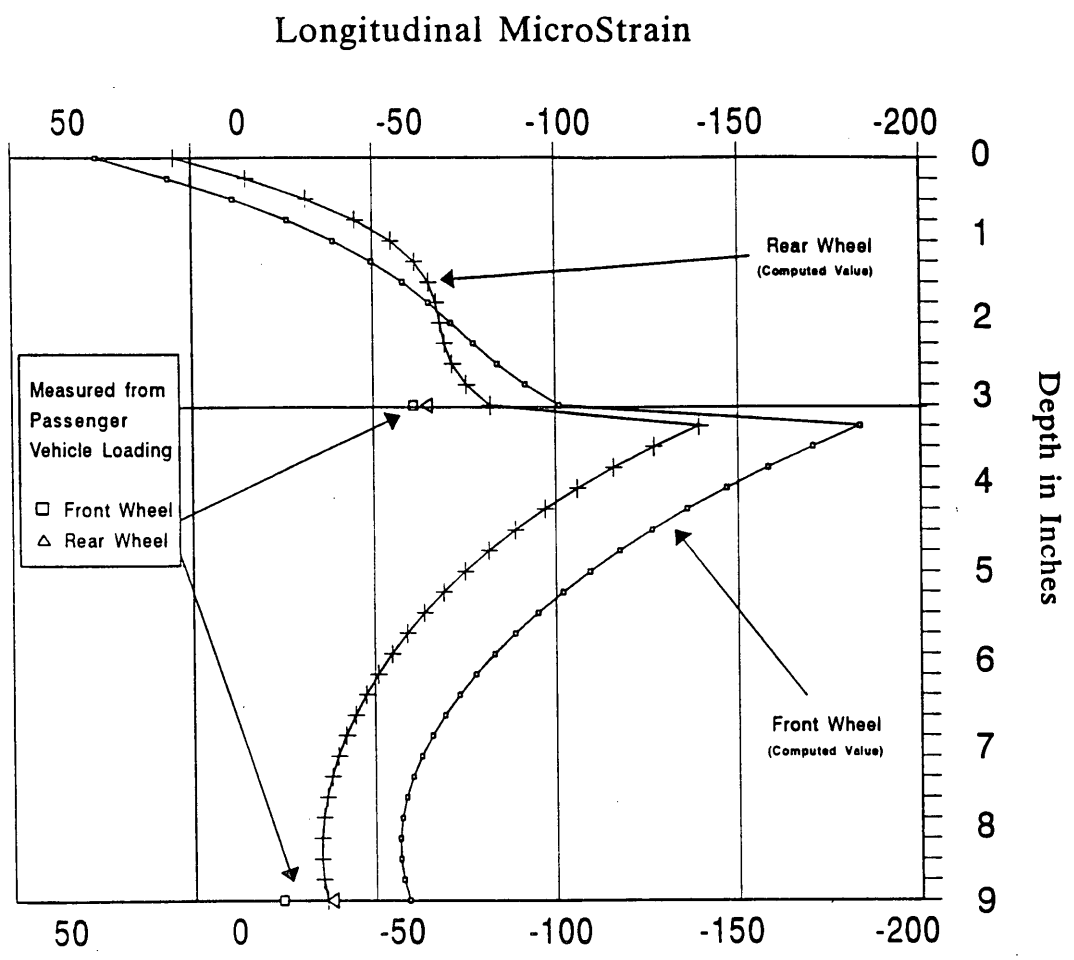

FIGURE 10 Comparison of the measured and computed longitudinal microstrain.

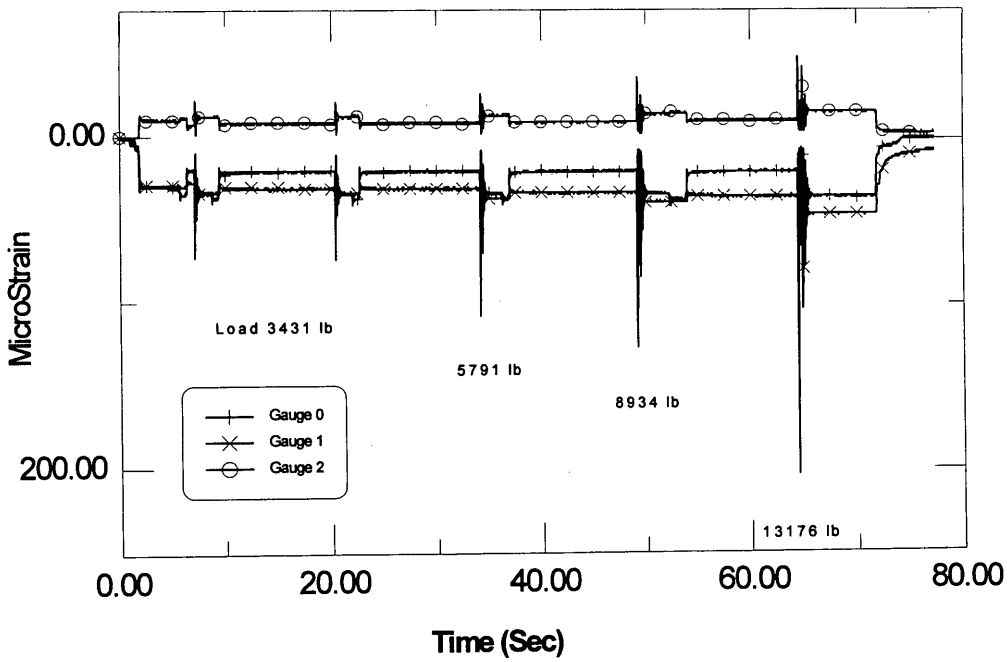

FIGURE 11 Typical response curve under FWD loading.

Sampling Rate

All the above results were obtained with a frequency of 40 Hz. To study the influence of sampling rate, a test with a frequency of 100 Hz was conducted. Figure 12 presents the comparisons between the test results of 10, 40, and 100 Hz. The trends of these deflection profiles appear to be similar except at certain peaks. The 40-Hz sampling rate appears to be sufficient from this type of loading.

Influence of Concrete Block

The loading of FWD was performed on a concrete slab that was placed above the pavement surface. Figure 13 compares the results with loading on a concrete block and without it. Lower strains were observed in the case of a loading with a concrete block. This is because the energy applied in loading is mostly taken by the block; therefore, the stresses applied to the pavement layers are substantially lower than those applied in a loading without a block. Also, the stiffness variations between the concrete and pavement layers can contribute to the above variation.

Phase 3

Phase 3 involves using a loading by using a Dynaflect. The loading system consists of two counter-rotating eccentric masses. A load of 4.45 kN at a frequency of 8 cps was applied through two steel wheels that are 0.51 m apart. Figure 14 shows the measured strains versus the time in seconds. It is interesting to note that eight deflection cycles are measured in each second, which is the Dynaflect frequency. This phase also proves the capability of the developed data acquisition system.

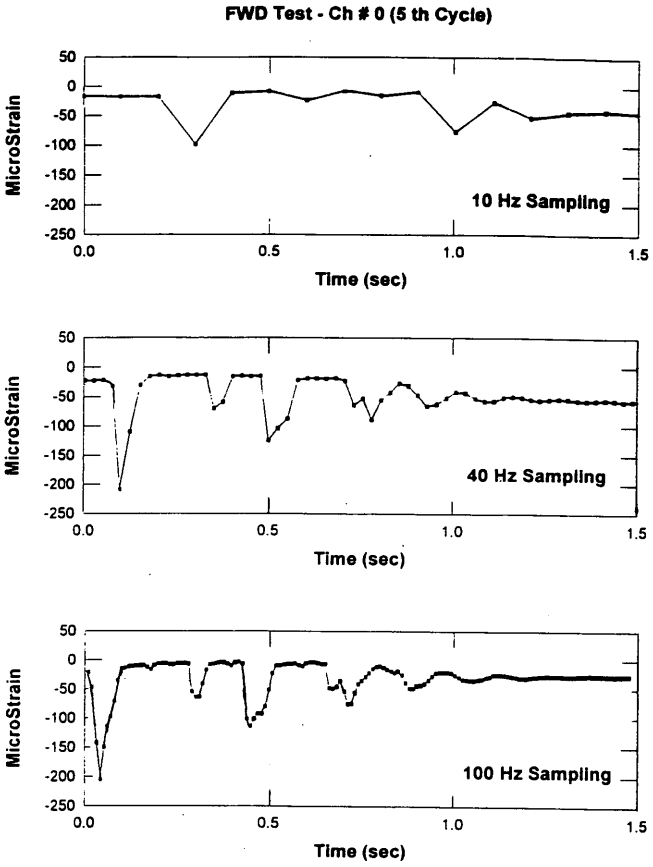

FIGURE 12 Influence of sampling rate on measured strain profile.

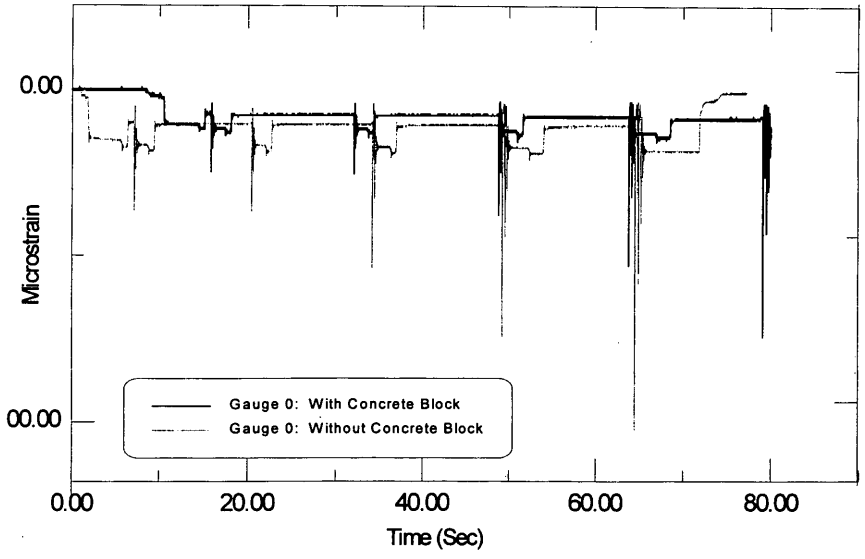

FIGURE 13 Influence of loading via concrete block on strains.

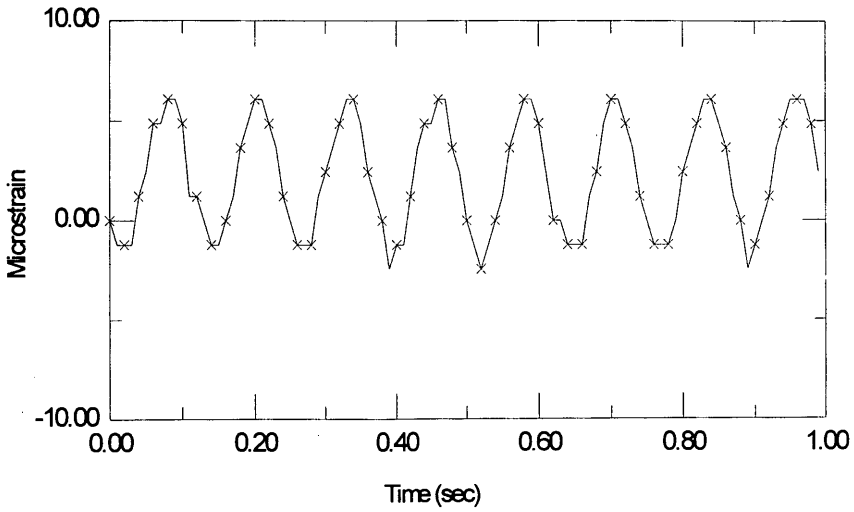

FIGURE 14 Typical strain response curve from Dynaflect loading.

SUMMARY AND CONCLUSIONS

A sophisticated data acquisition system was developed for use in monitoring various sensors under an ALD. Capabilities and reliability of this system are assessed by monitoring different sensors under various loadings. The results showed that this system is capable of capturing all types of responses under all types of loading at various frequencies. Also, H-gauges have demonstrated excellent capabilities in measuring the strains of different layers.

ACKNOWLEDGMENTS

This work was supported by the Louisiana State Transportation Research Center under Louisiana Department of Transportation and Development. The authors express their appreciation for this support.

REFERENCES

1. Cumbaa, S. L., et al. *Construction and Comparison of Louisiana's Conventional and Alternative Base Courses Under Accelerated Loading*. FHWA. Research Study, 1993–1996.
2. Mohammad, L. N., and S. K. Kathavate. *Design and Development of Data Acquisition System for the Louisiana Accelerated Loading Device*. Report FHWA/LA-92/250. Louisiana Transportation Research Center, Baton Rouge, La., July 1992.
3. Mohammad, L. N., and S. K. Kathavate. *Validation of the Performance of the Louisiana ALF Data Acquisition System*. Report LA-93/278. Louisiana Transportation Research Center, Baton Rouge, La., Aug. 1993.
4. National Instruments. *Catalog on IEEE-488 and VXI Bus Control, Data Acquisition and Analysis*. National Instruments Corporation, Austin, Tex., 1992.
5. Tabatabaee, N., P. Sebaaly, and T. Scullion. *Pavement Testing Facility, Instrumentation for Flexible Pavements*. Report FHWA/RD/89–084. FHWA, McLean, Va., 1989.

Publication of this paper sponsored by Committee on Pavement Monitoring, Evaluation, and Data Storage.

Correlation of Present Serviceability Ratings with International Roughness Index

SEDAT GULEN, ROBERT WOODS, JOHN WEAVER, AND VIRGIL L. ANDERSON

The Indiana Department of Transportation (INDOT) is using a pavement management system to identify roads for periodic maintenance and reconstruction. The present serviceability index (PSI), pavement riding comfort index, is one of the major factors in selecting roads for rehabilitation. This study searched statistically realistic models for PSI and international roughness index (IRI) correlation. Ten randomly selected subjects rated 1-mi-long test sections at three roughness levels for both concrete and bituminous pavements. Two nearly identical cars were used, and each subject rated the 20 test sections as a driver and as a front seat passenger. Each rater assigned a PSI value between 0 and 5 (0 for worst, 5 for best) and also marked whether the ride on the section was acceptable. The IRI of each test section was measured by a van equipped with noncontact laser sensors. The statistical analyses indicated that the PSI rating observations were normally distributed, the variances were homogeneous, and the position of the rater in the car was not significant. Then the average PSI ratings and IRI values of the test sections were used for model searches. Simple linear and exponential models were obtained to fit the data with r^2-values ranging from 0.80 to 0.95. The acceptable service level IRI values were obtained by a logistic regression model using the average IRI and acceptance-rejection data of the test sections. Now INDOT can predict PSI values from collected IRI data. Using the IRI data and acceptable service level values, INDOT can identify roads for rehabilitation.

The Roadway Management Division of the Indiana Department of Transportation (INDOT) is utilizing a pavement management system for optimum rehabilitation of their highway system. The present serviceability index rating (PSI ratings or simply PSI) is one of the major factors in selecting the roads for rehabilitation and reconstruction. A realistic prediction of the PSI values may be obtained from the measured international roughness index (IRI) or the measured roughness number (RN or RIDE-SCORE).

Three research studies have been performed in Indiana to correlate PSI ratings with RN values. The first one was a Joint Highway Research Project study (*1*) by Mohan in 1978 in which a total of 94 test sections were selected on four pavement types—flexible, asphalt overlay, continuously reinforced concrete, and jointed reinforced concrete. A 20-member panel rated the test sections for PSI values, and RN values were measured by the PCA road meter. The PSI rating data were correlated with the RN with r^2-values ranging from 0.46 to 0.78.

The second research study, performed in 1982 by Trezos and Gulen (*2*), was undertaken to reestablish the PSI versus RN relationship developed by Mohan. This study was similar in design to the first one, but with several improvements. The PSI rating data versus RN models developed in the second study resulted in r^2-values ranging from 0.68 to 0.71.

The third research study, performed in 1984 by Gulen et al. (*3*), examined the relationship between PSI ratings and RN as well as the effects of the pavement types, the rater's occupation, and the rater's vehicle type on the PSI ratings. Twelve raters (four highway engineers, four technical people, and four nontechnical people) rated 68 test sections for PSI on bituminous and concrete pavements. The PSI ratings were obtained by subjects who drove three car types (compact, mid-size, and full-size).

In the latest research study, performed outside Indiana, Al-Omari and Darter obtained data from Louisiana, Michigan, New Jersey, New Mexico, Indiana, and Ohio. Their results are reported in another paper in this Record. The relationships between IRI and PSI ratings were analyzed, and the following model was recommended:

$$PSI = 5 * e^{(-0.26 * IRI)} \quad (1)$$

where IRI is in millimeters per meter or

$$PSI = 5 * e^{(-0.0041 * IRI)} \quad (2)$$

where IRI is in inches per mile. The above prediction equations are not correct statistically; in fact, they are biased because they were forced to pass through PSI = 5 when IRI is zero.

For the current study only 10 randomly chosen raters were used to evaluate 20 randomly selected sections in Indiana to examine the relationships between PSI and IRI. There were 9 sections on bituminous and 11 sections on concrete pavement. The raters used two nearly identical cars (1992 Dodge Spirit) and made evaluations both as drivers and as right front seat passengers.

OBJECTIVE OF STUDY

The two main objectives of this study were as follows:

1. To establish statistically valid and realistic models between PSI ratings and IRI for both bituminous and concrete pavements using a minimum number of raters. For conversion of historical data, RIDE-SCORE was included in this study.
2. To define an unacceptable PSI rating value (critical PSI) for each pavement type or the types combined.

Division of Research, Roadway Management, Indiana Department of Transportation, P.O. Box 2279, West Lafayette, Ind. 47906.

SCOPE OF WORK

Design of Experiment

Ten subjects were selected to rate the test sections as a driver and passenger using one of the two nearly identical cars. Each person rated the sections once as a driver and once as a right front seat passenger. The design factors used in this study were

- Pavement type (fixed, two levels)
  - —Bituminous pavement and
  - —Concrete pavement.
- Roughness level (fixed, three levels)
  - —Low (smooth roads),
  - —Medium (medium smooth roads), and
  - —High (rough roads).
- Test sections (random). A minimum of three 1-mi-long sections per roughness level for each pavement type was selected.
- Raters (random). Ten subjects were selected to rate the sections for PSI ratings.
- Location of raters in the car (fixed, two levels)
  - —As a driver and
  - —As a passenger (front seat).

Procedures for PSI Rating Data Collection

Selection of Raters

Ten subjects were randomly selected from INDOT. It was necessary to select raters within INDOT because of budget constraints and insurance liability.

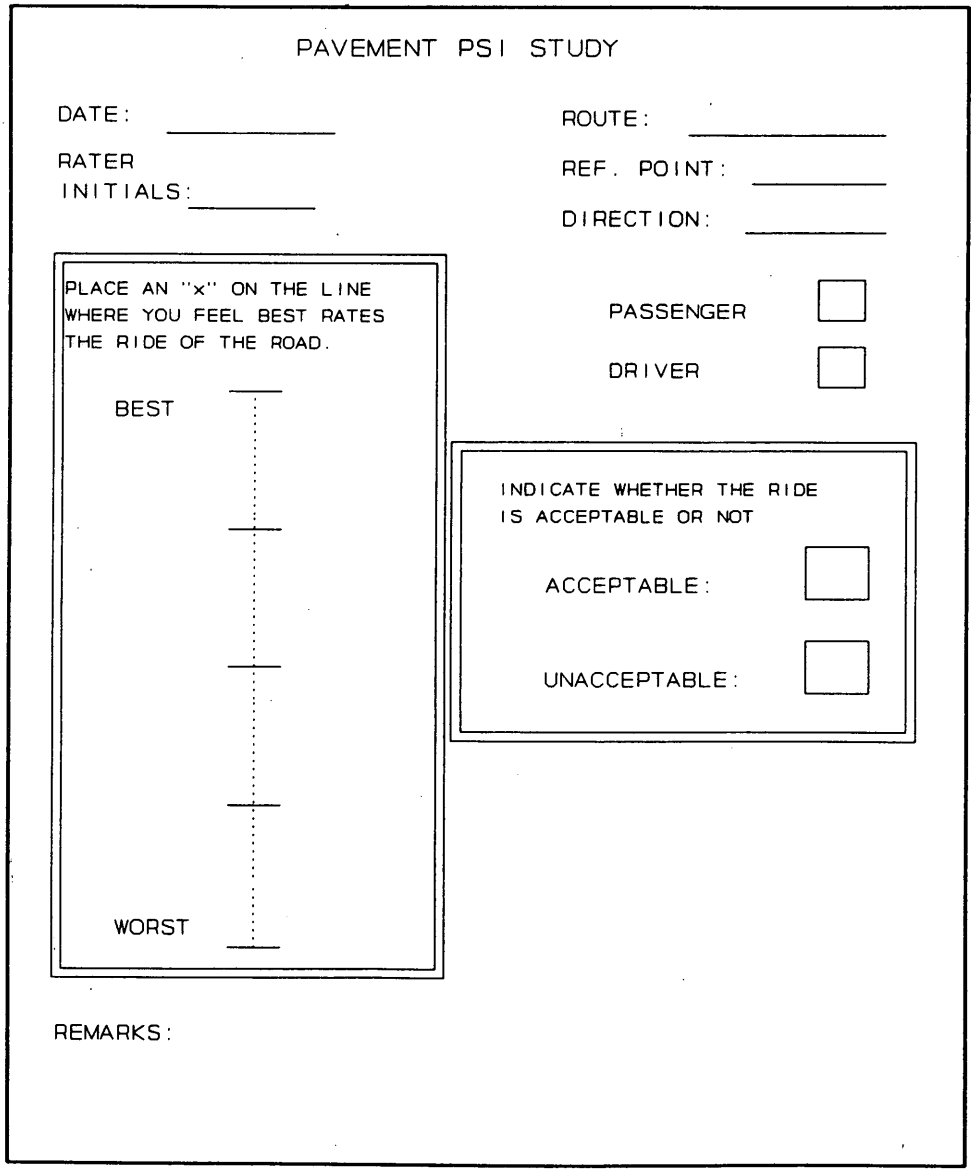

FIGURE 1 Data rating form.

TABLE 1 Expected Mean Squares for Full Model

	a F i	b R j	c R k	d F l	1 R n	EXPECTED MEAN SQUARES (EMS)
R_i	0	b	c	c	1	$\sigma^2+d\ \sigma^2_{SP}+bd\ \sigma^2_{RP}+cd\ \sigma^2_{S}+bcd\ \phi(R)$
$S_{(i)j}$	1	1	c	d	1	$\sigma^2+d\ \sigma^2_{SP}+cd\ \sigma^2_{S}$
P_k	a	b	1	d	1	$\sigma^2+d\ \sigma^2_{SP}+abd\ \sigma^2_{P}$
RP_{ik}	0	b	1	d	1	$\sigma^2+d\ \sigma^2_{SP}+bd\ \sigma^2_{RP}$
$SP_{(i)jk}$	1	1	1	2	1	$\sigma^2+d\ \sigma^2_{SP}$
L_l	a	b	c	0	1	$\sigma^2+\sigma^2_{SPL}+ab\ \sigma^2_{PL}+c\ \sigma^2_{SL}+abc\ \phi(L)$
RL_{il}	0	b	c	0	1	$\sigma^2+\sigma^2_{SPL}+b\ \sigma^2_{RPL}+c\ \sigma^2_{SL}+bc\ \phi(RL)$
$SL_{(i)jl}$	1	1	c	0	1	$\sigma^2+\sigma^2_{SPL}+c\ \sigma^2_{SL}$
PL_{kl}	a	b	1	0	1	$\sigma^2+\sigma^2_{SPL}+ab\ \sigma^2_{PL}$
$RPL_{(i)kl}$	0	3	1	0	1	$\sigma^2+\sigma^2_{SPL}+b\ \sigma^2_{RPL}$
$SPL_{(i)jl}$	1	1	1	0	1	$\sigma^2+\sigma^2_{SPL}$
$\epsilon_{(ijkl)1}$	1	1	1	1	1	σ^2 *random error term*

Selection of Vehicles

Two nearly identical mid-size vehicles (1992 Dodge Spirit), owned by INDOT, were selected.

Selection of Test Sites

Three 1-mi-long test sections in each of the three roughness levels were randomly selected for bituminous pavement. A total of eleven 1-mi-long test sections were randomly selected for concrete pavement: three high roughness sections, four medium roughness sections, and four low roughness sections.

Instruction to PSI Raters

The raters were given a 1-hr orientation in which the road PSI rating responsibilities were described. Figure 1 shows the data

TABLE 2 Expected Mean Squares for Reduced Model

	a F i	b F j	c R k	d R l	n R n	EXPECTED MEAN SQUARES (EMS)
T_i	0	b	c	d	n	$\sigma^2+n\ \sigma^2_{SP}+bcn\ \sigma^2_{TP}+dn\ \sigma^2_{S}+bcdn\ \phi(T)$
$R_{(i)j}$	0	0	c	d	n	$\sigma^2+n\ \sigma^2_{SP}+cn\ \sigma^2_{RP}+dn\ \sigma^2_{S}+cdn\ \phi(R)$
$S_{(ij)k}$	1	1	1	d	n	$\sigma^2+n\ \sigma^2_{SP}+dn\ \sigma^2_{S}$
P_l	a	b	c	1	n	$\sigma^2+n\ \sigma^2_{SP}+abcn\ \sigma^2_{P}$
TP_{il}	0	b	c	1	n	$\sigma^2+n\ \sigma^2_{SP}+bcn\ \sigma^2_{TP}$
$RP_{(i)jl}$	0	0	c	1	n	$\sigma^2+n\ \sigma^2_{SP}+cn\ \sigma^2_{RP}$
$SP_{(ij)k}$	1	1	1	1	n	$\sigma^2+n\ \sigma^2_{SP}$
$\epsilon_{(ijkl)r}$	1	1	1	1	1	σ^2 *random error term*

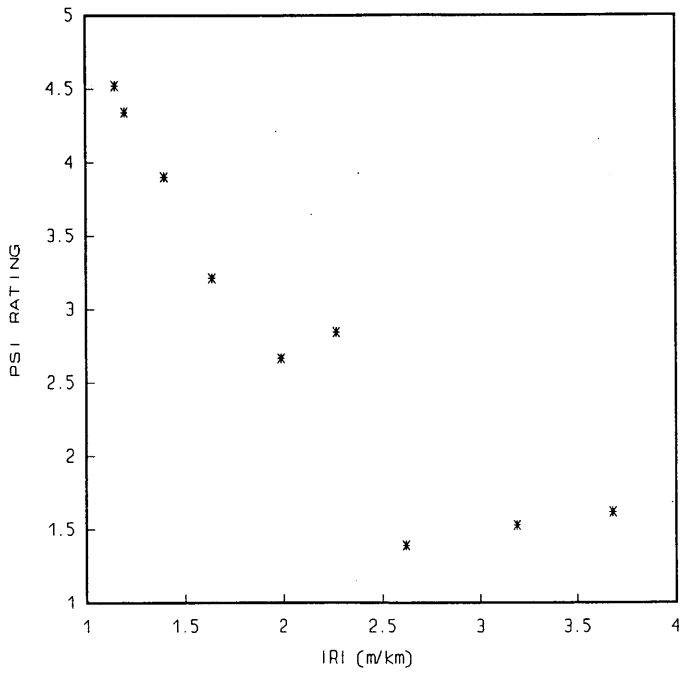

FIGURE 2 Average PSI versus average IRI (bituminous). [IRI in m/km (1 m/km = 1/63.36 in./mi).]

rating form used in this experiment. The raters were instructed to evaluate the sections as a driver and as a front seat passenger on different days to minimize being influenced by their previous rating. They were to mark their PSI rating opinion value on the scale on the form and were asked to note whether the section was acceptable. A constant speed of 55 mph was specified to be maintained during the rating procedure.

IRI Data Collection

The IRI data for the selected test sections were collected by a noncontact, laser-based profilometer, designed in accordance with the World Bank recommendations, installed in a van and meeting FHWA Class II specifications for Highway Pavement Management System data collection. Three runs were made for each section at a near-constant speed to determine the IRI value. The standard deviation of the instrument can be as low as 0.25 in/mi for uniform road surfaces.

RIDE-SCORE Data Collection

The RIDE-SCORE data were collected by the Ultrasonic Ranging Road Meter-CS 8000 Model E installed in a second van (*4*). Three readings were obtained at constant speed.

DATA ANALYSIS

Analysis of PSI Versus IRI and RIDE-SCORE

The following steps were taken in the data analysis of the PSI ratings.

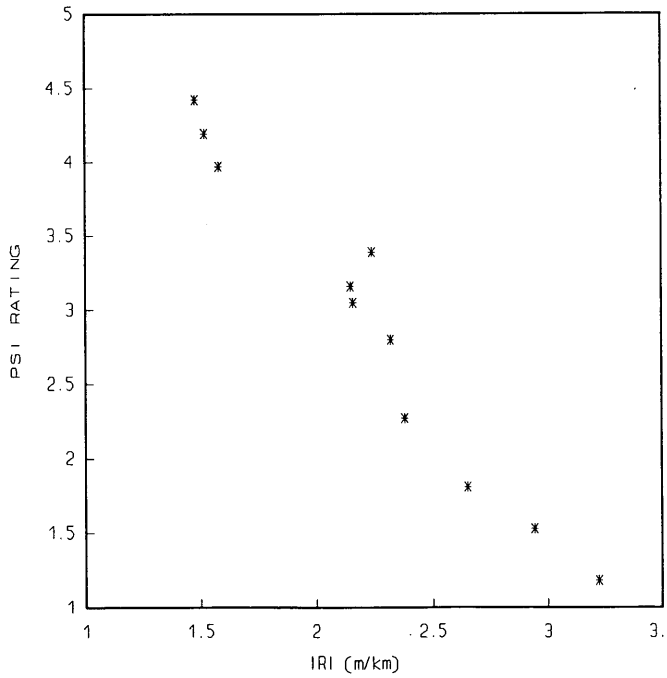

FIGURE 3 Average PSI versus average IRI (concrete). [IRI in m/km (1 m/km = 1/63.36 in./mi).]

TABLE 3 Prediction Equations for PSI Values

NO	SURFACE	PREDICTION EQUATION	r^2	MSE
1	Bituminous	$\hat{PSI} = 4.8 - 0.06\ RIDE$	0.86	0.232
2	Bituminous	$\hat{PSI} = 5.70\ e^{-0.02\ RIDE}$	0.94	0.165
3	Bituminous	$\hat{PSI} = 9.9 - 4.8\ Log_{10}(RIDE)$	0.92	0.131
4	Bituminous	$\hat{PSI} = 5.5 - 1.25\ IRI$	0.85	0.251
5	Bituminous	$\hat{PSI} = 7.21\ e^{-0.47\ IRI}$	0.84	0.143
6	Bituminous	$\hat{PSI} = 4.8 - 6.36\ Log_{10}(IRI)$	0.92	0.135
7	Bituminous	$\hat{PSI} = 8.3 - 3.78\ \sqrt{IRI}$	0.89	0.183
8	Concrete	$\hat{PSI} = 5.8 - 0.08\ RIDE$	0.88	0.155
9	Concrete	$\hat{PSI} = 8.75\ e^{-0.0302\ RIDE}$	0.90	0.149
10	Concrete	$\hat{PSI} = 13.7 - 6.9\ Log_{10}(RIDE)$	0.89	0.142
11	Concrete	$\hat{PSI} = 7.1 - 1.88\ IRI$	0.95	0.061
12	Concrete	$\hat{PSI} = 14.05\ e^{-0.74\ IRI}$	0.93	0.129
13	Concrete	$\hat{PSI} = 6.0 - 9.35\ Log_{10}(IRI)$	0.94	0.081
14	Concrete	$\hat{PSI} = 11.2 - 5.58\ \sqrt{IRI}$	0.95	0.066
15	Bit.& Conc.	$\hat{PSI} = 5.2 - 0.06\ RIDE$	0.83	0.229
16	Bit.& Conc.	$\hat{PSI} = 6.59\ e^{-.03\ RIDE}$	0.86	0.251
17	Bit.& Conc.	$\hat{PSI} = 10.5 - 5.0\ Log_{10}(RIDE)$	0.80	0.255
18	Bit.& Conc.	$\hat{PSI} = 6.1 - 1.46\ IRI$	0.86	0.183
19	Bit.& Conc.	$\hat{PSI} = 9.00\ e^{-0.56\ IRI}$	0.84	0.161
20	Bit.& Conc.	$\hat{PSI} = 5.2 - 7.16\ Log_{10}(IRI)$	0.87	0.162
21	Bit.& Conc.	$\hat{PSI} = 9.2 - 4.32\ \sqrt{IRI}$	0.88	0.163

Where:

r^2 : *Coefficient of Determination*

$$MSE = \frac{\sum_{i=1}^{N} (\hat{PSI} - PSI)^2}{N - u} \quad ; \textit{Mean Square Error}$$

N : *Number of data points*

u : *Number of Parameters in the Prediction Equation*

$\hat{PSI}$: *Predicted Present Serviceability Index-Rating*

PSI : *Observed Present Serviceability Index-Rating*

IRI : *International Roughness Number in inches / mile.*

Note: IRI is in units of mm/m. (1 mm/m = 63.36 in/mi).

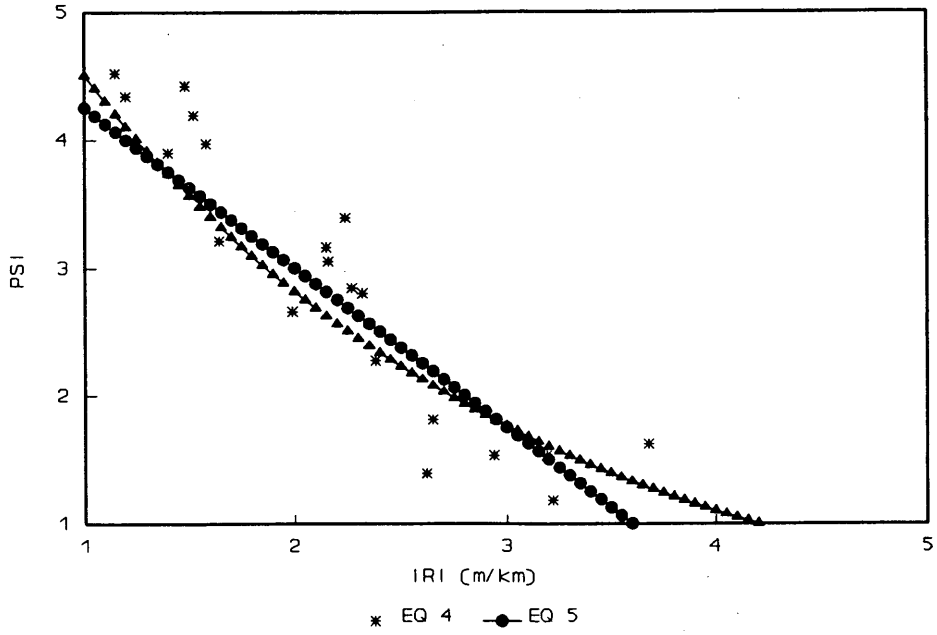

FIGURE 4 Prediction equations 4 and 5 for bituminous pavements (see Table 3). [IRI in m/km (1 m/km = 1/63.36 in./mi).]

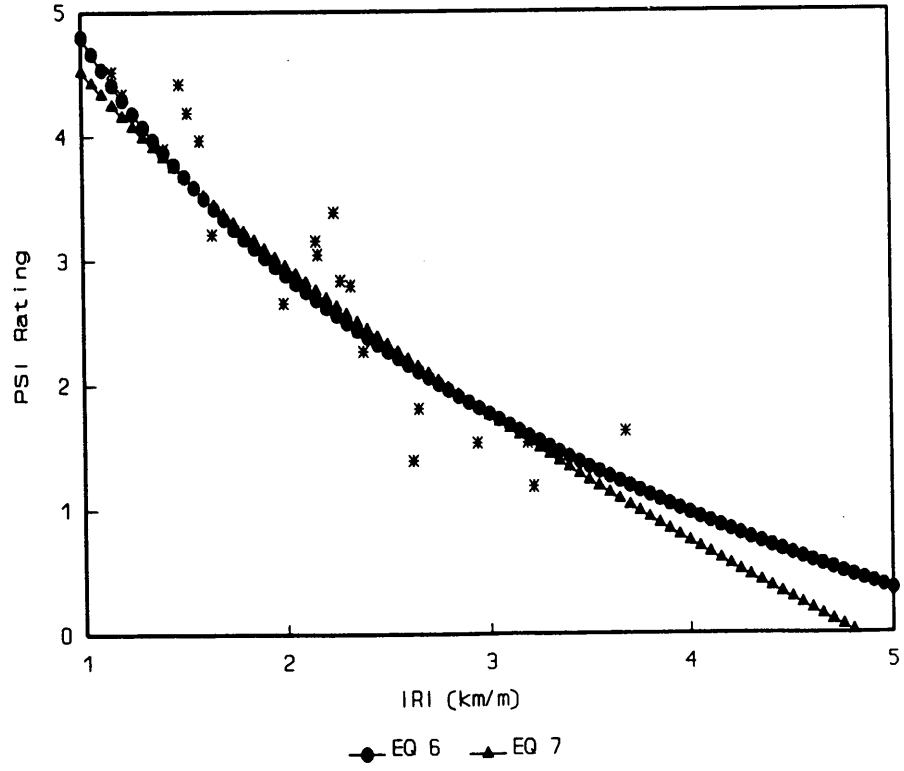

FIGURE 5 Prediction equations 6 and 7 for bituminous pavements (see Table 3). [IRI in m/km (1 m/km = 1/63.36 in./mi).]

Normality of PSI Rating and Homogeneity of Variances

The distribution of the PSI ratings for each test section was checked and found to be normal for both pavements types. The variances of the PSI ratings among the test sections were checked and found to be homogeneous for both pavement types.

Analysis of Variance

The main purpose of this step was to determine whether the position of the rater in the car was significant. Before the actual numerical procedure can be run, however, the expected mean squares (EMS) for the proposed model (Equation 3) must be derived (5–7).

The analysis of variance (ANOVA) model was as follows:

$$PSI_{ijkln} = \mu + R_i + S_{(i)j} + P_k + RP_{ik} + SP_{(i)jk} + L_l + RL_{il} + SL_{(i)jl} + PL_{kl} + RPL_{ikl} + SPL_{(i)jkl} + \epsilon_{(ijkl)1} \quad (3)$$

where

PSI = present serviceability index rating;
μ = overall mean;
R_i = roughness levels, fixed (i = 1,2,3);
$S_{(i)j}$ = test sections, random, within roughness levels;
P_k = raters, random (k = 1, . . . , 10);
L_l = rater's location in car, fixed (l = 1,2);
RL = interaction of roughness with rater's location;
RP = interaction of roughness with rater;
SP = interaction of section with rater;

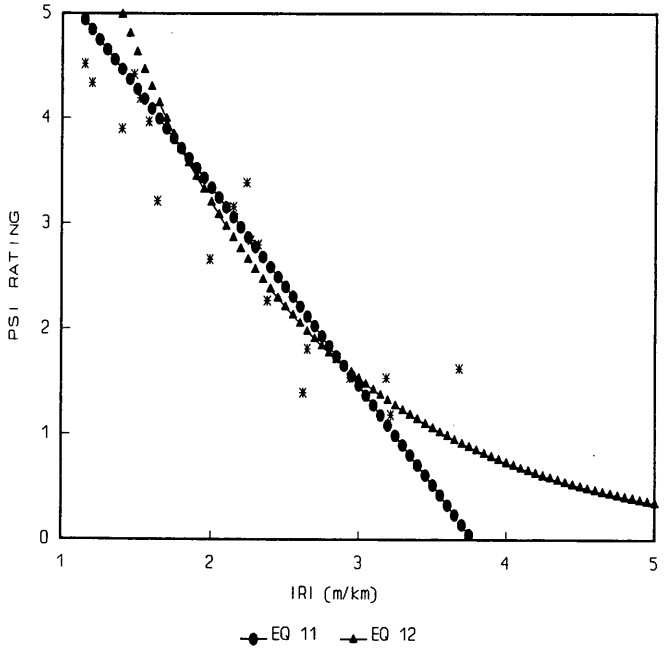

FIGURE 6 Prediction equations 11 and 12 and concrete pavements (see Table 3). [IRI in m/km (1 m/km = 1/63.36 in./mi).]

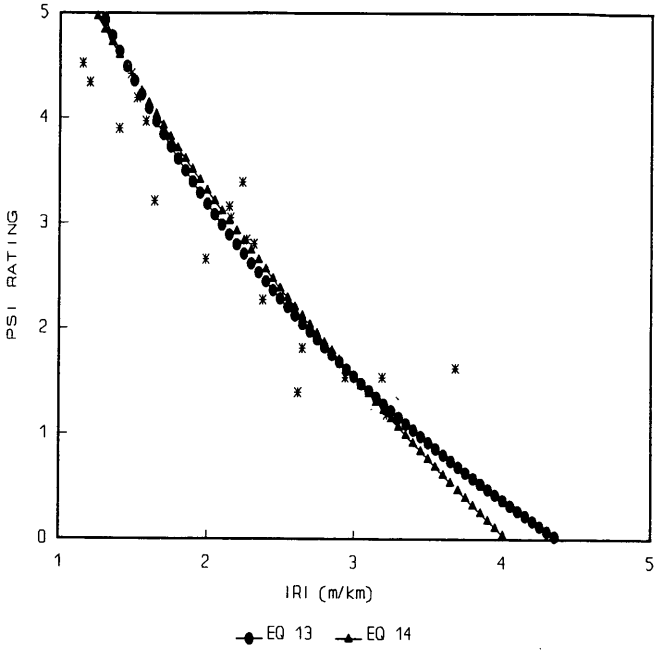

FIGURE 7 Prediction equations 13 and 14 for concrete pavements (see Table 3). [IRI in m/km (1 m/km = 1/63.36 in./mi).]

SL = interaction of section with rater's location;
PL = interaction of rater with rater's location;
RPL = interaction of roughness, rater, and location;
SPL = interaction of rater, section, and location; and
$\epsilon_{(ijkl)1}$ = experimental error assumed normal and independently distributed NID (0, σ^2).

Because there was no replication, the three-way interaction, SPL, was used as an error term. The EMS table (Table 1) shows how various F-tests should be performed.

F-test for L:

$$F = \frac{EMS(L) + EMS(SPL)}{EMS(PL) + EMS(SL)} \quad (4)$$

The number of test sections for concrete pavement was not the same for each roughness level; therefore the statistical analysis system (SAS) at Purdue University was used for statistical computations (*8*). The statistical computations indicated that the position of the raters in the car was not significant (F-value was less than 1). Then, the following reduced ANOVA model (Equation 3) was written to check the effect of the surface type as well as the other terms.

$$PSI_{ijkln} = \mu + T_i + R_{(i)j} + S_{(ij)k} + P_l + TP_{il} + RP_{(i)jl} + SP_{(ij)kl} + \epsilon_{(ijkl)n} \quad (5)$$

where

μ = overall mean;
T_i = pavement type, fixed (i = 1,2);
$R_{(i)j}$ = roughness levels, fixed;
$S_{(ij)k}$ = sections, random, within roughness levels;

P_l = raters, random;
TP = interaction of pavement with rater;
RP = interaction of roughness with rater;
SP = interaction of section with rater; and
$\epsilon_{(ijkl)n}$ = experimental error, $NID(0, \sigma^2)$.

The corresponding EMS table (Table 2) was prepared to show various F-tests.

F-test for T, pavement type:

$$F = \frac{EMS(T) + EMS(SP)}{EMS(TP) + EMS(S)} \quad (6)$$

Statistical computations indicated that pavement type was not significant (F-value was less than 1).

PSI Rating Versus IRI and RIDE-SCORE

Because the distribution of PSI ratings for each test section was found to be normal and the variances among the test sections were homogeneous, the PSI ratings for each test section were averaged. Similarly, the IRI and RIDE-SCORE values for test sections were averaged. Various plots were prepared to see the nature of the PSI ratings and corresponding IRI and RIDE-SCORE (see Figures 2 and 3 for overall average PSI ratings).

Regression analyses were performed using the average data to relate PSI ratings to the IRI and RIDE SCORE. Regression models that best fit the data are listed in Table 3 for each pavement type and combination of both pavements. The regression equations and combined actual data are plotted in Figures 4 through 11.

Figures 4 and 5 show the Prediction Equations 4 through 7 for bituminous pavements. Figures 6 and 7 show the Prediction Equations 11 through 14 for concrete pavements. Figures 8 and 9 show the Prediction Equations 18 through 21 for both pavement types combined.

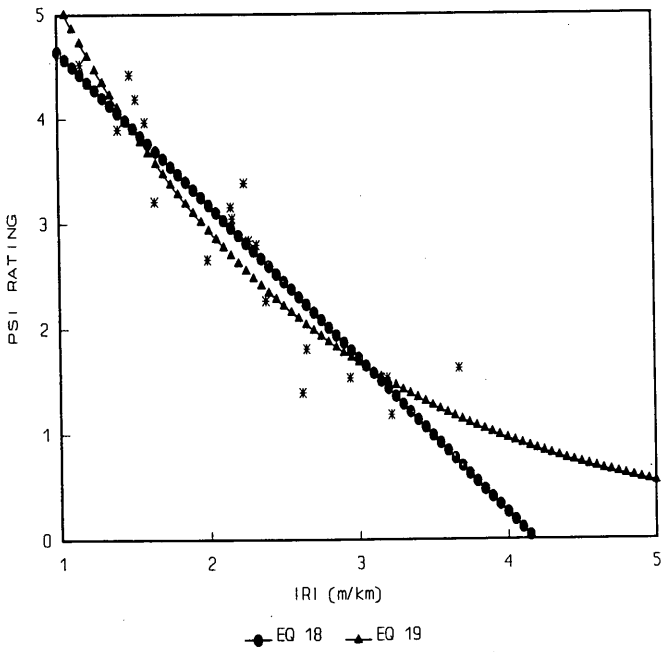

FIGURE 8 Prediction equations 18 and 19 for combined pavement (see Table 3). [IRI in m/km (1 m/km = 1/63.36 in./mi).]

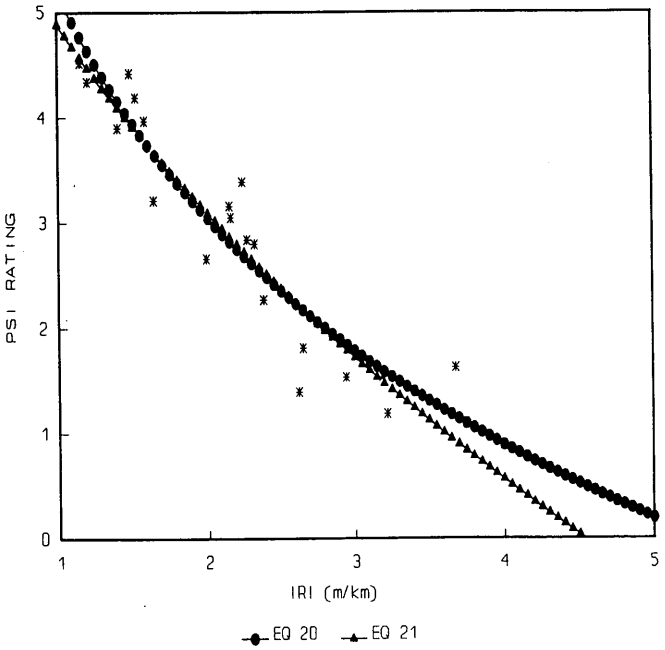

FIGURE 9 Prediction equations 20 and 21 for combined pavements (see Table 3). [IRI in m/km (1 m/km = 1/63.36 in./mi).]

The prediction equations in Figures 4 through 9 show that the predicted PSI rating values are very close when a PSI rating value is between 1.5 and 4.5, indicating that any of the prediction equations can be selected for practical purposes. Figure 10 shows linear prediction Equations 4, 11, and 18 for bituminous, concrete, and both pavement types combined, respectively. The predicted PSI rating values from these three equations are very close when a PSI rating is between 2.0 and 3.2. This indicates that any of these prediction equations can be used for rehabilitation analyses purposes because this range is of chief concern to the rehabilitation analysis.

Figure 11 shows the Prediction Equations 7, 14, and 21 in which the square root of IRI is used for bituminous, concrete, and both pavement types combined.

The predicted PSI rating values from these three equations are very close when the PSI rating is between 1.8 and 3.0, indicating that any of these equations can also be used for rehabilitation analysis purposes. For conservative rehabilitation analysis, Prediction Equations 19 and 21 are recommended. Table 3 also shows r^2 values, coefficients of determination, and MSE. Any equation listed in Table 3 can be used to predict PSI ratings from both the IRI and the RIDE-SCORE for bituminous and concrete pavements as well as the combination of both pavements.

Terminal-Critical IRI Values Determinations

The ten raters also identified whether the test sections were acceptable in terms of riding comfort. These two responses can be considered as two outcomes of a binary variable, Y. Denoting the

outcomes by 1 for acceptance and 0 for rejection gives the Bernoulli random variable. Therefore the logistic regression model (function) Equation 7 was used to obtain the critical IRI values (*9*).

$$E(y) = \frac{e^{\beta_0 + \beta_1 * (IRI)}}{1 + e^{\beta_0 + \beta_1 * (IRI)}} \tag{7}$$

where $E(Y)$ is the expected value of Y, the mean response. An interesting property of the logistic function is that it can easily be made linear. $E(Y) = p$ since the mean response is a probability when the dependent variable is an indicator (binary) variable. Then, with the following transformation,

$$L = \text{Log}_e\left(\frac{p}{1 - p}\right) \tag{8}$$

from Equation 7,

$$L = \beta_0 + \beta_1 * (IRI) \tag{9}$$

The transformation in Equation 9 is called the logistic or logit transformation of the probability p. β_0 and β_1 are parameters to be determined.

The field data were rearranged to enable use of the logistic software of SAS. The maximum likelihood estimation was used to estimate the parameters β_0 and β_1 using the following SAS commands:

PROC CATMOD; BY PVMT LOC; WEIGHT COUNT; DIRECT IRI; MODEL Y = IRI/PREDICT;

The computed maximum likelihood parameter estimates for the logistic model are given in Table 4. The likelihood p-values indicated that the linear models fit well except for bituminous as passenger. The predicted logits

$$\hat{L} = \hat{\beta}_0 + \hat{\beta}_1 * IRI \tag{10}$$

were computed for IRI from 0.79 m/km (50 in./mi) to 4.7 m/km (300 in./mi). Then the predicted probability of acceptance, $\hat{p}$, was computed from

$$\hat{p} = \frac{e^{\hat{L}}}{1 + e^{\hat{L}}} \tag{11}$$

and the results were plotted as in Figure 12.

For practical purposes, INDOT uses $p = 0.85$ for multiple purposes. For this reason, the corresponding average critical values of IRI were computed as follows from Equations 8 and 9 using $p = 0.85$:

- Bituminous pavement—as driver: 2.15 m/km (136 in./mi); as passenger: 2.25 m/km (142 in./mi).
- Concrete pavement—as driver: 2.30 m/km (146 in./mi); as passenger: 2.45 m/km (155 in./mi).

As seen in Figure 12, when p is approximately 0.80, the four curves are practically merging, and, because the difference between driver and passenger is not significant as found before, logistic regression analysis was performed by combining driver and passenger data. The average critical values of IRI using $p = 0.85$ were found to be 2.19 m/km (139 in./mi) and 2.38 m/km (151 in./mi) for bituminous and concrete pavements, respectively.

Figure 12 shows that passengers are more tolerant (less critical) of roughness than drivers for both pavement types. Above an IRI

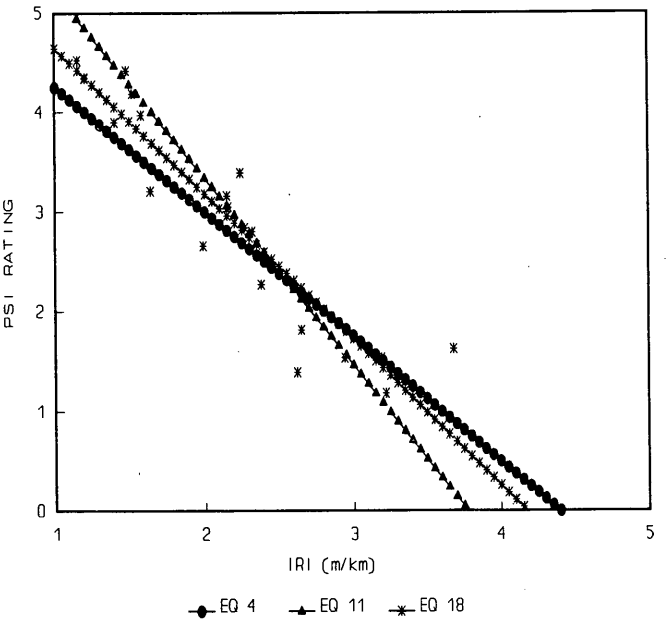

FIGURE 10 Linear prediction equations for combined pavements (see Table 3). [IRI in m/km (1 m/km = 1/63.36 in./mi).]

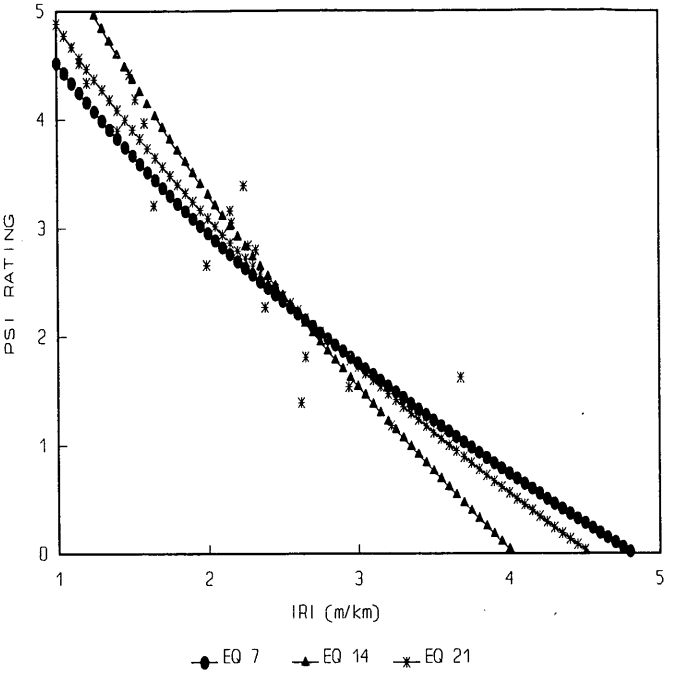

FIGURE 11 Square-root prediction equations for combined pavements (see Table 3). [IRI in m/km (1 m/km = 1/63.36 in./mi).]

TABLE 4 Maximum Likelihood Parameter Estimates

	PAVEMENT TYPE			
	Bituminous		Concrete	
	Driver	Passenger	Driver	Passenger
β_0	6.7942	6.5189	16.1588	16.8853
β_1 *IRI*	-2.3536	-2.1310	-6.2510	-6.1864
Likelihood Ratio p-value	0.11	0.04	0.80	0.81

Note: IRI is in units of mm/m. (1 mm/m = 63.36 in/mi).

of approximately 150, Figure 12 shows that both passenger and drivers are more tolerant (less critical) of bituminous surfaces than of concrete surfaces for the same IRI.

Confidence intervals at 95 percent for average probability of acceptance, p, were computed for particular IRI values and are shown in Table 5. As seen in this table, prediction intervals cover $p = 0.85$ when IRI is 2.27 m/km (144 in./mi) for bituminous and 2.32 m/km (147 in./mi) for concrete pavements. For this reason, a single overall value of 2.3 m/km (146 in./mi) could be used as a critical value for IRI for practical use in pavement management decisions in Indiana.

CONCLUSIONS AND RECOMMENDATIONS

The following conclusions and recommendations were made on the basis of this study:

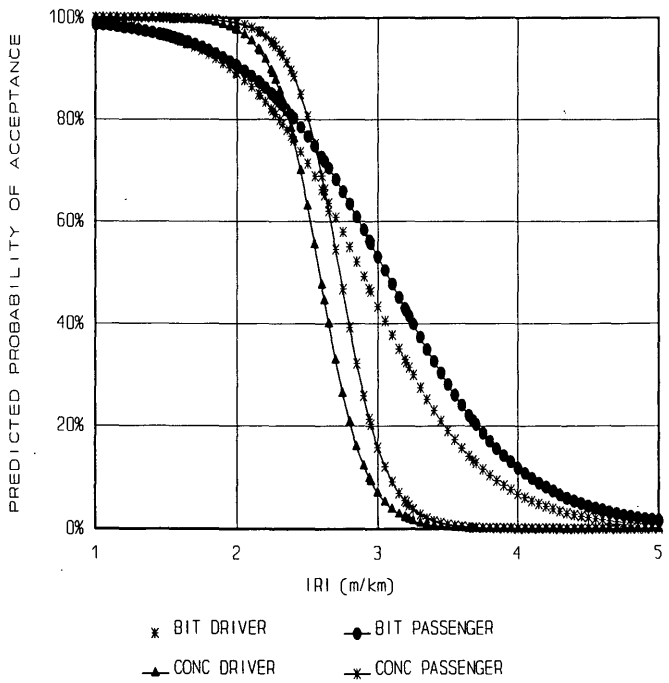

FIGURE 12 Predicted probability of acceptance versus IRI (see Table 3). [IRI in m/km (1 m/km = 1/63.36 in./mi).]

1. Ten or fewer randomly chosen raters may be sufficient to obtain PSI rating data for future studies.
2. The location of rater in the car (as a driver or as a front seat passenger) was found to be nonsignificant.
3. Prediction equations shown in Table 3 are all statistically sound. Selection of equations depends on the user's need. For practical purpose, INDOT may use any of the equations for combined pavement types.
4. Predicted critical IRI values shown in Table 5 are practical. However, a mean value of 2.3 m/km (145 in./mi) for IRI for all pavement types in Indiana is recommended for pavement management purposes.
5. The choice of prediction equations for PSI ratings depends on users. However, Prediction Equation 19 in Table 3 (Equations 12 and 13 in text) is recommended to predict PSI ratings from the IRI values for conservative rehabilitation. However, Linear Prediction Equation 18 in the table also can be used to predict PSI rating values from the IRI values.

$$PSI = 9.0e^{(-0.557 * IRI)} \quad (12)$$

TABLE 5 Confidence Intervals at 95 Percent for Average Probabilities of Acceptance

IRI	BITUMINOUS		BITUMINOUS Combined
	DRIVER	PASSENGER	
1.99	0.81 - 0.98	0.83 - 0.99	0.84 - 0.96
2.27	0.70 - 0.92	0.74 - 0.95	**0.75 - 0.90**
2.53	0.50 - 0.80	0.59 - 0.85	0.59 - 0.79
IRI	CONCRETE		CONCRETE Combined
	DRIVER	PASSENGER	
2.32	0.74 - 0.94	0.85 - 1.00	**0.82 - 0.95**
2.38	0.66 - 0.90	0.81 - 0.99	0.76 - 0.92
2.65	0.20 - 0.60	0.44 - 0.80	0.37 - 0.64

Note: IRI is in units of mm/m. (1mm/m = 1/63.36 in/mi).

where IRI is in millimeters per meter or

$$\hat{PSI} = 9.0e^{(-0.008784 * IRI)} \quad (13)$$

where IRI is in inches per mile.

6. It is highly recommended that this type of study be performed regularly with additional factors, such as vehicle type, to determine whether or not they are significant.

ACKNOWLEDGMENTS

The authors thank the raters David Andrewski, Cristine McFatridge, Ronald Walker, Karen MacDonald, Jay Marks, Cris McFall, Feleceia Turner, and Janie Marks for their cooperation in conducting this experiment. Appreciation is expressed to Murray Supple and Thomas Williams, who designed and assembled the IRI data collection vehicle and obtained the IRI data. Appreciation is also expressed to Idris Jones, who collected RIDE SCORE data, and Debra Thompson, who helped to prepare the report and various slides. Special thanks are given to David S. Moore of Purdue University, who helped with the categorical data analysis to determine the critical IRI values.

REFERENCES

1. Mohan, S. *Development of a System for the Evaluation of Pavements in Indiana.* Report FHWA/ISHC/JHRP-78/21. Purdue University, West Lafayette, Ind., 1978.
2. Trezos, K., and G. S. Gulen. *Correlation of Roughness Number with PSI.* INDOT, West Lafayette, Ind., 1983.
3. Gulen, S., M. Harness, V. L. Anderson, and K. J. Kercher. *Comprehensive Study of Road Meter Roughness Number with Riding Comfort of Indiana Pavements.* Report DRT-85-1 (HPR-1). INDOT, West Lafayette, Ind., 1985.
4. Cox, J. *Ultrasonic Ranging Road Meter, Model E: Operation Manual.* James Cox & Sons, Colfax, Calif., 1983.
5. Anderson, V. L., and R. A. McLean. *Design of Experiments.* Marcel Dekker, Inc., New York, 1974.
6. Neter, J., and W. Wassermann. *Applied Linear Statistical Models.* Richard Irvin, Inc., Homewood, Ill., 1974.
7. Ostle, B. *Statistics in Research.* Iowa State University Press, Ames, 1963.
8. *SAS Publications on Statistics and Linear Models.* SAS Institute, Inc., Cary, N.C., 1991.
9. Agresti, A. *Categorical Data Analysis,* John Wiley and Sons, Inc., New York, 1990.

Publication of this paper sponsored by Committee on Pavement Monitoring, Evaluation, and Data Storage.

Evaluation of Roughness System of Automatic Road Analyzer

JIAN LU, W. RONALD HUDSON, AND CARL BERTRAND

The automatic road analyzer (ARAN) is a multifunction road-quality surveying instrument. The roughness measuring system is one of the subsystems of the ARAN unit. To enhance the understanding of the response of this instrument (so as to apply it more efficiently to pavement management), a research study was conducted by the Center for Transportation Research, University of Texas at Austin, to comprehensively evaluate this instrument. The results of evaluating the roughness subsystem of the ARAN unit, including roughness correlation analysis and development of a new present serviceability index (PSI) model, are presented. In the correlation analysis, roughness data were collected in Texas by the ARAN unit and the Texas Department of Transportation modified K. J. Law profilometer that was used as a standard reference. The evaluated roughness statistics of the ARAN unit were root mean square vertical acceleration (RMSVA), mean absolute slope (MAS), and TEXTURE. These roughness statistics were correlated with the roughness statistics of the profilometer Maysmeter output, serviceability index (SI), and international roughness index. The PSI model developed in this study is based on the roughness statistic SI of the modified K. J. Law profilometer. This PSI model, including RMSVA and MAS that are independent variables, shows good correlation with SI of the profilometer.

Research leading to the development of roughness measuring equipment dates back more than 60 years (*1*). As a result of the AASHO Road Test in particular, increasing attention has focused on this research area, leading to the development of many types of pavement roughness surveying instruments. Gradually the use of these instruments to evaluate the ride quality of pavement surface grew more widespread such that now the evaluation of the relative smoothness of pavement surfaces has become an important factor affecting decisions about maintenance and the classification of pavement inventories.

Existing pavement roughness instruments generally can be divided into three classes, with each class defined by measurement techniques and the associated measurement errors (*2,3*).

Class 1. Manually operated instruments that accurately measure short wavelength profiles of the roads. Examples of such instruments include the rod and level, the face dipstick, and the TRRL beam.

Class 2. Dynamic direct profiling instruments that employ a variety of methods to produce elevation data from the road surface. Examples of these instruments include the APL trailer, GM profilometer, K. J. Law profilometer, and South Dakota profiler.

Class 3. Response-type road roughness measuring (RTRRM) systems, which accumulate suspension deflections (axle to body or acceleration values) from the roadway surfaces. Examples of these instruments include the Mays ride meter, Cox meter, BPR roughmeter, and the automatic road analyzer (ARAN) unit.

The basic concept of the Class 1 and Class 2 categories is the measurement of the shorter wavelengths contained in the pavement surface profiles. These categories and the associated instruments possess the highest resolutions and the least acceptable error associated with their operation.

The pavement surface ride quality can be directly related to the passenger's perception of the vehicle's vibrations in a certain frequency band rather than the absolute surface profiles. The passengers are more sensitive to the vertical acceleration of the vehicle body caused by the transfer of pavement surface smoothness through the suspension system of the vehicle than to the elevation of the pavement surface. This is the basic concept behind the instruments contained in Class 3.

The ARAN unit is classified as a Class 3 instrument. The vertical accelerations of the body and the axle of the unit are sampled and processed to produce the roughness indexes: root mean square vertical acceleration (RMSVA), mean absolute slope (MAS), and TEXTURE. Relatively speaking, the smaller the values of the reported roughness indexes, the better the corresponding pavement surface ride quality. In addition to the three indexes, the Texas Department of Transportation (DOT) is interested in also obtaining the serviceability index (SI), which is another roughness index. This roughness index can be obtained through a regression model with the variables RMSVA and MAS. The concept behind the SI is the same as that of the present serviceability index (PSI) (*4*).

The multiple functioning and high operating speed of the ARAN unit commend it as an important instrument in pavement management. In addition, a comprehensive evaluation of this unit, as provided in this study, will benefit the Texas DOT in the following ways:

1. The results of the research will provide useful information about the ARAN unit with respect to the performance of the subsystems.
2. The models developed and implemented for the ARAN unit will render it a more powerful instrument; moreover, the methodologies of the modeling and evaluation can be used for future application on other instruments of this type.

This paper presents the results of evaluating the correlation between the roughness statistics from the ARAN unit and the roughness statistics generated by the Texas DOT modified K. J. Law profilometer. The reference statistics from the profilometer are SI (*5*), Maysmeter output (MO) (*5,6*), and international roughness index (IRI) (*7*). The model providing RMSVA at various wave-

J. Lu, Transportation Research Center, University of Alaska Fairbanks, P.O. Box 755900, Fairbanks, Alaska 99775-5900. W. R. Hudson, Department of Civil Engineering, University of Texas at Austin, Austin, Tex. 78712-1001. C. Bertrand, Texas Department of Transportation, D-18, 125 East 11th Street, Austin, Tex. 78701.

lengths from the profilometer is also available. However, MO and SI are functions of RMSVA at the 4- and 16-ft wavelengths (*6*). It was considered unnecessary to use these three roughness statistics together for the correlation analysis. In this research effort, the researchers chose SI and MO, instead of RMSVA. As another research effort, a new present service ability index (PSI) model is presented that includes the independent variables RMSVA and MAS and is based on the roughness statistic SI of the K. J. Law profilometer.

DESCRIPTION OF ROUGHNESS SYSTEM OF ARAN UNIT

The ARAN unit is a van-mounted system that measures and records a wide variety of pavement performance parameters. The entire system is mounted inside a 1986 Ford 1-ton van with a modified motorhome chassis to facilitate its operation; enlarged windows enhance operator observation, while a raised roof provides more space for equipment. As a multifunction system, the ARAN unit is equipped with the following subsystems (*8*):

1. Pavement surface roughness measurement,
2. Rut depth and transverse profile measurement,
3. Gyro,
4. Right-of-way videologging,
5. Pavement condition videologging, and
6. Pavement rating.

The individual subsystems have specialized functions. Detailed description and evaluation results of these subsystems can be found elsewhere (*9,10*).

The roughness measuring subsystem block diagram is shown in Figure 1. This two-part subsystem is divided according to its hardware or its software. The hardware consists of axle and body accelerometers, analog signal amplifiers, analog low-pass filters, and a 12-bit analog to digital (A/D) converter. The software consists of digital band-pass filters passing wavelengths of 1 to 300 ft, digital high-pass filters passing wavelengths of 2 ft or less, and statistical models generating the reported roughness statistics (RMSVA, MAS, and TEXTURE). These roughness statistics are described as follows. RMSVA is defined by

$$\text{RMSVA} = \sqrt{\frac{1}{N}\sum_{i=1}^{N}[a(i)]^2}$$

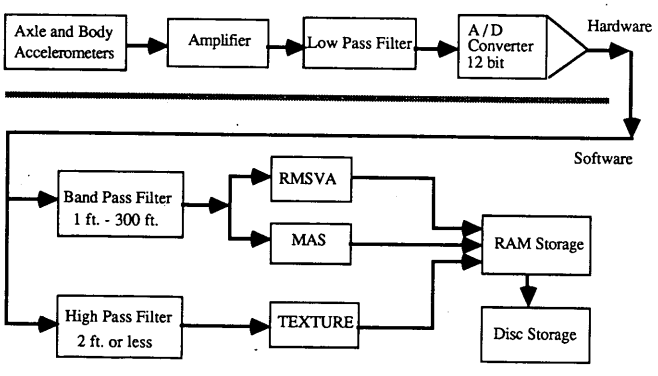

FIGURE 1 Roughness measuring subsystem.

where

$a(i)$ = ith discrete value of filtered acceleration that must be spatially filtered to remove any dc bias;
N = number of samples taken in the given pavement section; and
MAS = cumulative value of the absolute vertical axle or body displacement divided by the vehicle's traveled distance. Mathematically,

$$\text{MAS} = \frac{1}{2N}\left(\frac{T}{L}\right)^2(\Delta X)\sum_{i=1}^{N}|Z(i)|$$

where

T = elapsed time in a test section (station) (sec);
L = station length (mi);
ΔX = sample interval of raw acceleration values; and
$Z(i)$ = height calculated by double intergrating with this equation; thus $Z(i) = Z(i-1) + a(i) + a(i-1)$.

The acceleration signal, once it passes through an A/D converter, follows one of two signal paths. One signal path is through the high-pass filter, whereas the other is through the band-pass filter. The output of the high-pass filter allows more high-frequency (short wavelength) components of the input signal to pass, in the process eliminating the low-frequency signal (long wavelength) components. The high-frequency components of acceleration signal represent the detailed characteristics of surface roughness, such as texturing and cracking. The output signals of the high-pass filter go through the same mathematical model used to calculate RMSVA. The result of the model is TEXTURE.

FIELD DATA COLLECTION

Because most of the evaluation and modeling in this research effort were based on field testing and data collection, these activities were necessarily assigned a higher priority. In this study the ARAN unit had to be considered a "black box," that is, its performance had to be judged by its response (output) to a known input. The known input for the evaluation of correlation of the roughness subsystem was the Texas DOT modified K. J. Law profilometer—an instrument whose output had been verified using FHWA HPMS Appendix J procedures (*2,11*).

To obtain reliable correlation for the ARAN unit, 29 test sections were chosen for the field tests. With the exception of three rigid pavement sites, test sites were located in the Austin, Texas, area. Because no rigid pavements were accessible near Austin, three rigid pavement test sections near LaGrange, Texas, were chosen. The data collected from the flexible and the rigid pavements were combined without consideration of the type of pavement in the study.

The Texas DOT-modified K. J. Law profilometer, defined as a Class 2 pavement roughness monitoring instrument, was chosen as the standard reference instrument for correlation with the ARAN unit. From the standpoint of correlation analysis, it is better to correlate a Class 3 instrument with a Class 1 or Class 2 instrument. Class 1 and 2 instruments directly reflect the surface characteristics of a pavement, whereas Class 3 instruments reflect the response of a vehicle to, or the perception of the vehicle passengers of, the pavement surface roughness.

TABLE 1 Summary of Correlation Analysis of Roughness Statistics for ARAN Versus the Profilometer

		Profilometer					
		SI		MO (counts/.2mi.)		IRI (in./mi.)	
		20 mph	50 mph	20 mph	50 mph	20 mph	50 mph
ARAN - RMSVA (MG)	30mph	A=4.9065 B=-7.0212E-3 R^2=0.521 RMSE=0.763	A=4.9190 B=-7.3044E-3 R^2=0.514 RMSE=0.778	A=-4.8636 B=0.36917 R^2=0.461 RMSE=43.64	A=-6.5906 B=0.39226 R^2=0.436 RMSE=48.76	A=18.688 B=0.53548 R^2=0.504 RMSE=58.13	A=19.625 B=0.56516 R^2=0.455 RMSE=67.72
	40mph	A=5.1249 B=-5.5126E-3 R^2=0.577 RMSE=0.692	A=5.1435 B=-5.7276E-3 R^2=0.568 RMSE=0.733	A=-18.579 B=0.29593 R^2=0.533 RMSE=40.64	A=-21.563 B=0.31553 R^2=0.508 RMSE=45.58	A=-1.3517 B=0.42964 R^2=0.583 RMSE=53.30	A=-2.8514 B=0.45707 R^2=0.534 RMSE=62.57
	50mph	A=5.2972 B=-4.7422E-3 R^2=0.669 RMSE=0.612	A=5.3222 B=-4.9264E-3 R^2=0.657 RMSE=0.653	A=-30.730 B=0.26084 R^2=0.648 RMSE=35.27	A=-35.607 B=0.28046 R^2=0.628 RMSE=39.62	A=-17.375 B=0.37520 R^2=0.696 RMSE=45.50	A=-21.563 B=0.40275 R^2=0.650 RMSE=54.27
ARAN - MAS (Slope*1000)	30mph	A=5.4152 B=-0.94085 R^2=0.900 RMSE=0.337	A=5.4761 B=-0.99013 R^2=0.907 RMSE=0.339	A=-42.140 B=53.749 R^2=0.940 RMSE=14.52	A=-50.653 B=58.922 R^2=0.947 RMSE=14.95	A=-27.190 B=74.634 R^2=0.941 RMSE=20.23	A=-39.584 B=83.156 R^2=0.946 RMSE=21.23
	40mph	A=5.3098 B=-0.93483 R^2=0.891 RMSE=0.351	A=5.3698 B=-0.98577 R^2=0.902 RMSE=0.349	A=-35.778 B=53.261 R^2=0.926 RMSE=16.16	A=-44.199 B=58.607 R^2=0.940 RMSE=15.94	A=-18.783 B=74.136 R^2=0.931 RMSE=21.61	A=-30.764 B=82.833 R^2=0.942 RMSE=22.10
	50mph	A=5.2116 B=-0.91685 R^2=0.886 RMSE=0.360	A=5.2686 B=-0.96777 R^2=0.899 RMSE=0.355	A=-30.299 B=52.285 R^2=0.922 RMSE=16.58	A=-38.338 B=57.606 R^2=0.938 RMSE=16.16	A=-10.882 B=72.659 R^2=0.924 RMSE=22.69	A=-22.322 B=81.351 R^2=0.939 RMSE=22.70
ARAN - TEXTURE (MG)	30mph	A=4.5438 B=-1.5897E-2 R^2=0.451 RMSE=0.788	A=4.5362 B=-1.6478E-2 R^2=0.442 RMSE=0.833	A=13.589 B=0.84265 R^2=0.406 RMSE=45.83	A=12.638 B=0.89953 R^2=0.388 RMSE=50.82	A=44.024 B=1.2380 R^2=0.455 RMSE=60.93	A=46.320 B=1.3071 R^2=0.411 RMSE=70.38
	40mph	A=4.6382 B=-1.4275E-2 R^2=0.478 RMSE=0.769	A=4.6233 B=-1.4697E-2 R^2=0.462 RMSE=0.818	A=7.2714 B=0.76888 R^2=0.444 RMSE=44.33	A=6.2754 B=0.81724 R^2=0.421 RMSE=49.44	A=34.423 B=1.1326 R^2=0.500 RMSE=58.34	A=35.684 B=1.2005 R^2=0.455 RMSE=67.68
	50mph	A=4.6590 B=-1.0636E-2 R^2=0.448 RMSE=0.791	A=4.6434 B=-1.0942E-2 R^2=0.432 RMSE=0.841	A=6.2946 B=0.57190 R^2=0.415 RMSE=45.49	A=5.0451 B=0.60918 R^2=0.394 RMSE=50.55	A=32.773 B=0.84387 R^2=0.469 RMSE=60.16	A=34.498 B=0.89060 R^2=0.432 RMSE=69.66

Model: Index (Prof.) = A + B Index (ARAN)

To evaluate the effect of the operational speed on the reported roughness statistics, different testing speeds were used. Because the response of the ARAN unit with respect to speed could be nonlinear, more than two different testing speeds had to be considered. Thus three testing speeds—30, 40, and 50 mph—were selected for use in this evaluation effort.

Three different groups of test sections were chosen to provide a range of surface roughness. These test groups include pavements with smooth surfaces (PSI = 3.5 to 5.0), pavements with medium smooth surfaces (PSI = 2.0 to 3.5), and pavements with rough surfaces (PSI = 0 to 2.0). The relative smoothness of these sections was ranked on the basis of the profilometer's output. The test sections chosen covered a full range of pavement conditions in terms of PSI. In addition, for each combination of the above factors, three runs were made.

		Profilometer	
		20 mph	50 mph
ARAN	30 mph	Model 1	Model 2
	40 mph	Model 3	Model 4
	50 mph	Model 5	Model 6

FIGURE 2 PSI modeling factorial.

ROUGHNESS CORRELATION ANALYSIS

From the standpoint of instrumentation, three factors—repeatability, correlativity, and accuracy—indicate the performance of an instrument. The repeatability of an instrument can be evaluated by observing outputs on repeated runs on the same pavement surface, whereas the evaluation of an instrument's correlativity and accuracy must be quantified by using a standard instrument such as that described previously (*12*). The roughness measuring subsystem of the ARAN unit, classified as a response-type road roughness measuring system, provides the statistics—RMSVA, MAS, and TEXTURE—as described earlier. The accuracy of these statistics could not be evaluated directly because the researchers did not have access to a reference instrument that provides the same roughness statistics as the ARAN unit. Accordingly, the measurement accuracy of the roughness statistics is not considered in this evaluation of the ARAN roughness subsystem. Instead, a calibration model was developed through correlation analysis with the profilometer.

Choice of Reference

The profilometer must meet two basic requirements before it can be used as a reference instrument for correlation. The output statistics of the reference should be based on the results of an objective measurement and should not be vehicle dependent. If the reference instrument is vehicle independent, the models for correlation and calibration are stable in terms of time and the vehicle suspension system.

Two alternative approaches are available for developing the roughness statistics used in the correlation analysis and calibration of the roughness measuring subsystem of the ARAN unit. The first one is a dynamic modeling of a hypothetical device simulating the dynamic response of a vehicle with certain physical constants predefined. The dynamic model must have a sequence of pavement surface profiles used as the input. For example, a typical hypothetical device, called the reference quarter-car simulation (RQCS) (*7*), has been used as a standard reference for correlation and calibration. The corresponding statistical output of the RQCS, the quarter-car index (QI), was used for Maysmeter calibration in Brazil (*7*). Using RQCS makes it necessary to input the sequences of profile elevation measured by either a Class 1 or Class 2 instrument to the simulating model to develop a standard statistical output. This indirect procedure for obtaining reference standard statistical output is relatively complicated. The second approach uses the Class 2 profilometric method, directly developing roughness statistics from the relatively accurate measurement of the pavement surface elevations. This method, which measures the profile elevations and directly transfers elevations into roughness statistics, is comparatively simple, with the resulting roughness statistics relatively vehicle independent.

TABLE 2 Resulting Models of Equation 6 from Figure 2

	Coefficients				
Model	A	B	C	D	R^2 Value
1	5.4898	-0.001007	-0.873430	0.000206	0.904
2	5.5465	-0.001126	-0.930580	0.000801	0.915
3	5.4323	-0.001702	-0.855272	0.002919	0.896
4	5.4979	-0.002143	-0.917207	0.004613	0.907
5	5.3507	-0.000795	-0.795375	-0.000344	0.895
6	5.3837	-0.000722	-0.865102	-0.000118	0.904

TABLE 3 Values of Correlation Between New PSI Including TEXTURE (ARAN) and SI (Profilometer)

		Profilometer	
		20 mph	50 mph
ARAN	30 mph	0.904	0.915
	40 mph	0.896	0.907
	50 mph	0.895	0.904

The modified K. J. Law profilometer provided by Texas DOT for the purpose of making comparisons in this test has been chosen as the reference for the correlation analysis and calibration of the ARAN unit's roughness subsystem. The selection of this instrument was based on the following:

1. The modified K. J. Law profilometer is classified as a Class 2 pavement surface ride quality surveying instrument (*5*). This instrument automatically measures the pavement profile elevations at high operating speed with good accuracy and repeatability.
2. The profilometer is equipped with the software to compute the roughness statistics, RMSVA, SI, MO, and IRI. These statistics have been carefully evaluated (*5*) and are widely used in pavement surface ride quality surveys.
3. Because the profilometer belongs to Texas DOT, it was accessible for this evaluation effort.

Roughness Statistics of Modified K. J. Law Profilometer

The modified K. J. Law profilometer develops the roughness statistics SI, MO, and IRI. These statistics, which summarize the pavement roughness characteristics from different approaches, are relatively vehicle independent in principle because they are obtained through the processing of the raw profile elevations sequences. An explanation of each of these statistics follows:

Maysmeter Output

As explained previously (*5*) MO is the calibrated Maysmeter output value given in counts per 0.2 mi. This Maysmeter estimate is developed using the RMSVA values calculated for the 4- and 16-ft base wavelengths from profilometer, using the following equation.

$$MO = A_1 + A_2\ RMSVA_4 + A_3\ RMSVA_{16} \quad (1)$$

where $RMSVA_4$ and $RMSVA_{16}$ are the RMSVA values of the profilometer for the 4- and 16-ft base wavelengths, respectively. The constants A_1, A_2, and A_3 are different for various types of pavement (rigid or flexible).

Serviceability Index

The measure of riding quality with which engineers are most familiar is the SI. Representing the user's perception of pavement roughness, SI is given as a number between 0 and 5. Such unitless index can be developed on the basis of MO or RMSVA. The model for calculating SI in the profilometer (*6*) is

$$SI = 5\ e^{-\left(\frac{\ln (32\ MO)}{8.4933}\right)^{9.3566}} \quad (2)$$

where MO is calculated by Equation 1. The index SI is a measure of roughness primarily in the 8- to 35-ft wavelength range.

International Roughness Index

IRI (*7*) is a well-known measure of roughness. IRI is reported in inches per mile, as measured with a Class 1 or Class 2 instrument or as computed with a quarter-car simulation. IRI values from the profilometer are calculated from the profiles for both the left wheelpath and the right wheelpath. The reported IRI is the mean value of the left wheelpath IRI and the right wheelpath IRI.

Field Tests

To obtain the correlation and calibration models for the roughness measuring subsystem of the ARAN unit, 29 test sections were selected. These sections consisted of both rigid and flexible pavements and were evaluated with both the modified K. J. Law profilometer and the ARAN unit. The models developed for this research are based on the combined data collected from both the flexible and the rigid pavement test sections. The test sites were selected because they could provide the broadest range of roughness levels and could be safely run at the 50-mph test speed. The smooth sites were needed to ensure that the subsystem had the resolution necessary to correctly measure smooth pavements, whereas the rough sites ensured that the subsystem could handle the large amplitudes generated when traveling down rough pavement. The medium sections allowed data points to be located between the two extremes. This wide roughness distribution makes the correlation analysis results suitable across the wide roughness levels that are normally found in the Texas highway network.

TABLE 4 Values of Correlation Between Original SI (ARAN) and SI (Profilometer)

		Profilometer	
		20 mph	50 mph
ARAN	30 mph	0.903	0.908
	40 mph	0.890	0.897
	50 mph	0.894	0.901

TABLE 5 Correlations Between New PSI Using TEXTURE and SI from Profilometer

	Coefficients		
Model	a	b	R^2 Value
1	-3.1604e-4	1.0001	0.904
2	-3.8273e-2	1.0115	0.915
3	-1.5422e-5	1.0000	0.896
4	-1.5556e-5	1.0000	0.907
5	-1.9383e-4	1.0000	0.895
6	3.6650e-4	0.99994	0.904

Three repeat runs were made for each test section, testing speed, and both K. J. Law profilometer and the ARAN unit. The mean values of the reported roughness statistics were calculated and used as the summarized statistic. This was done to cancel the operational bias. The ARAN unit is designed for operation in the normal traffic speed range. The field tests were conducted at speeds of 30, 40, and 50 mph for each test section. The most frequently used operational speeds of the K. J. Law profilometer are 20 and 50 mph. Therefore, each test section was run at the testing speed of 20 and 50 mph for the K. J. Law profilometer.

Results

The linear correlation model proposed for the research evaluation effort is

$$\text{Roughness (profilometer)} = A + B\ \text{roughness (ARAN)} \quad (3)$$

where A and B are constants, and Roughness (profilometer) is the estimation of the roughness statistic corresponding to one of the profilometer outputs: SI, MO, or IRI. Roughness (ARAN) is the roughness statistic (RMSVA, MAS, TEXTURE) measured and generated by the ARAN unit. Two statistical indexes showing the correlativity of the two instruments are used. One is the R^2 value and the other is the root mean square error (RMSE) defined by

$$RMSE = \sqrt{\frac{1}{N}\sum_{i=1}^{N}(x_i - y_i)} \quad (4)$$

where

N = number of test sections (N = 29);
x_i = estimation of the roughness statistic of the profilometer at ith test section; and

y_i is the roughness statistic measured by the ARAN unit and generated by Equation 3 at ith test section. The comprehensive correlation analysis results with different operational speeds are shown in Table 1. From this table, it can be said that MAS has relatively good correlation with the roughness statistics of the K. J. Law profilometer. Research results also show that the roughness statistics of the ARAN unit are speed dependent; that is, the reporting statistics on the same road surface will be different if the operational speed differs. Models used to cancel speed effect were developed in the same research project but not reported in this paper. Detailed analysis and models regarding speed effect were reported previously (*9,13*).

PRESENT SERVICEABILITY INDEX MODEL FOR ARAN

HPI, the manufacturer of the ARAN unit, provided an SI model to the Texas DOT. This SI model has the following form:

$$SI = 5.6797 - 0.00134\ RMSVA - 0.7553\ MAS \quad (5)$$

Because the modified K. J. Law profilometer is considered by the Texas DOT to be the reference instrument for calibration of all of its roughness monitoring equipment, it is necessary that the SI model obtained from the ARAN unit be directly calibrated to the SI from the profilometer. In addition it can be expected that the operational speeds of the ARAN unit significantly affect its roughness statistics. The model estimating SI values should be used for a given operational speed. Because of these disadvantages a new PSI model, including TEXTURE, was proposed by research staff. This new model is

$$PSI = A + B\ RMSVA + C\ MAS + D\ TEXTURE \quad (6)$$

where A, B, C, and D are constant coefficients. These constant coefficients were obtained through a linear regression analysis of the ARAN unit's roughness output and that of the modified K. J. Law profilometer. Therefore, the PSI value resulting from this model is an estimate of the PSI values corresponding to the profilometer. According to the definitions of RMSVA, MAS, and TEXTURE, these variables are independent of each other. Conceptually, the more independent variables the model includes, the better the model will be.

As another alternative, a model that excludes the TEXTURE statistic was also generated. The model has the following form:

$$PSI = A + B\ RMSVA + C\ MAS \quad (7)$$

This new PSI model has the same form as the original SI model. The new model has the advantage of being obtained through the regression analysis of the ARAN unit and the modified K. J. Law profilometer. The data were collected in Texas.

TABLE 6 Models from Equation 7 and Figure 2

	Coefficients			
Model	A	B	C	R^2Value
1	5.4879	-0.000924	-0.873794	0.904
2	5.5391	-0.000801	-0.931996	0.916
3	5.3875	-0.000647	-0.867200	0.894
4	5.4269	-0.000475	-0.936057	0.904
5	5.3546	-0.000951	-0.787525	0.895
6	5.3850	-0.000775	-0.862404	0.904

New PSI Model Including TEXTURE

The factorial used in the modeling of the new PSI is shown in Figure 2. A FORTRAN program (MULT REGRESSION) developed by research staff was used to process the data collected from field tests. The resulting models correspond to the regression models seen in Figure 2.

Table 2 shows the linear correlation results representing the models shown in Figure 2. The R^2 values of the linear fits are also included in the table.

The sensitivities of PSI to each roughness statistic can be compared in terms of the absolute value level of each coefficient. In the resulting models, the absolute value level of Coefficient C is much higher than that of either B or D. Coefficients B and D are at the same relative level. Because Coefficient C was defined for MAS it can be said that PSI is more sensitive to MAS than to either RMSVA or TEXTURE. In fact, from the correlation analysis results, the R^2 values for MAS are much higher than those for either RMSVA or TEXTURE. This means that the correlation of MAS with the profilometer SI is better than that of RMSVA or TEXTURE.

Greater RMSVA or MAS values for the ARAN unit represent poorer serviceability or smaller PSI values. Mathematically, this relationship requires that the signs of Coefficients B and C be negative. Because TEXTURE reflects only the detail (short wavelength) characteristics of a pavement surface, it does not have an obvious direct relationship with PSI. Therefore, the sign of the coefficient of TEXTURE could be either positive or negative. From the resulting models shown in Table 2 it can be seen that the signs for Coefficients B and C are negative. Coefficient D is both positive and negative.

A comparison can be made between the new PSI model including TEXTURE and the original SI equation by considering the R^2 values resulting from the correlation analysis. The R^2 values resulting from the new PSI model are listed in Table 3 and correspond to the factorial shown in Figure 2. The R^2 values of the correlation between original SI for the ARAN unit and SI from the profilometer are shown in Table 4. All of the R^2 values from the new PSI model are greater than those from the original SI equation. It can be concluded that the new PSI equation fits the profilometer output better than the original SI equation.

The correlations of the new PSI equation using TEXTURE from the ARAN unit and SI from the profilometer at different speeds are presented in Table 5. The equation for those correlations is

$$SI\ (profilometer) = a + b\ PSI(ARAN) \quad (8)$$

From these figures and the resulting linear equations, it can be seen that

$a \approx 0, b \approx 1$

Therefore, the six new PSI models, including TEXTURE, that correspond to the various speeds of operations can be used effectively to estimate the SI values from the profilometer.

New PSI Model Excluding TEXTURE

The second set of PSI equations does not include TEXTURE. These equations have the same form as the PSI model shown in Equation 7. The factorial equations that omit TEXTURE are the same as those that include TEXTURE (Figure 2).

Table 6 represents the coefficients from the new PSI equations excluding TEXTURE, which have the form of Equation 7. The program MULT REGRESSION was again used with the data from the test sections.

As shown in Table 6 and discussed in the previous section, the second new PSI equation excluding TEXTURE has the same sign and sensitivity qualities as does the equation including TEXTURE. It can also be seen that the new PSI equations excluding TEXTURE are not significantly different from the ones that include TEXTURE. In this case, it is reasonable to use the equations without TEXTURE because they are similar and just as valid.

CONCLUSIONS

The correlation analysis compared the Texas DOT ARAN unit and the modified K. J. Law profilometer with the results showing good correlation between the outputs of these two instruments. However, because the correlation models developed are speed dependent, the correlation models must be used for a given operational speed if no speed-effect-canceling model is implemented. It is recommended that MAS be used to estimate the roughness outputs corresponding to the profilometer. Unfortunately, RMSVA and TEXTURE do not correlate well with any of the profilometer's outputs.

Two PSI models, developed as a result of this research effort, are reported in this paper: (a) the model including the roughness output TEXTURE, and (b) the model excluding TEXTURE. The test results demonstrated that the new PSI models developed are better than the original SI model. The new PSI model excluding TEXTURE has been implemented with the personal computer program presented previously (*9*).

The operational speed of the ARAN unit has a significant impact on its roughness outputs. The impact of the operational speed on the roughness outputs also depends on the roughness level of the pavement surface being evaluated. With respect to the operational speed, it was found that RMSVA and TEXTURE are more sensitive than MAS (*9,13*).

REFERENCES

1. Buchanan, J. A., and A. L. Catudal. Standardizable Equipment for Evaluating Road Surface Roughness. In *Highway Research Record 2* HRB, National Research Council, Washington, D. C., 1940, pp. 621–638.
2. *Highway Performance Monitoring Field Manual*, FHWA Publication 5600.1A, Appendix J, U.S. Department of Transportation, Washington, D.C., Dec. 1987.
3. Sayers, M. W., T. D. Gillespie, and W. D. O. Paterson. *Guidelines for Conducting and Calibrating Road Roughness Measurements.* World Bank Technical Paper 46. The World Bank, Washington, D.C., 1986.
4. Carey, W. N., and P. E. Irick. The Pavement Serviceability Performance Concept. *Bulletin 250*, HRB, National Research Council, Washington, D.C., 1960.
5. Claros, G. J., W. R. Hudson, and C. F. Lee. *Performance of the Analog and Digital Profilometer with Wheels and with Non-Contact Transducers.* Research Report 251-3F. Center for Transportation Research, The University of Texas at Austin, April 1985.
6. Mckenzie, D. W., W. R. Hudson, and Clyde E. Lee. *The Use of Road Profile Statistics for Maysmeter Calibration.* Research Report 251-1. Center for Transportation Research, The University of Texas at Austin, August 1982.
7. Sayers, M. W., T. D. Gillespie, and C. A. V. Queiroz. *The International Road Roughness Experiment, Establishing Correlation and a Calibration Standard for Measurement.* World Bank Technical Paper 45. The World Bank, Washington, D.C., 1986.
8. *ARAN III Manuals.* Version 1.3. Highway Products International, Inc., 1983.
9. Lu, J., C. B. Bertrand, and W. R. Hudson. *Evaluation and Implementation of the Roughness Measuring Subsystem of the ARAN Unit.* Research Report FHWA/TX-92 + 1223-1. Center for Transportation Research, University of Texas at Austin, Feb. 1991.
10. Lu, J., C. B. Bertrand, and W. R. Hudson. *Evaluation and Implementation of the Automatic Road Analyzer (ARAN).* Research Report FHWA/TX-92+1223-2F. Center for Transportation Research, University of Texas at Austin, July 1991.
11. Bertrand, C. B., R. Harrison, and B. F. McCullough. *Evaluation of the Performance of the Auto-Read Version of the Face Dipstick.* Research Report 969-2F, Center For Transportation Research, The University of Texas at Austin, 1989.
12. Gillespie, T. D., M. W. Sayers, and L. Segel. *NCHRP Report 228: Calibration of Response-Type Road Roughness Measuring Systems.* TRB, National Research Council, Washington, D.C., Dec. 1982.
13. Lu, J., C. B. Bertrand, and W. R. Hudson. Speed Effect Analysis and Cancelling Model of Response Type Road Roughness Measuring System. In *Transportation Research Record 1260*, TRB, National Research Council, Washington, D.C., 1990, pp. 125–134.

Publication of this paper sponsored by Committee on Pavement Monitoring, Evaluation, and Data Storage.

Image-Processing Methods for Automated Distress Evaluation

VINOD K. KALIKIRI, NORMAN W. GARRICK, AND LUKE E. K. ACHENIE

The collection and analysis of pavement distress data are the primary components of any pavement management system. There is an emerging trend over the last decade to automate this process of data collection and analysis. Current research work at the University of Connecticut aims at developing such an image data analysis system, compatible with the photolog system used by the Connecticut Department of Transportation for pavement distress surveys. The image data retrieved from the Connecticut photolog system cannot be used directly as input to the analysis system because of undesirable details such as shadows and random noise in the images. Therefore extensive image processing must be carried out before the image data are suitable for use as input for analysis. An image-processing strategy that can be used with the images obtained from the Connecticut photolog system is presented. Topics discussed include image data digitization, format conversion, feature extraction techniques, and binary image manipulation. The binary images resulting from the process were found to be a very good representation of the actual distress conditions of the pavement and can readily serve as input to a pattern recognition system for analysis.

An efficient pavement management system relies on the availability of comprehensive and accurate distress data for the road network (*1*). The conventional method for collecting these data is a manual survey whereby the rater goes out in the field to inspect the condition of the roadway. Many users believe that there is a need to replace this manual data collection system with an automated system that takes advantage of recent advances in computer technology. An automated system will eliminate problems such as safety hazards to field personnel, subjectivity of observations, and time constraints associated with the manual methods (*2*; K. R. Maser, unpublished data).

Vehicles capable of photographing the pavement surface and storing the photographed images in a convenient form already have been developed, and a number of such systems have been tested and evaluated over the years (*3*; K. R. Maser, unpublished data). Many of these are used successfully by various highway agencies.

Automation of the process of data analysis is the next step toward the development of a totally automated system (*4,5*). The emergence of computers with high-speed processing capabilities has laid the foundation for the application of image-processing and pattern-recognition techniques to achieve this objective.

The current research work at the University of Connecticut (UCONN) aims at tackling this problem by developing an automated pavement distress analysis system that is compatible with the photolog system already in use by the Connecticut Department of Transportation (ConnDOT). Principles of digital image processing, pattern recognition, and quantification through artificial neural networks are being adopted to realize this objective. The image data being used for processing and analysis in the research work are taken from the photolog laser videodisc (PLV) collection at ConnDOT.

The quality of the image data obtained by the Connecticut photolog system is not ideal for processing because of factors such as variable illumination and shadows in the images. An image-processing strategy capable of compensating for these factors must be developed before the image can be used as input to the automated system for analysis. In this paper one such strategy that was developed at UCONN to process the color images retrieved from the Connecticut PLV system will be described. The strategy is designed to generate the type of quality data that can serve as input for a distress data analysis system.

Department of Civil Engineering, University of Connecticut, Storrs, Conn. 06269-3037.

CONNECTICUT PHOTOLOG SYSTEM

ConnDOT uses a 35-mm movie camera to photograph the pavement surface. It is mounted in a photologging van that travels at average speeds of 40 to 50 mph. The camera is angled down the road for a full perspective view through the windshield. The film is exposed at regular intervals of 0.01 mi to record pavement distresses, shoulder conditions, and roadside inventory data. Information about route, mileage, and other details required to identify the roads being surveyed are also recorded through a keyboard.

The exposed film is processed and transferred onto double-sided laser video discs. Each side of the video disc stores all the information pertaining to 265 mi of the roadway. This information includes a windshield view (Figure 1) and a close-up view (Figure 2). The close-up view is the view that is used in the manual rating system.

At present the rating of the road images is carried out manually in the laboratory by personnel who record their observations directly into a personal computer. ConnDOT surveys show that the raters complete between 115 and 150 frames each hour (*2*). In an average year, the 7,700 mi (3,850 mi in each direction) of highway network in Connecticut requires approximately 2.5 months (1,000 person-hr) to be rated. In view of the time required to rate the sections manually, ConnDOT has determined that not all the frames recorded by the photolog system for rating can be used. Therefore a sampling procedure has been adopted in which only 10 percent of the frames are rated (*6*).

The overall cost involved with this setup is approximately $4.40/lane-mi surveyed (*2*). An automated system would significantly reduce the cost and time needed to survey the roads and at the same time result in an objective evaluation of the pavement condition. It would also enable ConnDOT to use all the frames for rating rather than just the small fraction that is used now.

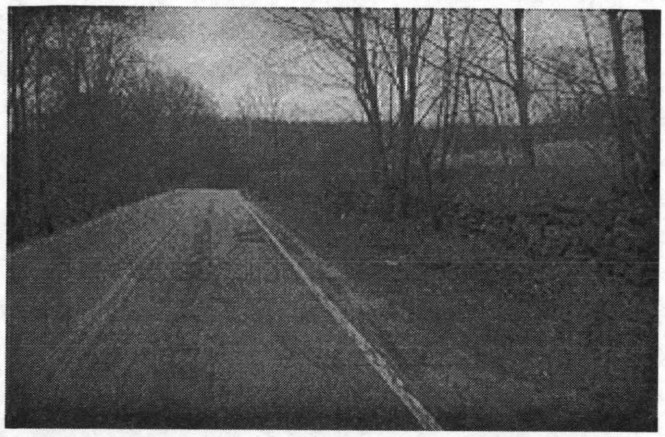

FIGURE 1 Windshield view captured by the photolog vehicle.

The image data available as input for the automated system needs to be processed before they can be used for analysis. The extent of processing depends on the configuration of the data acquisition system being used. Images from the ConnDOT PLV system are particularly difficult to process efficiently because of the following characteristic features of the system:

1. The windshield view, which facilitates the collection of roadside inventory data along with the pavement surface data, invariably imparts a perspective effect in the image. This effect reduces the accuracy of the information recorded in the upper portions of the image.
2. Nonuniform illumination and highly variable image brightness and contrast values are encountered because of the natural lighting conditions during the survey. These defects result in noisy images that must be corrected by adopting suitable image-processing techniques.
3. Redundant features recorded in the image (such as turfed shoulders, trees, and roadside inventory) must be eliminated to isolate distressed portions of the roadway.
4. Shadows cast on the pavement by overhead power lines and trees mimic the presence of distresses, thereby complicating the task of implementing a totally automated machine vision system.

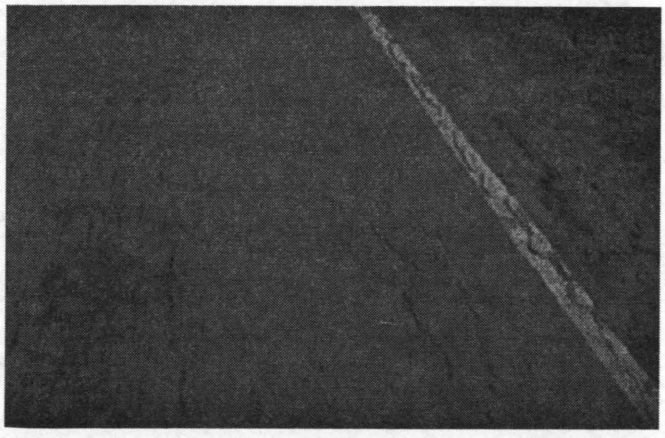

FIGURE 2 Close-up view of a portion of the windshield view.

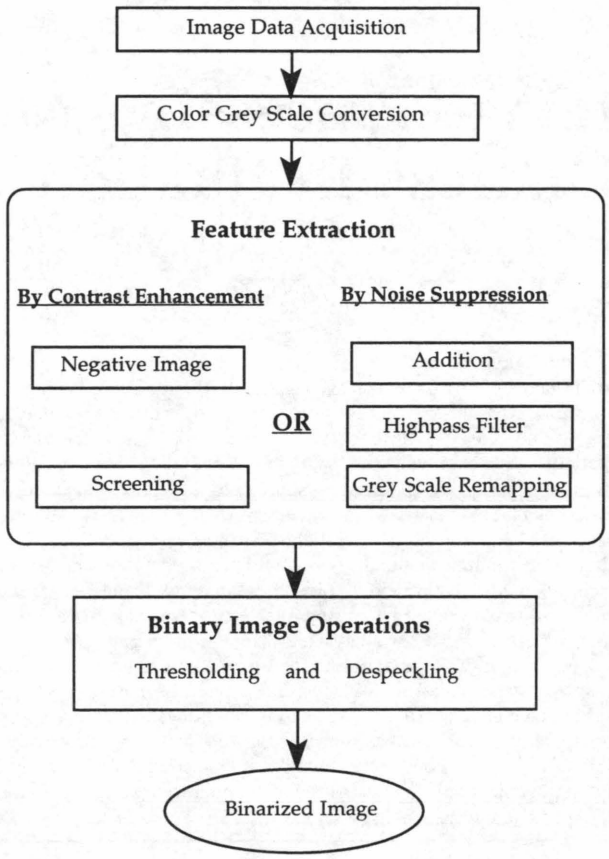

FIGURE 3 Processing strategy for analyzing ConnDOT photolog images.

In contrast, data acquisition systems such as the PASCO Roadrecon-70 provide a more suitable environment for the application of an automated system (*3*). The quality of image data recorded by the PASCO system is quite high because the system works under artificial illumination at night. Such illumination eliminates problems such as shadows and nonuniform contrasts and brightness values (*7*). In addition, the camera is oriented in such a way that a standard scale image (1:200 in the case of Roadrecon-70) is recorded with no optical aberrations. Processing requirements for such image data are minimal compared with the degree of processing required for the data collected using the Connecticut photolog system.

IMAGE-PROCESSING TECHNIQUES

The processing of the images from the ConnDOT laser video discs was carried out in the various stages that are outlined in the flowchart in Figure 3. The strategy tackles problem areas such as image enhancement, noise reduction, and shadow elimination. The stages outlined in the flowchart are the processes for color image acquisition, format conversion to gray scale, feature extraction by highlighting areas of interest, and binary operations to segment the gray scale images. These processes are discussed in more detail.

Image Acquisition and Digitization

Close-up views of the pavement sections were used for this project because the distresses are well defined in these views, and most background details such as vehicles and adjoining lanes are eliminated. The first processing step was the capturing and digitizing of a selected portion of the lane (approximately 8 ft^2). A video digitizing software supported by a 24-bit graphics adapter was used for this purpose.

Conversion from Color to Gray Scale

The color image that is captured by the digitizer is in a format of 24 bits/pixel that is essentially a combination of three 8-bit integer arrays. These arrays contain the brightness values for each of the three primary colors used to represent the image. The color image is then converted into a gray scale format of 8 bits/pixel for ease of processing and manipulation. Although this process results in the loss of all the color information in the image, it helps in reducing the file space required for storage by two-thirds. This conversion is achieved in image processing softwares by the application of color filters, which absorb complementary colors and result in a monochrome (gray scale) image in which the brightness level of each pixel is assigned an integer value between 0 (black) and 255 (white). Efforts to use color images directly instead of the gray scale images will be made in the future so that the concept of depth perception can be incorporated into the system.

Feature Extraction

The next stage after conversion to the gray scale involves the processing of these gray scale images to isolate the distress features. Two alternative processes, feature extraction by contrast enhancement and feature extraction by noise suppression, have been identified to accomplish this objective. Both the alternatives were found to work equally well on the images tested. The objective for both series is to eliminate undesirable elements such as shadows, random noises, and variable image contrasts. This is realized in each of the series by adopting different sequences of image-processing strategies.

Feature Extraction Through Contrast Enhancement

The objective of eliminating undesirable elements in the gray scale image is accomplished in this alternative by increasing the contrast between pavement distress and the background (*8*). In addition, the overall brightness range of the image is reduced. These effects are achieved by screening the gray scale image through a copy of its negative on the basis of the following operation.

A negative is first created by calculating the inverse value of each pixel in the original gray scale image on a scale of 256 values (0 to 255) (*9*). Thus, a pixel with a brightness value of 10 in the actual gray scale image will be assigned a value of 255 − 10 (or 245) in its inverted form. The negative and the positive are stored in two different channels on the system. The gray scale image is then subjected to a process known as negative screening that results in an image in which undesirable features are suppressed and

FIGURE 4 Gray scale image (contrast enhancement).

distressed features are sharpened in contrast to the background. The brightness value of each pixel in the resulting image generated by screening is calculated using the following operation:

$$X = K - [(K - A)(K - B)]/K$$

where

X = brightness value in the destination channel,
K = maximum allowable gray level (255),
A = gray value in Source A (positive image), and
B = gray value in Source B (negative image).

In essence the process highlights lines, edges, and discontinuities in the image by screening out all unrelated features. Uniformly varying regions such as shadows, which have lower pixel intensity in comparison with sharp transition regions such as cracks, are suppressed in this process. Figure 4 shows the distressed portion of a pavement section with shadows of trees across

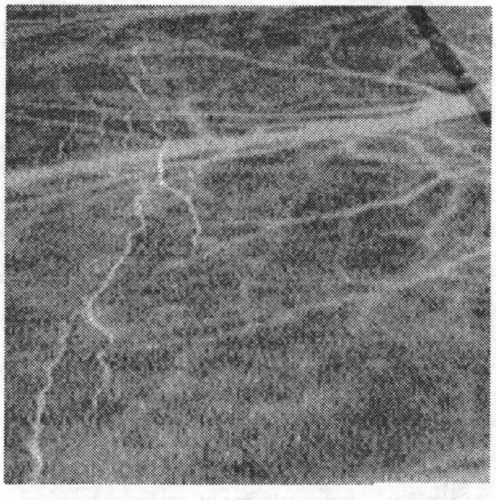

FIGURE 5 Negative screening.

the roadway. Figure 5 shows the localized contrast enhancement effect produced by the negative screening operation on the gray scale image. The overall brightness range of the image is also reduced significantly.

Feature Extraction Through Noise Suppression

In another alternative the objective of highlighting distressed features is achieved by the application of a succession of noise reduction techniques to the gray scale image. In the first step an averaging operation is performed on two or more copies of the gray scale image. This results in the smoothing out of excessive noise in the image. The underlying concept is that because random noise is typically characterized by low photon intensity registered on the film at the time of recording, an averaging operation performed on two or more copies of the image would result in the suppression of the brightness values corresponding to the noise. The improvement in quality is usually proportional to the square root of the number of frames added. The most commonly used noise suppression technique under averaging operations is the addition of two copies of the image numerically.

Figure 6 shows the gray scale image of a distressed pavement section. The addition of two copies of this frame resulted in the suppression of the noise to some extent and also increased the contrast of the image as shown in Figure 7.

Further reduction in random noise is achieved by removing low-frequency details in the image (*8*). This is done by the application of a high-pass filter, the most common of which is the Laplacian filter, which is a two-dimensional second-derivative operation represented by

$$\nabla^2 I = \frac{\delta^2 I}{\delta X^2} + \frac{\delta^2 I}{\delta Y^2}$$

where

FIGURE 6 Gray scale image (noise suppression).

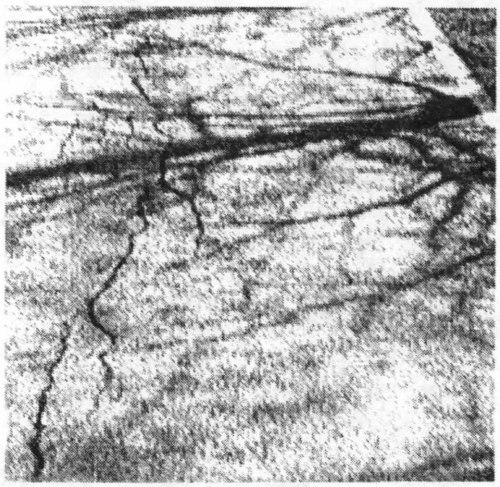

FIGURE 7 Averaging operator (addition).

$\nabla^2 I$ = Laplacian operator and

$\frac{\delta^2 I}{\delta X^2}, \frac{\delta^2 I}{\delta Y^2}$ = second derivatives of the image along X and Y directions.

The outcome, after the application of the high-pass filter, is an image in which features showing sharp transition are highlighted in contrast to the background. Figure 8 shows the effect of noise suppression achieved by the application of this filter to Figure 7.

The final stage in this series involves the reduction of the number of gray levels in the image so that edges between regions become abrupt (*8,10*). The process is usually referred to as *gray-level remapping*. A value of 3 to 5 gray levels was found to result in a clear demarcation between shadows and distress features in the ConnDOT images. Hence the number of gray levels in the image is reduced from over 100 to approximately 5. The brightness value of each of the pixels in the remapped image is calculated on the basis of a function defined for the number of gray values selected for remapping. A generalized function for such

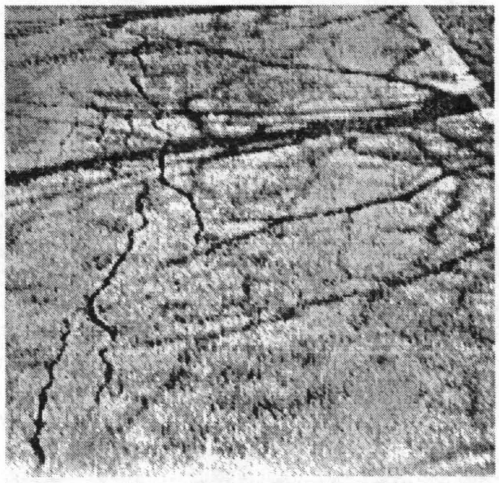

FIGURE 8 High-pass filter.

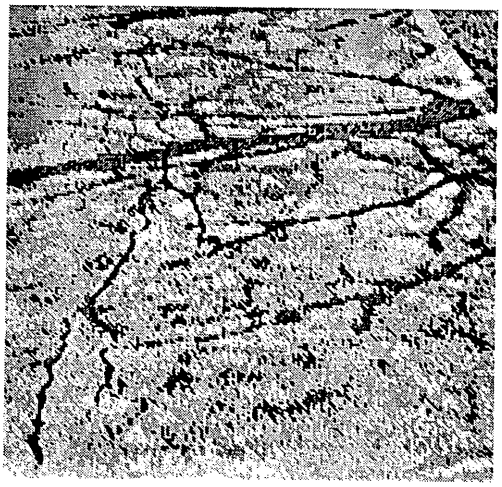

FIGURE 9 Gray scale remapping.

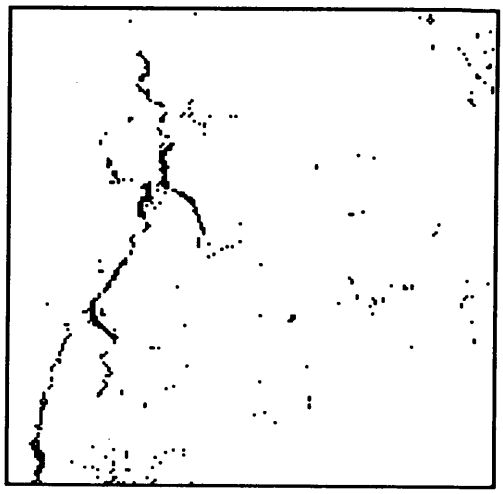

FIGURE 11 Thresholded gray scale image (contrast enhancement).

linear remapping from the source to the destination image is given as

$$R_i = (I_i - I_{\min})\left[\frac{R_{\max} - R_{\min}}{I_{\max} - I_{\min}}\right] + R_{\min}$$

where

I_i = ith pixel in input image I,
R_i = ith pixel in resultant output image R,
$I_{\min}$ = lowest value in input range,
$I_{\max}$ = highest value in input range,
$R_{\min}$ = lowest value in output range, and
$R_{\max}$ = highest value in output range.

Figure 9 shows the effect produced by the remapping of Figure 8 to three gray levels. Both methods of feature extraction, by contrast enhancement and by noise suppression, were found to work equally well on images with and without shadows. Histograms of gray scale values for the outputs from both of these series had characteristic geometry that facilitated a simplified thresholding process. This final stage of thresholding and noise elimination is explained in the following section.

Binary Operations

The final stage of processing involves a set of two operations; thresholding and despeckling. The objective of this stage is to isolate the distressed features by generating an image that has only two levels (black and white)—one level corresponding to the distress feature and the other to the background. A threshold value at which areas of interest can be isolated is first selected on the basis of the histogram of gray scale values (*8*). Brightness values of each of the pixels in the source image are then compared with the threshold. The pixel value in the destination image is assigned to 0 if the brightness value is less than the threshold and to 255 if the brightness value is greater than the threshold value. This operation can be represented mathematically as

$$R_i = H, \quad I_i \geq T \qquad R_i = L, \quad I_i < T$$

where

R_i = brightness value of ith pixel in output image,
I_i = brightness value of ith pixel in input image,
T = threshold value for segmentation,
L = below threshold value (in this case, 0), and
H = above threshold value (in this case, 255).

Selection of the actual threshold value plays an important role in the entire process because it is this value that ultimately defines the mapping of the distressed features in the destination image. To select this value, a histogram is plotted to show the pixel count for each of the gray level values in the image. The first feature

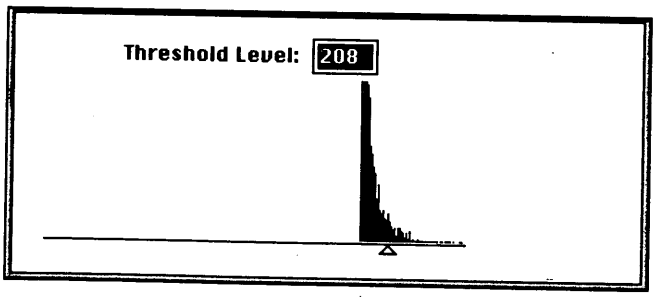

FIGURE 10 Histogram for screened image (contrast enhancement).

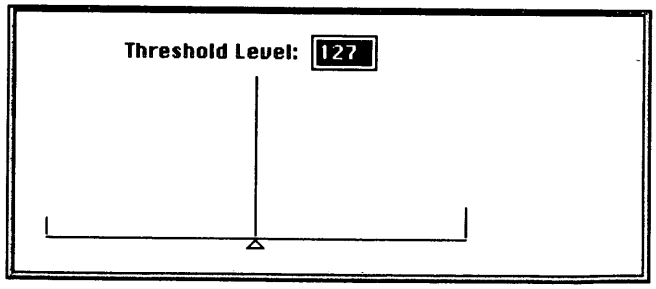

FIGURE 12 Histogram of remapped image (noise suppression).

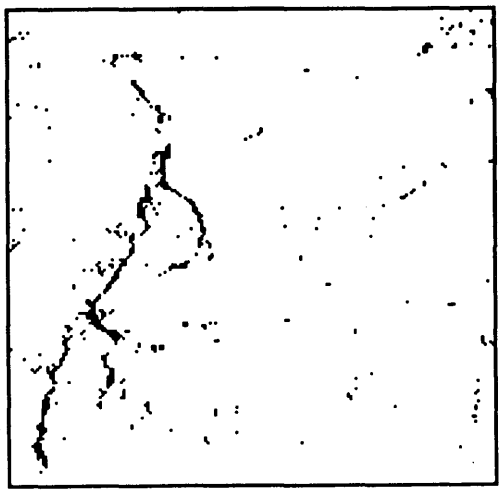

FIGURE 13 Thresholded gray scale image (noise suppression).

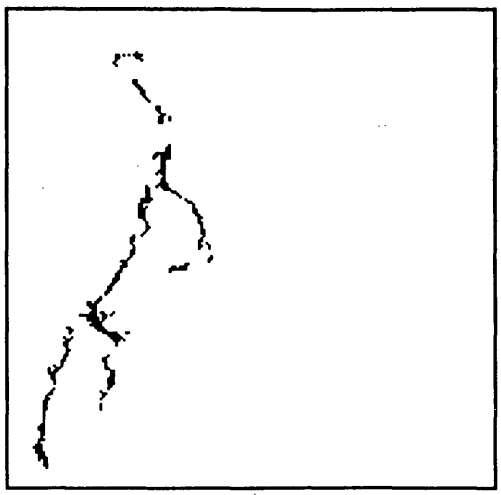

FIGURE 15 Despeckled gray scale image (noise suppression).

extraction method, contrast enhancement, results in a histogram that shows an abrupt peak, falling at a very steep slope and ending in a characteristic heel formation (see Figure 10). By trial and error, it was found that the gray scale value corresponding to the center of this heel is the optimum threshold value for feature extraction. Figure 11 shows the binary image obtained by thresholding Figure 5 at Level 208, corresponding to the center of the heel in the histogram shown in Figure 10. It can be seen that the geometry of the crack pattern is still retained while shadows and noise have been almost eliminated in the image.

Histogram for the noise suppression method of feature extraction (Figure 12) consists of a series of vertical lines (the number of lines is equal to the number of gray levels that were chosen for remapping). Each represents the count of pixels having that particular gray value. Many relevant features were eliminated when the image was thresholded at lower-level gray values. Thresholding at higher values left too much noise in the image. The gray value corresponding to the second vertical was found to be the optimum value for thresholding. Figure 13 shows the binarized image obtained by thresholding Figure 9 at a gray-level value of 127 that corresponded to the second vertical in the histogram shown in Figure 12. Most of the shadows and noise shown in the gray scale image (Figure 6) were eliminated in this process.

Finally the remaining noise in the binarized image is removed using a despeckling filter. On the basis of the size of the cluster (*7*), this filter eliminates isolated and small clusters of noise present in the image. Usually clusters of size 5 pixels or less can be safely eliminated as random noise. Figures 14 and 15 are the final binary images obtained after the application of the despeckling filter to images in Figures 11 and 13, respectively.

FIGURE 14 Despeckled gray scale image (contrast enhancement).

USE OF PROCESSED IMAGES

The binary images obtained at the end of the strategy described in this paper are suitable for use as input to an automated system for analysis. A neural network-based pattern recognition system for analyzing the processed binary images is being developed. The output from the system is a comprehensive report of the type, extent, and severity of the various distresses recognized on the laser disc. The process of fine tuning the parameters of the network to increase the efficiency of prediction is under way.

SUMMARY AND CONCLUSIONS

The Connecticut photolog system has the capacity to record pavement distress conditions. There is a need for a system that is capable of processing these recorded data and automatically reporting the type, severity, and extent of the various distress conditions. Work in progress at UCONN aims at realizing this objective by incorporating the principles of digital image processing and pattern recognition into an automated system that is compatible with the Connecticut data acquisition system. The images from the ConnDOT photolog system pose certain problems, such as variable illumination and shadows in the images, which add to

the challenge of developing an effective image-processing system. In this paper we discussed image-processing methods that address problem areas such as shadow removal and noise elimination.

The image-processing techniques adopted include image digitization, gray scale format conversion, feature extraction, and binary image operations such as thresholding and despeckling. The problems of shadows and random noise were successfully tackled by employing these processes. The strategy was tested on a variety of distress types and was found to yield images that were of sufficient quality to provide as input to an automated system for analysis.

A neural network-based pattern recognition system that will accept the processed images as input is being developed. The output from this system will be a report detailing the type, extent, and severity of the various distress types recognized. To date, the overall system has been found to be about 90 percent accurate. It is still necessary to integrate the various components of both image-processing and analysis systems before a goal of a fully automated pavement distress analysis tool can be achieved.

REFERENCES

1. Hudson, W. R., G. E. Elkins, W. Uddin, and K. T. Reilley. *Improved Methods and Equipment to Conduct Pavement Distress Surveys*. Final Report FHWA-TS-87-213, FHWA, U.S. Department of Transportation, April 1987.
2. Fundakowski, R. A., R. K. Graber, R. C. Fitch, E. L. Skok, and E. O. Lukanen. *NCHRP Research Results Digest 181: Video Image Processing for Evaluating Pavement Surface Distress*. TRB, National Research Council, Washington, D.C., 1991.
3. *Proc., Automated Pavement Distress Data Collection Equipment Seminar*, Iowa State University, Ames, Iowa, June 1990.
4. Wigan, M. R., Image Processing Techniques Applied to Road Problems. *Journal of Transportation Engineering*, Vol. 118, Jan./Feb. 1992.
5. Kaseko, M. S. and S. G. Ritchie. A Neural Network Based Methodology for Automated Distress Classification of Pavement Images. Presented at International Conference on Artificial Intelligence Applications in Transportation Engineering, San Buenaventura, Calif., June 1992.
6. Larsen, D. A., R. C. Hanley, and C. D. Larson. Connecticut Photolog Laser Videodisc-Based Pavement Rating System (PRS)—Overview. Research Project HRP-887. Report 887-20-90-11, Dec. 1990.
7. Jeyapalan, K., J. K. Cable, and R. Welper. Demonstration Project 72, Iowa DOT: *Evaluation of the PASCO Road Survey System*. Automated Pavement Data Collection Equipment. FHWA-DP-72-2, U.S. Department of Transportation, April 1987.
8. Lewis, R., *Practical Digital Image Processing*, Ellis Horwood Series, 1990.
9. Jain, A. K., *Fundamentals of Digital Image Processing*. Prentice Hall, 1989.
10. *Photoshop Users Reference Manual*, Adobe Systems, Inc.

Publication of this paper sponsored by Committee on Pavement Monitoring, Evaluation, and Data Storage.

Feasibility of Automating Pavement Distress Assessment Using Mathematical Morphology

DIMITRI A. GRIVAS, CHAKRAVARTHY BHAGVATI, MICHAEL M. SKOLNICK, AND B. CAMERON SCHULTZ

Surface distress assessment is an essential pavement management task. Developing and refining morphology-based image analysis techniques and evaluating the feasibility of their application to the automation of pavement distress surveys are discussed. Cracking and other distresses on asphalt and concrete pavement surfaces are analyzed. Significant advantages of the morphology-based approach include substantial reductions in data requirements and computational costs. Sample photographic images of pavements are analyzed, and the ability of the developed image-processing technique to identify distress types, severities, and extents is demonstrated. It is concluded that the developed morphology-based approach is capable of detecting noncracking distresses and assessing cracking on various types of pavement without manual intervention. It promises to become suitable for automating pavement distress surveys and thus to increase the effectiveness and efficiency of pavement condition assessment.

Surface distress assessment is an essential pavement management task. Available methods vary in cost as well as data quality and range from sketch mapping to visual surveys with automated data logging. However, the various manual methods are subject to nonrepeatability, subjectivity, and high personnel costs (*1*). Computerized image processing and analysis promise to reduce or eliminate the limitations associated with manual survey methods. Several computerized image-processing systems have been developed to analyze photographic or video images of the pavement surface (*1–4*). However, although they demonstrate the potential for distress survey automation, the simple edge detection and segmentation analysis schemes employed by these systems perform poorly on noncracking distresses and in the presence of pavement texture (*5,6*). Distress assessment on various types of pavement surfaces, especially those that exhibit extensive texture, has also proved problematic for existing systems. In the existing systems, analysis is typically based on interpreting differences between the intensity (gray scale) of distresses and the surrounding area. However, many situations occur in which the intensity ranges in an image do not provide sufficient discrimination between distresses and surrounding texture.

SCOPE OF WORK

The objectives of this study are to develop and refine mathematical morphology (MM)-based image analysis techniques and to evaluate the feasibility of applying this approach to improve the automation of pavement distress surveys. Preliminary tests are conducted to evaluate the ability of the developed image-processing technique to (*a*) identify cracking and other types of distresses on both asphalt and concrete surfaces and (*b*) assess cracking distresses to derive a rating in accordance with the linguistic scale currently used for manual distress surveying (*7*).

The tests were performed using digitized photographs of distresses on concrete pavements and asphalt shoulders of the New York State Thruway. Morphological measures were computed from the images, which were analyzed to obtain information about crack type, dimensions, and area, and the computed measures were then related to established distress rating scales. The algorithms designed as part of the current study were tested using 25 photographs representing various severities of slab cracking, slab surface defects, and shoulder defects, as defined by Thruway distress survey procedures. The distress types and scales used in the testing are summarized in Table 1.

The photographed pavement surfaces also were assessed manually by trained raters using the scales in Table 1 and the distress survey procedures defined previously (*7*). The rating obtained by morphology-based image processing is compared with the rating determined by the raters to test the performance of the current approach.

MATHEMATICAL MORPHOLOGY

The MM-based approach does not rely on intensity ranges to assess cracking and other distresses. Rather, it uses pavement texture as the basis for analysis and examines the distributions of sizes and shapes of "particles" in the image to evaluate distress types and severities. Thus, texture is analyzed to associate inhomogeneities in the texture with various types of distresses. MM operations and tools are not discussed rigorously in this paper. They are treated mainly from the functional perspective of their use in distress assessment. A rigorous treatment of this topic has been given in a previous publication (*8*).

MM analyzes textures on the basis of geometric features of textural particles such as size, orientation, shape, overlap, and so on. The power of the MM technique is based on a structural sorting of texture. Texture is analyzed through the use of geometric probes known as structuring elements. When various shapes and sizes of these elements are used, different features of interest are highlighted. For example, a circular structuring element of a specific diameter d sorts the texture under study so that structures

D. A. Grivas and B. C. Schultz, Department of Civil and Environmental Engineering; C. Bhagvati and M. M. Skolnick, Computer Science Department, Rensselaer Polytechnic Institute, Troy, N.Y. 12180.

possessing a similar geometry (i.e., circles of diameter d) are emphasized.

The morphological "opening" operation forms the basis for the current approach to assessment of pavement distresses. The approach is somewhat analogous to sieving a soil sample. Probing (or opening) an image with a structuring element has the effect of removing from the image all objects smaller than the structuring element. Performing a series of openings with increasingly larger structuring elements of the same shape is similar to shaking a soil sample through a series of sieves with increasing mesh openings, where the shape of the mesh corresponds to the shape of the structuring element. The generated morphological opening distribution based on the series of openings is analogous to the amounts of soil retained on screens of various sizes. Thus, an opening distribution provides important information about the size distribution of particles in an image.

IMAGE-PROCESSING METHODOLOGY

Morphology-based image processing for distress assessment is a four-step process. First, the pavement photographs are digitized and reduced to binary images by employing a threshold. Second, opening size distributions of pavement texture particles are computed from the images. Third, a "normalization" scheme is applied to increase the sensitivity of the distributions for capturing the essential distress features. Fourth, measures of the distributions are computed and related to features such as area, dimension, and type of distress, which are used to determine the linguistic ratings.

Thresholding

The simple relationship between morphological distributions and the particle size distributions discussed earlier is valid only in the case of binary images (black and white only; no shades of gray). Although opening distributions can also be used for computing size distributions in gray scale images, the methods are not as direct. For the purposes of the current feasibility study, the gray scale images produced from black-and-white photographs are digitized and then reduced to binary images by employing a "threshold."

Digitization translates the photographs into pixels of varying shades of gray. Because darker pixels generally occur in distressed areas (cracks appear darker than the surrounding texture), they are more useful in isolating pavement texture indicative of distress. In the current study, the threshold is automatically set such that 40 percent of the darkest pixels from the digitized photograph are converted to white in the binary image, and the remainder of the pixels are converted to black. The 40 percent value is determined empirically from the data set of 40 Thruway pavement images so that a sufficient amount of pavement texture is retained for subjecting each image to morphological analysis. Figure 1 shows an example of a digitized photograph and its corresponding binary image.

Opening Distributions

The morphological approach for crack assessment is illustrated in Figure 2. A thresholded image of alligator cracking on an asphalt shoulder is shown along with its opening distribution. There is a

TABLE 1 Manual Distress Assessment Scales

DISTRESS	SEVERITY	DESCRIPTION	EXTENT	RATING
Concrete slab cracking	None	No cracks	All slabs	N
	Small	Tight cracks spall free	1 or 2 slabs	SL
			$\geq$ 3 slabs	SG
	Medium	Full depth asphalt repairs	1 or 2 slabs	ML
			$\geq$ 3 slabs	MG
	Large	Open cracks spall free	1 or 2 slabs	LL
			$\geq$ 3 slabs	LG
	Total	Wide spalled cracks	1 or 2 slabs	TL
			$\geq$ 3 slabs	TG
Concrete slab surface defects	None	No defects	All slabs	N
	Small	Pitting	1 or 2 slabs	SL
			$\geq$ 3 slabs	SG
	Medium	Spalls < 6 inches	1 or 2 slabs	ML
			$\geq$ 3 slabs	MG
	Large	Spalls > 6 inches	1 or 2 slabs	LL
			$\geq$ 3 slabs	LG
Asphalt shoulder defects	None	No cracks	Entire Section	N
	Small	Longitudinal cracks or Transverse cracks	Occasional	SL
			Frequent	SG
	Medium	Alligator cracks	Occasional	ML
			Frequent	MG
	Large	Material loss or potholes or patches	Occasional	LL
			Frequent	LG

fine-grained texture in the original image caused by particles having dimensions of approximately 8 pixels or less. Two major cracks running vertically in the image have much greater widths (approximately 26 to 32 pixels).

The opening distribution is obtained by using a series of horizontally oriented line-shaped structuring elements with lengths varying from 2 to 46 pixels. As the image is opened with structuring elements of successively increasing lengths, the fine-grained texture is continuously removed until an element's length reaches 8 pixels. Thus, the opening distribution exhibits a large slope at scales less than 8 pixels. Since a line-shaped structuring element fits inside cracks (which are also long features), the structuring element preserves cracking until its length becomes longer than that of the crack. Structuring elements of lengths in the range of 26 to 32 pixels begin to remove the cracking from the image, which results in the sharper slopes at these scales in the distribution. Therefore, cracking is revealed by slopes in the opening distribution at "large" scales, where large, in most pavement images, implies exceeding 16 to 20 pixels.

Normalization

A normalizing scheme has been developed to remove the effects of the normal pavement texture from the opening distributions. Normalizing emphasizes deviations from normal surface texture, such as polishing, raveling, and pitting and also increases the sensitivity of crack detection.

"Raw" opening distributions are transformed into normalized distributions by removing information about normal texture. As a result, the normalized distribution for a pavement image with no distress (only normal texture is present) is a straight line parallel to the x-axis at $y = 1$. Deviations from the normal straight line indicate the presence of abnormal texture or distress. In an opening distribution generated from line-shaped structuring elements, cracks, which are large-scale features, are revealed as overshoots in the normalized distribution at scales corresponding to crack dimensions. Abnormal texture related to other types of distress is revealed as either an undershoot or an overshoot at scales corresponding to the scale of distress.

Figure 3 presents normalized distributions for four images of shoulder defects that were determined to have a severity of none, small, medium, and large in accordance with the Thruway's manual distress survey procedure (*7*). Note that the normalized distribution of the image rated none is almost a straight line parallel to the x-axis at $y = 1$, which indicates it has a normal pavement surface. The rest of the distributions show deviations from the flat line of varying magnitudes at varying scales. The images of small and medium severity distress exhibit cracking, and their normalized distributions reveal this as overshoots at large scales (26 to 32 pixels). The distribution from the image of large severity shows a large overshoot at scales between 4 and 12 pixels. It does not show any deviations at larger scales, indicating that it has little or no cracking. The distribution is thus consistent with the photograph, which shows that the distress is mostly material loss (a pothole).

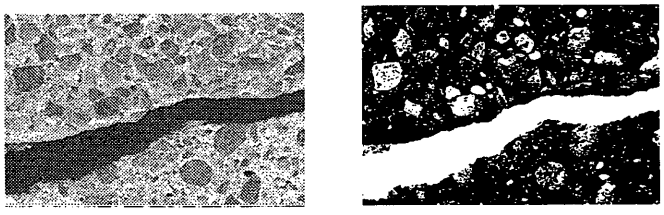

FIGURE 1 Gray scale and corresponding binary images.

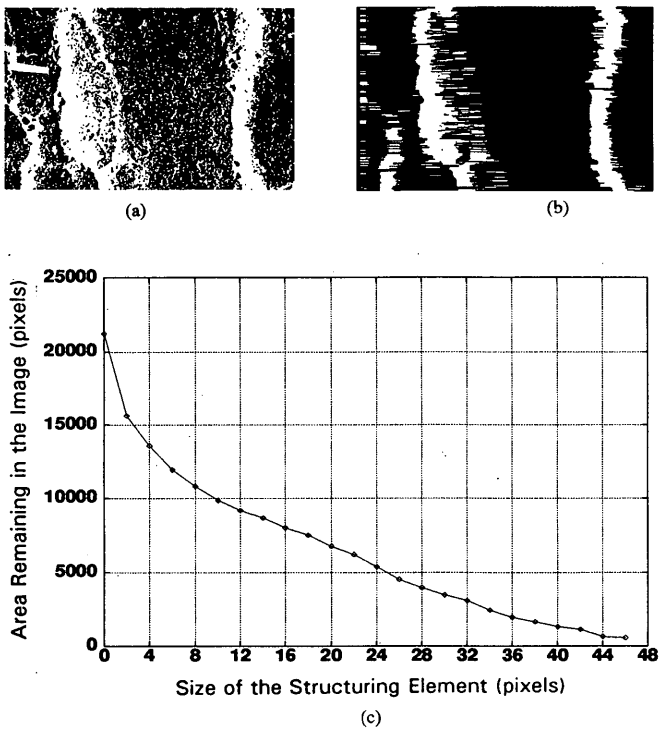

FIGURE 2 Process of developing an opening distribution: (*a*) binary image; (*b*) result of opening with a horizontal line-structuring element with a length of 8 pixels; and (*c*) opening distribution.

Distress Rating

Normalized distributions form the basis of the current morphology-based approach by capturing pavement texture information. The deviations from normal texture are analyzed to obtain numerical measures useful for determining distress ratings. The manual distress survey requires identification of distress type, severity, and extent. The automated procedure parallels this approach through development and application of rules for interpreting image analysis results. A summary of the distress rating algorithm is provided in Figure 4.

Type

Cracks are typically long, slender, large-scale features. Their presence is revealed by large-scale overshoots in normalized opening distributions. Determination of crack type is relatively straightforward, based mainly on the dominant direction of cracking. Crack direction is determined by comparing the differences be-

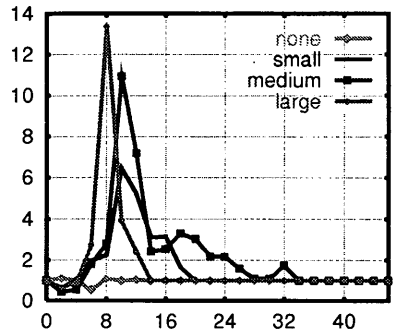

FIGURE 3 Normalized distributions of shoulder defects (*x*-axis, size of structuring element; *y*-axis, normalized area).

tween opening distributions made with structuring elements of various geometries. A vertical line structuring element preserves cracking in the vertical direction, and a horizontal line structuring element preserves cracking in the horizontal direction. If there is cracking in the horizontal direction, the normalized distribution in the horizontal direction shows overshoots at large scales. Similarly, normalized distributions in the vertical direction exhibit overshoots at large scales for vertical cracking. Based on the orientation of the photographs, vertical cracks are interpreted as longitudinal, and horizontal cracks are considered transverse. If both horizontal and vertical distributions show overshoots at large scales, there may be cracking in both directions, which is interpreted as alligator cracking. A simple quantitative rule embodies this logic: if $T^h_{cr} \geq 2\ T^v_{cr}$, then crack type is transverse; otherwise, if $T^v_{cr} \geq 2\ T^h_{cr}$, then crack type is longitudinal; otherwise, crack type is alligator, where T^h_{cr} is the largest scale at which an overshoot occurs in the horizontal direction, and T^v_{cr} is the largest scale at which an overshoot occurs in the vertical direction.

Determination of noncracking distress types (potholes, pitting, spalling, raveling, and so on) is similarly determined from consideration of properties of opening distributions. Such texture-related distresses are revealed on normalized distributions as undershoots and overshoots at small scales. Analysis at small scales, however, is less straightforward than that for cracking, and efforts are ongoing to improve discrimination between such cases.

Severity and Extent

In the manual survey procedure, severity and extent are defined by various measures, as appropriate for each distress type (see Table 1). The morphology-based procedure uses rules that duplicate the logic embedded in the manual distress scales (Table 1) to determine distress severities and extents from analysis of normalized opening distributions. For example, one rule for deducing the severity of concrete slab cracking is if the distress type is cracking, and cracking is tight and free of spalls, then the severity is small (*7*). Supplementary rules are added to aid quantification. For example, in the manual survey, tight cracks are defined as less than 1/4 in. wide. On an image, tight cracks are assumed to be

```
For each pavement image
1.  Threshold the input image into a binary image
2.  Compute Opening Distributions using horizontal line-shaped
    structuring elements (SE)
3.  Compute Opening Distributions using vertical line-shaped
    structuring elements (SE)
4.  Normalize the distributions extracted in (2) and (3)
5.  If the normalized distribution is 'close to' the ideal line Y = 1, then
        there are NO DEFECTS in the image
    If there are significant deviations from the ideal line at 'large'
    scales, then
        there is CRACKING present in the image
    If there are either undershoots or overshoots at 'small' scales, then
        there may be NON-CRACKING distresses in the image
6.  If there is CRACKING present in the image (see step 5) AND
    If the normalized distribution using horizontal line SEs exhibits
    overshoots at large scales,
        there is LONGITUDINAL CRACKING in the image
    else
        there is TRANSVERSE CRACKING in the image
    If there are deviations in both distributions at large scales, then
        there is ALLIGATOR CRACKING in the image
7.  Compute the area of distress from the magnitude of the deviations in
    the normalized distributions
8.  From the information obtained in steps (6) and (7), obtain severity
    and extent ratings
```

FIGURE 4 Summary of distress rating algorithm.

TABLE 2 Comparison of Morphology-Based and Manual Ratings of Shoulder Cracking Distresses

Image	Crack Measures			Crack Area	% Area	Automated Rating		Manual Rating	
	Type	T_{cr}^{h}	T_{cr}^{v}			Severity	Extent	Severity	Extent
1	–	8	8	78	0.04	N		N	
2	T	36	18	2544	12.72	S	L	S	L
3	T	>60	42	2579	12.84	S	L	S	L
4	A	42	50	4664	23.32	M	L	M	L
5	T	56	26	4119	20.59	S	L	M	L
6	A	>60	>60	7582	37.91	M	G	M	G

less than 30 pixels wide. (Crack width can be estimated from the scale at which overshoots occur.) For the purposes of the current feasibility study, no attempt is made to rigorously calibrate pixel size with true physical dimensions. However, the assumptions defining tight or open cracks appear reasonable on the basis of the data set used.

Determination of distress extent in a manner consistent with the manual procedure is somewhat problematic with the available test set of photographs. The individual photographs are from isolated locations, and each covers an area <1 ft^2. However, the manual survey defines distress extents by the amount of distress that occurs throughout a 0.10-mi sample section. On concrete pavement, extent is based on the number of slabs affected, while on asphalt pavement, it is the percentage of surface area affected. A simple rule was developed to test the potential of the technique to assess cracking extent on asphalt pavement: if less than one-third of the area in the photograph exhibits cracking, then extent is local; otherwise, extent is general (*7*).

TEST RESULTS

A total of 25 photographs representing various severities of concrete slab cracking, concrete slab surface defects (pitting and spalling), and asphalt shoulder defects (cracking and potholes) were analyzed to test the ability of the morphology-based approach to duplicate the ratings determined by the manual procedure. In the photographs, 16 contained cracking, and 9 contained noncracking types of distresses.

Cracking

Tables 2 and 3 present the test results for asphalt shoulder cracking and concrete slab cracking, respectively. Morphological measures, automated ratings from the morphology-based approach, and manual ratings from human raters are presented. In Table 2, no extents are reported for Image 1 because it has a severity of none. Extents are not shown in Table 3, because determination requires a count of slabs in a 0.10-sample section, and this information is not available for the test data set.

Of the 16 test images 14 were categorized correctly by morphological measures. The manual and automated severity ratings differed for two images. Severity in Image 5 was computed as small by the automated method but was classified as medium by the human raters. Image 15 was rated total by the automated analysis, but the human raters considered it large. Possible reasons for these discrepancies are as follows: (*a*) the rules for determining crack width on the basis of the number of pixels need adjustment; (*b*) the set of test photographs (which were taken for another purpose) are not exactly a constant height above the pavement surface and therefore, the correspondence between widths and number of pixels varies between photographs; and (*c*) there is a variety of uncertainties associated with subjective, human assessments using the manual scales.

Noncracking Distresses

Nine images representing various types of surface wear on asphalt and concrete pavements were analyzed. The results presented in

TABLE 3 Comparison of Morphology-Based and Manual Ratings of Slab Cracking Distresses

Image	Crack Measures			Crack Area	% Area	Severity (Auto.)	Severity (Manual)
	Type	T_{cr}^{h}	T_{cr}^{v}				
10	T	52	24	1378	6.86	S	S
11	T	48	10	440	2.20	S	S
12	T	50	28	2331	11.52	S	S
13	T	58	36	3523	17.62	L	L
14	T	56	32	3102	15.50	L	L
15	A	60	52	6887	34.44	T	L
16	A	60	60	6132	30.62	T	T
17	A	56	60	5912	29.56	T	T
18	A	>60	60	5992	29.96	T	T
19	A	56	44	3468	17.34	T	T

TABLE 4 Morphological Measures Indicating Noncracking Distress

Image	Distress	Manual Severity Rating	Surface	*Scales of Deviations*	*Distress Area*	*% Area*
7	Pothole	Large	Asphalt	34 – 48	3770	18.85
8	Material loss	Large	Asphalt	34 – 50	3352	16.76
9	Material loss	Large	Asphalt	28 – 40	2461	18.19
20	Pitting	Small	Concrete	32 – 40	2733	18.46
21	Pitting	Small	Concrete	34 – 44	4048	27.21
22	Spalling	Medium	Concrete	48 – 60	6371	54.18
23	Spalling	Medium	Concrete	36 – 46	2117	19.17
24	Spalling	Large	Concrete	46 – 60	6684	40.24
25	Spalling	Large	Concrete	48 – 60	11010	60.84

Table 4 indicate that the morphology-based method is capable of detecting such distresses. Work is currently in progress to develop morphological measures and rules for assessment of severities and extents of noncracking distresses. Two measures computed at the current stage of development are (*a*) the scale at which undershoots and overshoots occur and (*b*) the area exhibiting distress.

DISCUSSION OF RESULTS

The morphology-based approach provides a unified basis for automating distress surveys. This approach represents a significant departure from existing systems that use different image-processing algorithms for detecting different types of distress. Significant advantages of the morphology-based approach are (*a*) a substantial reduction in computational cost resulting from use of a single algorithm, (*b*) a substantial reduction in data requirements, and (*c*) reduction of manual intervention.

The morphological approach incorporates a thresholding procedure that reduces the effect of variations in gray scale intensities on various types of pavement surfaces. This decrease in variation effects will eliminate the need for manual intervention to indicate pavement type. Further reduction in manual intervention is made possible by the ability to assess different distress types.

Data needs are reduced because image data can be discarded once the distributions are computed. This ability to work from the distributions only is in contrast to existing systems, which detect distresses on the basis of selecting thresholds on original images. Therefore, with existing systems, performing various types of analysis may not be feasible if the image data are discarded. With the morphology-based approach, many different normalizing functions can be applied to the stored distributions to perform complex analyses and extract precise information about distresses. The distributions capture all essential distress information and are the basis for all further processing. Computational expense is thus significantly reduced because of the small size of the distributions. A typical image is 250,000 bytes in size, compared with its computed distribution, which may be about 200 bytes. Such a data reduction is extremely desirable.

Work is currently under way to establish whether morphological distributions capture all the information necessary to automate the distress survey procedures for all distress types, severities, and extents. If the distributions contain the needed information, and if they can be computed in real time, the choice of storing images versus storing only distributions will arise. The engineering use of the images has yet to be evaluated, but even if a visual data base of photographs is desired, a significant data reduction could be achieved by storing only those images whose distributions indicate the presence of "interesting" features such as large-scale distresses.

SUMMARY AND CONCLUSIONS

This study addressed the development of a new image-processing technique and evaluated the feasibility of applying this approach to improve the automation of pavement distress surveys. Significant advantages of the morphology-based approach are (*a*) reduction in computational cost resulting from use of a single algorithm, (*b*) reduction in data requirements, and (*c*) reduction of manual intervention.

Preliminary tests were conducted to evaluate the ability of the procedure to (*a*) identify and assess cracking and other types of distresses on both asphalt and concrete surfaces, and (*b*) derive ratings in accordance with a linguistic scale currently used for manual distress surveying. Results demonstrated that the approach is capable of

- Assessing distresses on various types of pavement surfaces without manual intervention;
- Detecting various distress types, such as cracking, material loss, surface wear, and spalling; and
- Evaluating crack types, severities, and extents.

These results demonstrate the potential of the approach in extracting measures for evaluating pavement surface condition. Further testing and refinement of the algorithm are currently under study to increase the utility and reliability of the computed measures. It is concluded that the developed approach is a feasible and promising technique for automating pavement distress surveys.

ACKNOWLEDGMENT

The research presented in this paper was sponsored by the New York State Thruway Authority. It is part of a broader effort to develop and implement a pavement management system for the Authority's pavements. The assistance provided by Thruway maintenance personnel is gratefully acknowledged.

REFERENCES

1. Copp, R. Field Test of Three Video Distress Recognition Systems. *Proc., Automated Pavement Distress Data Collection Seminar.* Ames, Iowa, June 12–15, 1990.
2. Lee, H. Accuracy, Precision, Repeatability, and Compatibility of the Pavedex PAS1 Automated Distress Measuring Device. In *Transportation Research Record 1311*, TRB, National Research Council, Washington, D.C., 1991, pp. 136–143.
3. Acosta, A. J., L. J. Figueroa, and R. L. Mullen. A Low Cost Video Image Processing System for Evaluating Pavement Surface Distress. Presented at 71st Annual Meeting of the Transportation Research Board, Washington, D.C., 1992.
4. Mohajeri, J. H., and P. J. Manning. ARIA: An Operating System of Pavement Distress Diagnosis by Image Processing. Presented at 70th Annual Meeting of the Transportation Research Board, Washington, D.C., 1991.
5. Mendelsohn, D. H. Automated Pavement Crack Detection: An Assessment of Leading Technologies. *Proc., 2nd North American Conference on Managing Pavements*, Toronto, Ontario, Canada, Vol. 3, Nov. 2–6, 1987, pp. 297–314.
6. El-Korchi, T., M. A. Gennert, M. O. Ward, and N. Wittels. System Design for Automated Pavement Surface Distress Evaluation. Presented at 70th Annual Meeting of the Transportation Research Board, Washington, D.C., 1991.
7. Grivas, D. A., B. C. Schultz, and C. A. Waite. Distress Survey Methodology of the New York State Thruway Authority's Pavement Management System. In *Transportation Research Record 1311*, TRB, National Research Council, Washington, D.C., 1991, pp. 166–172.
8. Serra, J. *Image Analysis and Mathematical Morphology.* Academy Press, Paris, 1982.

Views and opinions expressed herein do not necessarily reflect those of the New York State Thruway Authority.

Publication of this paper sponsored by Committee on Pavement Monitoring, Evaluation, and Data Storage.

Network-Level Performance Evaluation of Asphalt-Rubber Pavement Treatments in Arizona

GERARDO W. FLINTSCH, LARRY A. SCOFIELD, AND JOHN P. ZANIEWSKI

The disposal of waste tires is an important and unresolved problem in the United States. The addition of crumb rubber modifier to asphalt paving materials is a feasible solution for the disposal of scrap tires. For more than 25 years the Arizona Department of Transportation (ADOT) has been using asphalt-rubber materials in the construction and rehabilitation of pavements. Asphalt-rubber has been placed on more than 1360 km (850 mi) of the state system. The performance of various asphalt-rubber treatments was evaluated using the data available in the ADOT pavement management system data base. The performance of stress absorbing membranes (SAMs) and stress absorbing membrane interlayers (SAMIs) is analyzed considering treatment service life, survival curves, roughness, and cracking. Survival curves show that SAMs on Interstate highways have significantly shorter average service life than on state and U.S. routes. SAMs on state and U.S. routes show approximately the same roughness progression pattern. Interstate SAM sections show the fastest roughness increase. SAMs on Interstate sections also show higher rates of crack development than on state and U.S. routes. SAMIs on Interstate, state, and U.S. routes have approximately the same service life. SAMIs on Interstate sections show faster increases in roughness and cracking than on U.S. and state routes. Three-layer systems and asphalt-rubber asphalt concrete friction courses have performed satisfactorily for several years. No conclusion can be drawn about the performance of dense graded asphalt-rubber until more performance data are available.

The disposal of waste tires is an important and unresolved problem in the United States. Each year approximately 285 million tires are discarded. The Environmental Protection Agency (EPA) estimates that currently a backlog of 2 to 3 billion scrap tires requires disposal throughout the United States (*1*). One use for scrap tires that is thought to have an important potential is to incorporate their rubber into asphalt paving materials. The binder obtained by mixing scrap tire rubber, asphalt cement, and frequently a diluent is called asphalt-rubber.

The Arizona Department of Transportation (ADOT) has been using asphalt-rubber materials in the construction and rehabilitation of pavements for more than 25 years. These materials have been used in various types of treatments, prepared and applied following various techniques. Asphalt-rubber has been placed on more than 1360 km (850 mi) of the ADOT system. The main applications of asphalt-rubber rehabilitation treatments have been on state and U.S. routes.

Michael Heitzman of FHWA in a State of the Practice report on asphalt-rubber technology identified two principal unresolved engineering issues related to the use of asphalt-rubber in asphalt paving materials (*2*):

- At the national level, the ability to recycle these materials, and
- At the state and local levels, the evaluation of the performance of the materials in the field.

This paper focuses on finding answers for this last issue by analyzing the performance of pavement treatments involving asphalt-rubber in Arizona. Knowing the actual performance of the various asphalt-rubber treatments allows ADOT to determine which treatments have performed best and what treatments are the most appropriate.

The network-level pavement management system data base was used to statistically analyze performance of asphalt-rubber pavements. Using these data for the analysis did not provide the level of detailed performance information that normally would be used for the evaluation of various pavement treatments. However, using the pavement management data base allowed analysis of all of the pavement sections in the state. Furthermore, these data are the basis for pavement management in the state and therefore represent a real-world evaluation of the performance of the treatments. The network-level analysis included the evaluation of performance of the following asphalt-rubber pavement treatments: stress absorbing membranes (SAMs), stress absorbing membrane interlayers (SAMIs), three-layer systems (TLS), asphalt-rubber asphalt concrete friction courses (ARACFC), and dense-graded asphalt-rubber concrete (DGAR).

LITERATURE REVIEW

General Background

Crumb rubber modifier (CRM) for asphalt paving is one possible solution to the disposal of scrap tires. However, currently less than 1 percent of the tires discarded annually is used as CRM for paving purposes (*1*). The incorporation of CRM in asphalt surfacing materials can be done using two different processes. The wet process consists of blending the rubber with asphalt cement before incorporating the binder into the process. The dry process mixes the rubber with the aggregate before the mixture is charged with asphalt. Although, the dry process is limited to hot-mix asphalt concrete (HMAC) applications, the wet process has been applied to crack sealants, surface treatments, chip seals, and HMAC (*2*). Arizona uses asphalt-rubber prepared using the wet process. This

G. W. Flintsch and L. A. Scofield, Arizona Transportation Research Center, 7755 South Research Drive, Suite 106, Tempe, Ariz. 85284. J. P. Zaniewski, Civil Engineering Department, Arizona State University, Tempe, Ariz. 85287.

process mixes 70 to 80 percent asphalt with 20 to 30 percent scrap tire rubber at high temperature (160°C to 200°C). Frequently a low percentage of diluent (4 to 6 percent) is also required.

The main factors that affect the properties of the asphalt-rubber binder are rubber type and gradation, rubber concentration, asphalt type and concentration, diluent concentration and type, cure time, and reaction temperature (*3*). The main reasons for adding rubber to asphalt are to improve binder properties and to dispose of waste material (*4*). On the other hand, the main barriers to the development of the asphalt-rubber technology are the following (*3*):

1. Asphalt-rubber treatments have approximately twice the initial cost of conventional treatments, insufficient life-cycle cost data, and high capital cost required for equipment; and
2. Lack of complete long-term testing, conflicting test results, bad information transference, lack of material specifications, and patents.

The long-term performance of asphalt-rubber treatments in ADOT is discussed.

Historical Development

The modern concept of using wet process CRM in paving materials was developed primarily by Charles McDonald, Materials Engineer for the City of Phoenix, in the early 1960s. He developed an asphalt-rubber patching material called "Band-Aid." On the basis of the success of this material, the use of asphalt-rubber was expanded to surface treatments for entire projects. The resulting asphalt-rubber surface treatment is commonly referred to as SAM. ADOT placed its first experimental SAM on the frontage road of Interstate 17 in 1968 (*5*).

In 1972 ADOT placed its first experimental SAMI. This consisted of an asphalt-rubber membrane placed on an existing asphalt concrete surface before a conventional asphalt concrete overlay. The purpose of the membrane is to delay reflection cracking through the overlay and reduce pavement permeability. SAMI further evolved into a TLS as a solution for overlaying portland cement concrete pavements (PCCP). In the TLS the application of asphalt-rubber is placed between two asphalt concrete courses.

Further development resulted in asphalt-rubber binder use in hot asphaltic mixes. The first applications of asphalt-rubber as a binder in a hot-mix asphaltic concrete was in open-graded ARACFC. ADOT's first experimental ARACFC was placed in 1975. The first experimental section with DGAR was placed in 1986 (*6*).

Previous ADOT Reports

Gonsalves (*5*) presented the first comprehensive performance evaluation of asphalt-rubber treatments in ADOT. The principal applications by that time were SAMs and SAMIs. The analysis of pavement performance included surface condition, skid resistance, and roughness. The following were the main conclusions of the study:

1. Surface cracking was reduced by the use of rubberized asphalt and
2. Roughness is not adversely affected by rubberized asphalt.

Zaniewski (*4*) reported a review of the status of the research and performance of asphalt-rubber in Arizona. This report analyzed previous laboratory results, field experiments, and performance of highway sections containing asphalt-rubber treatments versus conventional treatments using ADOTs pavement management system (PMS) data bases. Comparisons between pairs of sections, where the only difference in construction history was that one received a SAM or SAMI and the other of the pair received a conventional treatment, showed mixed results. Finally, Zaniewski's report included a life-cycle cost analysis that concluded that if a conventional chip seal lasts 5 years a SAM application should last at least 10 years to be cost-effective. A 10-cm (4-in.) conventional overlay resulted in similar initial construction cost to a 5-cm (2-in.) SAMI treatment, but the conventional overlay had a lower life-cycle cost.

Scofield (*6*) presented a network level performance evaluation of SAMs, SAMIs, and asphalt-rubber membranes for pavement encapsulation, and a detailed project level analysis of eight experimental projects that included 47 test sections. Scofield concluded the following:

- SAMs had an average service life of 5.3 years on Interstate highways, 10.0 years on state routes, and 8.2 years on U.S. routes.
- SAMIs had an average service life of 9.0 years on Interstate highways, 9.5 years on state routes, and 7.8 years on U.S. routes.

The sections analyzed within each route class had different traffic, environmental, and support conditions. Therefore, the average service lives obtained represent average values for the entire route class. It will not be possible to accurately predict the service life of a particular section, but these average values can be used for network-level pavement management analysis.

NETWORK-LEVEL ANALYSIS USING ADOT PMS DATA BASE

The main body of the research consisted of an analysis of the performance of the various asphalt-rubber treatments using the information available in the ADOTs PMS data base. ADOT has constructed more than 1360 two-lane roadway km (850 mi) of pavement treatments containing asphalt-rubber. Usage consists of approximately 628 km (390 mi) of SAM, 476 km (296 mi) of SAMI, 13 km (8 mi) of TLS, 159 km (99 mi) of ARACFC, and 84 km (52 mi) of DGAR. The analysis concentrates on SAMs and SAMIs because more historical information is available relative to these treatments.

Asphalt-Rubber Membranes

A list of SAM and SAMI projects was obtained from the ADOT PMS data base. This list was compared with that from two previous reports (4,5) to prepare a comprehensive list of projects. For each of the identified projects, the pavement age at the time of the treatment and the time to the first rehabilitation treatment applied after the SAM or SAMI was extracted from the data base. In addition, pavement condition (surface distresses and roughness), traffic volumes, and maintenance costs were extracted from the main PMS data base. This information is available by mile-

TABLE 1 Descriptive Statistics for SAM Service Lives

Statistic	Total	Interstate	State	US. Routes
Mean	8.77	6.36	10.33	8.90
Standard Error	0.61	0.53	1.12	0.99
Standard Deviation	4.19	1.75	4.34	4.55
Coeff. of Variation	48	27	42	51
Range	17	6	14	16
Minimum	3	4	3	4
Maximum	20	10	17	20
Number of Sections	47	11	15	21

post, but average values for each section were computed for the analysis.

SAM Performance

There are 51 homogeneous SAM sections, 11 on Interstate highways, 18 on state routes, and 22 on U.S. routes. Four of these sections were experimental projects and were excluded from this analysis.

Service Life The service life for SAM sections was analyzed considering all route classes together and grouped by route class. Service lives were computed using ADOT's project data base by extracting the date of construction of the treatment and the date of application of the first rehabilitation treatment (mainly overlay or seal coat). However, three sections showed distress patterns (roughness and cracking), which indicated that a maintenance treatment was applied previous to the date shown in the data base. The date of rehabilitation was modified in all three cases. The statistics that describe SAM service lives are shown in Table 1. Survival curves were constructed by plotting the cumulative percentage of projects that have received major maintenance or rehabilitation (mainly seal coat or overlay) versus age of the pavement. The survival curves for Interstate, state, and U.S. routes are shown in Figures 1 through 3, respectively. For each survival curve a linear regression was fitted using the least-squares method. The corresponding fitted line, the coefficient of correlation, and the standard error of estimate are shown on each figure. Figure 2 shows that 50 percent of the SAM sections placed on state routes survived more than 10 years, and only approximately 25 percent were in service for more than 14 years.

Four fitted lines, corresponding to survival curves for all route classes, Interstate, state, and U.S. routes, are plotted in Figure 4. The Interstate sections have a significantly higher slope than the state and U.S. sections. Therefore, Interstate sections have significantly shorter average service life (in years) than state and U.S. routes. These results are consistent with those reported by Scofield (*6*) and can be explained by the fact that the Interstate sections receive, on average, approximately ten times more traffic than the others.

State sections performed slightly better than U.S. sections although they have approximately the same traffic load. This can be because the U.S. sections were significantly older at the time of construction of the SAM. The difference in performance on the two route classifications is less than was observed in 1989.

The average service lives and coefficient of variations of SAMs on each route class are as follows:

Route Class	*Average Service Life (years)*	*Coefficient of Variation (%)*
Interstate	6.4	27
State	10.3	42
United States	8.9	51

The service lives obtained were in all cases longer than those obtained in 1989. This is not surprising because in both cases

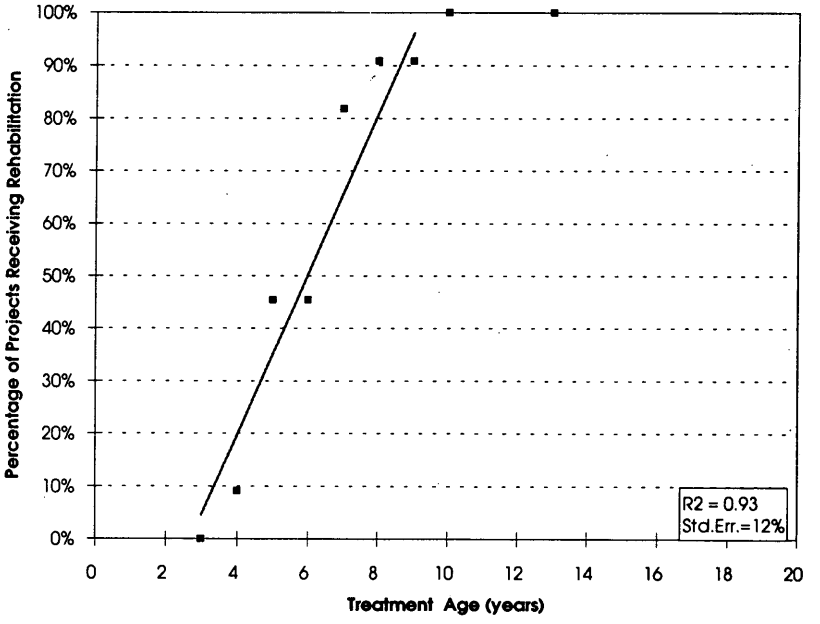

FIGURE 1 Survival curve for SAMs applied on Interstate routes.

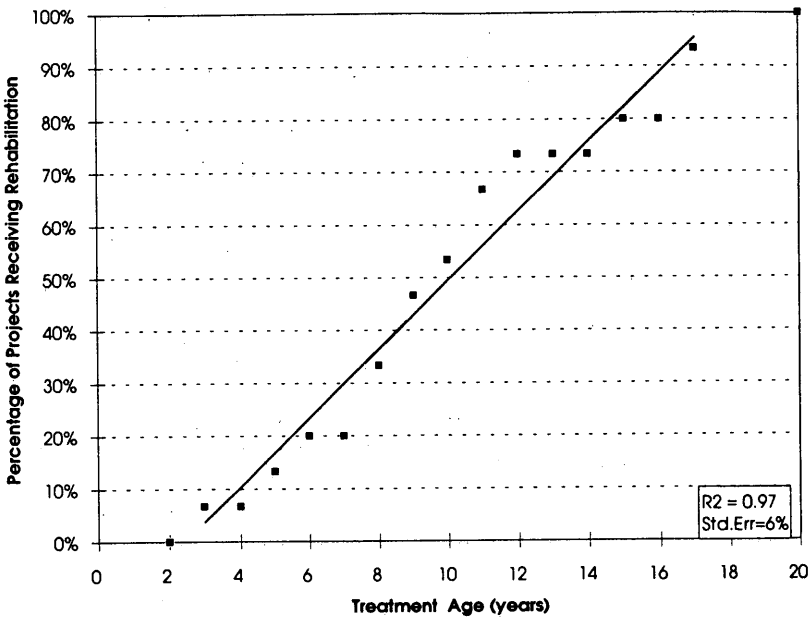

FIGURE 2 Survival curves for SAMs applied on state routes.

several sections have not received rehabilitation treatments and they are older now. The average service life has increased by 20 percent for Interstate, 3 percent for state and 9 percent for U.S. routes.

Roughness ADOT's PMS data base has annual roughness, expressed in inches per mile (in Maysmeter units), for every milepost of their highway network, starting in 1972. For every section considered, the average roughness values for the entire section were computed for the year before SAM placement and for each year of the SAM's service life. The average roughness of all sections and the corresponding standard deviation were computed for the year before SAM and for each year after SAM construction. Figure 5 shows a graphical representation of the average roughness progression with time and a 95-percentile band.

The average annual change in roughness was computed for each section by fitting a linear regression of the form

$$\text{Roughness} = m * \text{Age} + b \pm \epsilon \quad (1)$$

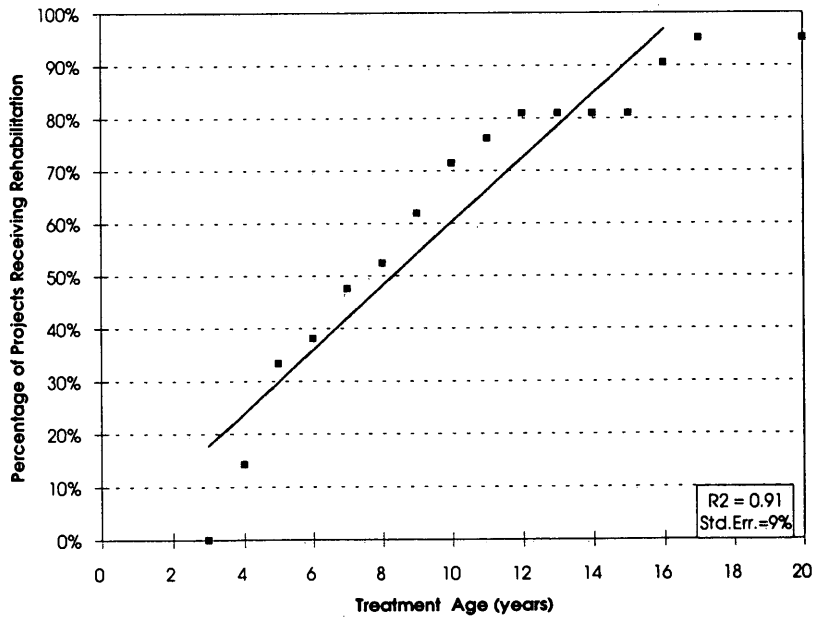

FIGURE 3 Survival curve for SAMs applied on U.S. routes.

The slope of this line (m) represents the average change in roughness for the roadway section. A line with slope equal to the overall average annual change in roughness (m) is shown superimposed on the average roughness plot in Figure 5. This line shows a relatively good fit until a pavement life of 12 years. Beyond that point it departs from the average roughness plot that indicates a reduction of roughness with age at the largest pavement ages. Two explanations are offered for this. First, only the sections that performed the best would survive beyond the 12-year horizon, and it could be expected that they had the lowest roughness. Second, fewer sections were used to compute the average roughness for the larger ages. Therefore, these averages are less representative. If the sections that lasted more than 14 years are analyzed separately, the overall average annual change in roughness (m) is only slightly different. However, in this case, a line with slope equal to the overall average m has a better fit with the plot of annual roughness averages. The averages for the older ages are higher, and therefore closer to the overall average roughness line, than are the averages that consider all sections.

SAM sections on state and U.S. routes show approximately the same roughness progression pattern. Therefore, they were grouped together for further analysis. Interstate sections show a faster increase in roughness probably because they carry heavier traffic load. Figure 6 shows the average roughness pattern for Interstate and state plus U.S. routes.

The performance equations that describe the average roughness for the two route classes are as follows:

$$\text{Average roughness} = 58 + 7.6 * \text{Age} \quad \text{for Interstate} \quad (2)$$

$$\text{Average roughness} = 88 + 5.5 * \text{Age} \quad \text{for state and U.S. routes} \quad (3)$$

The results reported by Zaniewski (*4*) are similar. However the values can be compared only after making an adjustment because ADOT has changed the calibration of the Maysmeter.

Cracking A problem was faced while analyzing cracking of SAM sections. Although a large percentage of sections were constructed in the mid-seventies, cracking data were available only starting in 1979. Consequently, the cracking data before SAM that would be expected to significantly affect the crack development are available only for a few sections. Therefore, the accuracy of the analysis is relatively poor because of the incomplete data in the early ages. The top portion of Figure 7 displays the annual percentage of cracking for all sections with a line that indicates the average of all sections for each year. A careful analysis of the cracking data showed that six SAM sections have particularly high percentages of cracking. Available information about these sections is limited to a few years close to the end of their service lives. Analyzing these sections separately reduces the dispersion, as shown in the bottom portion of Figure 7. Figure 8 shows the average percentage of cracking for Interstate, state, and U.S. routes. Interstate sections show a much higher rate of cracking development (1.7 percent per year) than state and U.S. routes (0.6 percent per year, and 0.4 percent per year, respectively).

SAMI Performance

Approximately 400 mi of SAMIs has been placed in Arizona. The analysis identified 77 homogeneous SAMI sections, 17 on Interstate highways, 25 on state routes, and 35 on U.S. routes. Nine of these sections were experimental and were not included in these analysis. Additionally, data for one of the sections analyzed previously was not in the current data base.

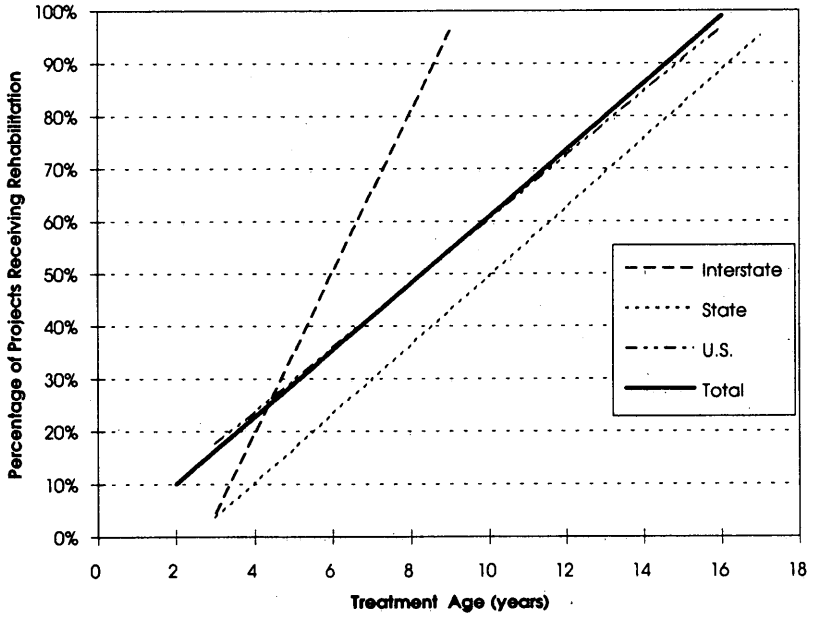

FIGURE 4 Comparison of fitted survival curves for SAMs on various route classes.

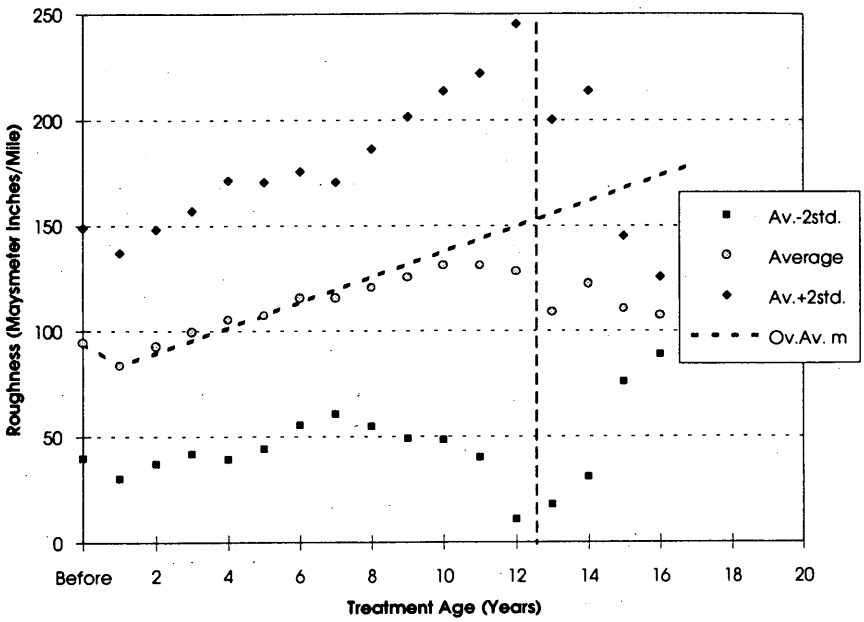

FIGURE 5 Average roughness progression for all SAM sections.

Service Life Service lives for SAMI sections were analyzed by considering all route classes together and grouped by route class. Service lives were computed on the basis of information stored in the PMS project data base. The statistics that describe SAMI service lives are shown in Table 2.

Survival curves for SAMIs on all route classes—Interstate, state, and US. routes—were constructed similar to that for SAM's sections. A linear regression was fitted for each curve. All regression lines showed good fit with coefficients of correlation (R^2) larger than 0.90.

The average service lives obtained for each route class are as follows:

Route Class	*Average Service Life (years)*	*Coefficient of Variation (%)*
Interstate	10.7	35
State	9.5	54
United States	10.7	42

Except for state routes that stayed the same, service lives were in all cases longer than those obtained in 1989. The average service life has increased by 19 percent for Interstate and 37 percent

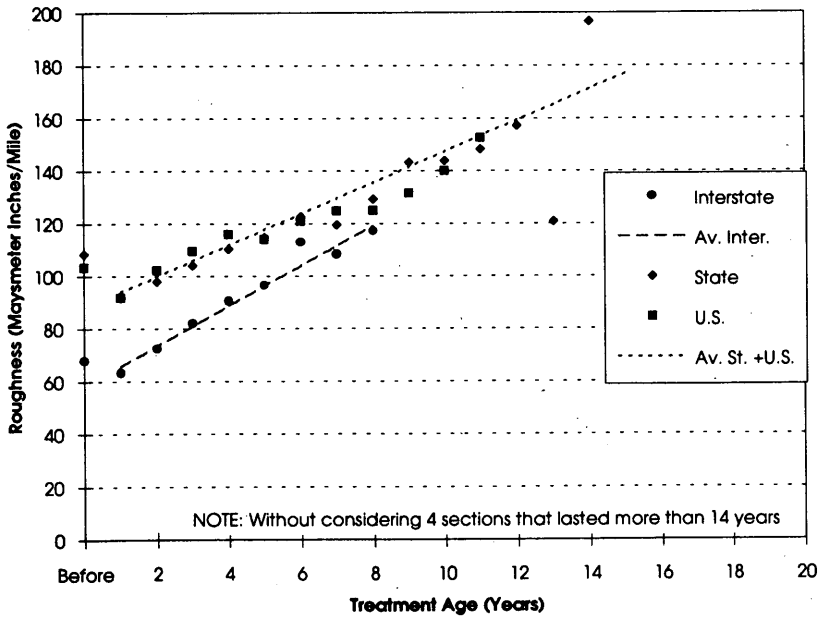

FIGURE 6 Average roughness progression for SAMs on various route classes.

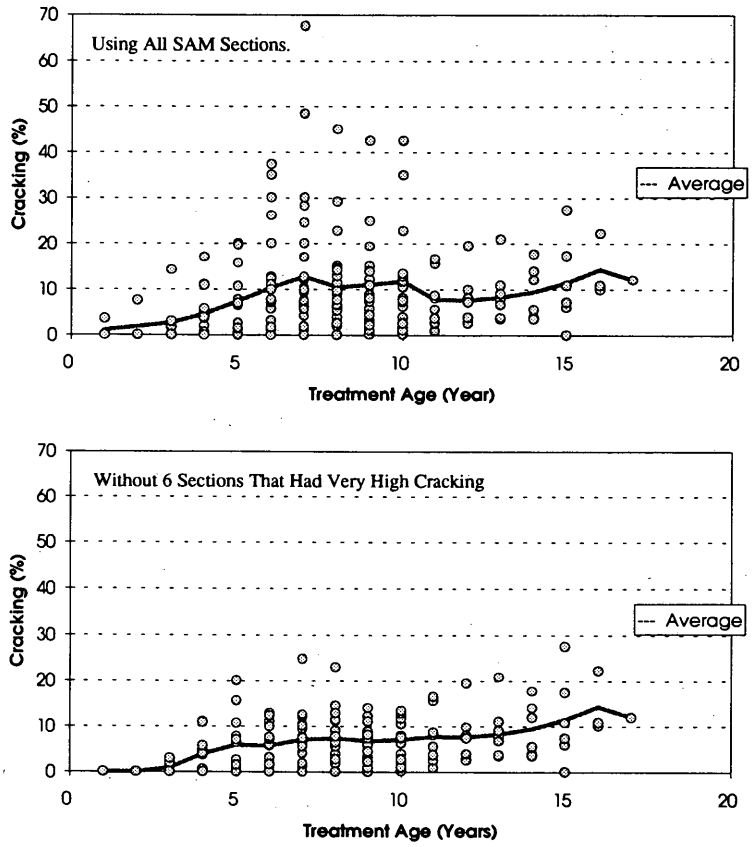

FIGURE 7 Average cracking development for SAM sections by year.

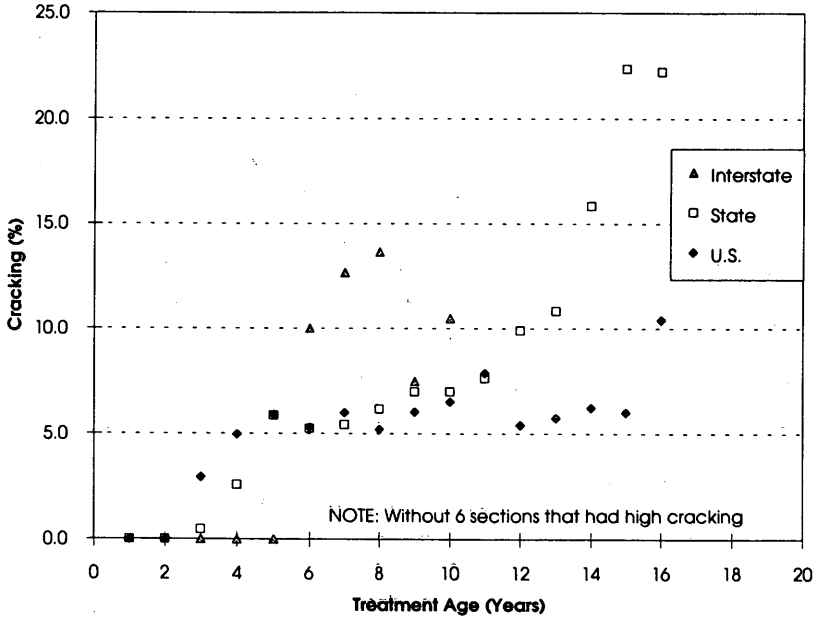

FIGURE 8 Average annual cracking for SAM sections grouped by route classification.

TABLE 2 Descriptive Statistics for SAMI Service Lives

Statistic	Total	Interstate	State	US. Routes
Mean	10.3	10.7	9.5	10.7
Standard Error	0.56	1.08	1.10	0.79
Standard Deviation	4.59	3.73	5.16	4.52
Coeff. of Variation	44%	35%	54%	42%
Range	14	11	14	14
Minimum	52	5	2	2
Maximum	16	16	16	16
Number of Sections	67	12	22	33

for U.S. routes. This increase is explained by the fact that several sections that were in service in 1989 have become older without being rehabilitated.

The four fitted lines obtained by linear regression show similar behavior (Figure 9). Consequently, SAMIs on Interstate, state, and U.S. routes have approximately the same service life. Because Interstate routes carry significantly higher traffic than the others, a shorter service life could have been expected. However, Interstate highways usually receive thicker overlays and in general are in better condition at the time of rehabilitation.

Roughness Roughness data were processed in the same way as those for the SAMs. The average roughness of all sections and the corresponding standard deviation were computed for the year before the SAMI construction and for every year of the treatment's service life. Figure 10 shows a graphical representation of the annual average roughness progression and a 95-percentile band. The average annual change in roughness was computed for each section using linear regression analysis. The overall average annual roughness changes for all sections by route classification are shown in Table 3. A line with slope equal to the overall average annual change in roughness shows a good fit with the annual average values, as shown in Figure 10.

Average roughness pattern for Interstate, state, and U.S. routes were compared. Interstate sections show the fastest increase in roughness probably because they carry a significantly heavier traffic load. Variations in annual roughness change (m) are very high. Performance equations for the average roughness are provided.

$$\text{Average Roughness} = 50 + 5.4 * \text{Age} \quad \text{for Interstate} \tag{4}$$

$$\text{Average Roughness} = 58 + 3.1 * \text{Age} \quad \text{for state routes} \tag{5}$$

$$\text{Average Roughness} = 58 + 2.3 * \text{Age} \quad \text{for U.S. routes} \tag{6}$$

These values are lower than those reported by Zaniewski (*4*) because in the previous report only the sections with high coefficient of correlation ($R^2 > 0.7$) were used to compute the average annual change in roughness.

Cracking Cracking data were evaluated following the same procedure described for SAM sections. Interstate sections show a much higher average rate of cracking development (0.5 percent per year) than sections on state and U.S. routes (0.2 percent per year). This rate can be caused by the heavier traffic load of Interstate highways.

TLS Performance

One section of Interstate Route 17 near downtown Phoenix (both roadway directions) had a TLS placed over PCCP in service for

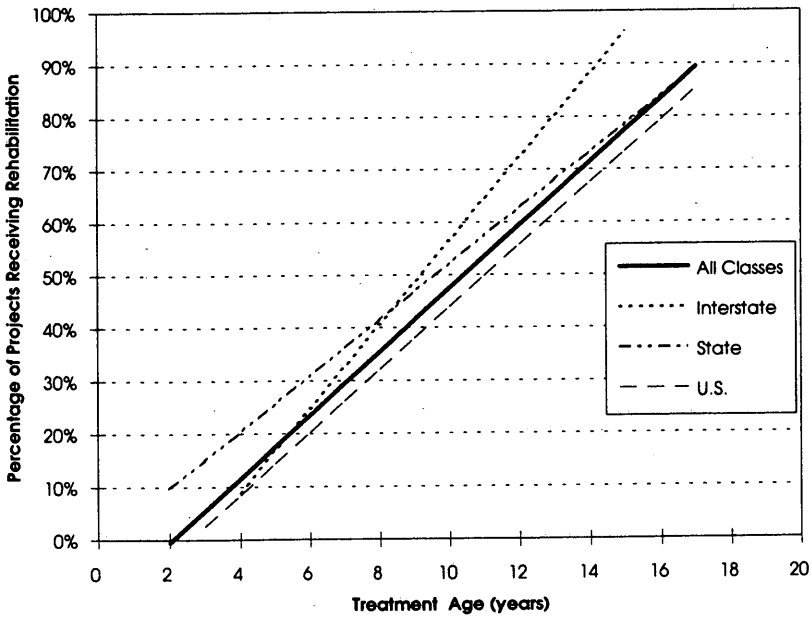

FIGURE 9 Comparison of survival curves for SAMIs on different route classes.

TABLE 3 Average Roughness Values for all SAMI Sections

Route	Roughness Before SAMI			Annual Roughness Change			Initial Roughness After SAMI		
Class	Av.	St.Dev.	Obs. #	Av.	St.Dev.	Obs. #	Av.	St.Dev.	Obs. #
Interstate	106.6	34.5	12.0	5.4	3.8	12.0	50.5	20.8	12.0
State	96.4	52.9	19.0	3.1	4.9	19.0	58.2	20.6	19.0
U.S.	117.7	38.2	31.0	2.3	3.0	31.0	57.8	17.2	31.0
Total	114.2	43.0	62.0	3.2	3.9	62.0	56.5	18.9	62.0

8 years, from 1985 until its rehabilitation in 1993. This section received approximately 7 to 8 million equivalent single axle loads during this period. The distress analysis showed the following:

- The average roughness was drastically reduced by approximately 120 in./mi (Maysmeter units) by applying the TLS.
- Average roughness showed almost no change through the 8 years of service life.
- Cracking developed during Year 4, reaching 3.5 percent in 1991. The average annual rate of crack development was 0.6 percent, similar to the average for SAMIs.

The section was performing satisfactorily at the time of rehabilitation but was removed as part of a larger rehabilitation project on the Interstate. The performance of this treatment is considered good. However, there are not enough statistical data to make strong conclusions about the long-term performance of TLS.

Asphalt-Rubber Concrete

ADOT has constructed several pavement sections using asphalt concrete mixes with asphalt-rubber binder. A brief description of the performance of these treatments is reported.

ARACFC Performance

ADOT's project data base includes 29 sections that have or had ARACFC treatments. Several of these are short experimental sections. Only eight of the ARACFC sections identified were constructed more than 3 years ago. One of these eight sections was a short experimental section and was reconstructed the year following construction, probably as part of a larger rehabilitation project. The average service life of the other seven sections is 10 years. However, only two of these sections have been rehabilitated: one at Year 5 and the other at Year 11. Therefore, the average service life of this treatment cannot be reliably estimated at this time, but it could be expected to be longer than 10 years.

DGAR Performance

A total of 24 sections that have DGAR in their structure were identified in ADOT's project data base. Several are short experimental sections, and only one section is older than 3 years. This section, constructed in 1986, is in service and, as of 1992, has not developed cracks. The roughness has only slightly increased from 1986 to 1992.

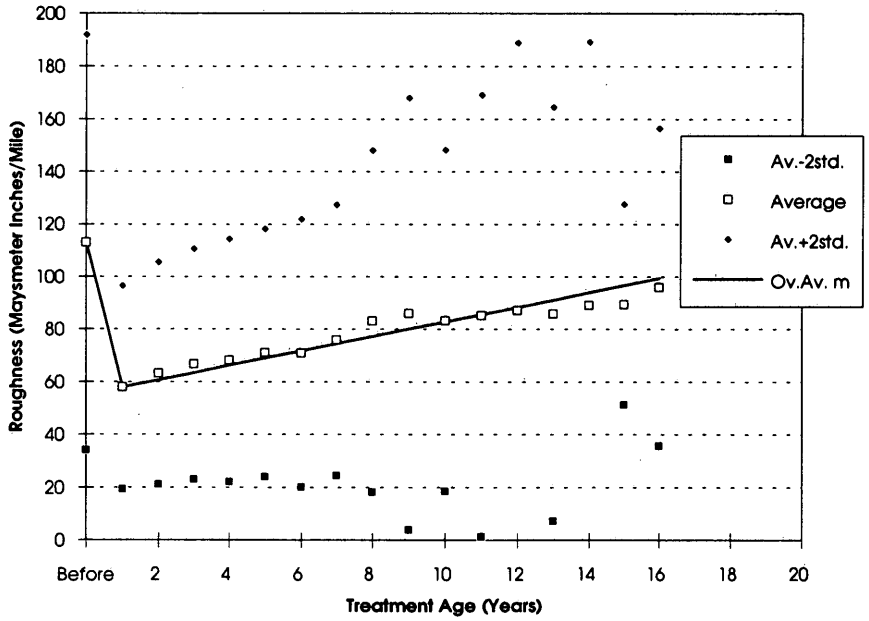

FIGURE 10 Average roughness progression for SAMI sections.

SUMMARY, CONCLUSIONS, AND RECOMMENDATIONS

The main asphalt-rubber applications in ADOT have been in SAMs, SAMIs, DGAR, and ARACFC. Network-level evaluations of the first two treatments were not conclusive about the relative effectiveness of the asphalt-rubber treatments with respect to conventional treatments. Experiences from other states and national studies also show mixed results.

The average service life for SAM sections on Interstate highways is significantly shorter than the average service life on state and U.S. routes. The average annual change in roughness was computed for each section using linear regression analysis. SAM sections on state and U.S. routes show approximately the same roughness progression. Interstate sections show a faster increase in roughness, probably because of heavier traffic loads. Additionally, SAMs on Interstates also exhibit a higher rate of crack development.

SAMIs on Interstate, state, and U.S. routes have approximately the same service life. Because Interstate routes carry significantly higher traffic than the others, a shorter service life is expected. However, Interstate highways usually receive thicker overlays and, in general, are in better condition at the time of rehabilitation. Interstate sections show the fastest increase in roughness probably because they carry significantly heavier traffic. Interstate sections also exhibit a higher average rate of crack development than state and U.S. routes.

A TLS placed over PCCP was in service under heavy traffic for 8 years until its rehabilitation in 1993. The section had a drastic decrease in roughness with the treatment and was still performing satisfactorily at the time of rehabilitation. ADOT has constructed several ARACFC sections. The average service life of this treatment cannot be reliably estimated as this time, but it could be expected to be longer than 10 years. No conclusion can be drawn about the performance of DGAR until more performance data are available.

To evaluate the effectiveness of using paving treatments that contain asphalt-rubber, their performance should be compared with the performance of conventional treatments of similar characteristics. A close long-term follow-up of treatments using asphalt-rubber concrete should be conducted to evaluate its effectiveness with respect to conventional asphalt concrete treatments.

REFERENCES

1. *Markets for Scrap Tires.* EPA/530-SW-90-074A. Environmental Protection Agency, Washington D.C., Oct. 1991.
2. Heitzman, M. *State of the Practice: Design and Construction of Asphalt Rubber Paving Materials with Crumb Rubber Modifier.* Report FHWA-SA-92-022. FHWA, U.S. Department of Transportation, Washington D.C., 1992.
3. Epps, J. A. *Uses of Recycled Rubber Tires.* (NCHRP Project 20-5, Topic 22-02), TRB, National Research Council, Washington, D.C., 1992.
4. Zaniewski, J. P. *Summary of Arizona Department of Transportation Experience with Asphalt Rubber.* State of the Art Report. Report FHWA-AZ88-818, Arizona Department of Transportation, Phoenix, 1988.
5. Gonsalves, G. F. D. *Evaluation of Road Surfaces Utilizing Asphalt Rubber.* Report 1979-663. Arizona Department of Transportation, Phoenix, 1979.
6. Scofield, L. *The History, Development, and Performance of Asphalt Rubber at ADOT.* Special Report. Report AZ-SP-8902. Arizona Department of Transportation, Phoenix, 1989.

Publication of this paper sponsored by Committee on Pavement Monitoring, Evaluation, and Data Storage.

Electrical Resistance Tomography Imaging of Spatial Moisture Distribution in Pavement Sections

OK-KEE KIM, WILLIAM A. NOKES, H. MICHAEL BUETTNER, WILLIAM D. DAILY, AND ABELARDO L. RAMIREZ

The Division of New Technology, Materials, and Research (NTM&R) of the California Department of Transportation sought a method to measure the spatial distribution and movement of moisture in a pavement section. Measurement of electrical resistivity was investigated because of the inverse relationship between resistivity and moisture content. NTM&R collaborated with Lawrence Livermore National Laboratory in applying electrical resistance tomography (ERT) to measure and subsequently image spatial resistivity. The results from two field experiments succeeded in showing images that correlate very well with layers in pavement sections. Images from sequential ERT measurements reveal water movement within the pavement and into the subgrade. Results suggest that ERT technology may be an important research tool in understanding moisture distribution and movement.

The Division of New Technology, Materials and Research (NTM&R) of the California Department of Transportation (Caltrans), sought a method to measure the spatial distribution and movement of moisture in a pavement section. Measurement of electrical resistivity, using electrical resistance tomography (ERT) was investigated because of the inverse relationship between resistivity and moisture content: high resistivity is interpreted as low moisture content and low resistivity is interpreted as high moisture content. NTM&R collaborated with Lawrence Livermore National Laboratory (LLNL) in evaluating ERT for measurement and subsequently for imaging. This paper presents a brief description of ERT technology and the results of two field experiments.

CONCEPT AND THEORY OF ERT

ERT is a method for determining the electrical resistivity distribution in a volume based on discrete measurements of current and voltage on the boundary. Resistivity data can be taken in a variety of configurations, including borehole to borehole or borehole to surface. Detailed technical concepts and theory used for ERT can be found elsewhere (*1*,*2*).

To obtain an image of the region between two boreholes, a number of electrodes are placed in each hole in electrical contact with the surrounding material. An aspect ratio of 2:1 for borehole depth to borehole spacing is common. A pair of adjacent electrodes is driven by a known current, and the resulting voltage difference is measured between other pairs of electrodes. The known current then is applied to another pair of electrodes, and the voltage is again measured between other pairs. This procedure is repeated until current has been applied to all pairs of electrodes (in both holes). The ratio of a voltage at one pair of terminals to the current causing it is a transfer resistance. For n electrodes there are $n(n-3)/2$ independent transfer resistances.

The next step is to calculate the distribution of resistivity between the boreholes given the measured transfer resistances and to construct an image. However, the calculation for the distribution of resistivity is highly nonlinear because the currents flow along the paths of least resistance and are dependent on the resistivity distribution. Finite element method (FEM) algorithms and least-squares methods are used to invert the transfer resistances.

Image construction can be on the same FEM mesh used to calculate the measurements or on a different array. An absolute image shows a resistivity structure, whereas a comparison image shows changes in resistivity with time. Comparison images can be used to study dynamic processes in pavement structure, such as percolation, by comparing data taken at different times. This paper presents both absolute images and comparison images.

Forward Solution

The forward solution to Poisson's equation uses FEM to compute the electrical potential response of a two-dimensional earth caused by a three-dimensional source. To avoid the difficulty of numerically solving a three-dimensional problem, Poisson's equation is formulated in the wave number domain via Fourier transformation in the strike direction. According to Hohmann (*3*), the governing equation is

$$\frac{\partial}{\partial x}\left(\sigma\frac{\partial V}{\partial x}\right) + \frac{\partial}{\partial z}\left(\sigma\frac{\partial V}{\partial z}\right) - \lambda^2\sigma V = -\mathrm{I}\delta(x)\,\delta(z) \qquad (1)$$

where

V = potential in Fourier transform domain,
σ = conductivity,
λ = the Fourier transform variable,
I = source current, and
$\delta(x)$ = delta function.

O-K. Kim, Division of New Technology, Materials and Research, California Department of Transportation, 5900 Folsom Blvd., Sacramento, Calif. 95819. W. A. Nokes, Division of State and Local Project Development, California Department of Transportation, 650 Howe Ave., Suite 400, Sacramento, Calif, 95325. H. M. Buettner, W. D. Daily, and A. L. Ramirez, Lawrence Livermore National Laboratory, P.O. Box 808, Livermore, Calif. 94551.

FIGURE 1 Location of experiment site.

The two-dimensional FEM algorithm is based on the theory described by Huebner and Thorton (*4*) and the implementation follows that described by Wannamaker et al. (*5*) for modeling two-dimensional magnetotelluric data. Using FEM, potentials are calculated for a discrete number of transform variables at the nodes of a mesh of quadrilateral elements. The potentials are then inverse transformed back into the Cartesian domain using the method described by LaBrecque (*6*).

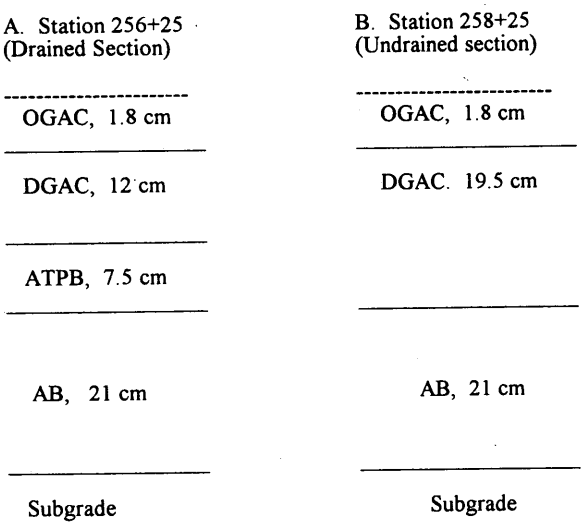

FIGURE 2 Pavement structural section of Experiment 1 site.

TABLE 1 Summary of Subgrade Soil Properties

Water content by weight, %	15.33
Dry bulk density of soil, gr/cc	1.72
Degree of saturation, %	70.9
Specific gravity of soil particle	2.73

Numerical Inversion

The inversion method uses the modified Marquardt algorithm (*7*) to jointly solve the nonlinear equation

$$\mathbf{WD} = \mathbf{W}*\mathbf{F(P)} \tag{2}$$

and the equation

$$\mathbf{P}^T\mathbf{RP} = 0 \tag{3}$$

where

D = vector of known data values,
W = weighting matrix,
P = vector of unknown parameters,
F(P) = the forward solution, and
R = the roughness matrix that is a numerical approximation to the Laplacian operator (*8*). To solve these equations jointly, the algorithm minimizes

$$\chi^2 + cL\,(\mathbf{P}) = 0 \tag{4}$$

where c is a constant and χ is the chi-squared statistic that is given by

$$[\mathbf{D}*\mathbf{F(P)}]^T\mathbf{W}^T\mathbf{W}[\mathbf{D}*\mathbf{F(P)}] = \chi^2 \tag{5}$$

Ideally the inverse algorithm would find the maximum value of c for which χ^2 is equal to some value known a priori. The constant (c) was determined by trial and error by calculating an inverse model with an a priori value of c and then adjusting (if necessary) to achieve the correct value of χ^2.

TABLE 2 Resistivity Test Results of Subgrade Soil (03-SUT-99, PM 4.9, Northbound, Sta. 256 + 25)

Water Content, % by Weight	Resistance (ohms)	Resistivity (ohm-cm)	
15.6	340	2322	
19.6	216	1475	
23.6	131	895	
27.6	110	751	
31.6	105	717	Minimum Resistivity
35.6	108	738	
39.6	110	751	
43.5	117	799	
55.5	120	820	

Resistivity = resistance*6.83

TABLE 3 Resistivity of Field Backfill Material

Station	Hole I.D.*	Resistance (ohms)	Resistivity (ohm-cm)
256+25 (Drained)	1	100,000	190,500
	2	160	304
258+25 (Undrained)	A	800	1,525
	B	80	152
	C	80	152

Hole I.D.* : corresponds to Figure 3.

TABLE 4 Mixing Formulation for Backfill Material

Mixing Components	Composition, % by Weight
Gravel (B-39)	47.2
Sand (B-11)	31.7
Coke breeze (DW-2)	10.2
Polyester resin	10.7
MEK (Methyl Ethyl Ketone)	0.2

FIELD EXPERIMENT

Experiment 1

Test Sites and Instrument Installation

Caltrans and LLNL researchers first installed ERT arrays on northbound Highway 99 near the Sacramento Metro Airport (shown as 03-SUT-99 in Figure 1) in December 1991. Test sites are located at stations 256 + 25 (built with a drainage layer) and 258 + 25 (without a drainage layer) on the outer (Number 2) lane. The elevation of the highway surface nearly equals that of the adjacent rice fields, which are usually filled with irrigation water from April to September and which typically are assumed to increase subgrade moisture during the dry summer.

Pavement cross sections in Figure 2 show similar designs. Station 256 + 25 has open-graded asphalt concrete (OGAC, 1.8 cm), dense-graded asphalt concrete (DGAC, 12 cm), asphalt-treated permeable base (ATPB, 7.6 cm), and aggregate base (AB, 21 cm) over subgrade soil. In contrast, station 258 + 25 has no ATPB (in Lane 2) and the DGAC is 19.5 cm thick. ATPB was inadvertently placed in Lane 1 at station 258 + 25 but was sealed with a slurry seal before placing the DGAC.

The subgrade soil at the test sites was sampled during construction for subsequent laboratory testing, which is summarized in Table 1. Soil from station 256 + 25 was used to measure resis-

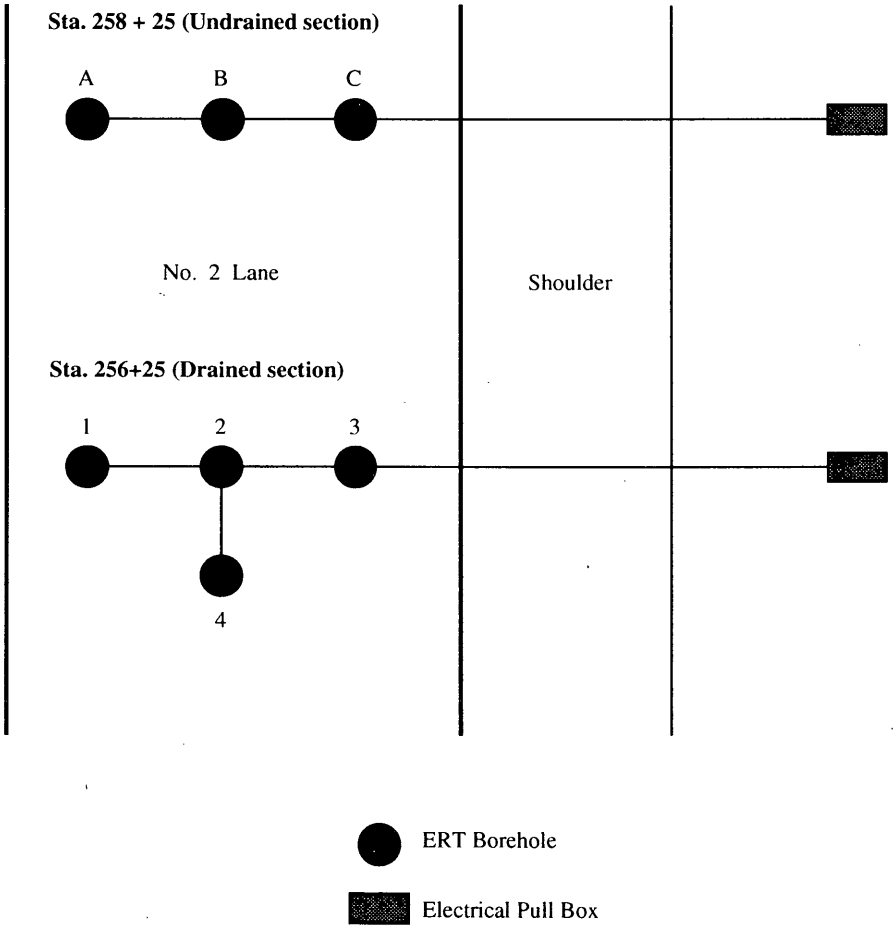

FIGURE 3 ERT layout at Experiment 1 site (note drawn to scale).

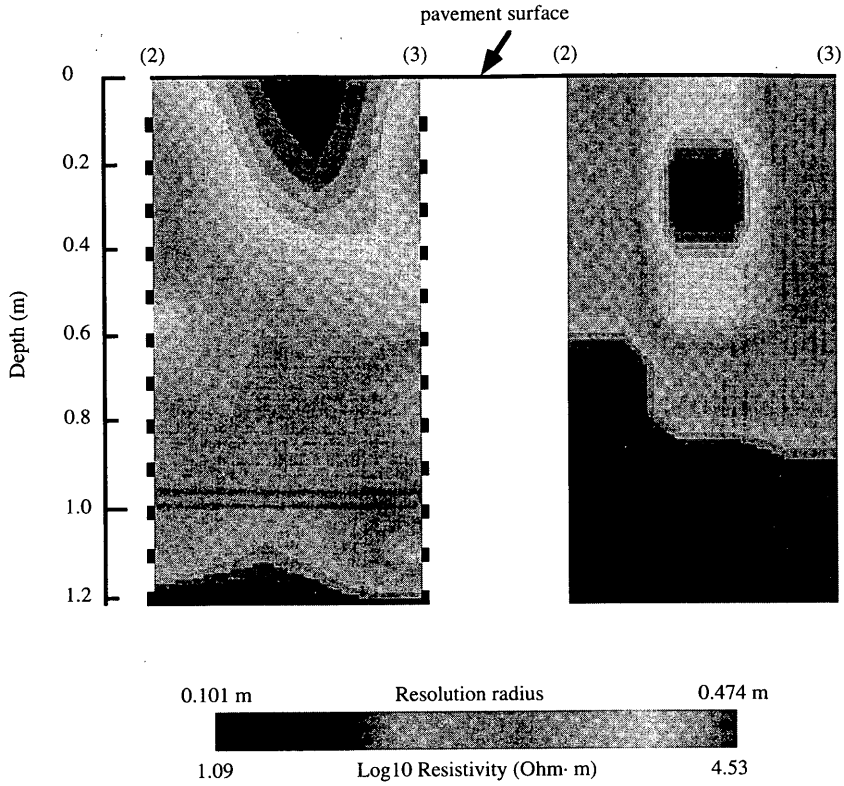

FIGURE 4 Absolute ERT image and resolution radius of Plane 2–3 for Experiment 1.

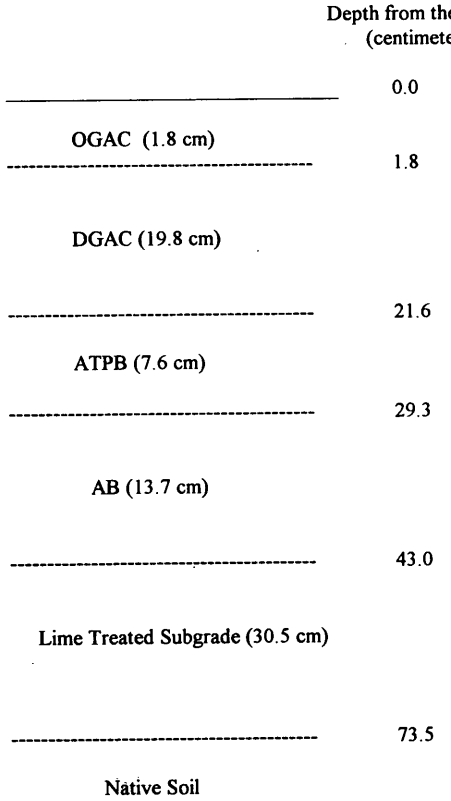

FIGURE 5 Pavement structural section of Experiment 2 site.

tivity on the basis of California Test Method 643 (*9*). Results shown in Table 2 show that resistivity ranges from 717 to 2322 ohm-cm depending on water content.

Conductive backfill material for ERT electrodes was prepared in the NTM&R laboratory and then mixed at the site using a small mechanical mixer. A nominal resistivity of 2000 ohm-cm was tar-

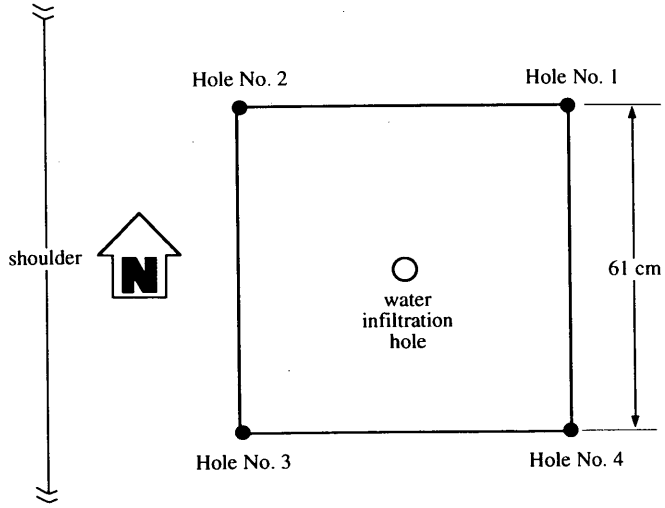

FIGURE 6 Layout of ERT boreholes for Experiment 2. Boreholes 1 and 2 were backfilled with the excavated native soil. LTS, AB, and cold AC patching material. Boreholes 3 and 4 were backfilled with cement-mortar and cold AC patching material.

geted for the backfill material surrounding the ERT arrays in each borehole. The backfill material was placed in the 3.8 cm ± annular space. Five-block specimens (7.5 × 7.5 × 30 cm) were made and brought back to the NTM&R laboratory to check the resistivity. The formulation of backfill material and its resistivity are presented in Tables 3 and 4.

The layout of ERT boreholes is shown in Figure 3. Spacing the holes 60 cm apart and 125 cm deep (each ERT array was 121.9 cm long) met the 2:1 aspect ratio requirement. Each hole diameter was 10 cm. Surface electrodes originally were to be placed in the AC surface layer, but stiff AC from the cold weather prevented installation.

Results and Discussion

The first two of three efforts to collect resistivity measurements yielded poor-quality data. LLNL researchers tried both sites, but data obtained from these two trips were insufficient for reconstructing images. The principal difficulties were (a) excessively high cross-hole resistance levels and (b) a dynamic range in the data too large for the measurement system to handle. The dynamic range refers to both the limits on injected current (1 amp maximum) and measured voltage (4 V maximum). Much of the data fell outside these limits.

On the third trip, in April 1992, the LLNL researchers tried to correct the difficulties mentioned above by (a) using higher drive voltages at the current injection electrodes and (b) splitting the measurement schedules into two parts to accommodate the large dynamic range of voltage measurements. It was necessary to break the measurement schedule into several parts, thus increasing the time required to collect data from both sites. A complete data set was collected for the plane between Boreholes 2 and 3, referred to as the "2–3" plane (see Figure 3), which resulted in an absolute image of resistivity shown in Figure 4. In the reconstruction, the dark end of the gray scale corresponds to low electrical resistivity (wet) and the light end to high resistivity (dry). The small solid rectangles on both vertical edges in the 2–3 plane indicate the location of electrodes spaced every 10 cm.

A distinct transition from high to low resistivity is shown in Figure 4 at a depth of about 40.6 cm below the pavement surface. This transition corresponds approximately to the boundary between the AB layer and the subgrade at 42.3 cm, as illustrated in Figure 3. The resistivity distribution in Figure 4 shows that, as expected, the upper layers are drier than the subgrade. It is difficult to interpret results further about the resistivity distribution in the plane 2–3 because the spatial resolution is no better than about 10 cm in the bottom of the plane and ranges from 30.5 to 50.8 cm in the upper part of Figure 4. Sampling for image reconstruction generally is better with smaller-resolution radius.

The poor resolution (or higher-resolution radius) is a consequence of the low-quality field data caused by backfill material having highly variable resistivity. Laboratory measurements shown in Table 3 show wide variations and nonlinearity in resistivity. Resistivity tests (called four-point measurements) on backfill material conducted at LLNL confirmed that the relationship between current and voltage was not linear. Undesirable properties were grossly evident when the LLNL researchers found that they could easily generate spark discharges and smoke at the current injection electrodes.

Experiment 2

Test Site and Installation

A second set of ERT electrodes was installed in September 1992 on the truck scale ramp just north of Riego Road on southbound Highway 99 (03-SUT-99). The site is located about 4 km south of the Experiment 1 sections and is built with OGAC (1.8 cm), DGAC (19.8 cm), ATPB (7.6 cm), AB (13.7 cm) and lime-treated subgrade (LTS, 30.5 cm) over native soil as illustrated in Figure 5.

Figure 6 shows a plan view of four boreholes 10.2 cm in diameter where electrode arrays were inserted. Four image planes were defined by four linear arrays of electrodes placed into holes at corners of a 61-cm square. The electrode arrays extended to 121.9 cm below the pavement surface. There are 12 electrodes in each hole and 5 surface electrodes on each edge of the square. Surface electrodes were placed into holes 1.3 cm in diameter drilled into the bottom of sawcuts (approximately 5.1 cm wide and 5.1 cm deep) on the pavement surface. These holes extended about 5.1 cm into the DGAC layer.

Electrodes in boreholes and at the surface were spaced every 10.2 cm. One hole 10.2 cm in diameter was drilled at the center of the square (see Figure 6) down to the bottom of the ATPB layer for a water infiltration experiment, which was conducted to better understand vertical and horizontal water flow.

Two kinds of backfill material were tried: cement mortar and excavated pavement materials. Cement mortar with a 1 to 3 ratio (by weight) was used with a water-cement ratio of 0.5. Boreholes 1 and 2 (see Figure 6) were backfilled with the excavated native soil, LTS, and AB materials, which were removed from the holes during drilling. Space in the ATPB, DGAC, and OGAC was filled with cold AC patching material. Boreholes 3 and 4 were filled with cement mortar up to the top of the aggregate base, and cold AC patching material filled the remaining space to the surface. A steel rod was used to compact the backfill materials to eliminate air pockets around the electrodes and to ensure good contact between the backfill materials and electrodes. Commercial concrete patching and cold AC patching materials were used to fill the sawcut trench.

Results and Discussion

Effect of Backfill Materials Measurements collected in March 1993 provided better-quality data than did the first experiment. Resistivity values vary from about 3 $\Omega \cdot$ m in the underlying native soil to about 10^5 $\Omega \cdot$ m in parts of the upper pavement section. As expected, the overall pattern indicated drier conditions in the upper layers than in the subgrade soil.

The absolute images presented in Figure 7*a* are much better than those in Figure 4, and there is better correlation with the pavement structure. The plane images in Figure 7 are similar despite the different backfill materials (the 1–2 plane has existing material for backfill and the 3–4 plane has cement mortar backfill). The resistivity in the upper half of the AB is similar to that in the lower half of the ATPB. This pattern is repeated between the AB and the LTS as well as the LTS and native soil. The DGAC and ATPB layers show relatively high resistivity as expected. However, an unexpected low resistivity (that is, relatively wet condition) appears in the upper portion of the DGAC layer at the interface with the OGAC. The OGAC shows a surprisingly lower

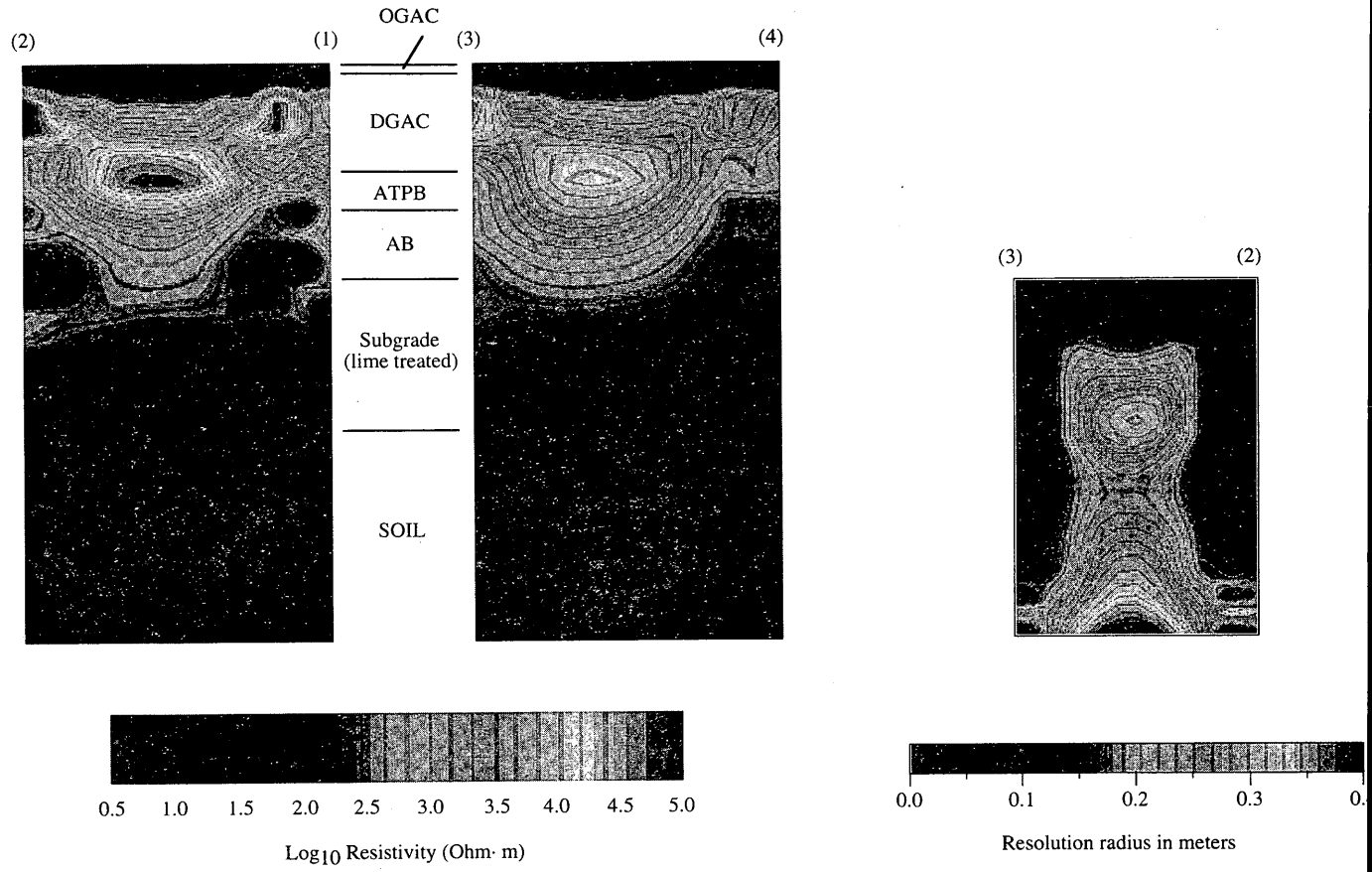

FIGURE 7 Plane images: (*left*), absolute ERT images of Planes 1–2 and 3–4; (*right*), resolution radius of Plane 3–2.

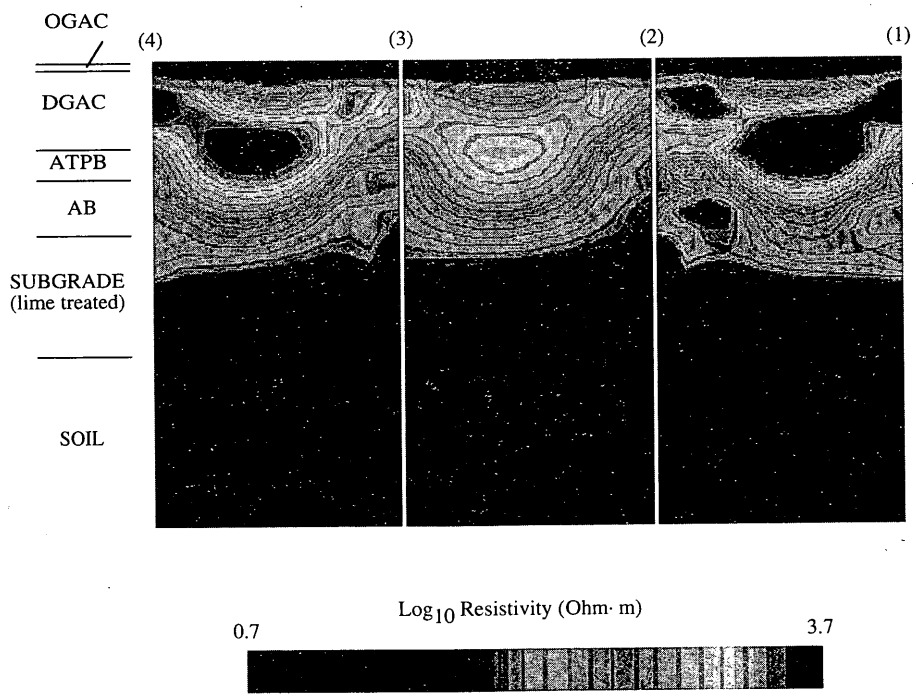

FIGURE 8 Baseline ERT images before water infiltration.

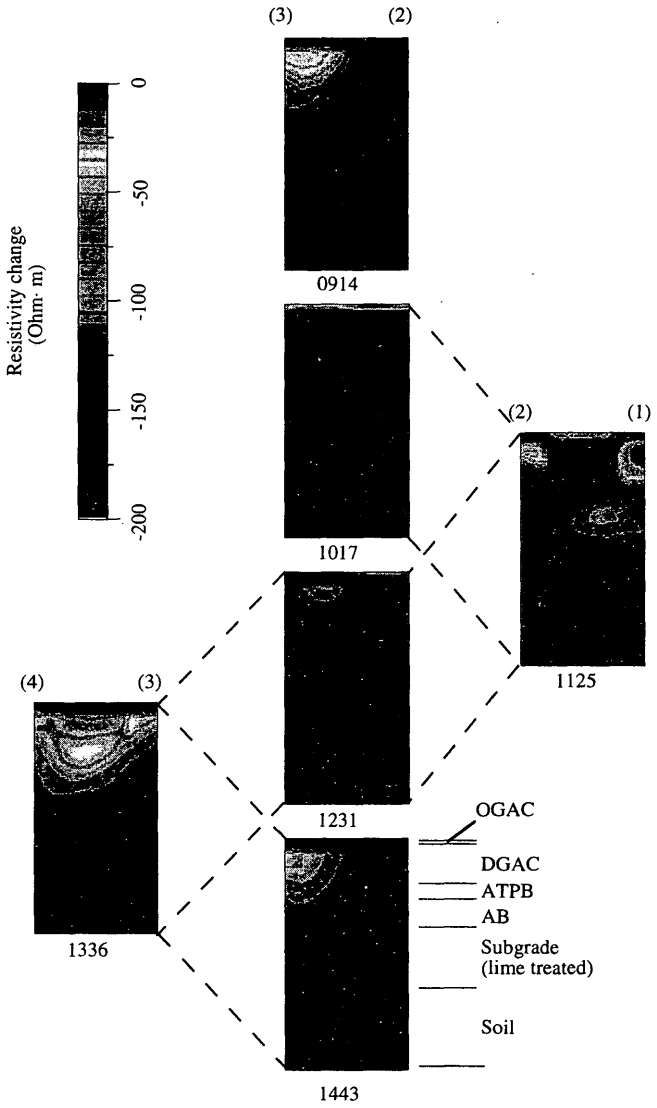

FIGURE 9 Comparison images during water infiltration.

resistivity than the DGAC despite sunny weather and a dry pavement surface that prevailed before and during data collection. One explanation for low resistivity at the DGAC/OGAC interface is vapor condensation. However, reasons for the low resistivity in the DGAC remain unknown until future research is done. The potential damages from high moisture content in these layers (e.g., asphalt stripping) justify further field study.

Figure 7*b* shows the resolution radius for the images in Figure 7*a*. The resolution radius can be thought of as a direct measure of the spatial resolution for the image: spatial resolution is better when the resolution radius is small and poorer when it is large. The resolution radius in this study varies from near zero to approximately 39.9 cm, whereas in Figure 4 it varies from about 10.2 to 50.8 cm. The resolution radius is better (smaller) near the electrodes and worse away from them because the pavement and soil materials are sampled more densely near the ERT arrays. In contrast to the first experiment, the improved resolution radius is largely a result of better-quality data and improved techniques.

Water Infiltration After obtaining good ERT images, an additional experiment was performed to measure horizontal and vertical water flow in the drained pavement section. The experiment was done in April 1993.

Before introducing water into the center hole (see Figure 6), ERT data were collected for baseline images. The baseline images of the 1–2, 2–3, and 3–4 planes, shown in Figure 8, match along their common edges and clearly show the expected resistivity structure (high resistivity in upper layers and low resistivity in the LTS and native soil). Like Figure 7*a*, the low resistivity is evident at the OGAC/DGAC interface.

The infiltration experiment was conducted during a period longer than 6.5 hr (from 8:40 a.m. to 3:00 p.m.) in which approximately 20.8 L of water was poured uniformly and slowly into the pavement through the center hole. Data were collected at several times during the infiltration period. The change in resistivity associated with moisture movement was imaged as a function of time. Four complete data sets were collected in the 2–3 plane (at 9:14 a.m. and 10:17 a.m. and 12:31 and 12:43 p.m.) because the researchers expected most of the water to drain through this plane. One data set was collected for the 3–4 plane at 1:36 p.m. and one for the 1–2 plane at 11:25 a.m. Because data collection required about 1 hr for each plane, the images represent time averages.

Water movement is inferred by contrasting the baseline data with those collected during water infiltration. Figure 9 shows a sequence of contrast images that show differences from the baseline conditions; that is, if there were no changes in resistivity because of water infiltration, the images would be a uniform single color. Progressive decreases in resistivity (i.e., increase in moisture) appear as progressively lighter as shown on the gray scale.

The sequence of images for the 2–3 plane shows decreased resistivity (interpreted as water flow) around the Borehole 3 at 9:14 a.m. At 10:17 a.m. this feature disappears, but ponding of water is evident across the section and in the LTS. By 12:31 p.m. this ponding disappears and there is more moisture movement around Borehole 3. Finally, at 2:43 p.m. there appears to be moisture movement around Borehole 3 much like that at 9:14 a.m. This sequence does not show a steady-state flow that is expected during slow constant infiltration.

The single image in the 3–4 plane at 1:36 p.m. shows moisture movement more evenly through the pavement section. This image matches well along the Borehole 3 edge with the 2–3 plane image at 2:43 p.m. The single image of the 1–2 plane at 11:25 a.m. shows moisture movement, although not as uniform, as the 3–4 plane at 1:36 p.m. The images in Figure 9 do not appear to show that infiltrated water drained preferentially to the shoulder through the 2–3 plane.

The sequence of images in this study shows that ERT can be used for further study related to drained pavement structures after improvement in some areas of ERT technology. For better understanding of the water flow in pavement system, it is recommended to improve ERT data collection system by decreasing the data collection time. In Experiment 2 the 1-hr data collection time is probably too long compared with the time scale of changes in the flow pattern in pavement structure. In addition, it would be valuable if data could be collected from multiple planes simultaneously and to provide better understanding of moisture movement in pavement system.

Finally, the following are concerns revealed during this study:

- There may be leaks or water movement between layers via boreholes,
- Image reconstruction introduces errors because it relies on two-dimensional analysis of three-dimensional water flow,
- Electrical properties (resistivity and change of resistivity) of pavement materials are not well known and correlation with moisture content is uncertain,
- Effects of water-soil-aggregate-asphalt binder interaction on water flow patterns are poorly understood, and
- All of the above are difficult to evaluate because of the long data acquisition time.

CONCLUSIONS AND RECOMMENDATIONS

ERT images showed moisture distribution and movement in pavement sections. These images correlate very well with known pavement structural sections where two different materials were used. Cold AC patching material was used successfully and is recommended as backfill in the ATPB and AC.

Further research to improve ERT technology will include laboratory testing of electrical properties of pavement materials, testing the water-soil-aggregate-asphalt binder interaction on water flow patterns, using reconstruction algorithms based on three-dimensional flow, and reducing data acquisition time.

Improved ERT technology will help pavement researchers and practitioners in many ways, such as visualizing moisture movement in pavement systems, understanding pumping mechanisms, determining traffic effects on water movement, and eventually designing pavement structures that are more resistant to water-induced damage.

ACKNOWLEDGMENT

Caltrans work was sponsored by FHWA, and LLNL work was performed under the auspices of the U.S. Department of Energy. The authors are grateful to John Carbino for fabricating the ERT probes and to Wayne Nakayama, John Morgan (District 4), and Kathy Coots (District 3) of Caltrans for their efforts in installing ERT probes.

REFERENCES

1. Daily, W. and E. Owen. Cross-Borehole Resistivity Tomography. *Geophysics*, Vol. 56, No. 8, Aug. 1991, pp. 1228–1235.
2. Daily, W., A. Ramirez, D. LaBrecque, and J. Nitao. Electrical Resistivity Tomography of Vadose Water Movement. *Water Resources Research*, Vol. 28, No. 5, May 1992, pp. 1429–1442.
3. Hohmann, G. W. Numerical Modeling for Electromagnetic Methods in Geophysics. In *Electromagnetic Methods in Applied Geophysics Theory*, Part 1, Vol. 3, (M.N. Nabighian, ed.), Society of Exploration Geophysicists, Tulsa, Okla., 1988, pp. 313–363.
4. Huebner, K. H. and E. A. Thorton. *The Finite Element Method for Engineers*. John Wiley and Sons, Inc., New York, 1982.
5. Wannamaker, P. E., J. A. Stodt, and L. Rijo. *PW2D Finite Element Program for Solution of Magnetotelluric Response of Two-Dimensional Earth Resistivity Structure*. Report ESL-158. University of Utah Research Institute, Salt Lake City, 1987.
6. LaBrecque, D. J. *Cross-borehole Resistivity Modeling and Model Fitting*. Ph.D. thesis, University of Utah, Salt Lake City, 1989.
7. Bard, Y. *Nonlinear Parameter Estimation*. Academic Press, San Diego, Calif. 1974, pp. 111–113.
8. Sasaki, Y. Model Studies of Resistivity Tomography Using Boreholes. Presented at the Society of Exploration Geophysicists International Symposium on Borehole Geophysics: Petroleum, Hydrogeology, Mining and Engineering Applications, Tucson, Ariz., Feb. 1990.
9. *Test Method 643*. Test Manual, Vol. 3. California Department of Transportation, Sacramento, 1978.

Publication of this paper sponsored by Committee on Pavement Monitoring, Evaluation, and Data Storage.

Long-Term Pavement Performance History of Sulfur-Extended Asphalt Test Roads in Eastern Province of Saudi Arabia

MADAN G. ARORA, ABDULAZIZ I. AL-MANA, ABDUL-HAMID J. AL-TAYYIB, REZQALLAH H. RAMADHAN, AND ZIAUDDIN A. KHAN

In 1978 the Metrology, Standards, and Materials Division of the Research Institute at King Fahd University of Petroleum and Minerals (KFUPM/RI) launched an in-house research study on sulfur-asphalt pavement development because sulfur produced in Saudi Arabia was available in abundance and the international price of paving asphalt was soaring because of the energy crisis. Among the various available techniques of substituting asphalt with sulfur, the sulfur-extended asphalt (SEA) paving technology developed by Gulf Canada was considered to be the closest to practical applications. Three SEA test roads were laid in the Eastern Province in cooperation with Gulf Canada and the Ministry of Communication (MOC), Saudi Arabia, as a part of the ongoing road development program of MOC. A sulfur/asphalt ratio of 30/70 by weight was used in Test Road 1 (Kuwait Diversion) and Test Road 3 (KFUPM), whereas a higher percentage of 45/55 was used in Test Road 2 (Abu Hadriyah Expressway). Performance of the three test roads has been monitored from time to time. For each test road, the control section using the normal asphalt concrete has shown a better performance than the SEA sections.

The Pavement Research Group of the Metrology, Standards, and Materials Division of the Research Institute, King Fahd University of Petroleum and Minerals (KFUPM/RI), Dhahran, Saudi Arabia, has been involved in design, construction, and monitoring of pavement conditions of three sulfur-extended asphalt (SEA) test roads as a part of an internal research project on sulfur-asphalt pavement development (PN15002). The project started in 1978 when sulfur produced in the kingdom as a by-product of the gas-gathering plants was available in abundance and was creating a disposal problem. Also, the energy crisis of the 1970s had significantly increased the cost of asphalt on a global market, and laboratory and field trials conducted in the United States and Canada proved sulfur to be a viable substitute for partial replacement of asphalt from both engineering and economic considerations (*1–3*). Of all the sulfur-based paving systems that were developed, the SEA type developed by Gulf Canada is the closest to a commercial application. Therefore, the KFUPM/RI entered into a joint venture with Gulf Canada to develop the SEA pavement technology within the kingdom.

Three full-scale SEA test roads were constructed between 1979 and 1982 as a part of the ongoing road development program of the Ministry of Communications (MOC), Kingdom of Saudi Arabia. The tasks pursued and the laboratory tests conducted to arrive at suitable mix designs have been reported elsewhere by Akili and Dabbagh (*4*), Akili and Uddin (*5*), Akili (*6*), Courval and Akili (*7*), and KFUPM/RI (*8*). Early performance results of the SEA test roads were reported by Akili and Arora (*9*).

This paper presents the long-term pavement performance history of the SEA test sections and compares their performance with the control sections composed of normal asphalt concrete (AC) specifications. The field data collection included traffic loads, pavement distress, surface roughness, skid resistance, and Benkelman beam and Dynaflect deflections. In addition, a number of cores were extracted periodically from the SEA and control AC sections and tested in the laboratory to evaluate the in situ percent air voids and mechanical properties, such as resilient modulus, split tensile strength, and fatigue resistance. The laboratory tests were performed at varying temperatures to determine the temperature susceptibility of the mixes. The results of the laboratory evaluation were used to interpret the observed pavement condition history of the SEA and control sections.

DESCRIPTION OF SEA TEST ROADS

The three SEA paving projects are located in the Eastern Province of Saudi Arabia near the towns of Dammam and Dhahran and were phased in with the ongoing MOC contracts. Pavement cross sections including sulfur/asphalt ratios used are shown in Figure 1. No substantial changes were introduced in design, materials, or construction procedures as a result of sulfur addition, except for the following:

1. A deliberate reduction in the base course thickness in one of the SEA sections of Test Road 2 to monitor the effect of thinning SEA pavement on performance and pavement life.
2. The addition of 1 percent portland cement to the SEA mix of Test Road 3, partially replacing its fine fraction. This was judged to be an expedient method of keeping the percent loss in a 24-hr Marshall stability within the specified limit.

Materials and Mix Design

The coarse aggregates used in the three paving projects were derived from shallow limestone beds, described at best as average in quality. The fine aggregates were a mixture of quartzitic dune sand and limestone crusher material ranging from about 5000 to 50 μm in diameter. A single asphalt type (60 to 70 pen grade) common to all three test roads was obtained from the Ras Tanura

Metrology, Standards, and Materials Division, Research Institute, King Fahd University of Petroleum and Minerals, Dhahran 31261, Saudi Arabia.

Refinery. The elemental sulfur added was a commercial grade with a minimum tested purity of 98 percent, a maximum carbon content of 1 percent, and a specific gravity of 1.977 at 23°C.

The Marshall method was used for the SEA mix design for all three test roads, as shown in Figure 2. Sulfur/asphalt (S/A) binders were prepared by blending heated sulfur and asphalt at a temperature of 140 ± 2°C by means of a high shear blender. Marshall briquettes were prepared in the normal manner with 75 blows per face. Table 1 shows the selected Marshall design data for the three test roads. Each result is an average of three separate determinations. The results of the SEA mixes followed the normal pattern except for somewhat higher stability exhibited compared with control samples, particularly at an S/A weight ratio of 45/55 for Test Road 2.

SEA Mix Production and Paving

The SEA mix production of Test Road 1 was accomplished with Société Nationale EIF Aquitane process and equipment. Gulf Canada process and equipment were deployed for the construction of SEA pavements of Test Roads 2 and 3. The two processes are similar in principles and use an add-on unit that blends hot sulfur and asphalt in desired proportions and delivers the blend to the pugmill. Methodology used is shown by a flow diagram in Figure 3. On all three test projects, blending of sulfur and asphalt resulted in homogeneous dispersion of minute sulfur particles in asphalt, as verified by periodic checks under a microscope. The construction steps in terms of transportation, placement, compaction, and quality control of all three SEA pavements were almost the same as those normally followed with conventional asphalt concrete pavements.

PAVEMENT EVALUATION SURVEYS

All three test roads are under periodic monitoring. The evaluation methodology used is shown in Figure 3 and briefly summarized as follows.

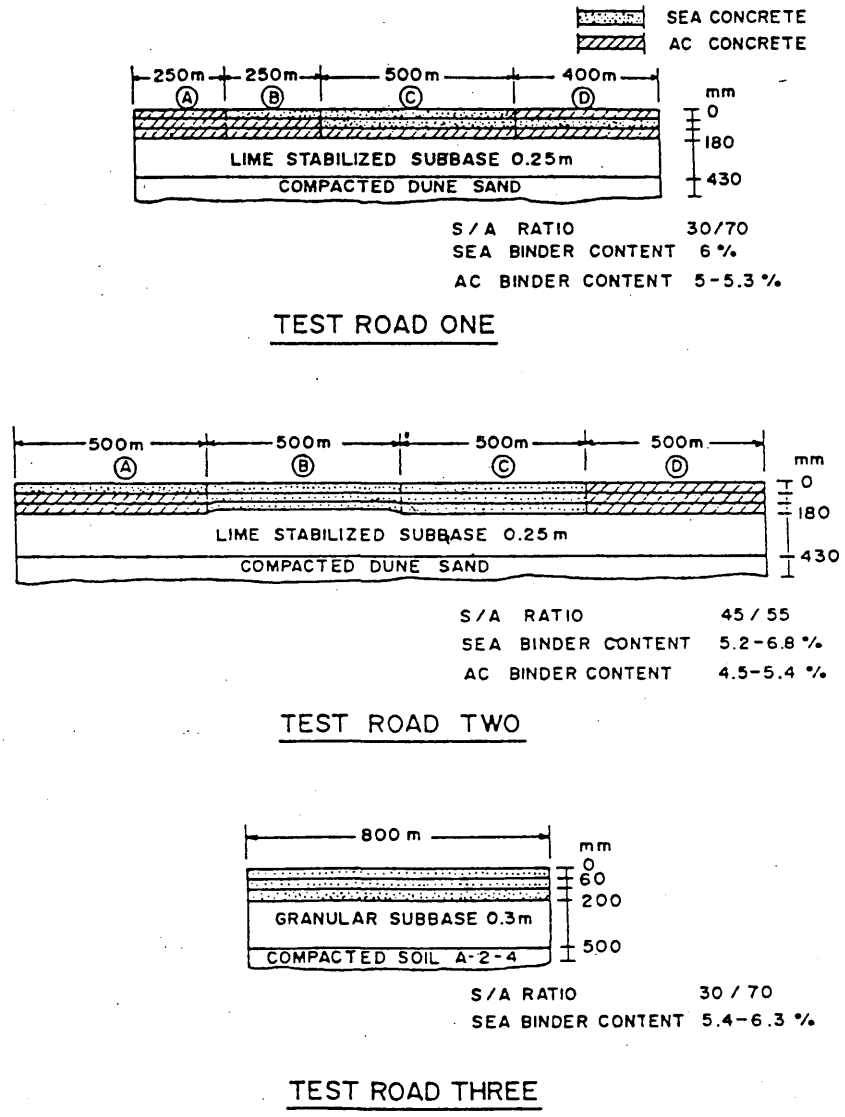

FIGURE 1 Pavement sections for three test roads.

Traffic Counts and Axle Load Survey

Traffic counts were made with manual counters as well as an automatic traffic counter. SEA Test Road 1 has an average daily traffic (ADT) of about 100 with 50 percent trailer truck traffic. Test Road 2 has very heavy traffic with an ADT of about 6,000 and 25 percent trucks. Test Road 3 has an ADT of about 3,000 with 5 percent light trucks. Axle loads of typical trucks operating on SEA Test Road 2 located on Abu Hadriyah Expressway were measured with the Trevor Deakin portable weighbridge designed by the Transport Research Laboratory (TRL), United Kingdom. About 26 to 72 percent of the loaded trucks were found to exceed the legal axle load limits set out by the MOC (*10*). Observed axle loads were converted into equivalent axle load applications of 8.2 tons and found to be about 5.5×10^6 applications per year for the slow lane (*11*).

Pavement Distress Survey

A distress survey for each test road was conducted following the method of pavement rating (PAVER) developed by the U.S. Army Corps of Engineers (*12*). Each SEA test section was divided into a number of sample units of 30-m length covering both lanes for SEA Test Roads 1 and 3. For the Abu Hadriyah Expressway, which was carrying very high traffic, the distress survey was conducted in the slow lane only, which was highly distressed. Severity was measured as low (L), medium (M), or high (H), whereas extent of distress was measured in linear meters or square meters, depending on the distress type as per the procedure of the U.S. Army Corps of Engineers (*12*).

Roughness and Skid Resistance Surveys

Pavement roughness was measured for Test Road 3 using the TRL bump integrator (*13*), which consists of a single-wheeled trailer that is towed on a wheel track at a speed of 32 km/hr. It measures the sum of the downward movements of the wheel relative to the trailer chassis produced by the unevenness in the pavement profile in the longitudinal direction. The integrated downward movement (in centimeters) divided by the distance traveled (in kilometers)

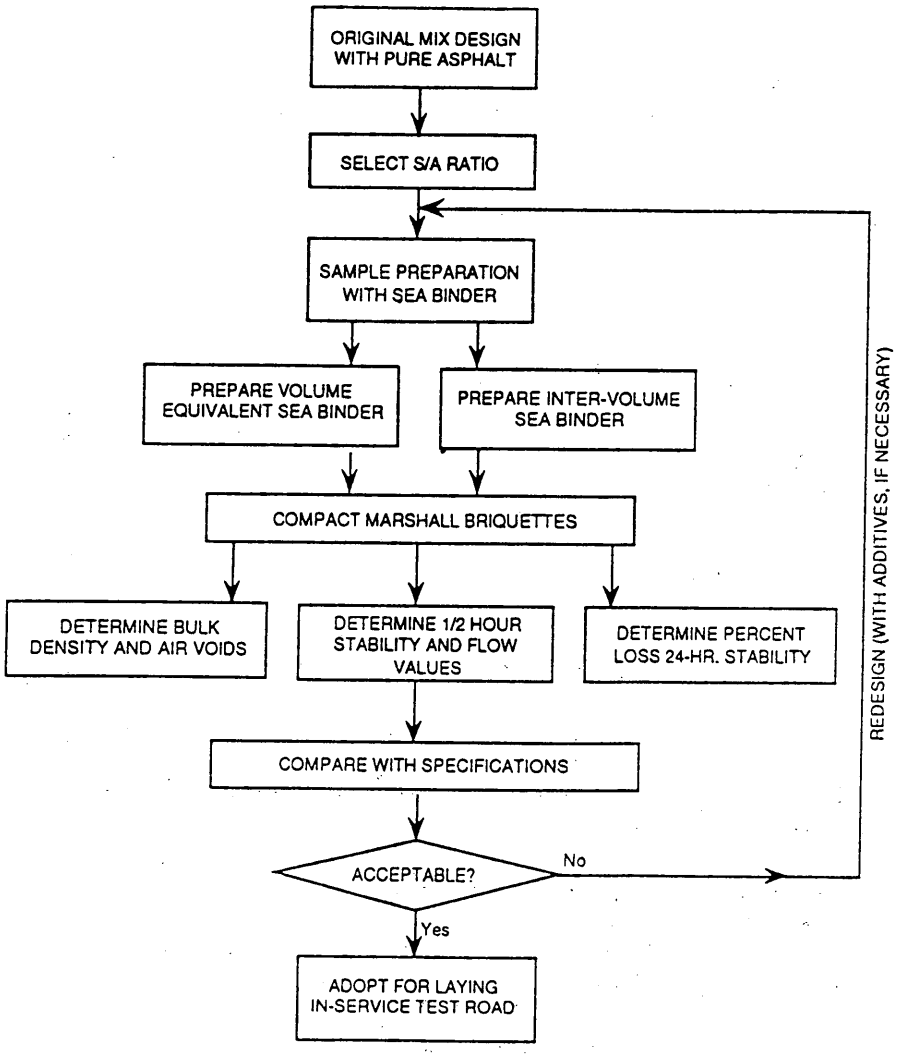

FIGURE 2 Flow chart showing Marshall method for SEA mix design.

gives the roughness of the pavement surface in centimeters per kilometer.

Skid resistance measurements were also made on Test Road 3 using the mu-meter following the procedure recommended by ASTM E670.

Deflection Surveys

Initially, the Benkelman beam rebound deflections (BBD) were measured along the outer wheelpath of the slow lane using the Western Association of State Highway Officials (WASHO) method (*14*). Test points were located 0.9 m from the pavement edge and at 20-m intervals along the entire pavement length. Pavement temperatures were also measured near the deflection points at a depth of 60 mm.

Later on, when Dynaflect was procured, the dynamic deflections were measured on Test Roads 2 and 3 using this equipment. Testing locations were selected at 0.9 m from the pavement edge at 50-m intervals. Pavement temperature was measured occasionally during the tests. The following parameters were computed for each test location from the five geophone deflection readings: Dynaflect maximum deflection (DMD) = D1 (reading of Geophone 1); surface curvature index (SCI) = D1 − D2; and base curvature index (BCI) = D4 − D5.

A significant correlation was observed between DMD and pavement mean temperature (T). On the basis of observed air and pavement temperatures in the Eastern Province of the kingdom, 35°C was selected to represent mean annual pavement temperature for the SEA test roads and the control AC sections. The following relationship was found to represent the temperature adjustment factor (TAF) for DMD at 35°C.

$$TAF = 1.658 - 0.0184T \quad R^2 = 0.9884, SE = 0.0138 \tag{1}$$

No adjustment was found necessary for SCI and BCI. By measuring DMD, SCI, and BCI, a qualitative analysis of the structural adequacy of pavement was obtained.

Field Coring and Testing

Field cores of 10-cm diameter were taken from the wheelpaths on the slow lanes of the test roads, initially upon the opening to traffic and later at periodic intervals. The following tests were performed on the cores.

Bulk Specific Gravity and Rice Maximum Specific Gravity and Percent Air Voids

ASTM D2726 and D2041 were used for these tests.

Resilient Modulus

Cores were tested for resilient modulus (M_R) in the split-tensile mode under dynamic loading (ASTM D4123). To determine the temperature susceptibility of SEA mixes, the tests were performed at various temperatures ranging from 5°C to 49°C. The resilient modulus was calculated from the following equation, assuming Poisson's ratio as 0.35.

$$\text{Resilient modulus (MPa)} = 618.3\ P/h \cdot d \tag{2}$$

TABLE 1 Marshall Laboratory Mix Design Data for Three Test Roads

Description	Composition S/A Ratio[a]	% Binder[b]	Bulk Density (g/cc)	Air Voids (%)	Marshall Stability (kN)	Marshall Flow (mm)
Test Road One-Wearing Course	0/100	5.0	2.345	3.5	12.05	1.9
	0/100	6.0	2.371	1.5	8.23	3.0
	30/70	5.25	2.380	3.8	19.95	2.7
	30/70	5.66	2.381	3.2	17.24	2.9
	30/70	6.10	2.394	2.2	9.60	2.5
Test Road Two-Base Course	0/100	4.5	2.341	4.6	18.54	2.1
	0/100	5.0	2.361	4.1	20.55	2.1
	0/100	5.5	2.348	3.9	15.53	2.5
	45/55	4.5	2.365	7.0	26.15	1.3
	45/55	5.2	2.366	6.2	26.28	1.8
Test Road Two-Wearing Course	0/100	5.5	2.385	6.3	15.16	3.8
	0/100	6.0	2.341	4.7	16.45	3.7
	0/100	6.5	2.341	3.2	13.03	3.9
	45/55	5.4	2.359	7.2	16.46	2.1
	45/55	6.0	2.357	6.4	16.29	2.4
	45/55	6.7	2.367	5.4	20.71	3.4
Test Road Three-Base Course	0/100	5.0	2.319	4.7	14.45	2.5
	0/100[c]	5.0	2.327	4.4	12.83	2.7
	30/70[c]	5.4	2.351	4.6	13.23	2.5
	30/70[c]	5.9	2.377	3.0	14.18	2.7
Test Road Three-Wearing Course	0/100	5.3	2.348	3.5	10.98	3.8
	1/100[c]	5.0	2.316	4.7	12.74	3.7
	30/70[c]	5.8	2.365	4.4	11.10	3.5
	30/70[c]	6.2	2.375	3.7	12.04	4.2

[a] *S/A ratio is weight percentage of sulphur and asphalt*
[b] *% binder refers to percentage binder by weight of total mix*
[c] *With one percent Portland cement by weight of aggregate*

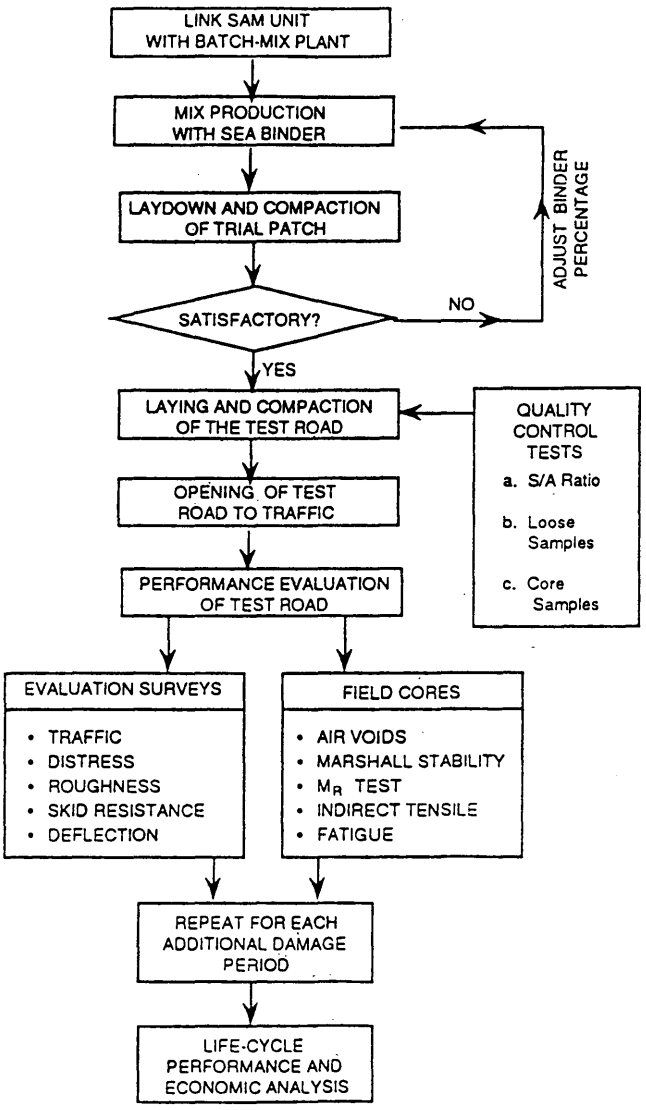

FIGURE 3 Steps involved in construction and evaluation of SEA test roads.

where

P = applied load (kN);
h = thickness of specimen (mm); and
d = recoverable horizontal deformation (mm).

Indirect Tensile Strength

Indirect tensile strength was carried out on a Marshall loading device at a loading rate of 50 mm/min. The load was applied on two opposite generators using stainless steel curved strips. The failure occurred instantaneously along the diametric plane at the maximum load sustained by the specimen. Cores were tested at room temperature and also at a low temperature of 5°C, simulating the local winter conditions when thermal cracking is more likely to occur.

Fatigue Resistance

Cores were tested in the split-tension mode using the dynamic loading equipment required for the M_R test. Initial elastic tensile-strain levels in the range of 55 to 130 μm were applied, and load was held constant until fracture occurred. The number of load repetitions to failure was recorded for each core. The test was performed at 35°C, which represents the mean annual pavement temperature for this region.

DISCUSSION OF RESULTS

Pavement Distress

Pavement distress data were analyzed to determine the most frequently occurring distress types and the pavement condition index (PCI). The PCI is a measure of a pavement's structural integrity and operational condition. Predominant distress types, considered here as those occurring in more than half the number of selected sample units in a section, are listed in Table 2. The SEA sections mostly developed longitudinal/transverse cracking in Test Road 1; alligator cracking and block cracking in Test Road 2; and block cracking and longitudinal/transverse cracking in Test Road 3. Some of these distresses are shown in Figures 4 through 6. On

TABLE 2 Predominant Distress Types Observed in Three Test Roads

Predominant Distress Types	Percentage of Selected Sample Units Showing Predominant Distress Types					
	Test Road One		Test Road Two		Test Road Three	
	SEA	AC	SEA	AC	SEA	AC
Alligator Cracking	–[a]	–	100	–	–	–
Block Cracking	–	–	80	–	63	–
Longitudinal/ Transverse Cracking	60	100	–	–	63	–
Polished Aggregate	–	–	–	100	–	65

[a] *Not predominant*

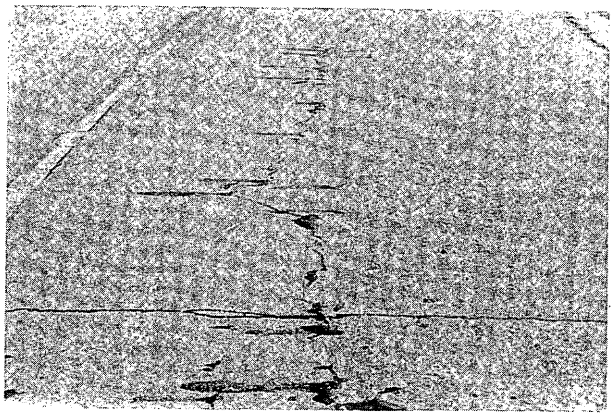

FIGURE 4 Typical longitudinal transverse cracking in SEA section of Test Road 1 (Kuwait diversion).

the control AC sections, the most predominant distress types were found to be longitudinal/transverse cracking and polished aggregate. Although alligator cracking is the load-associated distress and considered to be an indicator of structural deficiency, block cracking and transverse cracks are the climate-associated cracks caused by thermal stresses.

Table 3, which summarizes the pavement evaluation survey results, shows the latest (1993) PCI for each test road. The PCI variation with time for Test Road 3 is shown in Table 4. For each test road, the control section's PCI is higher than that of the corresponding SEA sections. The PCI of the control AC section varies from 85 to 98, indicating a very good to excellent pavement condition. The lowest PCI (41) is found for SEA Section B of Test Road 2, which indicates a fair pavement condition. The other two SEA sections of Test Road 2 are also characterized by lower PCIs compared with those of the SEA sections of Test Roads 1 and 3. Lower PCIs may be attributed to a much higher traffic loading on Test Road 2 and to the reduction in base course thickness in Section B. This is also corroborated by the presence of alligator cracking, which was observed only in the SEA sections of Test Road 2 because this distress type is known to be load-associated distress.

FIGURE 5 Typical alligator cracking in SEA Section B of Test Road 2 (Abu Hadriyah Expressway).

Pavement Roughness and Skid Resistance

Average roughness values of 170 cm/km and 150 cm/km were obtained for Test Road 3 for SEA and control AC sections, respectively, and are considered acceptable for riding quality. Similarly, average wet mu skid numbers of 62 and 73 were obtained for Test Road 3 for 300-m segments of SEA section and control AC section, respectively, which are also considered acceptable.

Pavement Deflection

The 85th-percentile deflection results are summarized in Table 3. Although the criteria used to interpret the deflection results are based on general rules of thumb, nevertheless they do provide relative measures of structural adequacies of the various test sections in question. The following observations were made from Table 3.

1. Benkelman beam deflections indicate lower BBD values for the control AC sections compared with the corresponding SEA sections. According to Lister (*15*), pavement life may be related to Benkelman beam deflection as follows:

$$\text{Life} \propto 1/(\text{deflection})^3 \quad (3)$$

Section B of Test Road 2, having the highest deflection, indicates the lowest life.

2. DMD values for Test Roads 2 and 3 indicate a trend similar to that observed for Benkelman beam deflections. DMD values of Test Road 2 are about 1.5 to 2 times those of Test Road 3, indicating lower structural capacity of Test Road 2. Further, like BBD, the DMD is the highest for SEA Section B of Test Road 2.

3. SCI, which is inversely proportional to the pavement upper-layer elastic modulus, is found to be the highest for Section B of Test Road 2, indicating the lowest elastic modulus of SEA layer for this section. Further, since the SCI of this section is greater than 6.25 μm, according to Teng and Sheffield (*16*), its SEA pavement layer is weak and needs an overlay. Distress survey results confirm this to be the worst section, characterized by the lowest PCI and fair pavement condition. SCI values of other SEA sections of Test Road 2 are also high, being about six to

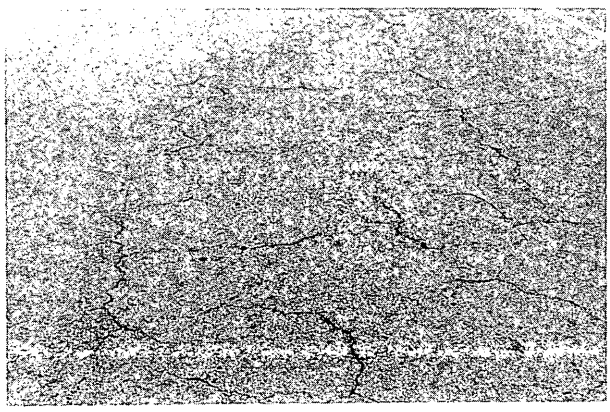

FIGURE 6 Typical block cracking in SEA section of Test Road 3 (KFUPM).

TABLE 3 Summary of Pavement Evaluation Survey Results for Three Test Roads

Item	Test Road One				Test Road Two				Test Road Three	
	AC(A)[a]	SEA(B)	SEA(C)	SEA(D)	SEA(A)	SEA(B)	SEA(C)	AC(D)	SEA	AC
PCI(%)	98	85	89	91	56	41	62	85	80	92
BBD(μm)	294	356	339	313	282	438	334	232	280	186
DMD (μm)	_[b]	–	–	–	13.72	14.48	11.94	13.21	8.64	6.35
SCI(μm)	–	–	–	–	4.93	9.02	3.86	4.90	0.61	1.68
BCI(μm)	–	–	–	–	1.19	0.66	1.47	1.50	0.48	0.58
Field Cores: Air Voids (%)	4.96	–	7.87[c]	–	–	–	9.28[c]	7.08	3.96	4.92
Field Cores: Resilient Modulus (1000 MPa), Room Temp (23°C)	11.20	–	11.83[c]	–	–	11.66[c]	–	11.35	7.30	5.95
Field Cores: Indirect Tensile Strength (KPa), Low Temp (5°C)	2129	–	1840[c]	–	–	1800[c]	–	–	2005	2263

[a] *AC Section A*
[b] *Not available*
[c] *Average value for SEA sections*

TABLE 4 Variation of Pavement Characteristics with Age for Test Road 3

Characteristics	Test Section	Year					
		1982[a]	1984	1986	1989	1991	1993
PCI (%)	SEA	100	_[b]	–	85	81	80
	AC	100	–	–	–	95	92
Field Cores: Air Voids (%)	SEA	5.15	4.12	3.96	3.96	–	–
	AC	–	6.50	4.92	6.68	–	–
Field Cores: Resilient Modulus (MPa), Room Temp (23°C)	SEA	2450	5760	7300	9980	–	10500
	AC	–	5110	5950	8860	–	–
Field Cores: Indirect Tensile Strength (KPa), Room Temp (23°C)	SEA	1021	1419	1405	1393		
	AC	–	1625	1732	1809	–	–

[a] *As constructed*
[b] *Not available*

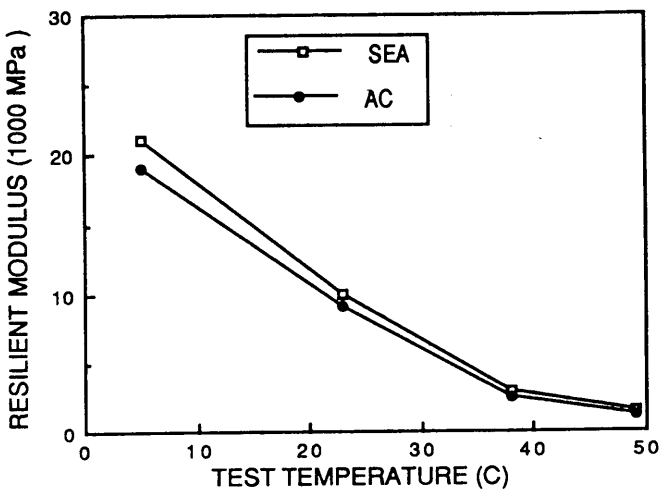

FIGURE 7 Effect of temperature on resilient modulus of field cores extracted from Test Road 3.

eight times those of Test Road 3. This trend may be attributed to load-associated alligator cracking observed in Test Road 2 as discussed earlier and shown in Table 2.

4. BCI values shown in Table 3 are indicators of subgrade strength. According to Teng and Sheffield (*16*), BCI values greater than 3.75 μm indicate a weaker subgrade. Because low BCI values are encountered for both Test Roads 2 and 3, strong subgrade conditions exist for these roads.

Field Core Properties

The average core properties presented in Tables 3 and 4 and Figures 7 and 8 are discussed.

Percent Air Voids

Percent air voids for the three test roads as determined from the cores extracted in 1986 are presented in Table 3. For SEA sections, the air voids range from 3.96 to 9.28 percent, compared with 4.92 to 7.08 percent for the control AC sections. Table 4 shows the percent air void variation with time for Test Road 3. There has been a consistent decrease in air voids for the SEA section, which may be attributed to further densification of the SEA layer under traffic.

Resilient Modulus

M_R values determined at room temperature (23°C) from 1986 cores are presented in Table 3 for the SEA and control AC sections of the three test roads. M_R values for the SEA sections ranged from 7300 to 11 830 MPa and are somewhat higher than those of the corresponding AC sections.

Table 4 shows a gradual increase in M_R values with age for SEA and AC sections of Test Road 3, which may be attributed to the combined effect of hardening of the binder and densification of the mix under traffic.

The effect of temperature on M_R studied on the 1989 cores from Test Road 3 is shown in Figure 7. As expected, M_R decreased with an increase in test temperature. The decrease is more significant in the temperature range of 5°C to 38°C and much less significant in the range of 38°C to 49°C. The above figure also shows that the temperature susceptibility of M_R is approximately similar in magnitude for both the SEA and AC mixes. In fact, the SEA cores showed somewhat higher stiffness at a low temperature of 5°C and almost similar stiffness at a high temperature of 38°C. These values are contrary to the requirement of an ideal mix, which should show less stiffness at low temperature to avoid cracking and an increased stiffness at high temperature to avoid rutting.

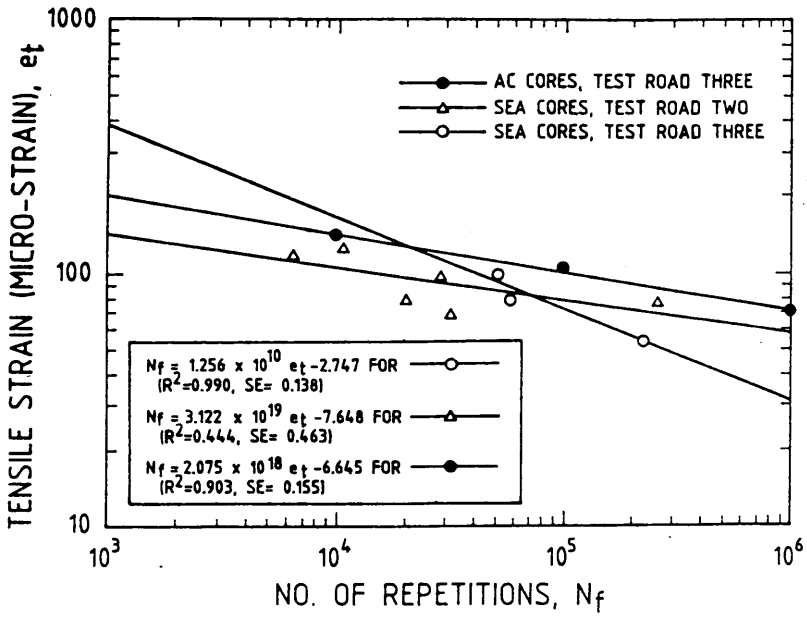

FIGURE 8 Fatigue resistance at a test temperature of 35°C.

Indirect Tensile Strength

Table 4 shows a variation in indirect tensile strength of cores taken from Test Road 3 during the period 1982 to 1989, as tested at room temperature (23°C). An increase in strength with age was noticed, particularly in the initial years after construction. Further, the SEA cores have shown somewhat lower tensile strength than the control AC cores. Low temperature (5°C) results, summarized in Table 3, also indicate lower tensile strength (by 11.4 to 13.5 percent) for SEA cores, which explains the greater extent of thermal cracking, in terms of block cracking and transverse cracking, observed in the SEA test sections in field.

Fatigue Resistance

Figure 8 shows the fatigue resistance of SEA and AC cores of Test Roads 2 and 3. For tensile strains of about 100 μm as expected under heavy traffic loads, the fatigue resistance of SEA cores is found to be lower than that of the AC cores. This explains the reason for early fatigue carcking in the form of alligator cracking observed in the SEA sections of Test Road 2.

CONCLUSIONS

Following are the major interim conclusions drawn from the pavement performance evaluation surveys of the three SEA test roads conducted to date. The evaluation surveys will continue until final conclusions are made on the life-cycle performance and economic viability of SEA pavement technology in Saudi Arabia.

1. The most predominant distress manifestations in the SEA test sections are the load-associated alligator cracking and the climate-associated block cracking and transverse cracking. Greater incidence of cracking is observed in the SEA sections than in the control AC sections.
2. The pavement distress condition rating characterized by PCI shows a lower rating for the SEA sections. SEA Section B of Test Road 2 on Abu Hadriyah Expressway has the lowest PCI of 41, indicating a fair pavement condition and an urgent need for an overlay. For this section, the SEA base course thickness was deliberately reduced by 20 percent to verify whether thickness reduction was possible with SEA pavement.
3. Roughness and skid resistance surveys conducted for Test Road 3 show acceptable values for both the SEA and control AC sections.
4. Dynaflect deflection surveys of Test Roads 2 and 3 show low BCI values in the range of 0.48 to 1.50 μm, indicating strong subgrade support conditions for the test roads. The very high SCI of 9.02 μm observed for Section B of Test Road 2 indicates a deteriorated condition of the SEA pavement layer of this section. This is also corroborated by the pavement distress survey that yielded the lowest PCI for this section.
5. Laboratory characterization of field cores extracted from SEA and control AC sections reveal lower indirect tensile strength and lower fatigue resistance of SEA cores. Lower tensile strength may be the cause of block cracking and transverse cracking observed in the SEA sections of the three test roads. Similarly, lower fatigue resistance may be the cause of alligator cracking observed in the SEA sections of the heavily trafficked Test Road 2.

ACKNOWLEDGMENTS

The authors acknowledge the support of the Ministry of Communications, Kingdom of Saudi Arabia; Gulf Canada; and the Research Institute of the King Fahd University of Petroleum and Minerals for this internally funded research work. Contributions from the Civil Engineering Department, particularly from W. Akili and H. I. Al-Abdul Wahhab, are greatly appreciated.

REFERENCES

1. Kennepohl, G. J. A., A. Logan, and D. C. Bean. Conventional Paving Mixes with Sulfur Asphalt Binders. *Proc., Association of Asphalt Paving Technologists*, Vol. 44, 1975.
2. Gallaway, B. M., and D. Saylak. *Sulfur/Asphalt Mixture Design and Construction Details—Lufkin Field Trials*. Report FHWA-TS-78-203. FHWA, U.S. Department of Transportation, Washington, D.C., 1976.
3. Frank, R. P., E. T. Meyer, G. J. Hignell, A. Kennepohl, and R. C. G. Haas. Temperature Susceptibility Evaluation of Sulfur Asphalt Mixtures. *Proc., Association of Asphalt Paving Technologists*, Vol. 46, 1977.
4. Akili, W., and A. E. Dabbagh. The Middle East—A Potential Market for Sulfur Asphalts and Concretes. *Proc., Sulfur-81*, Calgary, Alberta, Canada, 1981.
5. Akili, W., and W. Uddin. A Sulfur-Extended Asphalt Test Road in Eastern Saudi Arabia. *Proc., 3rd Conference of Road Engineering Association of Asia and Australia*, Taipei, 1981.
6. Akili, W. Laboratory Characteristics of Sulfur-Bitumen Sand Mixtures. *Proc., 11th Conference of Australian Road Research Board*, Part 3, Australia, 1982.
7. Courval, C. J., and W. Akili. Sulfur Asphalt Binder Properties Determined by the Sliding Plate Rheometer. *Proc., Association of Asphalt Paving Technologists*, Vol. 51, 1982.
8. KFUPM/RI. *Sulfur-Extended Asphalt (SEA) Road Experiment on Dammam-Abu Hadriyah Expressway—Construction and First Three-Year Performance*. Research Report PN 15002. Research Institute, King Fahd University of Petroleum and Minerals, Dhahran, Saudi Arabia, 1985.
9. Akili, W., and M. G. Arora. Early Performance Results of Sulfur-Extended Asphalt (SEA) Pavements in Saudi Arabia. 1st Saudi Engineers Conference, Jeddah, 1984.
10. Abdulghani, K., M. G. Arora, F. Balghunaim, F. Bayomy, and D. Pearson-Kirk. Taxation Model for Road Vehicles in Saudi Arabia. In *Transportation Research Record 1305*, TRB, National Research Council, Washington, D.C., 1991.
11. Arora, M. G., and F. Saleem. Structural Evaluation of Asphalt Pavements in the Eastern Province of Saudi Arabia. *Proc., Sixth International Conference on Structural Design of Asphalt Pavements*. Ann Arbor, Mich., 1987.
12. *Pavement Maintenance Management for Roads and Parking Lots*. Technical Report M-294. U.S. Army Corps of Engineers, 1981.
13. Jordan, P. G., and J. C. Young. *Developments in Calibration and Use of the Bump-Integrator for Ride Assessment*. TRRL Laboratory Report SR 604. U.K. Transport and Road Research Laboratory, Crowthorne, Berkshire, England, 1980.
14. Yoder, E. J.. Flexible Pavement Deflection-Methods of Analysis and Interpretation. *Proc., Association of Asphalt Paving Technologists*, Vol. 31, 1962.
15. Lister, N. W. *Deflection Criteria for Flexible Pavements*. TRRL Laboratory Report 376. Transport and Road Research. U.K. Crowthorne, England, 1972.
16. Teng, T. C., and J. P. Sheffield. *Pavement Rehabilitation Using Dynaflect Data*. Final Report. Mississippi State Highway Department, 1981.

Publication of this paper sponsored by Committee on Pavement Monitoring, Evaluation, and Data Storage.

Prediction of Tire-Road Friction from Texture Measurements

W. O. YANDELL AND S. SAWYER

A purely theoretical means for predicting tire-road friction has been the subject of research for the past two decades. It is based on a faithful simulation of a pneumatic tire sliding over the wet texture of the road surface. This involved the stress-gross strain analysis of the tread rubber, the effect of shear rate, heat, and lubrication. A device called the Yandell-Mee texture friction meter is described and is the end product of this research. When placed on a road surface, it samples a total texture profile 60 cm long to an accuracy of 0.05 mm and predicts side force and locked-wheel wet friction for three speeds in seconds. Because the result varies only with texture changes, this is an excellent control tool for pavement engineers.

A study has been under way since 1968 of the part played by surface texture on tire-road friction (*1–12*). Much of the work was influenced by that of Tabor (*13*) and Kummer and Meyer (*14*). It was assumed that tire-road friction was caused by hysteretic energy loss in the tread rubber as it flowed over the road surface texture and that intermolecular adhesion would not occur on wet roads. Yandell (*3*) summarized some of the basic elements involved in hysteretic sliding friction and the change in microtopology of road surfaces in service. In that paper (*3*) the principles of the mechano-lattice stress-strain analysis for gross deformations used in the prediction of hysteretic friction from one texture parameter—the average absolute slope—were shown. It was also shown how the friction of small stone surfaces lubricated with liquids of various viscosities sliding on tread rubber could be predicted in the laboratory.

Before the mechano-lattice stress-strain analysis can be used, the damping and resilient properties of the tread rubber as they vary with strain, rate of strain, and temperature must be known. This work was performed by Zankin and Yandell (*11*) using a temperature-controlled apparatus capable of measuring damping in rubber sliding at up to 80 km/hr. Taneerananon and Yandell (*10*) modified Reynold's equations for sliding and sinkage to use with the mechano-lattice stress-strain analysis so that masking water film thicknesses could be determined.

The authors' friction prediction was based on the concept that a profile of the road surface texture could be broken up into a number of components ranging from coarse to fine. Although large volumes of rubber were expending energy as they flowed over the coarsest scales, smaller shallower volumes of rubber simultaneously expended energy as they flowed over the finer scales of texture. The total hysteretic friction was the sum of frictions generated on each scale of texture. The friction on a scale was a function of the effective damping factor of the rubber and the average absolute slope of that scale. The damping factor is the energy lost divided by the energy applied in deforming rubber in a load-unload operation (*3*). The average absolute slope is a function of texture roughness.

The next stage in the development of a system for predicting wet friction from road surface texture involved measuring the texture of a number of roads of diverse surface texture with either bituminous or concrete surfacing (*12*). The coarse texture was measured with a profile former (row of needles), the fine texture by a Ziess light section microscope. The total texture was divided into four scales. The dry hysteretic friction was determined from the average absolute slope of that scale of texture and the damping factor of the tread rubber using the mechano-lattice analysis (*12*). The coefficients of wet sideways force and locked-wheel braking friction for speeds of 16, 48, and 80 km/hr were computed and compared with predicted values measured by a multimode friction measuring truck. An example of a correlation for locked-wheel braking is shown in Figure 1. The *R*-squared value was 0.7. This process, although reasonably accurate, was clumsy and time consuming. Accordingly a portable device that would do the same job in seconds was devised. It was called the Yandell-Mee (Y-M) texture friction meter. Mee designed the circuit boards and wrote the Pascal programs that controlled the original meter's operation. The meter simulates the behavior of a smooth pneumatic passenger car tire traveling on a wet pavement. A later version (Mark 2) of the Y-M texture friction meter was developed with the assistance of S. Sawyer and will now be described.

Y-M TEXTURE FRICTION METER MARK 2

The first portable Y-M texture friction meter was built under the sponsorship of Pavement Management Services, Ltd., in Sydney. This company incorporated it in their Australian Road Evaluation Vehicle with which friction measurements were made simultaneously with other pavement characteristics in Australia and Indonesia. The Y-M texture friction meter Mark 2 was developed from the Mark 1 model at the University of New South Wales (NSW) with the NSW State Road Authority's financial support. Mark 2 is superior to Mark 1 in that it is operator independent, has a texture profile sample 60 cm long, is surface brightness independent, and is faster.

General Description

The portable instrument has two main components: the compact surface texture measuring unit and the personal computer (PC) with screen that controls the entire operation. Figure 2 is a summarized flowchart showing the operation of the device. The following parts of the flowchart are described.

School of Civil Engineering, University of New South Wales, P.O. Box 1, Kensington, N.S.W. 2033, Australia.

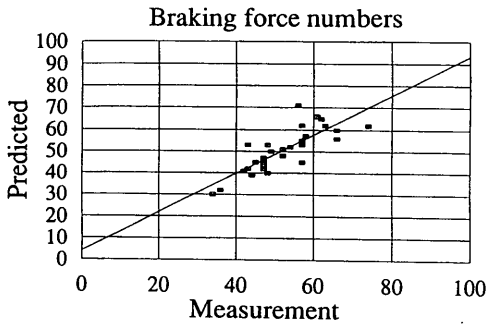

FIGURE 1 Braking force numbers at 48 km/hr versus those predicted from texture measured by light section microscope and profile former in 1982. $R^2 = 0.67$.

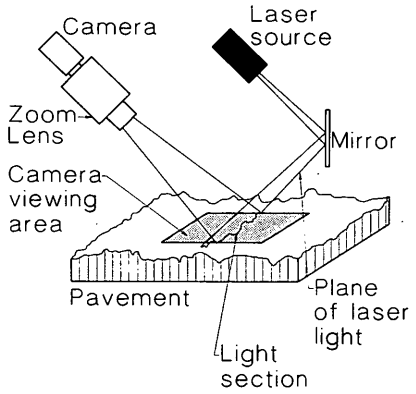

FIGURE 3 Schematic view of Y-M texture friction meter texture measurement.

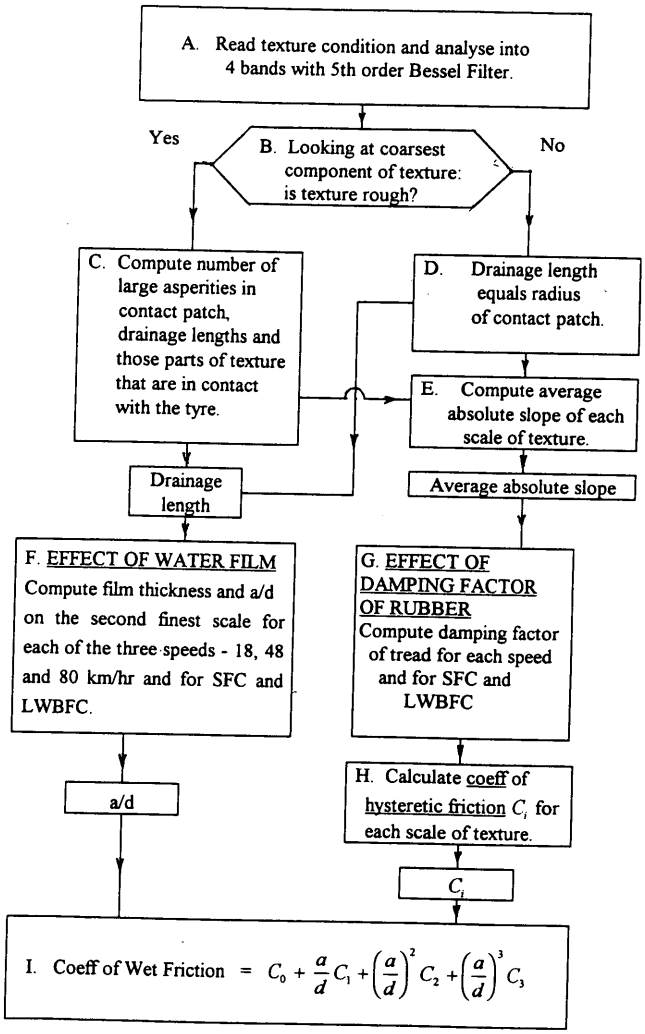

FIGURE 2 Simplified flow chart showing operation of the Y-M texture friction meter.

A. The profile 60 cm long is read with an accuracy of 0.05 mm by means of a black-and-white video camera viewing the image of a laser line projected at an angle onto the surface (Figure 3). Any gaps in the profile are filled in. This profile, recorded digitally as 12,000 ordinates, is divided into four bands with a fifth-order Bessel filter.

B. If the average absolute slope of the coarsest component is greater than an arbitrary 0.1, the surface is regarded as "rough" and the program goes to C for drainage path length computation. If the surface is "smooth," the program goes to D where a longer drainage path is computed.

C. The number of large asperities in the hypothetical contact patch of the tire on the rough surface—that part of the texture in contact with the tire and the drainage path lengths—is computed. Then move to E and F.

D. The drainage path length on the smooth surface is assumed equal to the radius of the contact patch. Then move to E and F.

E. The average absolute slope of the texture is computed of that part of each scale that is in contact with the tire. (The average absolute slope of the two sides of an equilateral triangle, for example, is $\sqrt{3}$.)

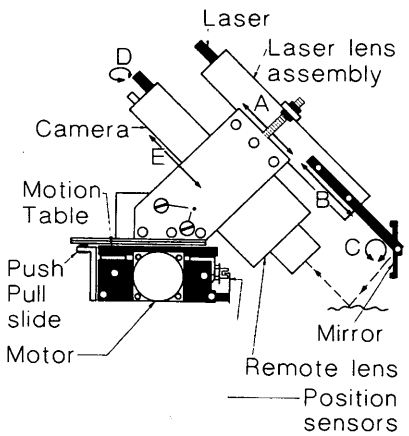

FIGURE 4 Side view of the laser camera carriage on the motion table.

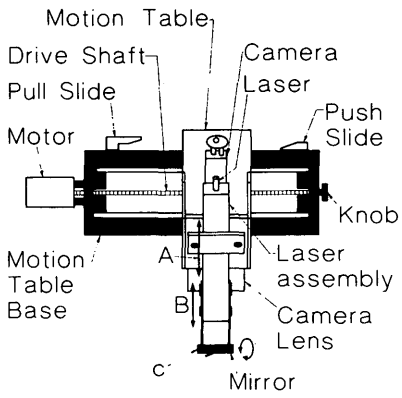

FIGURE 5 Plan view of the laser camera carriage on the motion table.

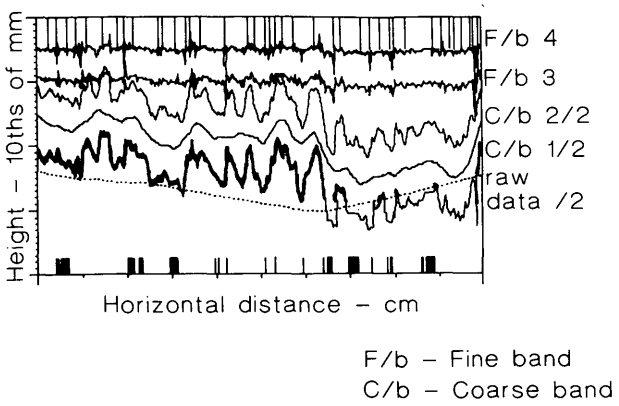

FIGURE 7 Monitor view of the total recorded texture and its four components.

F. The average water film thickness and the ratio of *a/d* is computed: *a* is the asperity height *d* of the second-finest scale of texture minus the water film thickness. This is done for each of the speeds (18, 48, and 80 km/hr) and for the sideways force coefficient and the locked-wheel braking force coefficient. Then move to I.

G. The damping factor of the rubber is determined for each of the three speeds of sliding and for sideways and for locked-wheel friction. The effect of temperature rise during locked-wheel braking is accounted for. Zankin and Yandell (*11*) provided this information.

H. The coefficient of dry hysteretic friction C_i is calculated for each scale of texture using the damping factor of the rubber and the average absolute slope of that scale of texture to give C_0, C_1, C_2, and C_3.

I. The coefficient of wet (not flooded) hysteretic friction is equal to the sum of the coefficients of dry hysteretic friction, each modified by the effect of surface water film, thus

$$\text{Coefficient of wet friction} = C_0 + \frac{a}{d} C_1 + \left(\frac{a}{d}\right)^2 C_2 + \left(\frac{a}{d}\right)^3 C_3$$

where

a/d = film thickness ratio from F;
a = height of the coarsest component of "microtexture" not masked by the water film;
d = average depth of the coarsest component of microtexture; and
C = coefficients of hysteretic friction computed from average absolute slope and tread damping factor using the mechano-lattice analysis (*10*). The expression is Taneerananon's hypothesis.

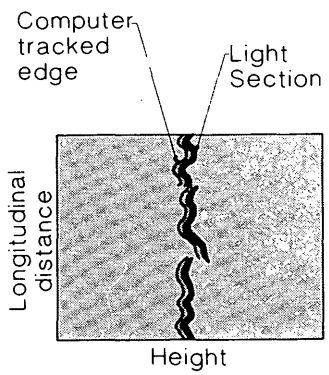

FIGURE 6 Monitor view of a laser image tracked by the computer.

Texture Measuring Device

The texture measuring device is housed in a lightweight case measuring 40 × 50 × 40 cm. A slot in the base of the case allows the laser to be projected onto the road surface and viewed by the video camera from inside the case. This portable unit is connected by a long cable to a 486 Compac PC that controls the operation. The components of the texture measuring device are the laser source, the camera, and the laser-camera transport.

Transport

The laser and the camera are fitted to a cross carriage that is sequentially moved into three alternative positions by fixed slides

PLACE: DESCRIPTION:		SURFACE: CHAINAGE:	AC 0.60 mm
Av. texture depth:	.456 mm. Std. Dev:	Pk. texture depth:	137 mm.
SPEED	LOCKED WHEEL FRICTION	SIDEWAYS FORCE FRICTION	
10mph (16kph)	.567	.589	
30mph (48kph)	.543	.568	
50mph (80 kph)	.523	.521	

Edit Mondo Data	Files	The Works
Take a Measurement	Print Report	Change Screens
Calculate friction	Adjust Video	Special Operations
Quit to DOS		

Esc=main menu Ctrl-t=T1 me/date F1=Erase line F2=Restore line F3=Full Edit

FIGURE 8 Main display of menu and output.

Yandell Mee Friction Device Results

Date: 25 Jul 1989
Time: 2.32

Client: Case study City Council
Id Number: 009
Place: Parkinson Ave from Cominara Parkway to Hart St
Surface: AC
Description: 10 metre intervals 1 metre from kerb

Chainage Km	Texture Depth mm	Locked Wheel Friction 10mph	30mph	50mph	Sideways Force Friction 10mph	30mph	50mph
0.00	.606	.461	.383	.369	.661	.618	.590
0.01	.564	.428	.349	.333	.658	.615	.586
0.02	.588	.458	.379	.364	.658	.615	.586
0.03	.580	.488	.403	.389	.702	.656	.626
0.04	.617	.532	.443	.430	.760	.714	.683
0.05	.559	.438	.360	.344	.634	.590	.561
0.06	.551	.466	.384	.369	.673	.628	.598
0.07	.547	.403	.335	.321	.577	.539	.514
0.08	.561	.392	.324	.310	.564	.525	.500
0.09	.566	.437	.358	.341	.636	.590	.560

FIGURE 9 Example of output block file (short form).

situated at each end of the main slide. The main carriage carrying the cross slide is driven by a motor through a lead screw for a distance of 20 cm as shown in Figures 4 and 5. In this way, three parallel profiles each 20 cm long can be recorded automatically in one operation.

Laser Source

The laser source is a 5-mw, 670-nm laser diode. Its fine cylindrical beam is changed to a flat knife by passing it through a cylindrical lens. It impinges on a mirror, which reflects it onto the road surface in view of the video camera. See Figures 4 and 5.

Camera and Lens

The black-and-white video camera views the laser line impinged on the road surface through powerful magnifying lenses. The laser beam and the line of sight of the camera are mutually at right angles so the line is always in focus. The aperture of the lens is adjusted automatically. The magnification of the lens is such that 1 cm of the surface is viewed at a time.

Client: Case study City Council — The Yandell-Mee Friction Texture Meter

Id. No.: 003 | File: 478003 pnt | Time: 17:13 | Date: 25 Jul 1989

Place: Parkinson Ave from Cominara Parkway to Hart St
Description: 10 metre intervals 1 metre from kerb
Surface: AC
Chainage: 6,000 km

Texture depth: .551 mm — Pk. texture depth: .878

Speed	Locked wheel friction	Sideways force friction
10mph (16kph)	0.468	0.673
30mph (48kph)	0.384	0.628
50mph (80kph)	0.369	0.598

Intermediate Result Summary for Current Measurement

Number of asperities in sample = 13
Weight per asperity = 10.76923lb
Texture depth = 1.02558mm
Max water holding depth (d1) = 0.01791ins
Film thickness ratios for speeds 10.30,50mph
1. Locked wheel 0.95120 0.94226 0.93668
2. Sideways force 0.96427 0.93691 0.91792

Absolute slope of frequency bands 1(coarsest) to 4(finest)
0.15493 0.38320 0.40388 0.35559

Partial friction coefficients for frequency bands 1 to 4

1. Locked wheel at 10mph:	0.0640	0.2176	0.2368	0.1933	Sum = 0.7117
2. Locked wheel at 30mph:	0.0639	0.2170	0.2362	0.1928	Sum = 0.7099
3. Locked wheel at 50mph:	0.0667	0.2291	0.2495	0.2034	Sum = 0.6820
4. Sideways force (spd.ind):	0.0645	0.2194	0.2388	0.1949	Sum = 0.7176

FIGURE 10 Example of output point file.

Computer Operation and Output

The texture measuring device is placed on the road. Upon initiation, the computer quickly tracks the edge of the laser line to give a profile of texture 10 mm long, as shown in Figure 6. Of these profiles, 60 are sequentially shown on the monitor and recorded while the carriage is automatically transported 1 cm at a time. Once the profile data are stored in the PC, the processing is effected as described earlier. The 60 parts of the profile are accurately connected and missing pieces are filled in. All the ordinates are divided by $\sqrt{2}$ to give the vertical resolution of the 45-degree view of the profile.

Figure 7 shows the total texture and its four components as shown on the monitor screen. Figure 8 shows the main screen display with coefficient of friction values, average and peak texture depths, and the menu for other operations. The inappropriate three decimal places will be modified to a more appropriate accuracy.

The contents of other files also can be shown on the screen or printed, or both. For example, Figure 9 is an example of a block file showing the chainage, texture depth, and locked-wheel and sideways force friction for any number of readings along a road. Figure 10 is an example of a point file that gives the six friction readings plus film thickness ratios and dry hysteretic friction values.

CORRELATION WITH DIRECTLY MEASURED FRICTION

A large number of devices that measure pavement friction directly with a test tire are available. There is seldom complete agreement between any two that measure friction on the same surfaces. For example, a runway friction tester (B. Miley, Florida Department of Transportation, unpublished data) and a pavement friction tester yielded an R-squared value of 0.02 for readings on about 25 wet open-graded textured roads using ribbed tires and an R-squared value of 0.75 on a large variety of wet asphalt surfaces using a smooth tire. Whitehurst (*15*) showed a 30 percent variation among seven different ASTM skid trailers reading identical surfaces. There are many reasons for this lack of agreement, among which are the vagaries of tread rubber behavior.

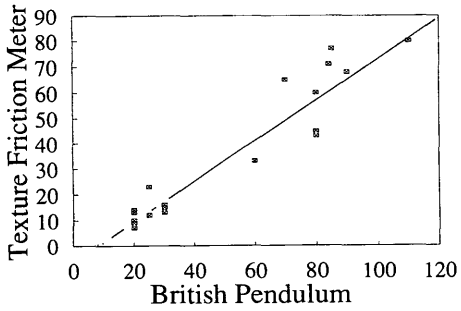

FIGURE 11 Relationship between friction numbers predicted with Y-M texture friction meter: braking force number at 16 km/hr and British pendulum numbers on rolled asphalt and floor tile surfaces, R^2 = 0.9.

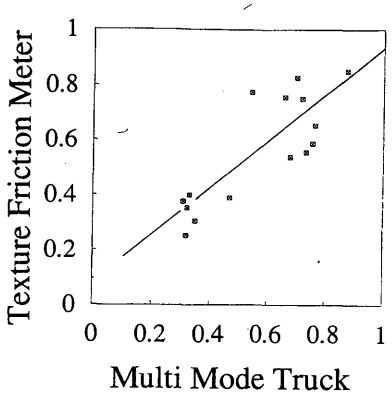

FIGURE 12 Relationship between friction coefficients predicted with the Y-M texture friction meter: sideways force coefficient at 48 km/hr and that measured by a friction test truck, R^2 = 0.7.

Relation Between Y-M Texture Friction Meter and Direct Measurement

A British pendulum friction tester and a Y-M texture friction meter were used to measure the friction on a number of wet rolled asphalt surfaces and also on very smooth surfaces such as floor tiles—surfaces where contact macrotexture was low. The correlation is shown in Figure 11 where the R-squared value was 0.9, which is high partly because of the inclusion of a large range of texture "harshness" and the absence of macrotexture.

A test truck that measures sideways force friction was used at 48 km/hr on a range of wet asphaltic and portland cement concrete surfaces. The results are seen plotted against the Y-M texture friction meter readings for SFC_{48} in Figure 12. The R-squared value was 0.7, which is similar to the agreement between the two peak friction tester results from Florida (B. Miley, Florida Department of Transportation, unpublished data).

Although the terms micro- and macrotexture are used, the texture is assumed to be continuous in scale, with no clear borderline between micro- and macrotexture. Others have developed devices for measuring road surface texture. For example, U.K. Transport Research Laboratory has a portable macrotexture measuring device. In addition, work by Henry and Hegmon (*16*) has led to the building of a fast texture-measuring van by the Pennsylvania Transportation Institute.

CONCLUSION

The main advantage to predicting tire-road friction from total texture measurements is based on the fact that the smooth pneumatic tire—the behavior of which is being simulated—has fixed characteristics. The initial hypothetical water film thickness is also fixed at 0.5 mm. Any variation in the predicted friction for a particular speed is solely a result of a change in the road surface texture. The surface texture is under the control of the road authority and so can be used as a trigger in pavement maintenance management. The recorded texture also can be used for other investigations, such as tire-road noise generation. A disadvantage,

of course, is the need for the measured surface to be free from water and detritus where tire contact occurs.

ACKNOWLEDGMENTS

The Roads and Traffic Authority of New South Wales supplied the funds for the authors to update the texture friction meter. The authors thank W. H. Cogill for his continued help and advice.

REFERENCES

1. Yandell, W. O. A Mathematical Simulation of Hysteretic Sliding Friction. *Proc., 4th Conference of the Australian Road Research Board*, Oct. 1968.
2. Yandell, W. O. The Effect of Surface Geometry on the Lubricated Sliding Friction and Polishing of Roadstones. *Australian Road Research*, Vol. 3, No. 10, 1969.
3. Yandell, W. O. A New Theory of Hysteretic Sliding Friction. *Wear*, Vol. 17, April 1971.
4. Yandell, W. O. The Use of Mechano-Lattice Analogy for Determining the Abrading Stresses in Sliding Rubber. *Rubber Chemistry and Technology*, June 1971.
5. Yandell, W. O. The Part Played by Microtexture in Skidding Resistance. *Proc., 6th Conference of the Australian Road Research Board*, 1972.
6. Yandell, W. O. The Simulated Traffic Polishing of Roadstones. In *Wear*, Vol. 21, 1972.
7. Yandell, W. O. The Relation Between the Stress Saturation of Sliding Rubber and the Load Dependence of Tire-Road Friction. Presented at International Symposium on the Physics of Tire Traction Theory and Experiment, Detroit, Mich., Oct. 1973.
8. Gopalan, M. K. and W. O. Yandell. Effect of Lubricants and Masking of Texture on Abrasion of Rubber. *Australian Road Research*, Vol. 5, No. 9, 1975, pp. 48–55.
9. Gopalan, M. K. and W. O. Yandell. The Relation Between the Surface Texture of Roads and the Friction and Abrasion of Tire Tread Rubber. *Proc., 8th Conference of the Australian Road Research Board*, Perth, Aug. 1976.
10. Taneerananon, P. and W. O. Yandell. Micro-Texture Roughness Effect on Predicted Road-Tire Friction in Wet Conditions. *Wear*, Vol. 69, 1981, pp. 321–337.
11. Zankin, V. and W. O. Yandell. High Speed Rolling Friction on Viscoelastic Substrates—Determination of the Hysteretic Damping Factor. *Wear*, Vol. 72, No. 2, 1981, pp. 157–185.
12. Yandell, W. O., P. Taneerananon, and V. Zankin. *Prediction of Tire-Road Friction from Surface and Tread Rubber Properties.* ASTM Special Technical Publication 793. ASTM, Philadelphia, Pa., 1982.
13. Tabor, D. *Philosophical Magazine*, Vol. 43, 1952, p. 1055.
14. Kummer, H. W. and W. E. Meyer. New Theory Permits Better Frictional Coupling Between Tire and Road. Presented at Conference of Federation Internationale des Sociétés d'Ingenieurs des Techniques de l'Automobile, Munich, 1966.
15. Whitehurst, E. A. Field Test Center's Experiences with Skid Trailer Problems. TRANSPLEX College of Engineering, Ohio State University, Columbus, 1978.
16. Henry, J. J. and R. R. Hegmon. *Pavement Texture Measurement and Evaluation.* ASTM Special Technical Publication 583, ASTM, Philadelphia, Pa., pp. 3–17.

Publication of this paper sponsored by Committee on Surface Properties–Vehicle Interaction.

Measurement of Truck Tire Footprint Pressures

JOHN T. TIELKING AND MOISES A. ABRAHAM

A triaxial load pin array to measure tire footprint pressures was recently purchased by Texas Transportation Institute (TTI). The triaxial load pin has two important advantages over the pressure-sensing film techniques that have been utilized by other researchers: (*a*) tire-pavement shear pressures can be measured, and (*b*) the load pin signal will respond to dynamic tire contact pressure. Preliminary results obtained with the TTI load pin array are described. Footprint pressure distributions were measured for two highway-type radial truck tires and a smooth-tread radial truck tire. The data obtained compared well with footprint pressures measured by pressure-sensitive film at the University of Texas. Comparisons with footprint pressures measured at two major tire companies are also given. Data showing the effects of tire inflation pressure and tire load on footprint pressure developed by conventional and wide-base truck tires are included. The effect of wheel flange offset on conventional truck tire footprint pressure distributions is detected. Recommendations are made for research to systematically investigate other influences, such as tire nonuniformity and the effect of tread wear on truck tire footprint pressures.

Determining tire-pavement contact pressure distributions has become an important research need for further advancement in pavement design (*1*). Today's truck tires, being radial with steel cord reinforcement, are known to operate with footprint pressures that are considerably different from those of the nylon cord bias-ply truck tires for which most of the nation's highways have been designed. Very little information on the tire-pavement pressure distributions produced by modern truck tires is available to the pavement designer.

A variety of methods has been used to measure contact pressure in the tire footprint. A pressure-sensing film and a scanner-digitizer-analysis system were recently used at the University of Texas (*2,3*) in laboratory measurements of truck tire footprint pressures. Piezoelectric sensors now being developed for weigh-in-motion (WIM) appear to provide realistic pavement pressure distributions (*4*) and are an approach that should be pursued for on-the-road measurements. The device that has been found most successful by the tire industry is the triaxial load pin. Several large tire companies and two government agencies (U.S. Air Force and National Aeronautics and Space Administration) have made their own load pins. Most of the work done by industry has been aimed at understanding tire wear and tread design. Goodyear has provided a set of footprint pressure measurements for pavement design purposes (*5*).

The Texas Transportation Institute (TTI) recently purchased a load pin array developed by the Precision Measurement Company of Ann Arbor, Michigan. This company has a long history of custom designing pressure-sensing equipment. Their load pins have the smallest contact area (11.4 mm^2 or 0.018 in^2) of those known to the authors and are currently used by Cooper Tire and the Pirelli-Armstrong Tire Company. The load pin has two important advantages over pressure-sensing film: (*a*) tire-pavement shear pressures can be measured with a triaxial load pin, and (*b*) the load pin signal will respond to dynamic tire contact pressure. This paper describes the initial experience and results obtained with the TTI load pin array. The footprint pressure data measured at Texas A&M (TAMU) are compared with data measured for the same size tires at the University of Texas, Cooper Tire Company, and the Goodyear Tire Company. Recommendations for a research program to further investigate tire-pavement contact pressures are outlined at the end of this paper.

Texas Transportation Institute, Texas A&M University, College Station, Tex. 77843-3135.

EXPERIMENTAL PROCEDURES

The normal contact pressures at various transverse locations for three different tires were obtained experimentally with tire loads applied by an MTS servo-hydraulic testing machine. A dual flange axle and U-shaped load frame were used to position both wide base and conventional tires in the testing machine. The U-frame was bolted to a load cell that measures the resultant force in the tire footprint. In this arrangement, the axle is fixed (nonrotating) and the load is applied by a contact plate attached to the servo-hydraulic actuator. The actuator moves the contact plate up against the tire until a specified load is reached. Figure 1 shows the laboratory setup.

The contact plate is a box 508 × 508 × 76.2 mm (20 × 20 × 3 in.) made of aluminum plates 12.7 mm (0.5 in.) thick. A movable shoe with 10 load pins slides in the box to obtain data at different transverse locations. Each load pin has three strain gauge channels from which a change in voltage caused by a change in load can be read. Figure 2 shows the contact plate with the shoe inside. A steel scale along the edge of the shoe channel locates the lateral position of the load pin array.

Data Acquisition

Data from the load pin array are acquired by a Daytronic Model 10K6 measurement and control unit. This unit is software controlled by a Compaq Portable 386 computer. A Daytronic program, DAS1, is used to obtain a live display of load pin data from the Daytronic unit. DAS1 displays data in sequential groups of 10 channels per screen page, which permits viewing of the vertical force signal from all 10 load pins simultaneously. The data displayed on the screen are bridge voltage (in millivolts), which changes with load.

As described earlier, the shoe is moved in the contact plate to obtain readings at different transverse locations. Figures 3 through

5 show the location of the pins with the shoe at three different positions along the median of the footprint of an 11R22.5 tire at a load of 26.9 kN (6,040 lb) and 720 kPa (105 psi) inflation pressure. The precise location of the pins is needed to quantify the distance from the center of the tire at which each contact pressure is obtained. The filled circles in Figures 3 through 5 show the actual contact areas of the load pins, as well as their locations, which are measured to the nearest 1.6 mm (0.0625 in.). The pin centers are spaced 24.5 mm (1 in.) apart.

The procedure adopted to measure the normal pressures is as follows. Initial channel readings are obtained for each load pin (no load applied). The tire load is applied by moving the contact plate up against the tire, and a second set of readings is obtained. Finally, the difference between the two voltage readings and the calibration line for each load pin are utilized to determine the measured pressure. This procedure was repeated for each position of the shoe along the transverse median of the footprint. Table 1 shows the readings obtained for the 11R22.5 tire. Pin 2 was inoperative when these data were taken, so two more shoe positions were used to collect data on Rib 5, using Pins 3 and 4.

The pin contact area is sensitive to tread pattern features. This is the reason a small pin area is desirable. For example, Pin 5 shows zero pressure at Position 3 (Table 1). Referring to Figure 5, one can see that Pin 5 is positioned over a groove (white space in footprint) and thus will not record a pressure.

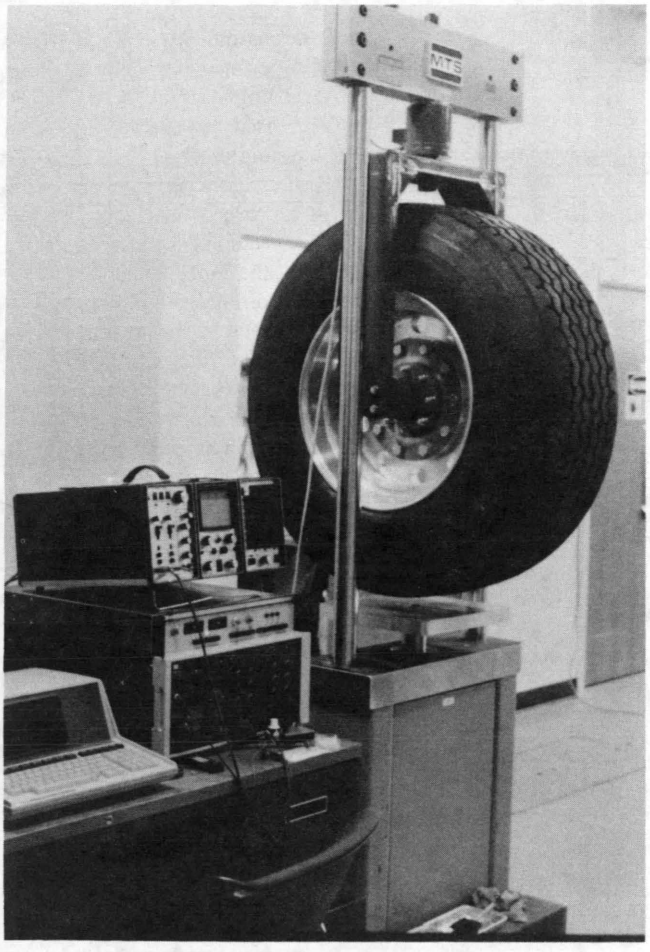

FIGURE 1 Wide base tire mounted in the testing machine.

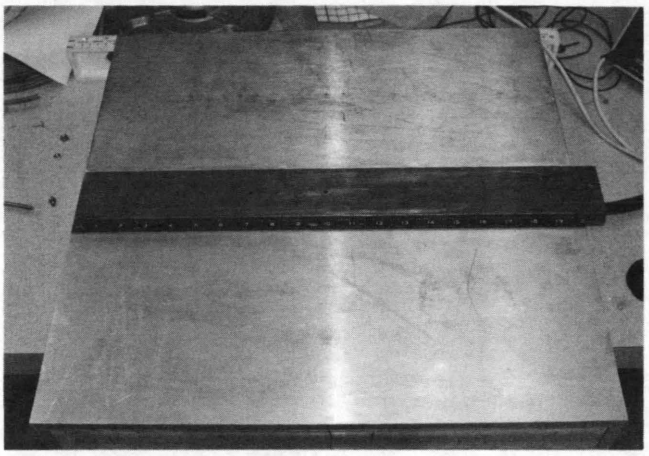

FIGURE 2 Contact plate and movable shoe with load pin array.

Table 2 shows the sequential data taken from Table 1 and two other shoe positions. These data show considerable variation in the pressures across the rib. The rib pressures were averaged to make the plots in this paper showing the effects of inflation pressure and tire load on the footprint pressure distribution. Table 3 shows the average rib pressures calculated from data in Table 2.

RESULTS

Footprint pressure measurements were made on three different tires, shown in Table 4. The load limits given in Table 4 are for single tire application with the tire inflated to the design pressure. A slightly lower inflation pressure and load limit are specified when the tire is used as a dual (*6*).

The 11R22.5 size is a conventional radial truck tire, used either as a single, in the steer position, or as duals on drive and trailer axles. The 385/65R22.5 is a wide base tire that is a possible replacement for a dual tire set. These two tires have highway rib-type tread patterns, as pictured in Figure 6. The 11R24.5 tire is a conventional radial truck tire made for research purposes with a patternless tread. The footprint pressures measured with each of these tires are given in the following sections. All pressure distributions in this paper are those found along the transverse median of the tire footprint.

Smooth Tread 11R24.5

This tire has a full tread layer molded without a tread pattern. The smooth tread eliminates the pressure gradients found at rib edges and avoids the difficulty of interpreting data when the load pin spans a kerf (a narrow cut in the tread pattern). This tire has been tested previously by the University of Texas using pressure-sensitive film, and by the Cooper Tire Company using a load pin array similar to that of TTI.

Figure 7 shows the contact pressures measured by the Center for Transportation Research (CTR) at the University of Texas (*2*). Slight tread imperfections are responsible for the scatter of the measured pressures. The 660-kPa (95-psi) peak at the center of

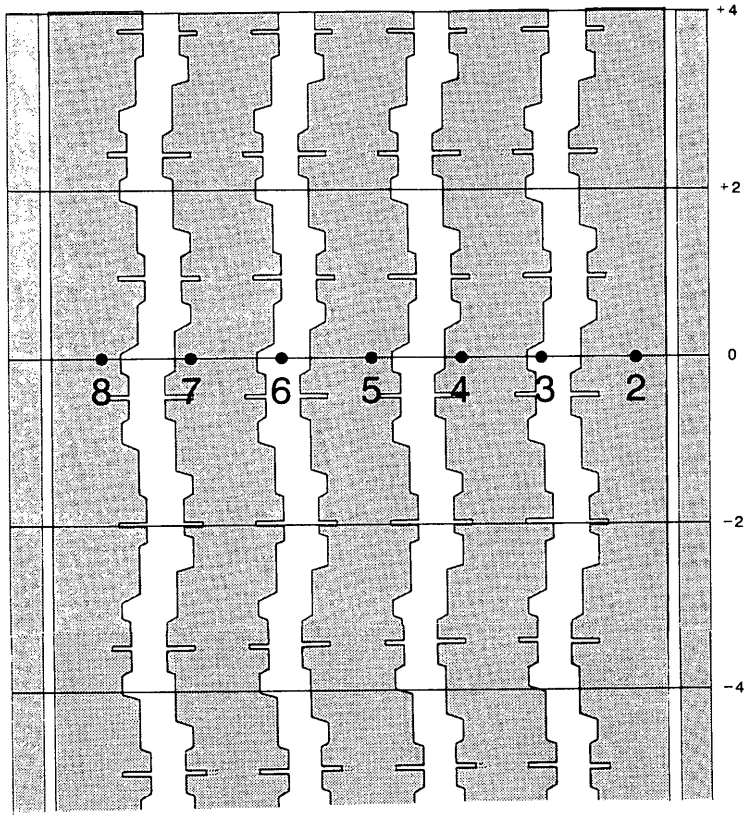

FIGURE 3 Load pin array with shoe at Position 1.

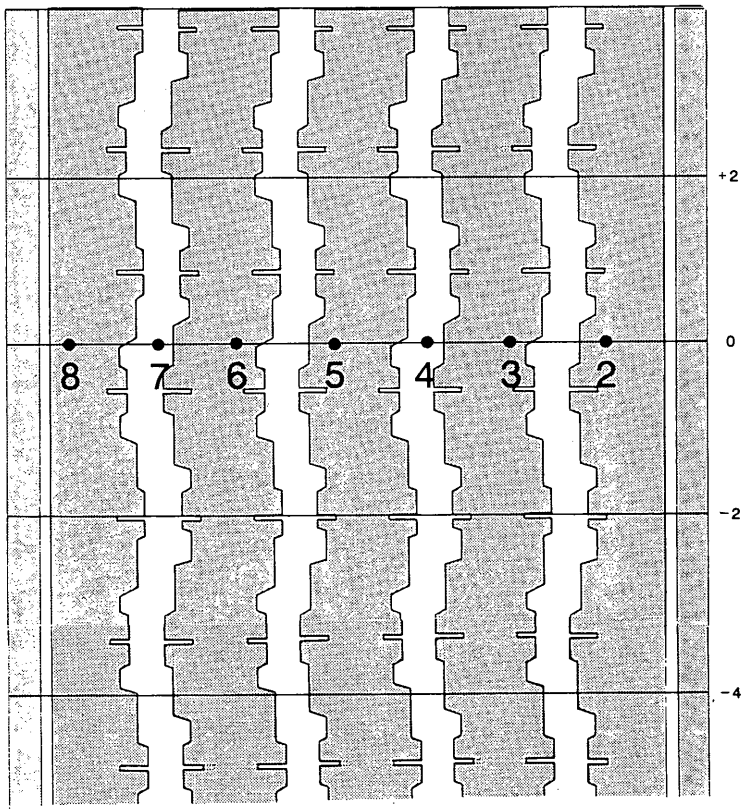

FIGURE 4 Load pin array with shoe at Position 2.

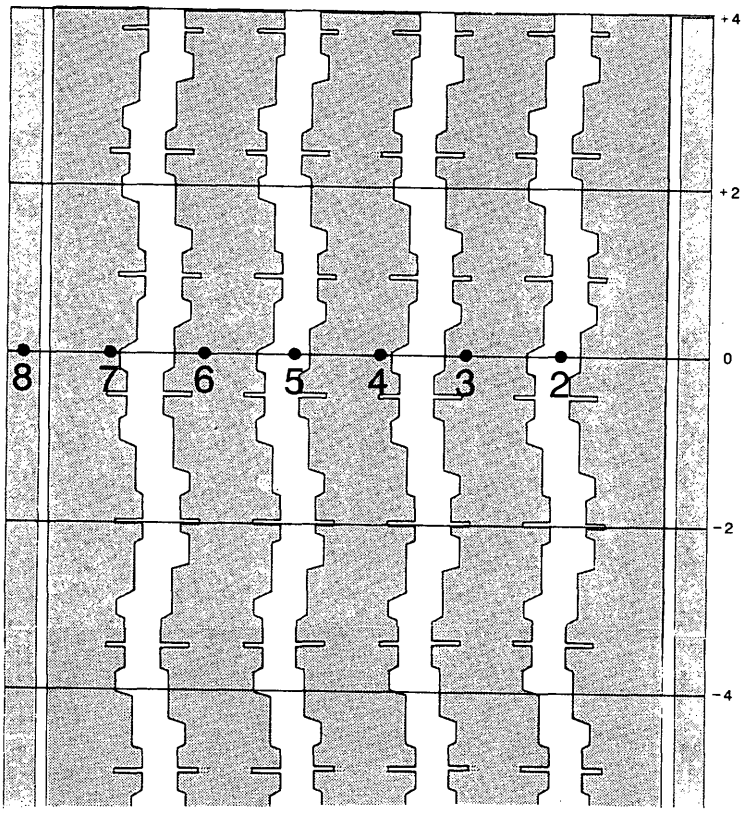

FIGURE 5 Load pin array with shoe at Position 3.

the footprint is caused by the mold parting line, a small ridge of rubber around the tread circumference. The data points measured by the TTI load pin array (TAMU data) are shown with an × in Figure 7.

Figure 8 shows the contact pressure distribution measured by the Cooper Tire Company load pin array, with the tire at a different inflation pressure and a different tire load. The data points measured at TAMU for this pressure and load are shown with an ×.

The agreement between TTI measurements and those of the University of Texas (CTR) and the Cooper Tire Company is very good, considering the sensitivity of interfacial pressure measurements. After test procedures with the smooth tread tire were developed, work with two tires having highway tread patterns was begun.

11R22.5 (Conventional Truck Tire)

Footprint pressures were measured for the 11R22.5 tire at two inflation pressures—720 and 550 kPa (105 and 80 psi)—and at two tire loads—26.9 and 35.6 kN (6040 and 8000 lb)—for each inflation pressure. Figures 9 and 10 show the effect of tire load on footprint pressure for this tire inflated at 720 and 550 kPa, respectively. The data in these and subsequent plots for tires having rib-type tread patterns give the average rib pressures. For example, the distributions across each rib of the 11R22.5 tire at 720 kPa and 26.9 kN load are given in Table 2. These rib distributions were averaged (Table 3) and plotted in Figure 9.

The data in Figures 9 and 10 show the pressure distribution to become somewhat more uniform as tire load increased. As may

TABLE 1 Example Data for 11R22.5 Tire at 720 kPa and 26.9-kN Load

	Position 1			Position 2			Position 3		
pin	Vi	Vf	p	Vi	Vf	p	Vi	Vf	p
3	-7354	-7354	0	-7354	-7874	814	-7354	-7844	744
4	-75	-538	766	-79	-81	0	-82	-906	1476
5	-2	-795	717	-3	-745	655	-5	-5	0
6	-49	-49	0	-45	-1014	1069	-47	-741	814
7	34	-301	372	33	33	0	33	-578	641
8	51	-577	821	62	-420	634	52	-363	586

Vi = initial voltage (mV)
Vf = final voltage (mV)
p = corresponding pressure (kPa)
1 kPa = 0.145 psi

TABLE 2 Measured Pressures

Distance [a] (mm)	Pressure (kPa)	
-98	586	
-83	634	rib 1
-74	820	
-72	641	
-48	372	
-46	814	rib 2
-38	979	
-32	1069	
-6	655	
3	717	rib 3
4.8	1475	
29	766	
30	793	
38	1034	rib 4
45	745	
46	814	
49	724	
72	593	
74	552	rib 5
100	814	

[a] Measured from tread centerline
1 mm = 0.039 in
1 kPa = 0.145 psi

be expected, the average pressure at the higher load is also higher. The average over the entire footprint will be somewhat different. It is well known to tire engineers that the average footprint pressure produced by a tire can be above or below the inflation pressure, depending on tire load. This effect also has been calculated with an analytic tire model (*7*).

It is noted in Figures 9 and 10 that the contact pressure is not exactly symmetrical about the tire plane of symmetry. This is largely because of tire non-uniformity. It is also believed to be because the conventional truck tire was mounted on a wheel with an offset flange. A typical truck wheel is sketched in Figure 11. The wheel mounting flange is offset about 150 mm (6 in.) from the tire plane of symmetry so that the same wheel can be used for dual tires or for single tires. In Figures 9 and 10, the tire load is applied through the wheel flange at 150 mm to the left of the center of the tread (transverse distance). This effectively cantilevers the tire and is believed to contribute to the slight dip in the contact pressure at about 38 mm (1.5 in.) to the right of the tread center. This effect apparently has not been previously noted. It

TABLE 3 Average Rib Pressure

Distance [a] (mm)	Pressure (kPa)	
-100.0	0	
-85.0	669	(rib 1)
-41.0	807	(rib 2)
-0.5	952	(rib 3)
-40.0	814	(rib 4)
85.0	655	(rib 5)
100.0	0	

[a] Measured from tread centerline
1 mm = 0.039 in
1 kPa = 0.145 psi

TABLE 4 Design Parameters of Tires Tested

Tire Size	Inflation Pressure (kPa)	Load Limit (kN)	Tread Pattern
11R22.5/G	720	26.9	5-rib
11R24.5/G	720	28.6	none
385/65R22.5/J	830	41.7	6-rib

Values given in the 1992 Tire and Rim Association Yearbook (*6*)
1 kPa = 0.145 psi
1 kN = 225 lb

should be investigated further because nearly all conventional truck tires are mounted on a wheel with an offset flange.

385/65R22.5 (Wide Base Truck Tire)

The wide base truck tire was mounted on a center flange wheel to eliminate the cantilever effect described above. Offset flange wheels are also used to mount wide base single truck tires, but the offset (nominally 96 mm) does not extend outside the contact

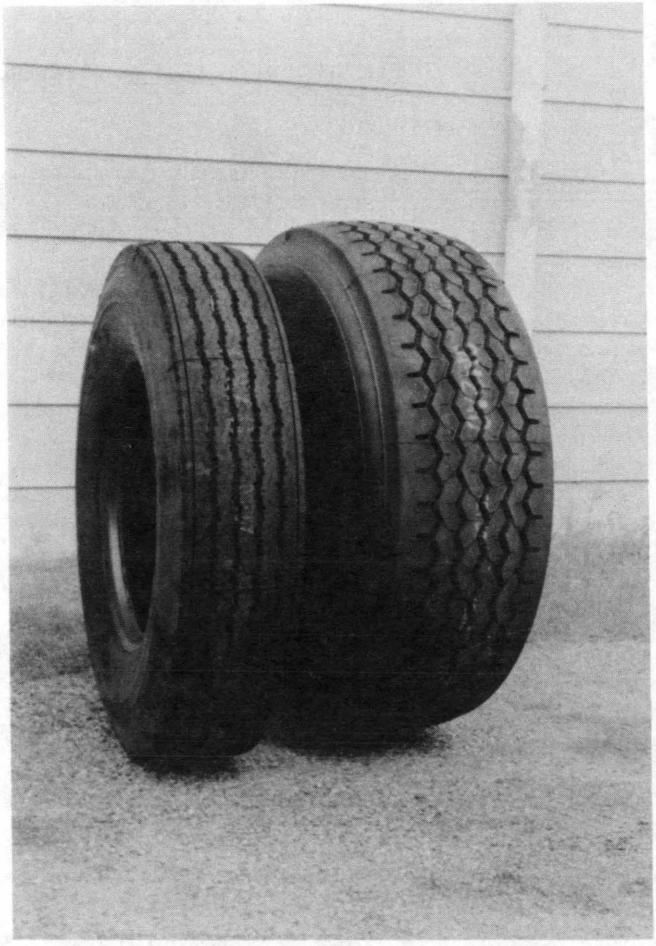

FIGURE 6 Conventional tire (*left*) and wide base truck tire (*right*).

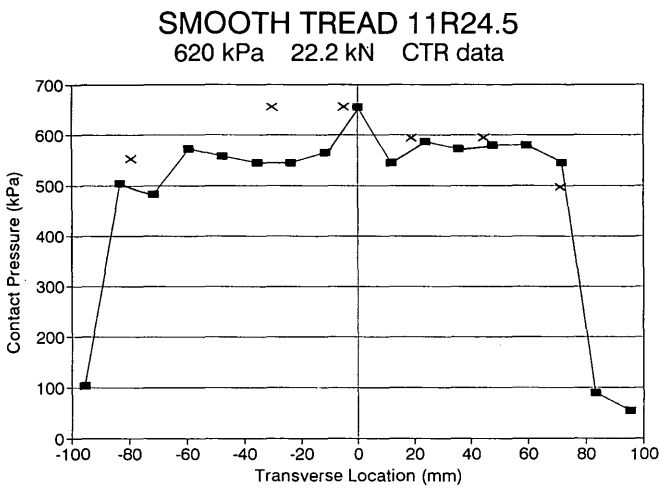

FIGURE 7 Comparison of data measured at TAMU (×) with data measured at the University of Texas (■).

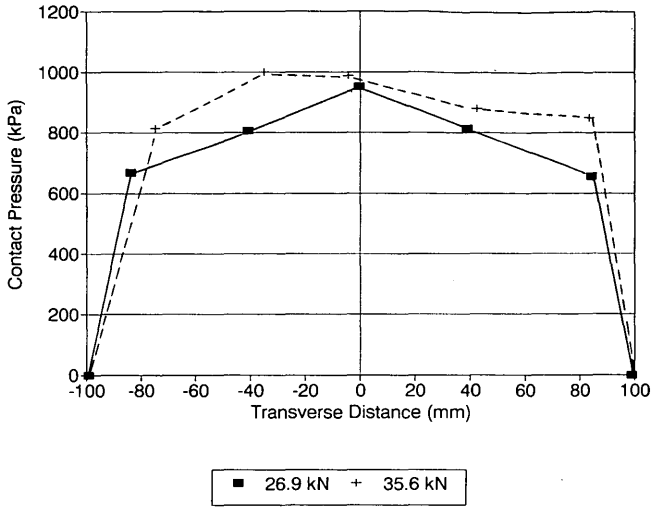

FIGURE 9 Effect of tire load on footprint pressure of 11R22.5 tire at inflation pressure of 720 kPa (105 psi).

region, so the cantilever effect with wide base tires probably will be imperceptible.

Footprint pressure data on this size tire were previously measured by Goodyear for pavement studies at the Pennsylvania Transportation Institute (*5*). Figure 12 compares the Goodyear data with the data from this study for this tire inflated at 900 kPa (130 psi) and with a 37.8-kN (8500-lb) load. The agreement here is fairly good except on the two central ribs where measurements show about 520 kPa (75 psi) higher contact pressure. It is believed that this can be because of tire variability, perhaps caused by a slight difference in the tire molds. It has not been determined that the tires tested by TAMU and Goodyear came from the same mold or from the same tire-building machine.

Footprint pressures were measured at two other tire inflation pressures, 830 and 660 kPa (120 and 95 psi) and at two tire loads, 26.7 and 40.0 kN (6,000 and 9,000 lb) for each of these pressures. Unlike the conventional truck tire, virtually the same footprint pressures along the transverse median were found for these two tire loads, with the tire at the same inflation pressure. However, inflation pressure has a significant effect when the tire load is held constant. This is seen in Figure 13, where the tire load is held at 26.7 kN.

Table 5 gives the average contact pressures for the inflation pressures and tire loads at which the wide base tire was tested. These averages are taken along the transverse median of the footprint and are not averages over the entire footprint.

CONCLUSIONS AND RECOMMENDATIONS

The work reported in this paper focused on measurement of tire-pavement pressure distributions, commonly called footprint pressures. Knowledge of footprint pressure distributions is necessary

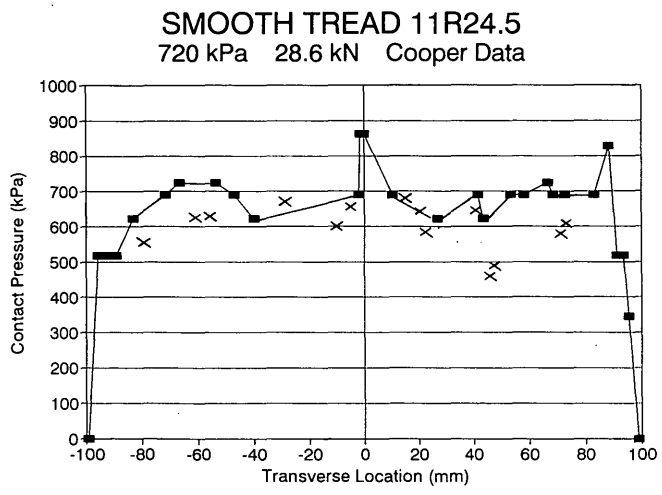

FIGURE 8 Comparison of data measured at TAMU (×) with data measured at the Cooper Tire Co. (■).

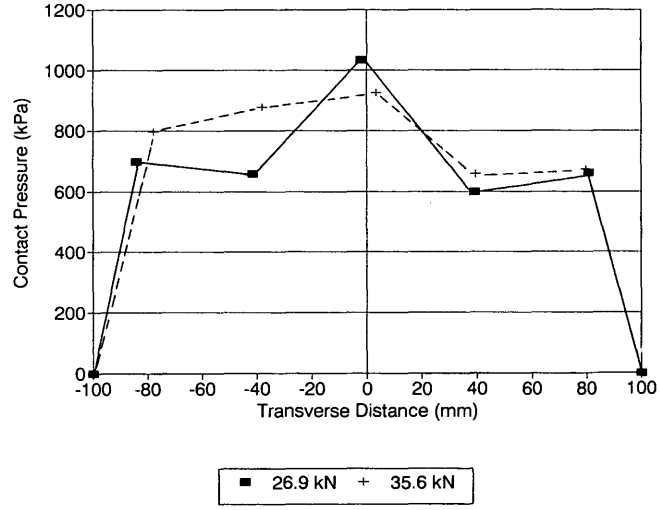

FIGURE 10 Effect of tire load on footprint pressure of 11R22.5 tire at inflation pressure of 550 kPa (80 psi).

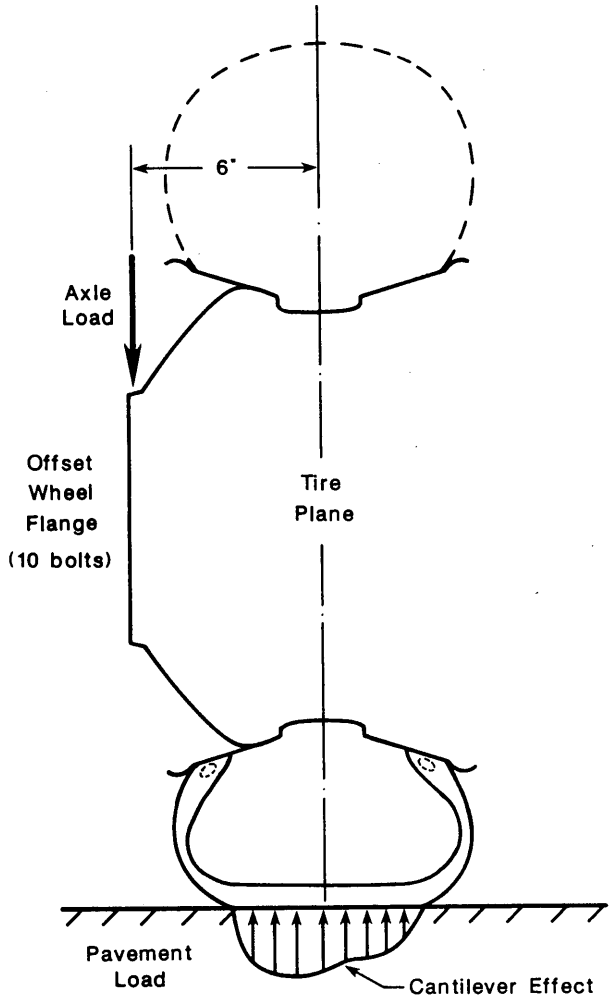

FIGURE 11 Truck wheel with offset flange: effect on pavement load.

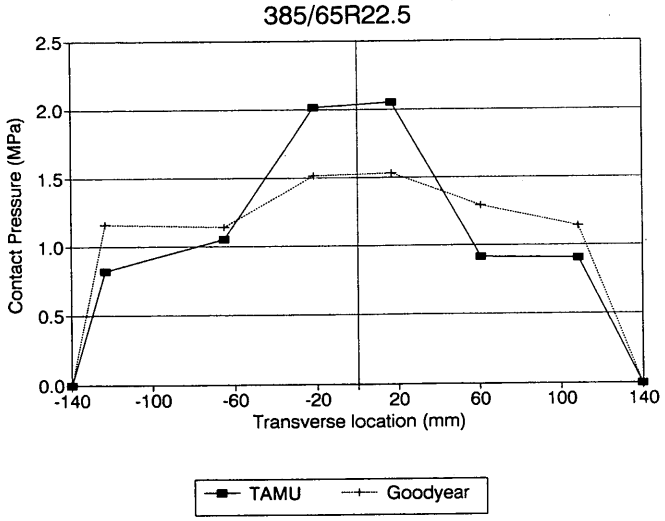

FIGURE 12 Comparison of data measured at TAMU with data measured by Goodyear Tire Company 385/65R22.5 tire at 900 kPa (130 psi) inflation pressure and 37.8 kN (8500 lb) load.

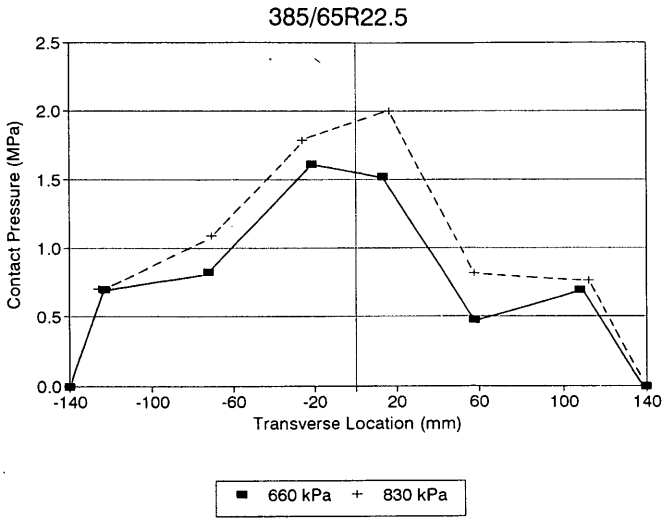

FIGURE 13 Effect of inflation pressure on footprint pressure of 385/65R22.5 tire with 26.7-kN (6,000-lb) load.

to accurately predict pavement damage. The results were found to compare well with data measured for the same size tires at the University of Texas, Cooper Tire Company, and the Goodyear Tire Company. The good agreement is encouraging in view of the extreme sensitivity of interfacial pressure measurements to surface imperfections and contaminants.

Preliminary measurements made to investigate the effects of tire load and inflation pressure have revealed considerable variability in the footprint pressure distributions. Tread wear and tire nonuniformity are two possible sources of footprint pressure variability. The following investigations are recommended to quantify the variability to be expected in tire-pavement contact pressures.

Effect of Tire Footprint Location

Tire uniformity (axisymmetry) has a significant effect on dynamic behavior such as noise and ride. However, no data are available on circumferential uniformity of the footprint pressure. This can easily be investigated by rotating the tire and repeating the footprint pressure measurements. It is recommended that this be done for four equally spaced footprints on each of the three tires tested in the pilot program reported here. It also will be worthwhile to

TABLE 5 Average Contact Pressures for 385/65R22.5 Truck Tire

Tire Inflation (kPa)	Tire Load (kN)	Contact Pressure (kPa)	Data Source
900	37.8	1303	Goodyear
900	37.8	1303	TAMU
830	40.0	1297	TAMU
830	26.7	1193	TAMU
660	40.0	1062	TAMU
660	26.7	972	TAMU

1 kPa = 0.145 psi
1 kN = 225 lb

repeat the measurements on a second tire of the same size and tread pattern to investigate tire-to-tire variability.

Effect of Tread Wear

It is well known that tread wear affects the cornering characteristics of a tire. This may be in part because of changes in footprint pressure caused by wear of the tread profile. A study that includes both worn and new tires of the same size and design is recommended.

Effect of Offset Wheel Flange

The offset wheel flange shown in Figure 11 is used on virtually all heavy trucks operating on U.S. highways. As nonuniformity of tire footprint pressure exacerbates pavement wear, it is worthwhile to test conventional truck tires on both a center flange wheel (specially made) and the usual offset flange wheel to quantify this effect on footprint pressure uniformity. It may be possible to extend pavement life by requiring center flange wheels for conventional tires. Wide base tires will not have this problem.

ACKNOWLEDGMENTS

This work was funded by the Texas Department of Transportation (DOT). The authors thank Bob Briggs of the Texas DOT and Tom Scullion of TTI for their support of this study. John Ragsdale of TTI provided invaluable instrumentation support, including alignment of the load pins.

REFERENCES

1. Smith, H. A. Synopsis of Tire-Pavements Interaction Research. SAE Paper 892455. SAE Truck and Bus Meeting, Charlotte, N.C. Nov. 6–9, 1989.
2. Hansen, R. W., C. Bertrand, K. M. Marshek, and W. R. Hudson, *Truck Tire Pavement Contact Pressure Distribution Characteristics for Super Single 18-22.5 and Smooth 11R24.5 Tires*, Report 1190-1. Center for Transportation Research, University of Texas at Austin, July 1989.
3. Pezo, R. F., K. M. Marshek, and W. R. Hudson, *Truck Tire Pavement Contact Pressure Distribution Characteristics for the Bias Goodyear 18-22.5, the Radial Michellin 275/80R24.5, the Radial Michellin 255/70R22.5, and the Radial Goodyear 11R24.5 Tires*. Report 1190-2F. Center for Transportation Research, University of Texas at Austin, Sept. 1989.
4. Kasahara, A., K. Himeno, K. Kawamura, and S. Nakagawa. Performance of Asphalt Pavements at Bibi New Test Road in Japan Related to Their Bearing Capacity. *Proc. 7th International Conference on Asphalt Pavements*, Vol. 1: Design 1992, pp. 106–123.
5. Sebaaly, P., and N. Tabatabaee. Effect of Tire Pressure and Type on Response of Flexible Pavement. In *Transportation Research Record 1227*, TRB, National Research Council, Washington, D.C., 1989, pp. 115–127.
6. *1992 Yearbook*. The Tire and Rim Association, Inc., Copley, Ohio, 1992.
7. Tielking, J. T. A Finite Element Tire Model. *Tire Science and Technology*, Vol. 11, Nos. 1–4, Jan.–Dec. 1983, pp. 50–63.
8. Tielking, J. T., and F. L. Roberts. Tire Contact Pressure and Its Effect on Pavement Strain. *Journal of Transportation Engineering*, Vol. 113, No. 1, Jan. 1987, pp. 56–71.

Publication of this paper sponsored by Committee on Surface Properties–Vehicle Interaction.

Sensitivity of Rear Wheel Pavement Loading to Variations in Heavy Vehicle Parameters, Speed, and Road Roughness

DONALD A. STREIT, WEN-KAN LIN, AND BOHDAN T. KULAKOWSKI

To construct a heavy vehicle simulation model, it is necessary to obtain vehicle parameters. A sensitivity analysis has been completed that studies the effects of ±15 percent variations in vehicle parameters on rear wheel dynamic load coefficients and maximum vertical rear wheel/pavement forces. Four speeds and road profiles of low, medium, and high roughness were considered. Variations in wheelbase, vehicle curb weight, and payload weight were observed to cause significant variations in values of rear wheel dynamic load coefficients and rear wheel peak forces. In addition, inaccuracies in determination of rear suspension spring rate, rear suspension unsprung weight, and rear tire spring rate were shown to have a significant effect on rear wheel dynamic load coefficients, but not on rear wheel peak forces.

The process of deterioration of the nation's highway structures has accelerated considerably in recent years because of a significantly higher percentage of truck traffic on the highway system. Moreover, trucks have become longer and wider and they carry heavier loads. Many research studies are currently under way to determine the effects of heavy vehicle parameters on dynamic tire forces and on the pavement damage for which these forces are responsible. Computer simulation of heavy vehicle dynamics offers a useful tool for investigation of dynamic pavement loading. The accuracy and the validity of computer simulation results depend very strongly on the accuracy of the vehicle parameters used in the simulation. In this study of vehicle-pavement loading, a two-axle, 155 750-N (35,000-lb) truck with an empty weight of 66 750 N (15,000 lb) and a payload of 89 000 N (20,000 lb) was modeled using the Phase-4 simulation program. During the course of measuring the truck parameters, it was important to know the measurement accuracy necessary to ensure reasonable accuracy of computer simulation results. A sensitivity analysis was performed to determine the effects of truck parameter variations on the simulated truck tire forces. The results of the sensitivity analysis allow identification of the most critical parameters, which have to be measured with high accuracy, as well as the parameters that can be roughly estimated without significantly degrading the quality of the overall vehicle dynamics model. Actual truck parameters were measured (*1*), and the results of the measurements were used as the baseline in the sensitivity analysis. Simulation results using the measured parameters were also compared with dynamic experimental results (*1*).

Pennsylvania Transportation Institute, The Pennsylvania State University, 201 Research Office Building, University Park, Pa., 16802.

BACKGROUND

Various researchers have studied the effects of vehicle geometry, inertial parameters, and speeds on pavement loading (*2–8*). Such efforts considered how pavement loading increased or decreased as parameters were varied. Lin et al. (*9*) focused on changes in front tire pavement load sensitivity to variations in parameter values at various vehicle speeds and pavement roughness values. The present effort focuses on change in rear tire pavement load sensitivity to variations in parameter values at different vehicle speeds and pavement roughness values.

Lin et al. (*9*) discuss various truck simulation models including the ASTM Dynamics model (*10*), VESYM and MAKEVIN, a personal computer (PC)-based pitch plane model (*11*), and the Phase 4 simulation program (*12*). They state

> The Phase 4 simulation program includes a reasonable level of complexity for vehicle simulation and parameter studies and was the program of choice for the present studies. Issues involved in this decision included the availability and familiarity of this code, as well as its history of use over the past few years.

Phase 4 was also the simulation program of choice for the present study. A linear spring-damper model was used for the tires, and a nonlinear model including coulomb friction was employed to represent the truck suspension. Comparison of the Phase 4 program with other simulation programs and with experimental data was previously reported (*13–15*).

Definitions of quantitative pavement load measures are first presented. Actual road profiles were used as inputs for a vehicle parameter sensitivity analysis. Parameter simulation results are studied to gain insight into the effects of various vehicle parameters on rear wheel/pavement loads. Results offer qualitative as well as quantitative insight into parameter variation effects on rear wheel dynamic pavement loading.

QUANTITATIVE MEASURES OF PAVEMENT LOADS

To systematically interpret and analyze vehicle dynamics simulation data, quantitative measures of mean force ($\bar{F}$), maximum force (F_{max}), and dynamic load coefficient (*DLC*) are first defined. These measures are calculated in terms of Phase 4 outputs of tire force F (left front, right front, left rear, and right rear) versus time

t. For N, data points representing tire force (time function), mean force ($\bar{F}$), maximum force (F_{max}), and dynamic load coefficient (DLC) are defined for each tire as follows:

$$\bar{F} = \frac{\sum_{i=1}^{N} F_i}{N} \quad (1)$$

$$F_{max} = \text{Max } \{F_i, i = 1, N\} \quad (2)$$

$$DLC = \frac{s}{\bar{F}} \quad (3)$$

where s is the standard deviation of tire force F. All tire forces in this study are positive.

Mean force represents the time average of tire force in the entire simulation period. It should be similar in magnitude to the static tire force. Maximum force represents the largest tire factor in the entire simulation time history. The dynamic load coefficient is a statistical measure reflecting tire force deviation from a mean value. It is helpful to note that the DLC is more a measure of oscillation about a mean value than a reflection of peak pavement loading (*9*).

SENSITIVITY ANALYSES

DLC and F_{max} were calculated for each wheel. These two quantities are considered the desired measures in the sensitivity analysis. Sensitivity (λ) is defined in the same manner as in a previous study (*9*). Sensitivity (λ) is defined as the percentage change in the desired output when an input parameter changes by 30 percent (115 to 85 percent). Sensitivity λ is calculated as follows:

$$\lambda(Y, x_i) = \frac{[Y(x_1, x_2, \ldots, x_i + \delta x_i, \ldots, x_n) - Y(x_1, x_2, \ldots, x_i - \delta x_i, \ldots, x_n)]}{[Y(x_1, x_2, \ldots, x_i, \ldots, x_n)]} * 100 \text{ percent} \quad (4)$$

TABLE 1 Nominal Vehicle Parameters Used in Phase 4 Simulations

	VALUE	UNIT
1.TRUCK PARAMETERS		
Wheelbase	218.25	in
Base vehicle curb weight on front suspension	5890	lb
Base vehicle curb weight on rear suspension	3776	lb
Sprung mass CG height	39	in
>Roll moment of inertia	8630	in-lb-sec^2
>Pitch monent of interia	127000	in-lb-sec^2
>Yaw moment of inertia	135600	in-lb-sec^2
Payload weight	10000	lb
>Distance ahead of rear suspension center	20	in
>CG height (in. above ground)	85	in
>Roll moment of inertia	16000	in-lb-sec^2
>Pitch moment of inertia	39000	in-lb-sec^2
>Yaw moment of inertia	39000	in-lb-sec^2
2. FRONT SUSPENSION AND AXLE PARAMETERS		
Suspension spring rate	850	lb/in/side
Suspension viscous damping	50	lb-sec/in/side
Coulomb Friction	300	lb/side
Axle roll moment of inertia	3630	in-lb-sec^2
Roll center height (in. above ground)	18.6	in
Auxiliary roll stiffness	7410	in-lb/deg
Lateral distance between suspension spring	35	in
Track width	80.5	in
Usprung weight	1260	lb
3. FRONT TIRES AND WHEELS		
Cornering stiffness (app. 10% of static load)	355	lb/deg/tire
Longitudinal stiffness (app. 4 times tire static load)	14200	lb/slip/tire
Aligning moment	1200	in-lb/deg/tire
Tire spring rate	5173	lb/in/tire
Tire loaded radius	19	in
Polar moment of inertia	103	in-lb-sec^2/wheel
4. REAR SUSPENSION AND AXLE PARAMETERS		
Suspension spring rate	3790	lb/in/side
Suspension viscous damping	20	lb-sec/in/side
Coulomb friction	1312.5	lb/side
Axle roll moment of inertia	4474	in-lb-sec
Roll center height (in. above ground)	31	in
Roll steer coefficient	0.0235	deg steer/deg roll
Auxiliary roll stiffness	12577.5	in-lb/deg
Lateral distance between suspension spring	40.5	in
Track width	72	in
Unsprung weight	2310	lb
5. REAR TIRES AND WHEELS		
Dual tire separation	13.5	in
Cornering stiffness	855	lb/deg/tire
Longitudinal stiffness	34200	lb/slip/tire
Aligning moment	1200	in-lb/deg/tire
Tire spring rate	5173	lb/in/tire
Tire loaded radius	19	in
Polar moment of inertia	103	in-lb-sec^2/wheel

where

Y = desired measure (*DLC* or F_{max}),
x_i = input parameter (nominal values of truck parameters as given in Table 1),
$\delta x_i = 0.15x_i$, and
$y = Y(X) = Y(x_1, x_2, \ldots, x_i, \ldots, x_n)$ = function of all Phase 4 input truck parameters.

No cross sensitivity is considered here, and parameters are changed one at a time. Although the test truck model is assumed symmetrical around its center, differences between left and right wheel forces arise because of differences in left and right input road profiles. Roll motion of both the body and axles is included in the Phase 4 simulations.

First, sensitivity of left front and rear tire forces to variations in each of the Phase 4 input parameters is considered at a highway cruise speed of 97 km/hr (60 mph) and for a medium roughness road. Second, the effect of vehicle speed and road roughness on tire force sensitivity is studied for a subset of Phase 4 parameters.

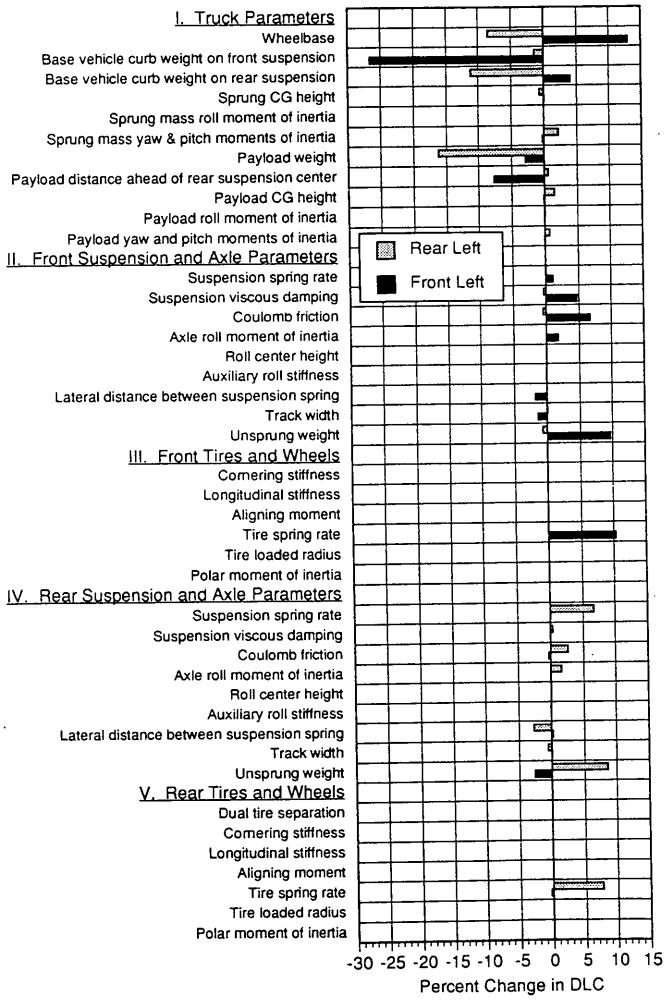

FIGURE 1 Effects of 30 percent increase in truck parameters on left front and rear tire *DLC* at 97 km/hr (60 mph) (*9*).

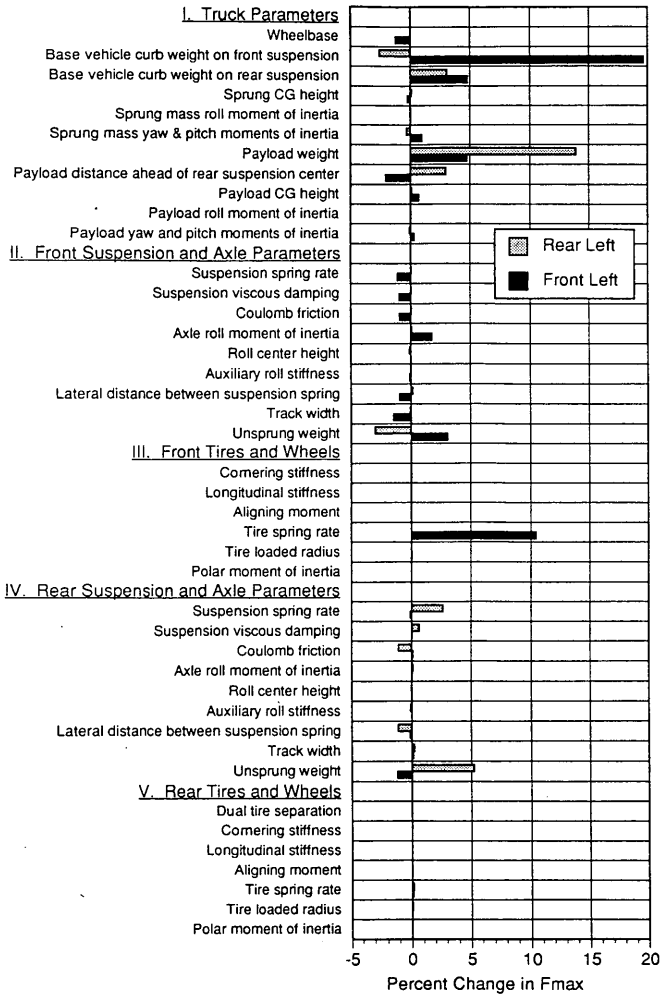

FIGURE 2 Effects of 30 percent increase in truck parameters on left front and rear maximum tire force at 97 km/hr (60 mph) (*9*).

Road Profiles

Three road profiles were used in this study: low, medium, and high roughness. Experimental road profile data were used, and left and right wheel track roughness numbers according to the international roughness index (IRI) were as follows: low roughness, right—1.24 m/km (78.3 in./mi); left—1.11 m/km (70.2 in./mi); medium roughness, right—2.64 m/km (167.4 in./mi), left—3.01 m/km (190.8 in./mi), high roughness, right—3.97 m/km (251.2 in./mi), left—3.86 m/km (244.8 in./mi). A 152.4-m (500-ft) pavement length was used in this study. All large irregularities (potholes) in road profiles were removed (*16*).

Results of Sensitivity Analysis

Sensitivity of *DLC* and of F_{max} to variations in system parameters is reported in Figures 1 and 2, respectively. A highway cruise speed of 97 km/hr (60 mph) and the medium roughness profile were used for the simulations of Figures 1 and 2. The sensitivity plots of Figures 1 through 10 are used as follows. To study the

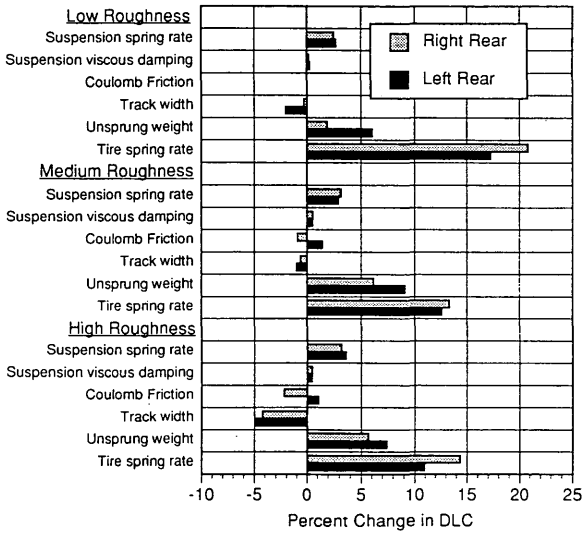

FIGURE 3 Effects of 30 percent increase in truck parameters on left rear tire *DLC* for three roughness levels at 48 km/hr (30 mph).

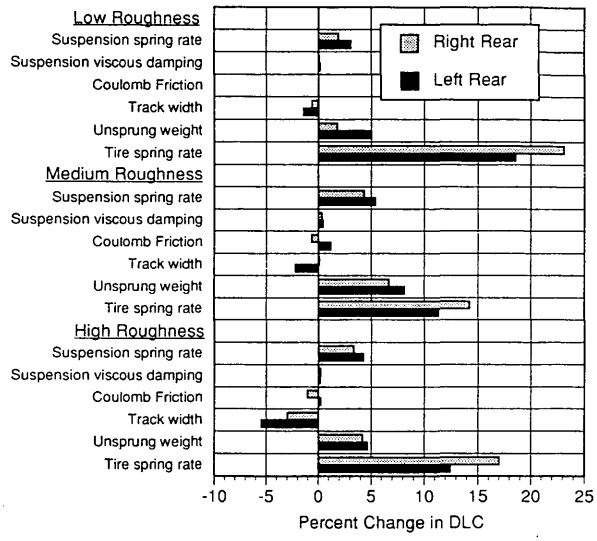

FIGURE 5 Effects of 30 percent increase in truck parameters on left rear tire *DLC* for three roughness levels at 72 km/hr (45 mph).

effect of a 30 percent increase in rear suspension spring rate (115 percent × rear suspension spring rate − 85 percent × rear suspension spring rate), the first line in Section IV of Figure 1 would be considered. A 30 percent increase in rear suspension spring rate is observed to result in a rear left tire *DLC* increase of about 7 percent and a front left tire *DLC* change of less than 1 percent. It can be seen that base vehicle curb weight, payload weight, and payload suspension location each have a significant influence on *DLC* and F_{max}. This is not surprising because each of these parameters has a direct and immediate impact on mean tire forces and on the heave mode resonance. In addition, it is not surprising that the wheelbase has a noticeable effect on *DLC* because the pitch mode oscillation is greatly affected by this parameter. Lin et al. (*9*) present a discussion of the effect of vehicle speed on the front wheel *DLC* and F_{max} sensitivities. In that study, parameters in Sections II and III of Figure 1 were varied and front wheel *DLC* and F_{max} were recalculated and reported for four speeds and three values of road roughness. Now a similar study has been completed for rear suspension and tire parameter variations listed in Sections IV and V of Figure 1. Specifically, the parameters in these sections, which are considered along with speed variations, are rear suspension spring rate, rear suspension viscous damping, rear suspension coulomb friction, rear wheel track width, rear suspension unsprung weight, and rear tire spring rate.

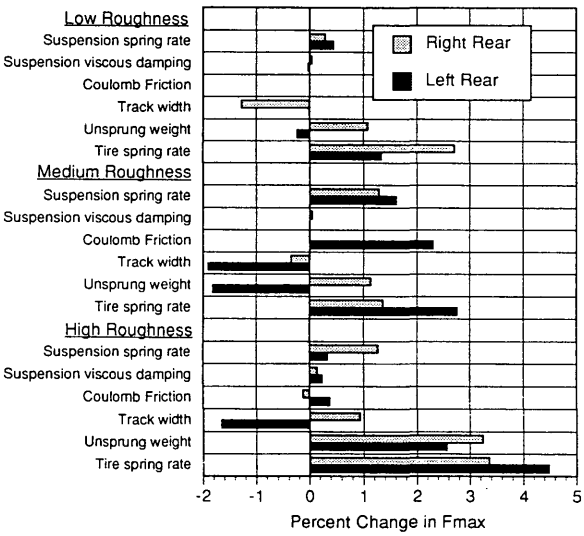

FIGURE 4 Effects of 30 percent increase in truck parameters on left rear maximum tire force for three roughness levels at 48 km/hr (30 mph).

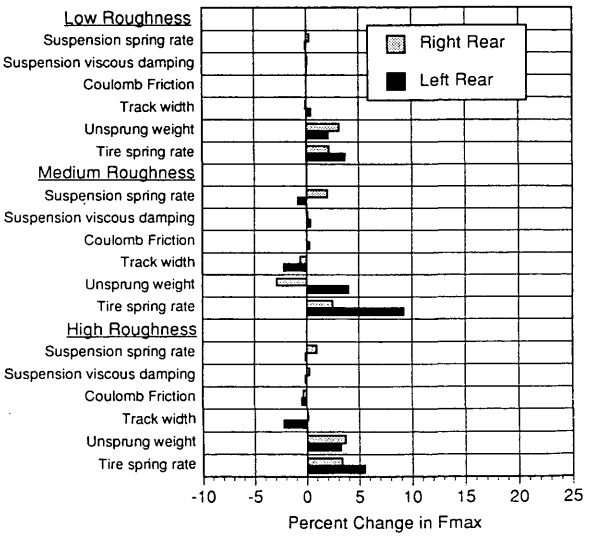

FIGURE 6 Effects of 30 percent increase in truck parameters on left rear maximum tire force for three roughness levels at 72 km/hr (45 mph).

DLC Sensitivity to Speed and Road Roughness

Figures 3 through 10 present *DLC* and F_{max} rear wheel sensitivity for speeds of 48, 72, 97, and 121 km/hr (30, 45, 60, and 75 mph), respectively. *DLC* and F_{max} are given for low, medium, and high roughness roads in each of these plots. The effects of both speed and road roughness, shown in Figures 3 through 10, have some very definite trends. At low speeds, 48 km/hr (30 mph), and for all three road roughness values, Figure 3 demonstrates that the predominant influence on *DLC* sensitivity is the tire spring rate. *DLC* is most sensitive to tire spring rate variation for low roughness roads. This is true for all four vehicle speeds, as shown in Figures 3 through 10. It is interesting to note that the effect of tire spring rate on *DLC* sensitivity tends to decrease with increasing speeds for all three road roughness values. An explanation of this phenomenon is given by recognizing that this sensitivity analysis says nothing about the magnitudes of *DLC* and F_{max} values. Rather, this study considers only the change in magnitude for variations in system parameters. Hence, the actual *DLC* value for a medium roughness road at high speeds might be larger than at low speeds, whereas the variation in spring rate on *DLC* sensitivity is observed to decrease with increasing speeds. It is likely that the magnitude of *DLC* increase as a result of a change in tire spring rate is relatively constant for increasing speeds. However, if the *DLC* magnitude increases with increasing speed, then the percentage increase in *DLC* will vary inversely with speed. The result is that inaccuracies in tire spring rate measurements will introduce less error into *DLC* calculations at high speeds and on high roughness roads than at low speeds and on low roughness roads. Usually there is more concern for dynamic pavement loading at high speeds and on rough roads than at low speeds and on relatively smooth roads because pavement damage increases with road roughness and speed (*2*). [Although pavement damage increases with vehicle speed, it may decrease at higher speeds as a result of decreasing dynamic response of the vehicle to pavement profile (*2*).]

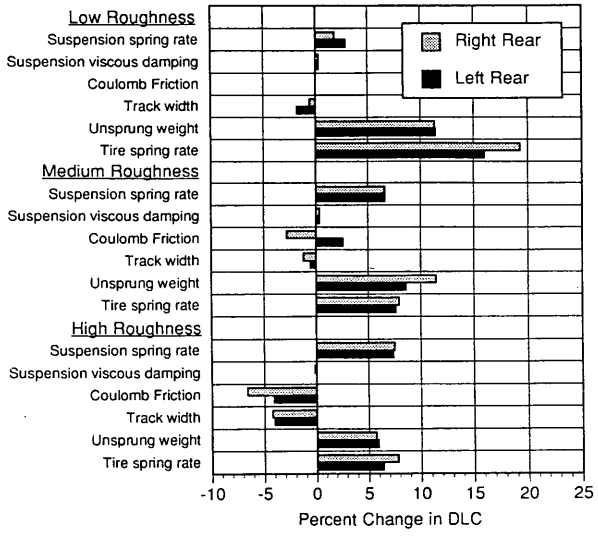

FIGURE 7 Effects of 30 percent increase in truck parameters on left rear tire *DLC* for three roughness levels at 97 km/hr (60 mph).

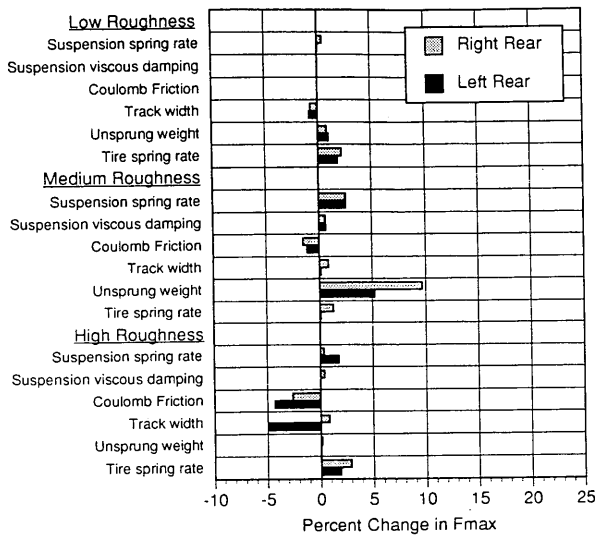

FIGURE 8 Effects of 30 percent increase in truck parameters on left rear maximum tire force for three roughness levels at 97 km/hr (60 mph).

In Figures 3, 5, 7, and 9, the effect of track width on *DLC* sensitivity at all speeds is seen to be greatest for the high roughness road. This observation might offer insight into the debate on the influence of vehicle roll on dynamic vertical wheel/pavement loads. Vehicle/tire roll oscillations are significantly affected by track width. For lower roughness roads the influence of track width and, hence, of vehicle or suspension roll, or both, is small. For high roughness roads the influence of track width and, hence, of vehicle or suspension roll, or both, is noticeable. A similar observation was made when front wheel *DLC* sensitivity was studied.

The results demonstrate that, for low roughness roads, vehicle speed has little effect on *DLC* sensitivity to suspension spring rate variation. However, when speed increases from 72 to 97 km/hr (45 to 60 mph) *DLC* sensitivity to a 30 percent variation in suspension spring rate more than doubles for both medium and high roughness roads.

DLC sensitivity to unsprung weight is relatively unaffected by speed for the high roughness road (see Figures 3, 5, 7, and 9). However, on the low roughness road, Figures 7 and 9 demonstrate that *DLC* sensitivity more than doubles when speed is increased from 72 to 97 km/hr (45 to 60 mph).

Coulomb friction variation primarily affects *DLC* sensitivity at the higher speeds of 97 and 121 km/hr (60 and 75 mph) and only for medium and high roughness roads.

Suspension viscous damping variation results in less than a 2 percent variation in rear tire *DLC* for all speeds and road roughness values considered. This might have been anticipated since there is relatively little viscous damping in the rear suspension of a two axle steel suspension vehicle. The effect of front suspension viscous damping on front tire *DLC* was observed to be more significant (*9*).

Table 2 is a *DLC* sensitivity matrix, summarizing the parameter effects that are shown in Figures 3 through 10. In this table, an "X" is entered in the appropriate row and column for each 5 percent change in *DLC*. Matrix locations are marked only when a 30 percent change in a system parameter resulted in a change

in *DLC* of more than 5 percent. The average change between left and right wheel *DLC* was used in compiling this table, and numbers larger than 5 percent were rounded to the nearest 5 percent. A quick look at this table highlights the importance of accurate unsprung weight and tire spring rate measurements when simulations are used to calculate *DLC*. Suspension spring rate accuracy is most important at high speeds and high road roughness values. A 30 percent variation in coulomb friction measurement has greater than a 5 percent effect on *DLC* for only one speed and road roughness.

F_{max} *Sensitivity to Speed and Road Roughness*

Figure 4 demonstrates that, at 48 km/hr (30 mph), none of the parameters studied results in greater than a 5 percent change in F_{max}. In fact, the average rear left/right *DLC* variation is greater than 5 percent for only two parameter combinations: 30 percent tire spring rate variation at 72 km/hr (45 mph) on medium roughness road and 30 percent unsprung weight variation at 97 km/hr (60 mph) on medium roughness road. F_{max} is relatively insensitive to variations in suspension and tire system parameters. Variations in system parameters are observed to have a greater effect on rear *DLC* than on rear F_{max} for all three pavement roughness values and at all four vehicle speeds considered. This observation was also made in the study of front wheel *DLC* and F_{max} sensitivity (*9*). This conclusion, which should be very important for researchers studying pavement loading caused by dynamic forces applied by heavy vehicles, can be restated as follows: The maximum tire force that is capable of being generated on actual roads depends primarily on the vehicle curb weight and payload weight and is not significantly affected by variations and inaccuracies in suspension and tire parameters. The suspension and tire parameters are, however, critical for the manner in which the vehicle forces vary within the range of 0 to F_{max}. This also explains why *DLC* is sensitive to suspension and tire parameters since *DLC* depends on both the maximum tire force as well as on the variation of the tire force.

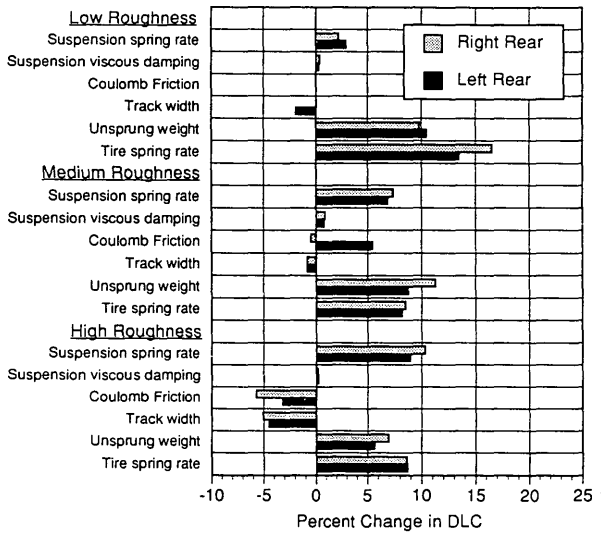

FIGURE 9 Effects of 30 percent increase in truck parameters on left rear tire *DLC* for three roughness levels at 121 km/hr (75 mph).

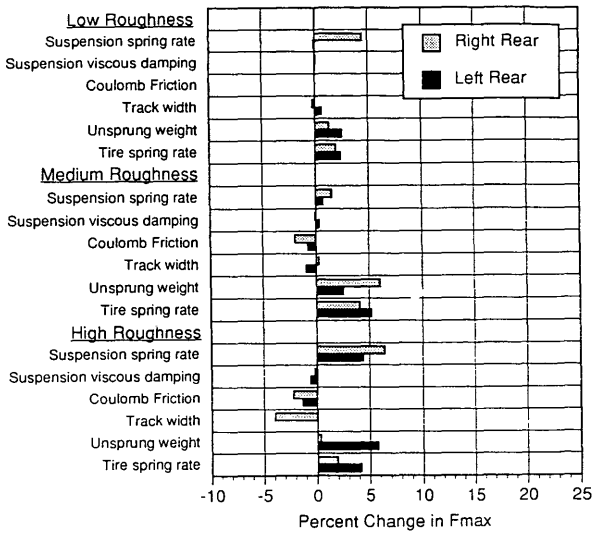

FIGURE 10 Effects of 30 percent increase in truck parameters on left rear maximum tire force for three roughness levels at 121 km/hr (75 mph).

CONCLUSIONS

A two-axle, steel suspension truck model was assembled using the Phase 4 simulation program. Initial simulations using a medium roughness profile and a vehicle speed of 97 km/hr (60 mph) identified vehicle parameters having the largest effect on rear wheel *DLC* and F_{max}. Variations in rear suspension and rear tire parameters (suspension spring rate, suspension viscous damping, coulomb friction, track width, unsprung weight, and tire spring

TABLE 2 Rear Tire DLC Sensitivity Matrix

Figure #	3	4	5	6
Speed Km/hr (Speed mph)	48 (30)	72 (45)	97 (60)	121 (75)
1. Low Roughness				
Suspension spring rate				
Suspension viscous damping				
Coulomb friction				
Track width				
Unsprung weight			XX	XX
Tire spring rate	XXXX	XXXX	XXX	XXX
2. Medium Roughness				
Suspension spring rate			X	X
Suspension viscous damping				
Coulomb friction				
Track width				
Unsprung weight	X	X	XX	XX
Tire spring rate	XX	XX	XX	XX
3. High Roughness				
Suspension spring rate			X	XX
Suspension viscous damping				
Coulomb friction			X	
Track width				
Unsprung weight		X	X	X
Tire spring rate	XXX	XX	X	XX

rate) were reported for four vehicle speeds and three road profiles of low to high roughness. For a 30 percent variation in each of these six parameters, rear suspension spring rate, rear suspension unsprung weight, and rear tire spring rate were observed to have the greatest effect on *DLC* over any range of speeds and road roughness values (see Table 2). Of the six rear suspension/tire parameters considered and for every speed and road profile used in these simulations, *DLC* was most sensitive to variations in tire spring rate.

The increased effect of track width on *DLC* for high roughness roads suggests that roll mode oscillations increase in importance with increased road roughness.

None of the six rear suspension/tire parameters was observed to significantly affect F_{max} over any range of speeds and road roughness values considered. The maximum rear tire force depends primarily on the vehicle curb weight and payload weight and is not significantly affected by variations or inaccuracies in suspension and tire parameters. The suspension and tire parameter measurements are, however, critical for the accurate determination of *DLC*

Future work might select vehicle parameters to be varied simultaneously, thereby studying parameter coupling effects on pavement loading. Also, alternative suspension systems, such as walking beam and air and more complex truck models such as tractor-trailer systems, might be studied.

ACKNOWLEDGMENTS

The work reported in this paper was partially sponsored by FHWA. Valuable input received from reviewers is gratefully acknowledged.

REFERENCES

1. Hsu, K.-M., D. A. Streit, and B. T. Kulakowski. Heavy Vehicle Loads on Pavement: Analytical and Experimental Comparison. Presented at 72nd Annual Meeting of the Transportation Research Board, Washington, D.C., 1993.
2. Cebon, D. Vehicle-Generated Road Damage: A Review. *Vehicle System Dynamics*, No. 18, 1989, pp. 107–150.
3. Sweatman, P. F. A Study of Dynamic Wheel Forces in Axle Group Suspensions of Heavy Vehicles. Special Report SR27. *Australian Road Research Board*, 1983.
4. Woodrooffe, J. H. R., P. A. LeBlanc, and A. T. Papagiannakis. Suspension Dynamics—Experimental Findings and Regulatory Implications. SAE Paper 881847. *Society of Automotive Engineers*, Warrendale, Pa., 1988, pp. 69–77.
5. Mitchell, C. G. B., and L. Gyenes. Dynamic Pavement Loads Measured for a Variety of Truck Suspensions. Presented at 2nd International Conference on Heavy Vehicle Weights and Dimensions, Kelowna, British Columbia, 1989.
6. Bonaquist, R., C. Churilla, and D. Freund. Effect of Load, Tire Pressure, and Tire Type on Flexible Pavement Response. *Public Roads*, Vol. 52, No. 1, June 1988, pp. 1–7.
7. Sayers, M., and T. D. Gillespie. Dynamic Pavement/Wheel Loading for Trucks with Tandem Suspensions. *Proc., 8th IAVSD Symposium on the Dynamics of Vehicles on Roads and on Railway Tracks*, Cambridge, Minn., 1983, pp. 517–533.
8. Whittemore, A. P., J. R. Wiley, P. C. Schultz, and D. E. Pollock. *NCHRP Report 105: Dynamic Pavement Loads of Heavy Highway Vehicles*. HRB, National Research Council, 1970.
9. Lin, W., Y-C. Chen, B. T. Kulakowski, and D. A. Streit. Dynamic Wheel/Pavement Force Sensitivity to Variations in Heavy Vehicle Parameters, Speed and Road Roughness. *International Journal of Vehicle Design*, in press.
10. Todd, K. B., and B. T. Kulakowski. Simple Computer Models for Predicting Ride Quality and Pavement Loading for Heavy Trucks. In *Transportation Research Record 1215*, TRB, National Research Council, Washington, D.C., 1989, pp. 137–150.
11. Hu, G. Use of a Road Simulator for Measuring Dynamic Wheel Loads. *Proc., Future Transportation Technology Conference and Exposition*, San Francisco, Calif., Society of Automotive Engineers, 1988.
12. MacAdam, C. C., P. S. Fancher, G. T. Hu, and T. D. Gillespie, *A Computerized Dynamics of Trucks, Tractor Semi-Trailers, Doubles, and Triples Combinations: User's Manual—Phase 4*. Report UM-HSRI-80-58. Highway Safety Research Institute, Ann Arbor, Mich., 1980.
13. Gillespie, T. D., C. C. MacAdam, G. Hu, J. Bernard, and C. Winkler. *Truck and Tractor-Trailer Dynamic Response Simulation*. Technical Report FHWA-RD-79-124, Vol. 2, FHWA, U.S. Department of Transportation, Dec. 1980.
14. El-Gindy, M., and J. Y. Wong. A Comparison of Various Computer Simulation Models for Predicting the Directional Responses of Articulated Vehicles. *Vehicle Systems Dynamics*, Vol. 16, No. 5–6, 1987.
15. Kenis, W., B. T. Kulakowski, and D. A. Streit. Heavy Vehicle Pavement Loading: A Comprehensive Testing Programme. *Proc., 3rd International Symposium on Heavy Vehicle Weights and Dimensions*. Cambridge, 1992, pp. 260–265.
16. Dodds, C. J., and J. D. Robson. The Description of Road Surface Roughness. *Journal of Sound and Vibration*, Vol. 31, No. 2, 1973, pp. 175–183.

The findings and conclusions in this paper are those of the authors and do not necessarily represent the views of the FHWA.

Publication of this paper sponsored by Committee on Surface Properties–Vehicle Interaction.

Heat Transfer from Vehicular Catalyst to Pavement

KENT S. FINDLEY AND HONG-JER CHEN

A study was undertaken to assess the effect of vehicle heat on bituminous pavement by comparing it with the effect of solar radiation. The catalytic converter (or catalyst) was chosen to represent a vehicle exhaust system. Catalysts transfer heat to pavements primarily by radiation, which can be calculated on the basis of existing theories. Two methods were used to calculate radiation from catalyst to pavement: view factor and solid angle. A simplified experiment showed that view factor calculation was closer to measured heat transfer. Data from catalysts of three vehicles were taken. Solar radiation absorbed by the pavement can be estimated from existing models and meteorological data. Results indicate that for one vehicle, pavement directly under the catalyst with an area the same as or smaller than the catalyst absorbed more radiation from it than from the sun. Size and temperature of the catalyst, distance between catalyst and pavement, and oxidation level of the catalyst material were all important factors. Because of the very small sample of vehicles studied, no general conclusions were drawn about whether vehicles on highways increase pavement surface temperature and cause rutting damage.

Rutting of bituminous pavements has been a subject of national attention in recent years. New York State had a few critical rutting failures before the New York State Department of Transportation (NYSDOT) Materials Bureau developed new heavy-duty flexible pavement mixes, specified from 1991 for all new construction. Combinations of weak foundations, poor-quality aggregates, improper mix designs, inadequate compaction, heavy truckloads, and high temperatures all contribute to rutting.

Properties of bituminous concrete make it highly susceptible to temperature. In 1988, a rutting failure had occurred on the Cross-Bronx Expressway in an abnormally hot summer. Heat emitted from vehicle exhaust systems is another possible source contributing to high temperatures. It was suspected that vehicles may worsen the rutting problem by causing further increase in pavement surface temperatures, particularly at intersections or on highly congested roadways where vehicles must stand with idling motors or move very slowly, if at all, for long periods. Recently, some minor rutting was also noted in Albany on the Route 5 approaches to the busy intersection of Routes 5 and 155. Route 5 had been reconstructed less than 3 years earlier, and no rutting had occurred in other areas.

The possible effect of heat transferred to pavements from standing or slow-moving vehicles does not appear to have been explored elsewhere, and, consequently, was selected for a short-term study by the Engineering Research and Development Bureau. The objectives were to determine the total heat transferred to the pavement surface from a catalytic converter, commonly called a catalyst, and whether its effect on pavement is significant compared with the effect of solar radiation. Although various parts of exhaust systems all contribute to this effect, it was decided to study only the catalyst because it produces particularly high temperatures, its area is easy to define, and it is unobstructed from the pavement surface, thus fitting this study's requirements: to produce results with limited resources and time.

In this paper, heat-transfer phenomena—especially radiation—are briefly reviewed. Then radiation from a catalyst to a pavement is calculated, using appropriate theories and data from three vehicles. The calculated radiation heat transfer was verified by a simplified test. Results are compared with those from calculated solar radiation that a pavement receives to determine whether catalysts have any significant effect on pavement temperatures.

Engineering Research and Development Bureau, New York State Department of Transportation, Albany, N.Y. 12232.

HEAT TRANSFER

Heat transfer is a science that involves the prediction of energy transfer between bodies as a result of a temperature differential (*1*). This prediction tries to explain how and at what rate energy is exchanged. The transfer of heat energy may take any of three forms: conduction, convection, or radiation.

1. Conduction occurs when a temperature gradient exists within a single body or two bodies in contact. It cannot take place without a material medium.
2. Convection is the process in which a gas or liquid with a given velocity carries heat away from a hot body. Its two types are (a) forced and (b) free or natural. Forced convection occurs when velocity of the fluid is driven by an external force such as a fan. Free convection occurs without external force; velocity is induced by the temperature gradient near the hot body. Convection also requires a material medium for it to occur.
3. Radiation, unlike convection and conduction, does not need a medium and is transmitted by electromagnetic waves. Thermal radiation is propagated by temperature differences. "Black-body" radiation consists of electromagnetic waves emitted from an object radiating according to the T^4 law. In this form, it is directly proportional to the area of the radiating object. Black-body radiation is calculated as follows:

$$q = \sigma_b A T^4 \quad (1)$$

where

q = black-body radiation (W),
σ_b = Stefan-Boltzmann constant (5.67×10^{-8} W/m$^2 \cdot$ K^4),
A = area of radiating object (m^2), and
T = absolute temperature of radiating object (°K).

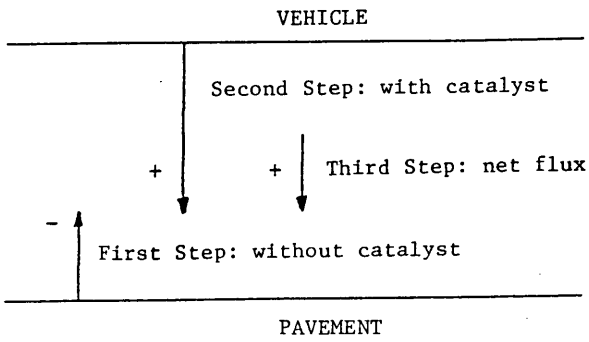

FIGURE 1 Net radiation between vehicle and pavement.

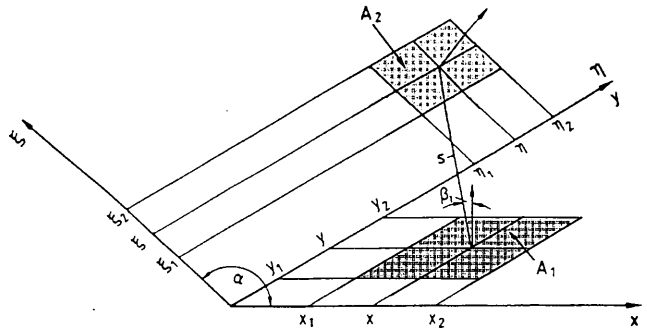

FIGURE 3 Two areas on two arbitrary planes.

If two objects face one another, and one has a higher temperature but the same area, thermal radiation transmitted to the cooler object is equal to

$$q = \sigma_b A(T_H^4 - T_C^4) \quad (2)$$

where

q = radiation heat transfer (W),
T_H = absolute temperature of hotter object (°K), and
T_C = absolute temperature of cooler object (°K).

Equations 1 and 2 are valid if the objects are "black," a term referring to their ability to radiate or absorb energy according to the T^4 law.

RADIATION FROM A CATALYST

Theory

Thermal radiation is the main form of heat transfer between catalyst and pavement. Convection heat transfer between vehicle and pavement may be neglected because the hotter body is above the cooler body so that gravity reduces heat flow. Because catalyst and pavement are not in contact, heat transfer does not occur as conduction.

A "gray" body, such as a catalytic converter, radiates proportionately to the T^4 law, with the proportionality constant called "emissivity" (ϵ). Its value depends on the material's composition, type of finish, level of oxidation, and surface temperature. The darker the surface, the higher is its emissivity, and vice versa. "Black" bodies have an emissivity of 1.

Net heat exchange in the form of radiation from catalyst to pavement can be calculated in a three-step process. The first is to calculate radiation transfer to the pavement from a vehicle without a catalyst. The second step is to calculate the additional radiation contribution from adding a catalyst to the vehicle. In the third step, these results should then be added to obtain total heat transfer; this process is shown in Figure 1. Throughout this study, the conventions of radiation leaving the pavement upward and leaving the vehicle downward were assumed to be negative and positive, respectively.

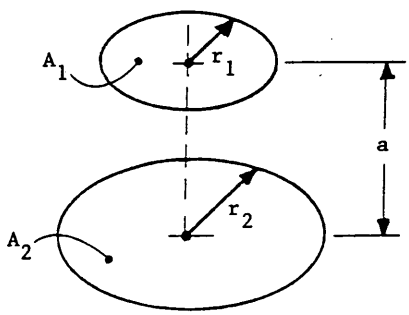

FIGURE 2 Two parallel concentric disks.

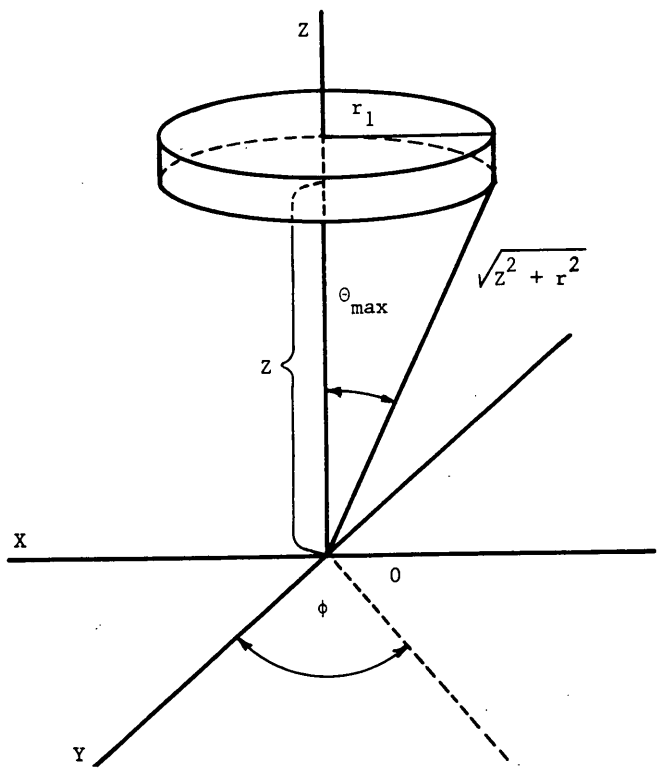

FIGURE 4 Solid-angle approach.

Step 1 is calculated as follows:

$$q_1 = -\sigma_b A_p (T_p^4 - T_v^4) \tag{3}$$

where

q_1 = radiation (W) between pavement and vehicle without a catalyst,
A_p = pavement area of interest (m^2),
T_p = pavement temperature (°K), and
T_v = temperature of underside of vehicle (°K).

Step 2 involves using a view factor (explained later in detail) and an emissivity for catalyst radiation. Step 1 does not require a view factor because the vehicle acts as an infinite plane compared with the pavement section that is of interest. No emissivity is used because pavement surface and vehicle underside are both assumed to radiate as black bodies because of their dark colors. The additional radiation contributed by the catalyst is calculated as follows:

$$q_2 = \epsilon_c F_{1-2} \sigma_b A_c (T_C^4 - T_v^4) \tag{4}$$

where

q_2 = additional radiation (W) from catalyst,
ϵ_c = emissivity of catalyst,
F_{1-2} = view factor,
A_c = area of catalyst facing pavement (m^2), and
T_c = temperature of catalyst surface (°K).

Step 3 is the summation of Equations 3 and 4, yielding the net radiation between a catalyst and an area of pavement beneath it:

$$q_t = q_1 + q_2 \tag{5}$$

or

$$q_t = \sigma_b [\epsilon_c F_{1-2} A_c (T_c^4 - T_v^4) - A_p (T_p^4 - T_v^4)] \tag{6}$$

where q_t is total radiation flux (W) between a vehicle catalyst and a pavement area.

The view factor (F_{1-2}) is the portion of total radiation from the catalyst that reaches the pavement area of interest (A_p). The view factor is a function of the geometry of the catalyst and pavement area in question (2). The most common geometry of two parallel concentric disks of varying radii was used in this study, as shown in Figure 2. F_{1-2} for this arrangement is calculated as follows:

$$F_{1-2} = \tfrac{1}{2}\left\{X - \left[X^2 - 4\left(\frac{R_2}{R_1}\right)^2\right]^{\frac{1}{2}}\right\} \tag{7}$$

where

$$X = 1 + \frac{(1 + R_2^2)}{R_1^2} \tag{8}$$

and

$$R_1 = \frac{r_1}{a},$$

$$R_2 = \frac{r_2}{a},$$

r_1 = radius of catalyst (m),
r_2 = radius of pavement area of interest (m), and
a = distance between catalyst and pavement (m).

Because most catalysts are not circular, r_1 is the equivalent radius and is calculated as follows:

$$r_1 = \sqrt{\frac{A_c}{\pi}} \tag{9}$$

Gross et al. (*3*) have explained that if surfaces of the radiating bodies are not parallel but inclined with respect to each other, the view factor is calculated as follows (with all variables defined as in Figure 3):

$$A_c F_{1-2} = \int_{\xi_1}^{\xi_2} \int_{\eta_1}^{\eta_2} \int_{y_1}^{y_2} \int_{x_1}^{x_2} \frac{x\xi}{[x^2 - 2x\xi \cos\alpha + \xi^2 + (y - \eta)^2]^2}\, dx\, dy\, d\eta\, d\xi \tag{10}$$

where

A_n = areas of radiating bodies,
x, y, η, ξ = coordinates,
β = direction angle relative to normal surface,
α = angle of inclination between two planes, and
s = distance between two planes.

A second possible method to calculate radiation from catalyst to pavement is to use the solid angle concept instead of the view factor, as shown in Figure 4 and described as follows:

$$I_{q_2} = \epsilon_c \sigma_b \frac{\text{solid } \angle}{2\pi} (T_c^4 - T_v^4) \tag{11}$$

where I_{q_2} is the radiation intensity of q_2 directly below the center of the catalyst at a distance Z, and solid $\angle$ is the solid-angle catalyst carved out to a point Z distance below the center.

Equation 11 gives the radiation intensity directly below the center of the radiating body. This intensity drops off for locations away from the Z axis. I_{q_2} reduces to half when the radial distance is about 0.76 Z from the Z axis. It also decreases as Z increases, and vice versa.

The solid angle is calculated by

$$\text{solid } \angle = \int_0^{2\pi} \int_0^{\theta_{max}} \sin(\theta)\, d\theta\, d\phi \tag{12}$$

Integration yields

$$\text{solid } \angle = -\cos(\theta) \Big|_0^{\theta_{max}} \cdot 2\pi$$

$$= 2\pi [1 - \cos(\theta_{max})] \tag{13}$$

From Figure 4

$$\cos(\theta_{max}) = \frac{Z}{\sqrt{Z^2 + r^2}} \tag{14}$$

where r is the radius of catalyst (Equation 9), and Z is the distance between catalyst and pavement.

Substituting Equation 14 into Equation 13 and then into Equation 11 will give the intensity. Total radiation absorbed by the pavement is obtained using the three-step process described earlier by adding q_1 and q_2. q_2 is the intensity (I_{q_2}) multiplied by the pavement area (A_p). That produces the following calculation:

$$q_t = \epsilon_c \sigma_b A_p \left[1 - \frac{Z}{\sqrt{Z^2 + R^2}}\right] (T_c^4 - T_v^4) + q_1 \quad (15)$$

Data and Calculations

From these theories, radiation heat transfer from catalyst to pavement can be calculated by knowing pavement temperature, catalyst temperature, vehicle underside temperature, catalyst geometry, and emissivity of the catalyst.

Pavement surface temperatures were computed using the NYTEMP computer model developed by Chen (*4*). Pavement surface temperatures on midsummer afternoons were calculated to range from 40.5°C to 54°C, and a pavement surface temperature of 49°C (322°K) was used throughout the calculations.

Three vehicles (a van, a pickup truck, and a station wagon) were available for testing in this study. Temperatures of their catalysts were measured with copper constantan thermocouples attached by pipe clamps, using thermally conductive grease to ensure good contact. A multichannel data collector recorded the thermocouple readings, which were taken inside a garage at 19.5°C air temperature. It is suspected that measured catalyst temperatures might have been higher if the surrounding air temperature had been warmer, as in summer. Other vital measurements included distance from catalyst to the ground and catalyst width, length, and inclination angle. These data are summarized in Table 1.

Average temperatures of the vehicle undersides were not directly measured but should range from 30°C to 45°C. A vehicle underside temperature of 38°C (311°K) was assumed for all three vehicles. Exhaust systems were all stainless steel. Its emissivity may range from 0.17 to 0.7, depending on oxidation level and temperature. Without a scale to estimate emissivity of the three catalysts, an ϵ of 0.7 was used in this study, assuming that critical conditions existed.

Using this method, view factors had to be estimated before calculating radiation. Equation 7 was used to compute view factors for the van and pickup. Equation 10 had to be used for the station wagon, whose catalyst inclined 20 degrees with respect to the ground. Integration of Equation 10 was performed by a specialized software using numerical methods. The wagon's catalyst also had additional shielding covering its lower half, resulting in two different catalyst surface temperatures and requiring additional calculation of view factors. As shown in Figure 5, pavement beneath the catalyst was also derived into two areas. Four view factors (F_{1-3}, F_{1-4}, F_{2-3}, and F_{2-4}) were calculated using Equation 10. For the first half of the pavement (A_3), second half of the pavement (A_4), and whole pavement area, the radiation absorbed is simply the sum of both halves of the catalyst:

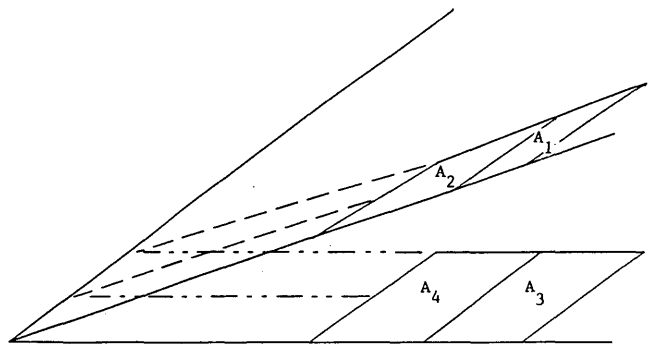

FIGURE 5 Radiation calculation for station wagon catalyst.

$$q_{A_3} = q_{A_1-A_3} + q_{A_2-A_3} \quad (16)$$

$$q_{A_4} = q_{A_1-A_4} + q_{A_2-A_4} \quad (17)$$

$$\text{Whole area: } q = q_{A_3} + q_{A_4} \quad (18)$$

Radiation heat transfer can be calculated using the three-step process described earlier. Three different pavement areas (A_p) in Equation 3 were used: half, the same, and twice the area of the catalyst (A_c). (A_p twice the area of A_c was not used for the wagon because calculation of view factors was too time consuming.) Results are given in Table 2.

The solid-angle approach was used for the van and pickup, but not for the station wagon, because this method assumes two parallel disks with uniform radiation, which the wagon did not have. Radiation was calculated with the assumption that the intensity calculated by Equation 11 decreased linearly with the increase in radial distance. Results of the solid-angle approach are given in Table 3.

TABLE 1 Catalyst Data

Vehicle	Angle of Incline	Length, m	Width, m	Area, m^2	Distance to Pavement, m	Highest Measured Temp, K
Van (8 cyl)	0	0.46	0.30	0.1380	0.28	427.44
Pickup (8 cyl)	0	0.33	0.23	0.0759	0.29	369.11
Wagon (4 cyl)						
1st Half	20	0.15	0.23	0.0345	0.19	459.11
2nd Half	20	0.15	0.23	0.0345	0.14	386.89

TABLE 2 Catalyst Radiation by View-Factor Method

Vehicle	Catalyst Area, m^2	Pavement Area, m^2	View Factor	Radiation Absorbed by Pavement, W
Van	0.138	0.069	0.160	15.6
		0.138	0.286	26.7
		0.276	0.463	39.1
Pickup	0.076	0.038	0.103	-0.15
		0.076	0.076	-0.76
		0.152	0.325	-3.01
Wagon	0.069			
1st Half		0.0345	$F_{1-3} = 0.005$ $F_{2-3} = 0.004$	6.26
2nd Half		0.0345	$F_{1-4} = 0.003$ $F_{2-4} = 0.007$	5.01
Whole Area		0.0690	--	11.28

The view factor for parallel concentric disks (Equation 7) and the solid angle (Equations 13 and 14) are similar mathematical functions. Both converge to 1 when the distance between catalyst and pavement (a or Z) approaches 0, and both approach 0 when distance approaches infinity. They differ somewhat in that the view factor takes into account the areas of both radiating bodies, whereas the solid angle directly considers only the hotter body area. Figure 6 compares the two functions using the van's catalyst data. This figure shows that the solid-angle factor (i.e., solid angle divided by 2π) is less than the view factor when pavement area exceeds or equals catalyst area, or both. When pavement area is half the catalyst area, the solid-angle factor is greater than the view factor. At this point, the authors do not know why these two approaches for the same problem yield quite different results, as shown in Tables 2 and 3.

Tests

To verify the foregoing theories and calculations, a simple experiment was conducted. Knowing that the enthalpy of air-saturated water is about 4.18 J/(g · °C) heat absorbed by water can be calculated. A known volume of water with the same surface area as the pickup truck catalyst was placed beneath it for a measured duration, and temperature change was recorded. About 3000 ml of distilled water with a surface area (facing the catalyst) of 0.0759 m^2 and depth of 39.5 mm was enclosed in plastic, covered with black paper, and placed 114.3 mm beneath the pickup catalyst for 51 min. Water temperature increased by 2.5°C. The calculated heat absorbed by the water was 10.24 W. Performing the radiation calculation using the view-factor method yielded a net flux of 8.5 W. The solid-angle method yielded an intensity of 69.6 W/m^2, corresponding to a net flux of 5.3 W.

This test indicates that the view-factor radiation calculation procedure is fairly accurate. The difference between calculated and measured heat transfer can be attributed to omission of convection heat transfer in the calculation because a considerable amount of heat could be transferred through convection during the 51-min period. The test also suggests that the solid-angle calculation is less accurate than the view-factor method.

SOLAR RADIATION

Radiation delivered to the pavement can be calculated by knowing the extraterrestrial radiation and percent of possible sunlight on a given day, using the following equation:

$$H = (a + b \cdot S) \cdot H_0 \tag{19}$$

TABLE 3 Catalyst Radiation by Solid-Angle Method

Vehicle	Solid Angle/2π	Pavement Area, m^2	Average Intensity I_{q_2}, W/m^2	Radiation Absorbed By Pavement, W
Van	0.1994	0.069	156.1	5.31
		0.138	142.5	8.76
		0.276	123.3	12.20
Pickup	0.1186	0.038	37.9	-1.56
		0.076	35.7	-3.29
		0.152	32.5	-7.08

where

H = solar radiation delivered to pavement (W/m^2),
a, b = constants,
S = percent of possible sunlight, and
H_0 = extraterrestrial radiation (W/m^2).

H_0 is obtained by using the NYETRI computer program developed by Chen (*4*) and is about 1100 to 1200 W/m^2 at 1:00 p.m. on a typical day in July or August. S on clear days is normally 90 percent or more. For Albany it was estimated that a = 0.15 and b = 0.556. Using these parameters, with good weather conditions solar radiation reaching the pavement may be as high as 800 W/m^2, with an average of 600 W/m^2 at 1:00 p.m. in July. Table 4 lists calculated solar radiation on hottest day and monthly averages for July and August of 1990 through 1992, using actual weather data from the Albany County Airport. From these data, 800 W/m^2 was used for solar radiation reaching the pavement.

Before calculating the amount of radiation that the pavement absorbs from the sun, one must subtract the portion that is reradiated and returned upward after reaching the pavement surface. This "black-body" radiation was calculated using Equation 1. Using the previous assumption that the pavement surface temperature was 322 K, the pavement radiated at 610 W/m^2. This resulted in a net absorption (by the pavement from the sun) of 190 W/m^2. This intensity was used in the comparisons of catalyst radiation.

TABLE 4 Solar Radiation Reaching Pavement at 1:00 p.m.

Month	Year	Average, W/m^2	High, W/m^2	Date of High
July	1990	596.3	701.3	4
	1991	650.0	830.8	1
	1992	509.2	707.4	6
August	1990	512.7	750.9	31
	1991	601.3	777.8	5
	1992	481.0	553.2	12

RESULTS AND DISCUSSION

Calculated radiation (using the view-factor method) that pavements absorbed from catalysts of the three tested vehicles and the sun is listed in Table 5. The pavement absorbed less radiation than it emitted to the environment, primarily because of the pickup catalyst's relatively low temperature and high position. The van catalyst radiated slightly more heat to the pavement directly beneath it than did the sun to that same pavement area. For the wagon, catalyst radiation was slightly less than solar radiation for the pavement area beneath the catalyst. For pavement areas twice as large as the catalysts, solar radiation far exceeded catalyst radiation.

These results indicate that (compared to the sun) some catalysts may significantly affect pavement temperature, but this is limited only to areas directly beneath the catalysts. Some combination of vehicles in a traffic stream having hot, old, low, and large catalysts located at various lateral positions across their widths might increase pavement temperature and contribute to rutting damage at intersections or along congested roadway sections.

The fact that the wagon had a shield over the lower half of its catalyst and that all three vehicles had shielding between the catalysts and passenger compartments indicates that vehicle designers are concerned about protecting the pavement and surrounding objects from excessive heat generated by catalysts and other high-temperature engine parts. Catalysts of vehicles of average age (3 to 5 years) have midrange emissivity. Vehicles with low centers of gravity, such as sports cars, may significantly affect the pavement because the catalyst is so near its surface. On the other hand, trucks are likely to have less effect because the exhaust system is farther from the pavement. Because so few vehicles were included in this study, the real effect of vehicle catalysts remains unknown.

The relation between vehicle heat and pavement temperature is highly complex. Not only vehicle configuration, but also vehicle movement and the effect of small-area heating on pavement temperature must be considered. Any specific area of pavement at intersections or along congested roadways is subjected to con-

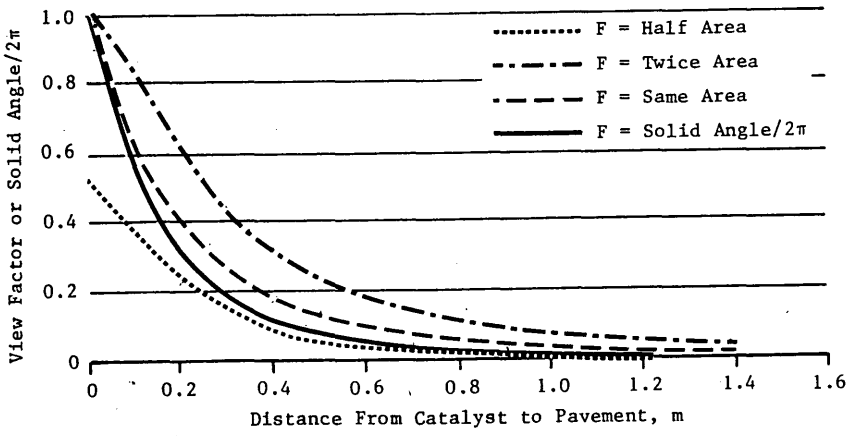

FIGURE 6 Comparison between view factor and solid angle.

TABLE 5 Comparison of Catalyst and Solar Radiation

Vehicle	Catalyst Area, m^2	Pavement Area, m^2	Radiation Absorbed From Catalyst, W	Radiation Absorbed From Sun, W
Van	0.138	0.069	15.6	12.8
		0.138	26.7	26.2
		0.276	39.1	52.4
Pickup	0.076	0.038	-0.15	7.2
		0.076	-0.76	14.4
		0.152	-3.01	28.9
Wagon	0.069			
1st Half		0.0345	6.26	6.55
2nd Half		0.0345	5.01	6.55
Whole		0.0690	11.28	13.10

stantly changing radiation as a result of vehicle movement and varying catalyst characteristics (temperature, location, size). The mechanism of temperature rise in pavement caused by small-area heating by catalysts and its relation to rutting are yet to be investigated.

Including the convection effect in this problem increases the calculated heat transfer because some heat can be transferred through the air between vehicle and pavement, even against gravity if enough time elapses. Vehicle movement to some extent disturbs this process and reduces its effects.

CONCLUSIONS

Heat transfer by radiation from catalyst to pavement is a function of catalyst temperature, pavement temperature, temperature of the vehicle underside, catalyst emissivity (in turn affected by its level of oxidation, color, and finish), distance from catalyst to pavement, catalyst size, and the pavement area being considered. According to the calculations, catalysts of some vehicles can radiate more heat than the sun to the small pavement areas beneath them. Because of the very small vehicle sample in this study and the problem's complexity, no general conclusion can be drawn about whether vehicles cause additional temperature increase and thus rutting damage to bituminous pavements.

RECOMMENDATIONS

This relationship between vehicle heat and bituminous pavement does not appear to have been studied in the past, and many unanswered questions remain. From this investigation, the following future research is suggested:

1. Pavement temperature measurement
   - Simple: Measure pavement temperatures at about 1:00 p.m. on hot summer days, with and without vehicles parking over thermocouples, to determine whether running engines emit more radiation to the pavement than does the sun.
   - Detailed: Place thermocouples in approach and nonapproach sections at a busy intersection (such as Routes 5 and 155), to determine whether the combined effect of several vehicles and their movement causes any increase in pavement temperature. The same measurement plan can also be tried on highly congested and less-traveled sections of a roadway.
2. Convection study. Investigate how properly to include convection into heat-transfer theory and calculation for this problem.
3. Simulation study.
   - Comprehensive vehicle sampling: Obtain necessary data (catalyst location, size, and temperature, and vehicle underside temperature) for a sample of vehicles reasonably representing those on the road.
   - Simulation: Compute expected radiation distribution for intersections and congested pavement areas, using data from sampling and simulation techniques. This can assess effects of mixed vehicles and their movement and may help clarify the results from Study 1.
4. Temperature and modulus model. Establish temperature distribution across a pavement lane width under the influence of prevailing vehicle heat. From this temperature model, compute the corresponding in situ modulus distribution within the bituminous pavement.
5. Finite element analysis and rut prediction. Mechanistic responses of the pavement can be computed by the finite element method, using the modulus obtained in Study 4. Then rutting may be predicted on the basis of these responses with existing rut models or new ones to be developed.

ACKNOWLEDGMENTS

This study was initiated and conducted under general supervision of Robert J. Perry, Director of Engineering Research and Development, New York State Department of Transportation. The authors thank John Kimball of the Physics Department, State University of New York at Albany, for providing considerable technical supervision throughout the study.

REFERENCES

1. Holman, J. P. *Heat Transfer*, 7th ed. McGraw-Hill, Inc., New York, 1990.
2. Howell, J. R. *A Catalog of Radiation Configuration Shape Factors*. McGraw-Hill, Inc., New York, 1982.
3. Gross, U., K. Spindler, and E. Hahne. Shapefactor-Equations for Radiation Heat Transfer Between Plane Rectangular Surfaces of Arbitrary Position and Size with Parallel Boundaries. *Letters in Heat and Mass Transfer*, Vol. 8, 1981, pp. 219–227.
4. Chen, H. J. *NYTEMP User's Manual: A Pavement Temperature Model*. Special Report 111. Engineering Research and Development Bureau, New York State Department of Transportation, Albany, July 1993.

Publication of this paper sponsored by Committee on Surface Properties–Vehicle Interaction.

Kansas Experience with Smoothness Specifications for Concrete Pavements

WILLIAM H. PARCELLS, JR., AND MUSTAQUE HOSSAIN

Because it affects road users directly, smoothness, or riding comfort, determines the quality of newly constructed pavements. There is a growing interest in the industry in attaining increasingly smoother pavement surfaces. Smoothness specifications for portland cement concrete pavements (PCCP) now in effect in Kansas have evolved through applications over the last 8 years. Pavement profiles of short wavelengths and smaller amplitudes than the industry-accepted 5.1 mm (0.2 in.) can decrease the ride quality of pavements. This experience has led the Kansas Department of Transportation (KDOT) to eliminate the blanking band width in the profilograph trace reduction process. The implementation of this zero or null blanking band was successful and has resulted in better-quality pavements. The latest proposed specifications will increase the amount of bonus that can be achieved but might result in more grinding unless the PCCP pavers were able to improve the pavement smoothness in the middle (full-pay/grind) ranges. An analysis of effect of as-constructed smoothness on the roughness history of pavements has shown that the ride quality over the service life of pavements is highly dependent on the smoothness achieved during construction. Limited cost analysis has shown an increasing amount of bonus achieved in PCCP construction over the last few years, indicating quality paving.

Pavement smoothness or roughness can be described by the magnitude of profile irregularities and their distribution over the measurement interval. The road surface smoothness on newly constructed pavement is a major concern for the highway industry. Because it affects the road users directly, this smoothness, or riding comfort, is a measure of the quality of the newly constructed pavements. According to Hudson (*1*), the primary purpose for smoothness measurement is to maintain construction quality control. There is a growing interest in the industry for attaining increasingly smoother pavement surfaces. Results from a 1992 NCHRP study show that of the 22 states reporting, 91 percent utilized smoothness criteria on new pavement construction (*2*). A 1990 NCHRP Synthesis study (*3*) showed that of the 36 states reviewed, 80 percent used smoothness criteria on new pavement construction. The increasing trend in the use of ride quality specifications is also evidenced by the 1992 study in which respondents from 21 states out of 25 queried believe that there will also be a future increase in ride quality requirements. The 1987 AASHTO survey results showed that 53 percent of the states using profilographs for acceptance of concrete pavements used incentive and disincentive specifications (*4*). The incentive/disincentive values in smoothness specifications typically ranged from 1 to 5 percent of the bid item price, with 31 percent of these states reporting allowable incentives up to 5 percent. The relatively high incentives now possible with many of the profilograph specifications place an ever-increasing burden on the measurement and data reduction processes. Variability in test results can significantly affect contractor payments (*5*).

W. H. Parcells, Jr., Bureau of Materials and Research, Material and Research Center, Kansas Department of Transportation, 2300 Van Buren, Topeka, Kans. 66611-1195. M. Hossain, Department of Civil Engineering, Kansas State University, Manhattan, Kans. 66506.

DEVELOPMENT OF PORTLAND CEMENT CONCRETE PAVEMENT SMOOTHNESS SPECIFICATIONS

In 1985 the Kansas Department of Transportation (KDOT) selected a 7.63-m (25-ft) California-type profilograph using the 5.1-mm (0.2 in.) blanking band for evaluation of the profilogram for determining smoothness of portland cement concrete pavement (PCCP) construction (*6*). In 1985 the first three PCCP projects having smoothness requirements were constructed. The specifications implemented on these projects are shown in Table 1. However, the incentive clauses were not exercised. Profilograph measurements were taken on each wheelpath. The profilograph results in terms of profile roughness index (PRI) on 0.16-km (0.1-mi) intervals on these projects were analyzed and are shown in Table 2. The first two projects had a high percentage of sections in the bonus range, indicating smoothness of 0 to 63 mm/km (0 to 4 in. mi) was practical and easily achievable. The relatively high percentage of sections in the penalty range on the I-70 project was caused by contractor negligence.

The eastbound lanes of the I-70 project paved in 1986 by the same contractor were remarkably smoother. The profilograph results showed that on the eastbound lanes there were 84 sections with 41 sections (49 percent) in the bonus range, 41 sections (49 percent) in the full-pay range, and 2 sections (2 percent) in the penalty zone. These figures showed a significant improvement in 1 year. These projects showed that the smoothness specifications shown in Table 1 were achievable and resulted in better-quality pavements. In 1990 the specifications shown in Table 3 were adopted as standards for control of concrete pavement smoothness in the state of Kansas.

REVISED TRACE REDUCTION PROCEDURE

In 1990 there was a noticeable high-frequency vibration on a PCCP reconstruction project on I-70. However, this vibration was not noticed for another concurrent new PCCP project on I-470. A closer review of the profilograph traces on these projects showed that on the I-70 project there was a significantly consistent sine

TABLE 1 Schedule for Adjusted Payment for PCCP (Special Provision 80P-232)

Profile Index millimeter per kilometer per 0.16 km segment	Price Adjustment Percent of Contract unit bid price
190 or less	100
191 to 206	98.0
207 to 222	96.0
223 to 238	90.0
238 or higher	Corrective work required or replace

Incentive was based on the initial profile index and on a section which was a break in paving such as a bridge or day's end joint or other interruption.

0 to 64 millimeter per kilometer	105.0 Percent of unit bid

TABLE 2 Specification Compliance of 1985 Projects

Roadway	No. of 0.16 km sections	Compliance with specified PRI (mm/km)					
		Bonus (0 - 64)	(%)	Full Pay (65 -191)	(%)	Penalty (>191)	(%)
US 73*	80	24	30	51	64	5	6
US 50 EB**	99	64	65	28	28	7	7
US 50 WB**	103	64	62	26	26	13	12
I-70 WB*	94	5	5	43	46	46	49
All 1985	376	157	42	148	39	71	19

* PRI values were average of four traces (one trace in each wheel path)
** PRI values were average of two traces (one trace in each wheel path)
Note: 1 in = 25.4 mm, 1 mile = 1.6 km

TABLE 3 Schedule for Adjusted Payment for PCCP (1990 Specification 502.06)

Profile Index millimeter per kilometer per 0.16 kilometer segment	Price Adjustment Percent of Contract unit bid price
48 or less	106
49 to 64	103
65 to 159	100
160 to 191	96
192 to 222	92
223 to 238	90
239 or more	88 (Corrective Work required or replace)

Note: 1 in = 25.4 mm
1 mile = 1.6 km

wave cyclic oscillation of about 2.44-m (8-ft) spacing and with 5.1-mm (0.2-in.) amplitudes, as shown in the example trace of Figure 1. Most of these surface deviations were covered up by the 5.1-mm (0.2-in.) blanking band during trace reduction. On the I-470 project, the oscillation waves had a spacing of about 9.14 m (30 ft) and an amplitude of about 5.1 mm (0.2-in.) (also shown in Figure 1), which were, again, covered up by the 5.1-mm (0.2-in.) blanking band during trace reduction. This issue of the effects of short wavelengths on PRI was tied to the question about the proper blanking band width. It is interesting to note that this issue is not new and dates back to the mid-sixties when General Motors decided to use a 2.54-mm (0.1-in.) blanking band for the construction of one of their test facilities, even though the practice of using the 5.1 mm (0.2-in) blanking band was then well established. According to the engineers of General Motors (*7*),

> On-site evaluations of the roughness of recently constructed California roads indicated that, while they exhibited very few long wavelength irregularities, they seemed to have a considerable amount of short wavelength roughness of very low amplitude. This is felt in the vehicle more as a sensation of wheel motion than of noticeable road roughness. It was reasoned that this problem could be caused by the existence of many small-amplitude bumps that might well lie within the 5.1 mm (0.2 inch) tolerance California allows. In an attempt to minimize this, the Proving Ground decided to reduce this band to 2.54 mm (0.1 inch), but otherwise adopt the California method.

The blanking band concept was originally developed as a convenient method for analyzing mechanical profilograph traces 30 years ago. This makes the resulting PRI an artifact of the test and data reduction procedures. According to Hveem (*8*), developer of the profilograph:

> While the profile index appears to be reasonably satisfactory for use in specification, it fails to differentiate between bumps or irregularities of different shape and of different lengths. This numerical expression does not adequately emphasize the annoyance in terms of

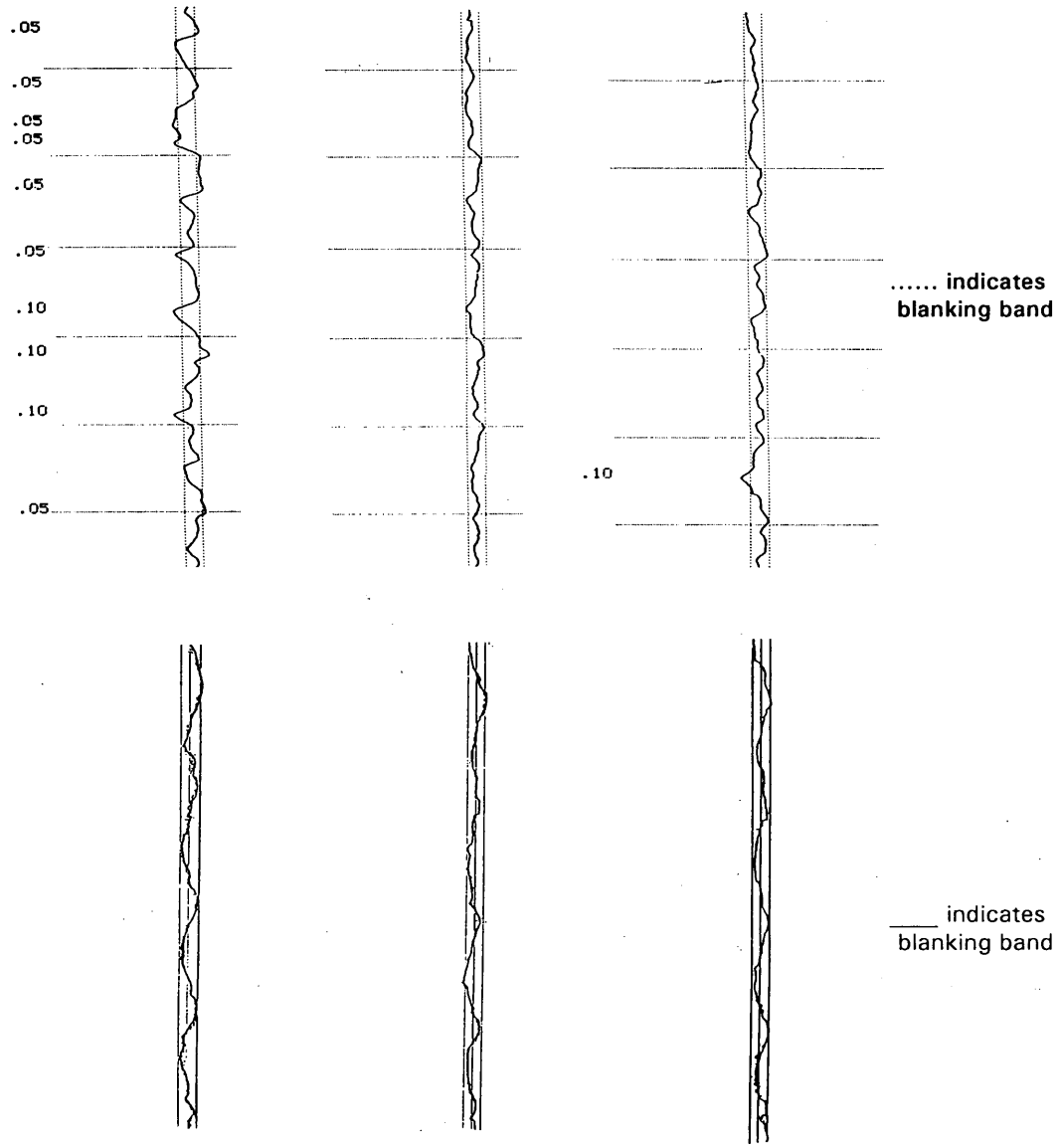

FIGURE 1 Profilograph traces from I-70 and I-470 projects: sample traces from I-70 Geary County (*top*) and I-70 Shawnee County (*bottom*) (*6*).

riding qualities generated by badly faulted pavement for example. A somewhat more elaborate system of deriving a numerical index will be necessary if it becomes important to assign numbers to existing highways or airfields.

Research conducted by the Pennsylvania Transportation Institute (*9*) has shown that the blanking band concept is not acceptable for smoothness levels of less than 110 mm/km (7 in./mi).

The I-70 and I-470 projects of 1990 prompted KDOT to experiment with the blanking band width to quantify the apparent visual difference of profilograph traces on these projects. It was decided to use a zero blanking band width or null blanking band. The null blanking band is nothing but a reference line usually placed approximately at the center of the trace having the line equally dividing the scallops above or below the center line. In addition to these projects, traces from all the PCCP projects on which profilographs had been used in 1990 were reanalyzed using the null blanking band. Tables 4 and 5 show the results of this comparative study of blanking band widths on I-70 and I-470 sections, and all 740 of the 0.16-km sections.paved in 1990. Results from Table 5 indicate that the majority of the sections on the I-70 projects were in the bonus range when analyzed with the 5.1-mm (0.2-in.) blanking band even though the ride quality on this project was perceived by the state personnel to be very poor. As shown in Table 5, the use of zero blanking band results in a wider distribution of PRI values and movement of data points away from the range of 0 to 158 mm/km (0 to 10 in./mi) [proposed to replace the previously used range of 0 to 64 mm/km (0 to 4 in/mi) or bonus range]. This apparently indicates that achieving bonus would be harder with the zero blanking band. However, it is beyond any doubt that this improved the ability of the profilograph to measure PCCP smoothness quality, taking into account the lower-quality ride produced by roughness waves of short wavelengths and smaller amplitudes with no increased demand or hardship on the contractor or the inspector. Only the trace reduction procedure was changed, and the entire procedure for using the zero blanking band was included in KT-461, the revised KDOT test method for operation of a profilograph and trace reduction (*10*). On the basis of these results, a new set of special provisions (90P-111) were incorporated for the 1992 construction projects. This required use of the null blanking band (0.25 mm or 0.01 in. for the computerized profilographs) for profilograph trace reduction and established separate limits on the calculated PRI for roadways with posted speed limits higher or lower than 72 km/hr as shown in Table 6. The profilograph results for the 1990 through 1992 projects with zero blanking band are shown in Table 7. The results indicate almost no change in the number of sections in the three broad ranges. The PRI limits required by the specifications were easily achievable with the current practice of paving. One of the concerns for the "null" blanking band was whether the repeatability of trace reduction could be achieved with this type

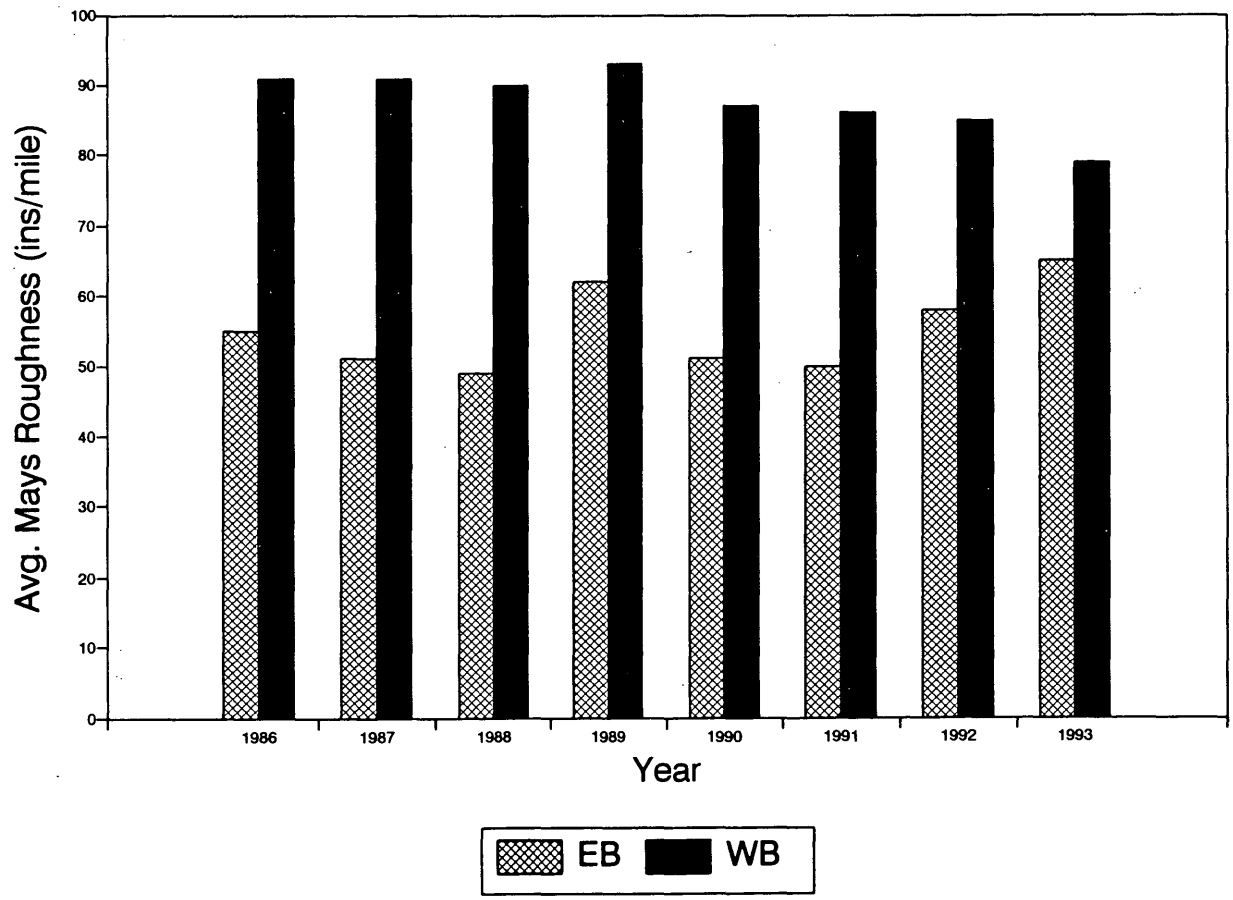

FIGURE 2 Mays roughness history of 1985 I-70 PCCP project, MP 9.27–17.00.

of blanking band. KDOT, in cooperation with Kansas State University, has fully automated the process of trace reduction using a user-friendly personal computer-based methodology (*10*).

REVIEW OF PROPOSED SPECIFICATIONS FOR 1993

Currently, special provisions 90P-111-R1 shown in Table 8 are being proposed for 1993. The maximum amount of bonus has been increased from 6 percent of the bid item price to 8 percent; however, the full-pay range has been narrowed to include slightly more rigid grind-back provisions. Table 9 compares the compliance with the proposed 1993 specifications using data from the 1992 projects for roadway segments with posted speed limits greater than 72 km/hr. It is evident that the revised ranges in the proposed specifications might result in more grinding unless the PCCP pavers were able to improve the pavement smoothness in the middle (full-pay/grind) ranges (*11*).

EFFECT OF INITIAL SMOOTHNESS ON ROUGHNESS HISTORY OF PAVEMENTS

Roughness histories of the 1985 and 1986 I-70 PCCP projects were analyzed using the Mays roughness data from the pavement management system (PMS) data base. The Mays roughness data are collected annually for the PMS data base on each mile of the KDOT highway system. Figure 2 shows the average Mays roughness for 13 km (8 mi) for each year the pavement has been in service since 1985. The eastbound direction was built smoother and, thus far, has remained so as compared with the westbound direction.

The roughness history of the 1990 I-70 PCCP project was also analyzed as shown in Figure 3. As-built smoothness on both directions of this project were comparable and has remained so 3 years after construction with slightly rougher eastbound lanes. However, because of poor ride quality, predominantly large portions of the eastbound lanes were ground in the fall of 1992.

COST ANALYSIS

It is well known that there is a speculation in the industry that changes in specifications result in higher cost. Table 10 shows an analysis of average statewide PCCP unit bid costs from 18 projects between 1990 and 1992. The results indicate that the contractor price differs slightly from the state estimate and may be higher or lower without any definite trend. Table 11 shows the smoothness-related payments made out to the contractors in 1990 and 1991. Data from eight projects covering 72.2 lane-mi in 1990 and three projects with 4.4 lane-mi in 1991 are shown. Most of

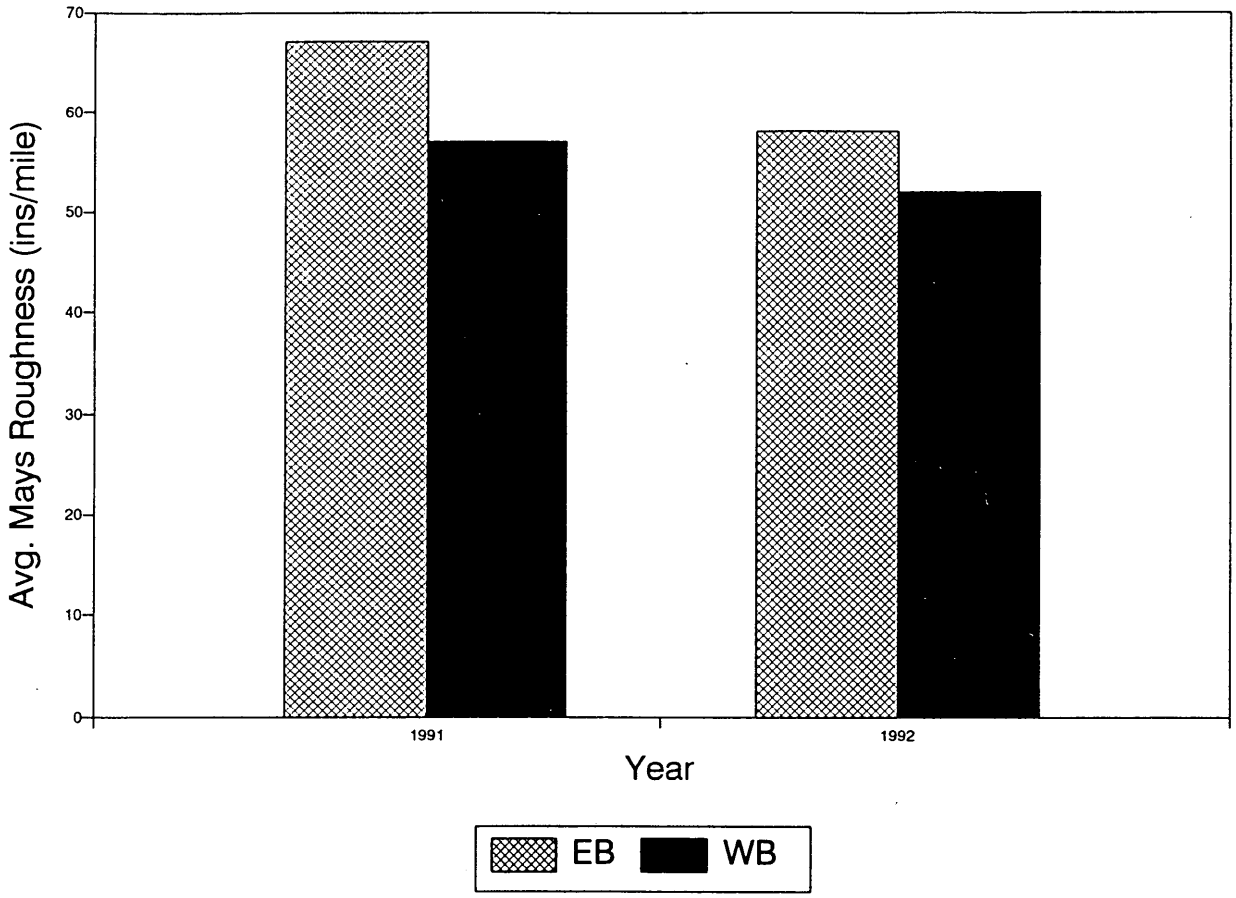

FIGURE 3 Mays roughness history of 1990 I-70 PCCP project, MP 0.00–7.00.

TABLE 4 Specification Compliance of Projects Blanking Band

Roadway	No. of 0.16 kilometer sections	Compliance with specified PRI (mm/km)					
		Bonus (0 - 64)	(%)	Full Pay (65 - 159)	(%)	Penalty (>159)	(%)
I 70	132	62	47	51	64	5	6
I 470	77	50	65	26	34	1	1
All 1990	740	469	63	197	27	74	10

Note: Profilograph results were attained with a 5.1-mm (0.2-in.) blanking band width.

TABLE 5 Profilograph Results with Null Blanking Band and Proposed Specified Ranges

Roadway	No. of 0.16 kilometer sections	Compliance with specified PRI (mm/km)					
		(0 - 159)	(%)	(160-635)	(%)	(>635)	(%)
I 70	132	0	0	91	69	41	31
I 470	77	0	0	77	100	0	0
ALL 1990	740	10	1	656	89	74	10

Note: 1 in = 25.4 mm
1 mile = 1.6 km

TABLE 6 Schedule for Adjusted Payment for PCCP (Special Provision 90P-111)

Profile Index millimeter per kilometer per 0.16 kilometer section (> 72 km/h)	Profile Index millimeter per kilometer per 0.16 kilometer section (72 km/h or less)	Price Adjustment Percent of contract unit bid price
175 or less	238 or less	106
176 to 238	239 to 397	103
239 to 635	398 to 794	100
636 to 952	795 to 1111	100 (Grind Back)
953 to more	1112 to more	95 (Grind back or remove & replace)

TABLE 7 Profilograph Results on PCCP in Kansas for 1992 Special Provisions 90P-111

Roadway	No. of 0.16 kilometer sections	Compliance with specified PRI (mm/km)					
		PRI (0 - 238) Bonus	(%)	PRI (239 - 635) Full-pay	(%)	PRI (>635) Penalty	(%)
1990 (reanalysis)	740	111	15	555	75	74	10
1991 (reanalysis)	290	55	19	203	70	32	11
1992	682	123	18	484	71	75	11

Note: 1 in. = 25.4 mm
1 mile = 1.6 km
Results were attained using zero or 0.254-mm (0.01-in.) blanking band.

TABLE 8 Schedule for Adjusted Payment for PCCP (1992 Special Provisions 90P-111-R1)

Profile Index millimeter per kilometer per 0.16 km section (72 km/h or greater)	Profile Index millimeter per kilometer per 0.16 km section (72 km/h or less & ramps)	Price Adjustment Percent of Contract unit bid price
175 or less	238 or less	108
176 to 238	239 to 397	104
239 to 476	398 to 715	100
477 to 794	716 to 1032	100 (Grind back)
795 or more	1033 or more	95 (Grind back or remove and replace)

TABLE 9 Effect of Proposed 1993 PCCP Smoothness Specifications (90P-111-R1) on Construction in Kansas

Specification	No. of 0.16 km sections	Compliance with specified PRI (mm/km)							
		PRI (0 - 238) Bonus	(%)	PRI (239 - 635) Full-pay	(%)	PRI (636-952) Full-pay/ Grind	(%)	PRI (>952) Penalty	(%)
90P - 111	529	127	24	370	70	27	5	5	1
90P - 111- R1	529	(0-238)	(%)	(239-477)	(%)	(478-794)	(%)	(> 794)	(%)
		127	24	280	53	111	21	11	2

Note: 1 in. = 25.4 mm
1 mile = 1.6 km
Roadways were marked as having speed limits greater than 72 km/hr (45 mph).

TABLE 10 Average PCCP Unit Bid Cost for 1990–1992

Year	No. of Projects	Avg. PCCP unit bid cost ($/ meters sq.) state	Avg. PCCP unit bid cost ($/ meters sq.) contractor	Difference (%)
1990	7	21.4	21.7	+1.4
1991	5	27.03	24.27	-10.0
1992	6	21.89	24.17	+10.0

TABLE 11 Cost Analysis of Smoothness Specifications

Year	No. of Proj-ects	Smoothness-related Cost ($)						
		Total	Bonus	% of Total	Full-Pay	% of Total	Pen-alty	% of Total
1990	8	16,703,551	599,258	3.6	16,041, 437	96	62,856	0.40
1991	3	1,639,067	80,083	4.9	1,541, 159	94	17,825	1.1

the projects of 1991 are still not closed. In 1990, the contractors received 3.6 percent bonus and 96 percent full payments. The penalty represented only 0.4 percent of total payment. The penalty rose to 1.1 percent of total payments in 1991. However, bonus payments also rose to 4.9 percent (an increase of 1.3 percent) over 1990, negating a higher penalty. It appears that incentive payments have had a positive impact and resulted in quality paving.

CONCLUSIONS

Smoothness specifications for PCCP pavements now in effect in Kansas have evolved over the last 8 years. Pavement profiles with short wavelengths and smaller amplitudes than the industry-accepted 5.1 mm (0.2 in.) can adversely affect the ride quality of pavements. This experience has led KDOT to eliminate the blanking band width in the profilograph trace reduction process. The implementation of this zero or null blanking band was successful and has resulted in better-quality concrete pavements in Kansas. The latest proposed specifications will increase the amount of bonus that can be achieved by a contractor but might result in more grinding unless the PCCP pavers were able to improve the pavement smoothness in the middle (full-pay/grind) ranges. An analysis of effects of as-constructed smoothness on the roughness history of pavements showed that the ride quality over the service life of pavements is dictated by the initial smoothness, i.e., the smoothness achieved during construction. Limited cost analysis has shown that an increasing amount of bonus achieved in PCCP construction over the last few years indicated quality paving.

ACKNOWLEDGMENTS

The authors acknowledge the financial support provided by KDOT for this study. Thanks are due to Dean Testa, of the Bureau of Construction and Maintenance, Loni Ingram, of the Bureau of Materials and Research, and Dick McReynolds, of the Research Department for their continued interest and support for smoothness research in Kansas.

REFERENCES

1. Hudson, W. R. Road Roughness: Its Elements and Measurement. In *Transportation Research Record 836*, TRB, National Research Council, Washington D.C., Dec. 1981.
2. Scofield, L. A. *NCHRP Project 20-7, Task 53: Profilograph Limitations, Correlation, and Calibration Criteria for Effective Performance Based Specifications.* Final Report. TRB, National Research Council, Washington D.C., Dec. 1992.
3. Woodstrom, J. H. *NCHRP Report 167: Measurement, Specifications, and Achievement of Smoothness for Pavement Construction.* TRB, National Research Council, Washington, D.C., Nov. 1990.
4. *Summary of Results of the 1987 AASHTO Rideability Survey.* AASHTO Highway Subcommittee on Construction, AASHTO, Washington, D.C., 1988.
5. Scofield, L. A., S. Kalevela, M. Anderson, and A. S. M. Hossain. *A Half Century with the California Profilograph.* Report FHWA-AZ-SP9102, Arizona Department of Transportation, Phoenix, Feb. 1992.
6. Parcells, W. H. Jr. *Control of Pavement Trueness in Kansas.* Interim Report. Kansas Department of Transportation, Topeka, Jan. 1992.
7. Lundstrom, L. C. and P. C. Skeels. *Surface Control Methods Employed on General Motors Proving Ground Circular Test Track.* Internal Report. General Motors Engineering Services, Milford, Mich. May 1964.

8. Hveem, F. N. *Profilograph 2*. California Highway and Public Works, March–April 1960, pp. 51–57.
9. Kulakowski, B. T. and J. W. Wambold. *Development of Procedures for the Calibration of Profilographs*. Report FHWA-RD-89-110. Pennsylvania Transportation Institute, Pennsylvania State University, University Park, Aug. 1989.
10. Devore, J. and M. Hossain. *An Automated System for Determination of Pavement Profile Index and Location of Bumps for Grinding from the Profilograph Traces*. K-TRAN Project 92-2. Kansas State University, Manhattan, July 1992.
11. Parcells, W. H. Jr. *Control of Pavement Trueness in Kansas*. Interim Report. Kansas Department of Transportation, Topeka, Jan. 1993.

Publication of this paper sponsored by Committee on Surface Properties–Vehicle Interaction.

Correlation Study of California Profilograph and K. J. Law Profilometer

SYLVESTER A. KALEVELA, ESTOMIH M. S. KOMBE, AND LARRY A. SCOFIELD

The Arizona Department of Transportation (ADOT) uses the California profilograph and the K. J. Law 690 DNC profilometer for measuring pavement roughness. However, ADOT has not used the K. J. Law profilometer on portland cement concrete (PCC) pavement construction contracts because the current smoothness specifications are given in terms of the California profilograph index (PRI). This study was initiated to determine the feasibility of including the K. J. Law profilometer as one of the principal devices for testing PCC pavement surface smoothness. To accomplish that objective (a) PCC pavement sections were selected for use in the testing of the K. J. Law profilometer and the California profilograph, (b) pavement roughness data were obtained from the selected sections by both the profilometer and profilograph, and (c) correlation analysis was conducted for the two types of devices. It was found from this study that (a) between three and five replicates are required to obtain a good estimate of the PRI and (b) a good linear relationship is obtainable for the mean values of profilometer Mays index and PRI and also between the profilometer international roughness index and PRI values. On the basis of this study, it was concluded that (a) the California profilograph and the K. J. Law profilometer can be linearly correlated, (b) it is feasible to calibrate the California profilograph by the profilometer, (c) the profilometer must be calibrated first before it can be used to calibrate profilographs, and (d) it is not practical to interchangeably use the profilometer and profilographs because each device is more suited for some jobs than others.

The most common devices used by Arizona Department of Transportation (ADOT) for measuring pavement profile roughness are the Maysmeter, the California profilograph, and the recently acquired K. J. Law 690 DNC profilometer. Pavement roughness measurements obtained with these devices are used for (a) quality control of pavement surface smoothness during construction, (b) pavement acceptance at project completion time, and (c) pavement condition monitoring for the implementation of pavement management systems.

The California profilograph and the K. J. Law profilometer are not equally suited for the various data collection needs and operating environments because of their different characteristics. For instance, the California profilograph is operated by pushing and steering it along a wheelpath. This profilograph is clearly not suited for large-scale data collection projects because of its speed limitations. The K. J. Law 690 DNC profilometer is much heavier but is operated at highway speeds. ADOT's current specification for the profilometer speed is 50 mph. The K. J. Law profilometer is not suited for use at project sites with inadequate acceleration or deceleration distances and on new PCC pavements that cannot support the weight of the profilometer system.

S. A. Kalevela and L. A. Scofield, Arizona Transportation Research Center, Arizona Department of Transportation, 7755 South Research Drive, Suite 106, Tempe, Ariz. 85284. E. M. S. Kombe, Department of Industrial and Management Systems Engineering, College of Engineering and Applied Sciences, Arizona State University, Tempe, Ariz. 85287-5906.

During the summer of 1992, ADOT successfully introduced its new asphalt concrete (AC) smoothness specifications. The specifications provide for performance-based bonuses and penalties and call for the use, in the measurement of pavement roughness, of either the General Motors Research (GMR) profilometer or the Maysmeter that has been calibrated by the GMR profilometer. During the 1992–1993 fiscal year, construction projects were built according to these specifications. None of the construction projects resulted in large bonuses because the attained overall pavement smoothness levels were just slightly better than the standard specified by ADOT. In this case, pavement roughness was measured with a K. J. Law 690 DNC profilometer.

At the same time, concern was expressed about the reproducibility of profilograph test results for portland cement concrete pavement (PCCP) acceptance. Subsequently, ADOT began evaluating the feasibility of performing final acceptance of PCCP smoothness with a K. J. Law 690 DNC profilometer.

ADOT currently has an incentive/disincentive scheme in place for its PCCP construction contracts. Upon completion of PCCP construction, contractors are rewarded with a bonus for PCCP roughness that is lower than the specified standard. Similarly if the roughness is higher than this standard, the contractor is penalized. Current PCCP construction specifications are in California profilograph index (PRI) units.

It was ADOT's goal to have the specifications in both PRI and profilometer equivalent measures so that the two types of devices could interchangeably be used during the different phases of a PCCP construction contract. Since the PCCP smoothness specifications exist and are based on the PRI values, it was decided to study how profilograph measurements correlate with profilometer measurements.

ROUGHNESS INDEX UNITS

Apart from the different physical characteristics and speed of operation, the California profilograph and the profilometer produce different pavement roughness indexes. The California profilograph computes a profilograph index (PRI) for the full length of the run in inches per mile. Typically these values are between 0 and 15 in./mi. On the other hand, the profilometer can be set to compute either a Mays index or an international roughness index (IRI) or both. Both IRI and Mays are given in inches per mile and can be reported for desired section lengths irrespective of the actual total length of the test run. The Mays index is based on profile measurements from both of the wheelpaths traversed by the profilometer vehicle. The measurements are computed simultaneously to obtain the Mays index. IRI is an index computed by the computer system for each wheelpath. If desired, a mean IRI for the lane can

also be computed by averaging the individual IRIs from the wheelpaths for that lane.

PROJECT OBJECTIVE AND SCOPE

In a preliminary investigation of the correlation between profilometer roughness index values (Mays/IRI) and California profilograph index (PRI) values, roughness data using California profilograph devices were sampled from project measurements taken a few months earlier. The results of this exercise showed very poor correlation between the two devices. It was strongly felt that the problem was caused by the variability of California profilograph roughness measurements and the fact that the profilograph roughness index values had been computed on the basis of unreplicated tests using the California profilograph.

The low precision of the California profilograph made the use of single measurements from the device for correlation analysis statistically inappropriate. However, it was believed that if both devices were measuring the same physical quantity, there was reason to expect correlation between the measurements obtained with the two devices. Previous studies (*1,2*) showed that indeed there was correlation between profilometer and profilograph roughness indexes.

The principal objectives of the study were (a) to review the feasibility of correlating the California profilograph PCCP smoothness measurements with profilometer measurements and (b) to establish whether the profilometer can be used to calibrate the profilograph. To accomplish this objective, the following tasks were proposed:

- Review relevant literature about profilograph calibration methodologies and determine their suitability for this study;
- Review historical data obtained during acceptance testing of PCCP constructed for ADOT since 1986 in the Phoenix metropolitan area;
- Select, on the basis of historical data, concrete pavement sections that represent the roughness levels typically encountered during new construction;
- Test the pavement sections with both the profilograph and profilometer devices; and
- Develop a model for the relationship between profilograph and profilometer measurements of PCCP surface roughness.

REVIEW OF PROFILOGRAPH CALIBRATION PROCEDURES

The calibration of a measuring device assumes that one has a means of determining the true value of the parameter being measured. The true value can then be compared to the value obtained with the measuring device. Depending on the nature of this measurement, and the established cause of the observed difference from the true value, appropriate corrective measures may be taken. Alternatively, if an observed deficiency on the device(s) is known to result in systematic errors, a correction factor can be applied to the output from the device. In this study, the following procedures were reviewed to determine possible use for profilograph calibration:

- Use of a test section in conjunction with the Pennsylvania Transportation Institute (PTI) program for the computation of a California profilograph index,
- Use of profilometer profile data with the PTI program for the computation of a California profilograph index, and
- Calibration of profilograph by a linear regression model for the relationship between profilograph and profilometer indexes.

The procedures, their underlying assumptions, limitations, observed problems, and the results of test runs are described next.

PTI Program for Computation of Profilograph Roughness Index

The program, written in Microsoft FORTRAN for the IBM personal computer (PC) and compatible computers, was developed by Meau-Fuh Pong and reported by Kulakowski and Wambold (*3*). Its function is to calculate profile roughness index for a given set of profile elevation data obtained with a California or Rainhart procedure. The computer program requires input of profile elevations data collected at 2-in. intervals.

Test Section for Index Computation

The profilograph roughness index computation program was developed for use where a test section of known elevations exists. The known elevations are input to the program, which computes the appropriate profilograph index. The profilograph to be calibrated is used on this section, and the resulting index is compared with the computed value. Typical examples for such test sections are suggested by the authors as (a) a sinusoidal profile and (b) a horizontal section with rectangular bumps at particular locations. Because of the difficulty in the construction of a sinuosoidal section, the rectangular bumps are a more practical alternative.

LINEAR REGRESSION ANALYSIS

The following needed to be determined to conduct the regression analysis: (a) determination of the testing devices and operators; (b) identification of pavement roughness levels; (c) determination of measurements used in the analysis and of regression model and formulation of a hypothesis; and (d) procedure for data collection.

Test Devices

The correlation study investigated the correlation between profilometer pavement roughness index values (Mays and IRI) and profilograph PRI values. It was decided to initially use one profilometer (the only one available) and one automated profilograph at a filter setting of 8000. An automated profilograph is one that processes the profile readings and automatically computes the roughness index at the end of a test run.

Pavement roughness index values obtained with the profilograph and the profilometer are both expressed in inches per mile. The former is referred to as a California profilograph index (PRI) whereas the latter is computed as either a Mays index or an IRI. Although the units for these indexes are the same (inches/mile),

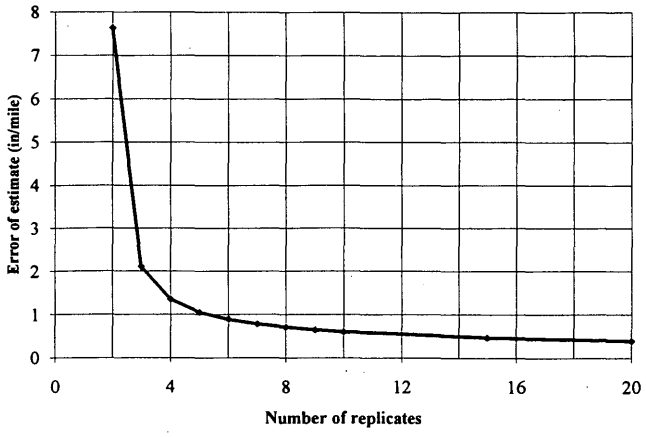

FIGURE 1 Plot of error of estimate for profilograph roughness index versus number of replications.

the magnitudes are different. Typically, PRI values for new PCCP have been found to lie in the range between 0.0 and 15.0 in./mi. The corresponding Mays index values have been found to lie in the range between 40 to 120 in./mi. Corresponding IRI values are only slightly larger than Mays index values.

Pavement Roughness Levels and Number of Test Sections

The importance of identifying the possible range of roughness values was based on how the results of the analysis can be generalized over this range. For the purpose of this study, it was believed that satisfactory results could be obtained by sampling highway pavement sections that were representative of low (PRI = 0 to 5 in./mi), moderate (PRI = 5 to 10 in./mi), and high (PRI = 10 to 15 in./mi) pavement roughness. The selection of pavement sections and the execution of the data collection task for the study were performed as follows:

- Twelve sections 0.1 mi representing three levels of pavement surface roughness were included. The roughness levels were (a) low, (b) moderate and (c) high, as described earlier.
- Five roughness measurements (replicates) were made for each wheelpath for each selected 0.1-mi section of a project. The mean of the replicate values for the 0.1-mi section constituted one data point for the analysis.
- It was initially considered desirable that more than one operator take part in the data collection, using the profilograph devices. The decision to use only one profilograph device was based on the preliminary nature of this phase of the study. For the same reason, a single profilograph operator was used.

Number of Replicates for Regression Data

The determination of a desirable number of replicates is an important consideration in influencing the quality and usefulness of the results of the analysis. There are a number of ways of obtaining the number of data points to be used in the regression. The most common of these are (a) data points based on a single measurement value from each test section for each device, and (b) data points based on average values from several replicate measurements from each test section for each device. The first case would be appropriate only in a situation in which measurements are obtained with very precise devices.

Because profilograph and profilometer measurements are not easily repeatable, a single measurement does not provide a good estimate of the true value of the roughness index. A good estimate of the value can be obtained by averaging a large number of replications. However, it is usually not practical or economical to obtain large numbers of replications. Therefore, a compromise that allows some degree of error in the estimate is normally adopted. The compromise provides for the use of a feasible number of replicates. For example, Figure 1 shows how the magnitude of the error of estimate (E) for the mean PRI value varies with the number of replications. The calculation of the error of estimate was based on a 95 percent confidence level and a repeatability standard deviation of 0.85 in./mi obtained during an earlier study.

The student t-distribution approximates the distribution of the measurement values for each individual section in this experiment. The mean is the theoretical average measurement for a 0.1-mi section, assuming a very large number of replicate measurements. An individual measurement can therefore lie within the range between $-E$ and $+E$ 95 percent of the time. The width of the con-

TABLE 1 Regression Equations for Index Variables

Response Variable (index)	Independent Variable (index)	Regression Equation	Coefficient of Determination (R^2)
Mays	PRI (both wp)	Mays = 43.3 + 5.7 * PRI	0.95
IRI (both wp)	PRI (both wp)	IRI = 52.9 + 6.1 * PRI	0.93
IRI (left wp)	PRI (left wp)	IRI = 53.5 + 6.6 * PRI	0.95
IRI (right wp)	PRI (right wp)	IRI = 54.5 + 5.0 * PRI	0.68

Note: '**wp**' used for "wheel path".

fidence interval narrows with an increasing number of replications, approximately according to the following expression:

$$E = \frac{(t_{(a/2,n-1)}) * S}{\sqrt{n}}$$

where

E = half width of confidence interval, permitted error for estimate of mean;
S = pooled standard deviation (for one data set it is standard deviation of applicable measurements);
t = value from student t-distribution for significance level and degrees of freedom ($n - 1$) given;
n = number of replicates used to estimate parameter; and
a = significance level for desired confidence interval.

During an earlier study on the precision of profilograph measurements, it was determined that the pooled standard deviation (S) was approximately equal to 0.85 in./mi. In the above expression both the numerator and denominator vary as the number of replicates change. In this case, the values of error of estimate (E) at the 95 percent confidence level were computed as

- $E = 2.11$ for $n = 3$,
- $E = 1.0$ for $n = 5$,
- $E = 0.6$ for $n = 10$, and
- $E = 0.4$ for $n = 20$.

As the number of runs are increased beyond 10, the benefit per additional run in terms of the reduction in the error of estimate diminishes. At the same time the ratio of the error of estimate to the mean would be about 31.0 percent for $n = 3$, and 14.0 percent for $n = 5$, if the mean of pavement roughness index value were 7 in./mi. The profilograph roughness index of 7 in./mi is the target roughness index value for ADOT construction projects.

The research team decided that a relative error of 14 percent could be tolerated. Therefore, it was recommended that at least five replicate profilograph runs be made on each wheelpath and that the mean value obtained from the five runs be used as one data point during correlation analysis. In addition, it was recommended that project sections be picked from several levels of pavement roughness so that the results of the correlation could be generalized over a wide range of pavement roughness.

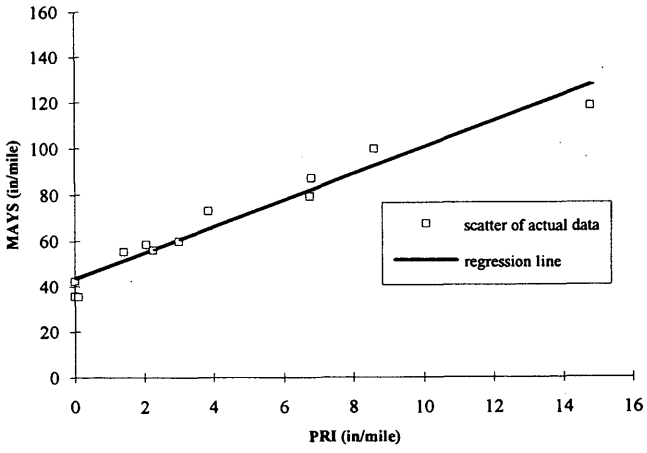

FIGURE 2 Plot of Mays index versus profilograph roughness index (both wheelpaths).

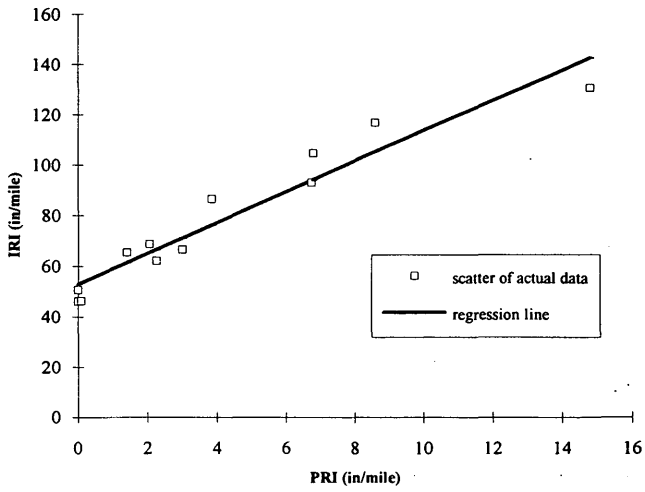

FIGURE 3 Plot of profilometer IRI versus profilograph roughness index (both wheelpaths).

Although desirable, the use of more than one profilograph was deemed unnecessary because results from an earlier study had indicated that variability between ADOT profilographs was not statistically significant.

To make a valid comparison between the variability of profilometer and profilograph measurements, it was decided to compare the coefficients of variation computed from data collected with the two devices. The coefficient of variation is used to express the standard deviation as a percentage of the mean. From the mean values for the data used in this study, which were 4.13 in./mi for profilograph roughness index and 66.5 in./mi for profilometer Mays index, the respective coefficients of variation were 13.0 percent for the profilograph and 3.0 percent for the profilometer. These coefficients of variation were computed on the basis of standard deviation values of 0.53 in./mi for the California profilograph and 2.0 in./mi for the K. J. Law profilometer.

Data Collection

A total of 120 tests were conducted with the profilograph on recently built PCCP sections in Phoenix, Arizona. The data collection plan was based on three levels of pavement roughness, four sections for each level of roughness, two wheelpaths for each section, and five replicate tests for each wheelpath (three roughness levels × four sections × two wheelpaths × five replicates = 120 total number of tests). Although the 12 sections did not constitute a large number of data sets for statistical purposes, it was considered sufficient for the preliminary task of establishing whether a linear model could indeed describe the relationship between the profilometer and profilograph indexes.

The majority of the data for the study were collected between July 9, 1992, and August 20, 1992. Additional data were collected in mid-September 1992 to replace some data that were inadvertently collected with a faulty profilometer. In most cases California profilograph measurements and profilometer measurements were

made on the same day or within a few days. The final breakdown of projects included in the data collection and the number of sections used from each project are as shown. Details about the actual locations of the tested sections are given in a report (*4*) that was prepared for the correlation study.

- Loop 101: University Dr.–Southern Ave., 4 sections;
- SR-360 at Ellsworth, 3 sections;
- SR-51: Glendale Ave.–Northern Ave., 2 sections;
- I-10: 99th Ave.–115th Ave., 2 sections; and
- SR-143: Washington St.–Sky Harbor Blvd., 1 section.

For each section, 10 measurements were taken using the California profilograph (5 for each wheelpath). The average of set of five replicate measurements was computed and used in the development of the regression model.

Three replicate measurements were made on each section with the profilometer. The average of the three replicates was then computed and used as the measured Mays index or IRI index for the correlation. Therefore, only 36 profilometer tests were needed during the study.

A preliminary inspection of the profilometer data raised serious concerns on three sets of profilometer roughness measurements because

- The differences in the readings between the right and left wheelpaths were uncharacteristically high.
- When compared to profilometer readings taken 4 months earlier on the same highway sections, there were about 50 to 100 percent differences in the observed Mays/IRI index values. This was in contrast to most of the other sections for which the differences in magnitudes between the data sets were less than 5 percent.

After a careful review of all data and the historical records of the profilometer performance, it was determined that the sensor on the left wheel of the profilometer had malfunctioned during the collection of the suspect data sets. Therefore, the three sets of bad data were discarded and, to replace them, new profilometer

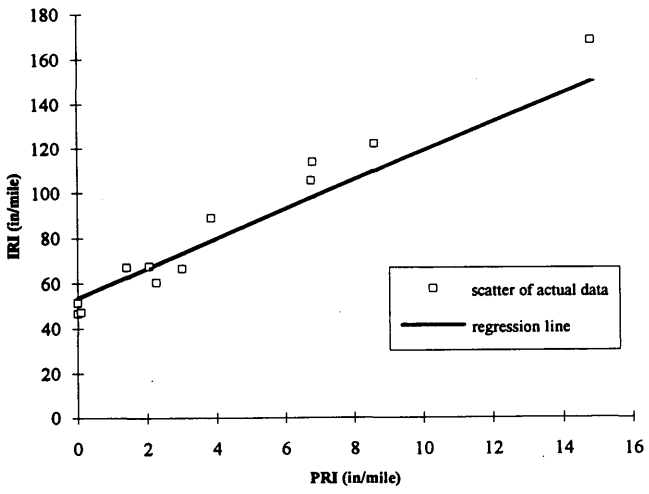

FIGURE 4 Plot of profilometer IRI versus profilograph roughness index (left wheelpath).

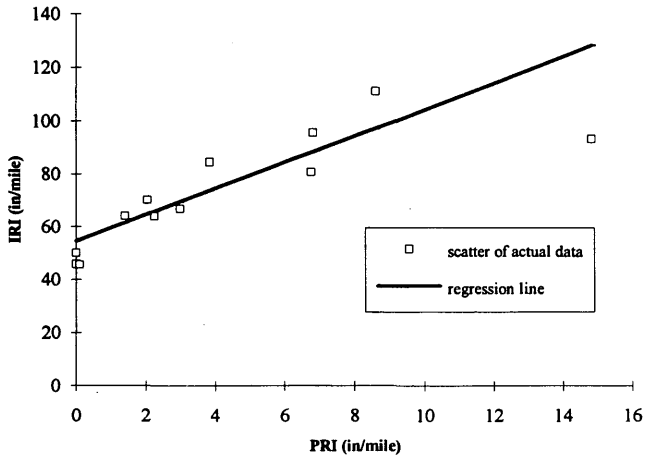

FIGURE 5 Plot of profilometer IRI versus profilograph roughness index (right wheelpath).

data sets were collected from the same sections. The new data showed no major discrepancy between the two wheelpaths and were similar to the values obtained 4 months earlier.

DATA ANALYSIS AND RESULTS

Data analysis was conducted to establish correlation and to develop regression models for the following pavement roughness variables: (a) Mays index with PRI (average of two wheelpaths in one lane), (b) IRI with PRI (based on the average of two wheelpaths in one lane), and (c) IRI with PRI (based on individual IRI and PRI for each wheelpath).

Scatter plots of the respective data suggested a linear relationship between the variables. In particular, the scatter plots for Mays against PRI, IRI against PRI (both wheelpaths) and IRI against PRI (left wheelpath) had a distinctive linear trend, with the data points falling within a very narrow band on the trend line. The scatter plot for IRI against PRI (right wheelpaths) was more spread out in comparison to the other three.

Simple linear regression models were developed for each pair of correlated variables. Statistical tests were conducted to determine if inclusion of x^2 and $x^{1/2}$ terms in the model would improve the regression model. The test results showed that the addition of one or both terms did not significantly improve the model. Therefore, the nonlinear terms were not included in the final regression equations. Table 1 gives the summary of the simple linear regression equations from the analysis. Plots of profilometer index values (Mays or IRI) against profilograph roughness index values, showing the respective regression lines are shown in Figures 2 through 5. The 95 percent prediction confidence intervals for Mays index values, based on three and five profilograph replicates, are shown in Table 2.

SUMMARY AND CONCLUSIONS

The principal objectives of the study were (a) to review the feasibility of correlating the California profilograph concrete pavement smoothness measurements with profilometer measurements

TABLE 2 Mays Index Prediction Confidence Intervals for Three and Five Profilograph Replicates

PRI in/mile	Predicted Mays Index (in/mile)	95% Confidence Limits for Mays Index Prediction			
		Limits from three Replicates		Limits from five Replicates	
		Lower	Upper	Lower	Upper
0	43.3	33.5	53.1	34.9	51.7
1	49.0	39.6	58.4	41.0	57.0
2	54.7	45.5	63.9	47.0	62.4
3	60.4	51.4	69.4	52.9	67.9
4	66.1	57.1	75.1	58.7	73.5
5	71.8	62.8	80.8	64.4	79.2
6	77.5	68.4	86.6	69.9	85.1
7	83.2	73.8	92.6	75.3	91.1
8	88.9	79.2	98.6	80.6	97.2
9	94.6	84.5	104.7	85.9	103.3
10	100.3	89.7	110.9	91.0	109.6
11	106.0	94.9	117.1	96.1	115.9
12	111.7	100.0	123.4	101.2	122.2
13	117.4	105.1	129.7	106.2	128.6
14	123.1	110.1	136.1	111.2	135.0
15	128.8	115.1	142.5	116.1	141.5

and (b) to establish whether the profilometer can be used to calibrate the profilograph. To accomplish this objective, the following principal tasks were done: (a) identification and selection of pavement sections that represent the roughness levels typically encountered during new construction, (b) testing of pavement sections with both the profilograph and profilometer, and (c) development of a model for the relationship between profilograph and profilometer profile roughness indexes.

This study showed that a linear model can be used to describe the relationship between California profilograph index values and profilometer Mays or IRI index values. It was demonstrated that a good regression model can be obtained if it is developed on the basis of mean values of the respective indexes, averaged from several replicates. It was also found that between three and five replicates are required to obtain a good estimate of the profilograph index.

On the basis of this study, it was concluded that (a) the California profilograph and the K. J. Law profilometer can be linearly correlated, (b) it was feasible to calibrate the California profilograph by the K. J. Law profilometer, (c) the profilometer must first be calibrated before it can be used to calibrate profilographs, and (d) it is not practical to interchangeably use the profilometer and profilographs because each device is more suited for some jobs than for others.

REFERENCES

1. Walker, R. S., and H. T. Lin. *Profilograph Correlation Study with Present Serviceability Index: Automated Pavement Data Collection Equipment.* University of Texas at Arlington, March 1988.
2. Uddin, W., G. E. Elkins, and W. R. Hudson. *Measurement of Pavement Roughness.* Interim Report. Arizona Department of Highways, Phoenix, Sept. 1986.
3. Kulakowski, B. T., and J. C. Wambold. *Development of Procedures for the Calibration of Profilographs.* Pennsylvania Transportation Institute, Pennsylvania State University, University Park, Aug. 1989.
4. Kombe, E. M., and S. A. Kalevela. *Evaluation of Initial Pavement Smoothness for the Development of PCCP Construction Specifications.* Special Report AZ-SP-9302. Arizona Department of Transportation, Phoenix, March 1993.

Publication of this paper sponsored by Committee on Surface Properties–Vehicle Interaction.

Relationships Between International Roughness Index and Present Serviceability Rating

BASHAR AL-OMARI AND MICHAEL I. DARTER

Relationships were developed between the international roughness index (IRI) and the present serviceability rating (PSR) for flexible, rigid, and composite pavement types. PSR is defined as the mean user panel rating for rideability on the conventional 0 to 5 scale. Relationships between IRI and PSR were developed for each pavement type for the states of Louisiana, Michigan, New Jersey, New Mexico, Ohio, and Indiana, and for all six states together. There were no significant differences between the models for different states and pavement types. The following nonlinear model that fits the boundary conditions is recommended: $PSR = 5 * e^{(-0.26 * IRI)}$ where IRI is in millimeters per meter or $PSR = 5 * e^{(-0.0041 * IRI)}$ where IRI is in inches per mile.

This paper documents relationships between the international roughness index (IRI) and the present serviceability rating (PSR) for pavement types included in the FHWA Highway Planning and Monitoring System (HPMS) data base. FHWA has requested that states report roughness data in the form of the IRI, which was developed by the World Bank in an effort to provide consistent data about roughness. The IRI is an objective and consistent measure of pavement condition that was chosen as the HPMS standard reference roughness index to provide more consistency between states. FHWA directed all states to report pavement roughness data by IRI for all paved rural arterials and urban freeways and expressways, including Interstates, beginning in 1989.

Currently, states are required to report both IRI and PSR to FHWA. The PSR ranges from 0 to 5 (very poor to very good) as defined in Figure 1 and includes a description of rideability, physical distress such as cracking, and rehabilitation needs. The PSR is determined by the states using this general definition but also by other methods. Another method is to first correlate some type of roughness measurement (using a state's equipment) with a mean user panel rating of rideability and then to use this correlation to obtain an estimate of PSR from the roughness index measurement on pavement sections. Another approach is to use a state's visual rating scheme, such as a scale between 0 and 100, and just divide ratings by 20 to estimate a value in the 0 to 5 range. The fact that various methods are used by states to estimate PSR makes consistency nationwide a very significant problem. The definition of PSR used in this report is that defined under NCHRP Project 1-23 (*1*) as subsequently described.

The PSR concept is important because it is built into the HPMS analytical software and is a vital part of the procedures used to estimate long-term pavement rehabilitation needs. The PSR is also a well-known indicator of pavement condition in the highway community. Not much is currently known about the IRI on the nation's highways, especially critical levels at which pavements should be rehabilitated.

Department of Civil Engineering, 1208 Newmark Civil Engineering Lab, 205 North Mathews Avenue, University of Illinois at Urbana-Champaign, Urbana, Ill. 61801.

RESEARCH OBJECTIVES

The primary objective of the first phase of this research was to develop a predictive model for PSR as a function of profile IRI that is applicable to flexible, rigid, and composite (asphalt over concrete) pavements. In the second phase of this study, additional data from the LTPP data base and other sources that included pavement distresses and IRI were analyzed to determine the relationships of key distress types to IRI and critical levels for rehabilitation. These results will be useful in the HPMS analytical process to achieve improved and consistent estimates of the future highway pavement rehabilitation needs in the United States.

PREVIOUS RESEARCH IN CORRELATING PROFILE TO PSR

The first major attempt to relate pavement profile to subjective highway user ratings of a highway was in 1958 by the AASHO Road Test research staff (*2*). The researchers found a reasonable correlation between longitudinal profile slope variance and PSR (mean panel rating). The following equations, which also include some physical distresses, were obtained (*2*):

- Asphalt concrete (flexible) pavements

$$PSR = 5.03 - 1.91 \log (1 + SV) - 1.38 (RD)^2 - 0.01 \sqrt{C + P} \quad R^2 = 0.84, SEE = 0.38, n = 74 \quad (1)$$

- Jointed concrete (rigid) pavements

$$PSR = 5.41 - 1.78 (1 + SV) - 0.09 \sqrt{C + P}$$

$$R^2 = 0.92, SEE = 0.32, n = 49 \quad (2)$$

where

SV = slope variance over section from CHLOE profilometer,
RD = mean rut depth (in.),
C = cracking (m^2/1000 m^2) (flexible),
= cracking (m/305 m^2)(= 1 ft/1,000 ft^2) (rigid),

P = patching (m^2/1000 m^2),
SEE = standard error of estimate, and
n = number of sections.

The most significant factor by far in each equation is the slope variance, which is calculated from the pavement longitudinal profile. The distress terms do not contribute much to the estimation of PSR and could have been left off without significant loss of accuracy.

Many other studies have been conducted since that time that relate various longitudinal profile statistics to highway user panel ratings. For example, a Purdue University study in 1964 provided several models showing slope variance and other roughness indicators correlating well with PSR without distress variables (*3*). Researchers from Texas completed a major study in 1968 into the relationship between profile characteristics and PSR (*4*). The World Bank sponsored a large research study in Brazil from 1976 to 1981 that resulted in the development of the IRI. Some correlations between IRI and PSR from various sources were given by Paterson (*5*) as shown in Figure 2 where a wide variation of relationships exists when different data sources from around the world are used. A nonlinear relationship between PSR and IRI that generally fits through the data set taken from Brazil, Texas, South Africa, and Pennsylvania is as follows:

$$PSR = 5 * e^{(-0.18*IRI)} \quad (3)$$

where IRI is in meters per kilometer.

Another major study was conducted under NCHRP Project 1-23 by Janoff et al. (*1*) and Janoff (*6*) in the 1980s. The objective of NCHRP Project 1-23 (*1*) was to correlate mean user panel rideability ratings using the Figure 3 scale of selected pavement sections with objective parameters derived from the measured profile. The main experiment was conducted on 81 test sections in Ohio, including 25 asphalt concrete (AC), 22 portland cement concrete (PCC), and 34 composite (COMP) sections. The user panel included 36 Ohio Department of Transportation employees and laypersons driving in four K-cars of similar age who rated the pavement sections for rideability only on the same subjective scale (0 to 5) as that for the AASHO Road Test, and the mean panel rating (MPR) was computed for each section. Thus, the MPR was similar to the PSR as defined for the AASHO Road Test, but only rideability was rated.

Chapter IV
DRAFT

FHWA ORDER M 5600.1A, Chg. 4
February 24, 1993

Table IV-2

Pavement Condition Rating

(Use full range of values)

PSR & Verbal Rating	Description
5.0	
Very Good	Only new, superior (or nearly new) pavements are likely to be smooth enough and distress free (sufficiently free of cracks and patches) to qualify for this category. Most pavements constructed or resurfaced during the data year would normally be rated very good.
4.0	
Good	Pavements in this category, although not quite as smooth as those described above, give a first class ride and exhibit few, if any, visible signs of surface deterioration. Flexible pavements may be beginning to show evidence of rutting and fine random cracks. Rigid pavements may be beginning to show evidence of slight surface deterioration, such as minor cracks and spalling.
3.0	
Fair	The riding qualities of pavements in this category are noticeably inferior to those of new pavements, and may be barely tolerable for high speed traffic. Surface defects of flexible pavements may include rutting, map cracking, and extensive patching. Rigid pavements in this group may have a few joint failures, faulting and cracking, and some pumping.
2.0	
Poor	Pavements in this category have deteriorated to such an extent that they affect the speed of free-flow traffic. Flexible pavement may have large potholes and deep cracks. Distress includes ravelling, cracking, rutting, and occurs over 50 percent, or more, of the surface. Rigid pavement distress includes joint spalling, faulting, patching, cracking, scaling, and may include pumping and faulting.
1.0	
Very Poor	Pavements in this category are in an extremely deteriorated condition. The facility is passable only at reduced speeds, and with considerable ride discomfort. Large potholes and deep cracks exist. Distress occurs over 75 percent or more of the surface.
0.0	

FIGURE 1 PSR ranges from 0 to 5 based on a description of rideability, physical distress, and rehabilitation needs.

The results of the frequency study of Ohio and Florida data revealed that the total profile index (PI) in the band of frequencies from 0.125 to 0.630 cycles/ft was correlated with the MPR. The PI is defined as the root mean square of elevation for the profile. Relationships were developed to relate PI to the MPR for each pavement type and for all sections combined. A log transformation provided the best fit. Also, the PI and quarter car index were found to correlate well with the MPR.

The objectives of the second phase of NCHRP 1-23 were to expand the methodology developed in the first phase to more states and also to study the effects of region and vehicle size on panel rating and the effect of measuring one wheelpath instead of both wheelpaths in calculating the objective roughness index (*6*). An additional four states besides Ohio participated in this phase. AC, PCC, and COMP sections from New Jersey (46 sections), Michigan (68 sections), New Mexico (64 sections), and Louisiana (52 sections) were selected. Panel ratings and profile measurements were performed on each section.

The same analysis as before was performed on the data. The MPR versus the PI curve was similar for all states except New Mexico. The differences between the five states did not exceed 0.3 MPR. Therefore, it was concluded that the region did not have a significant effect on the ratings.

Data from New Jersey were used to compare the PI from one and two wheelpaths. It was concluded that data from either wheelpath could be used to estimate MPR with as much accuracy as data from both wheelpaths. In all cases the difference was lower than 0.15 MPR. In general, the right wheelpath showed slightly more roughness than the left wheelpath.

A full-size car and a compact car were used to study the effect of vehicle size on the panel rating. No significant effect was observed. The effect of road class on the analysis was also determined. Data from New Jersey, Michigan, and New Mexico were classified by road class (Interstate/non-Interstate). No significant difference in the MPR-versus-PI relationship was observed between the two road classes for AC and PCC pavement types (the sample size for COMP was not sufficient) (*6*).

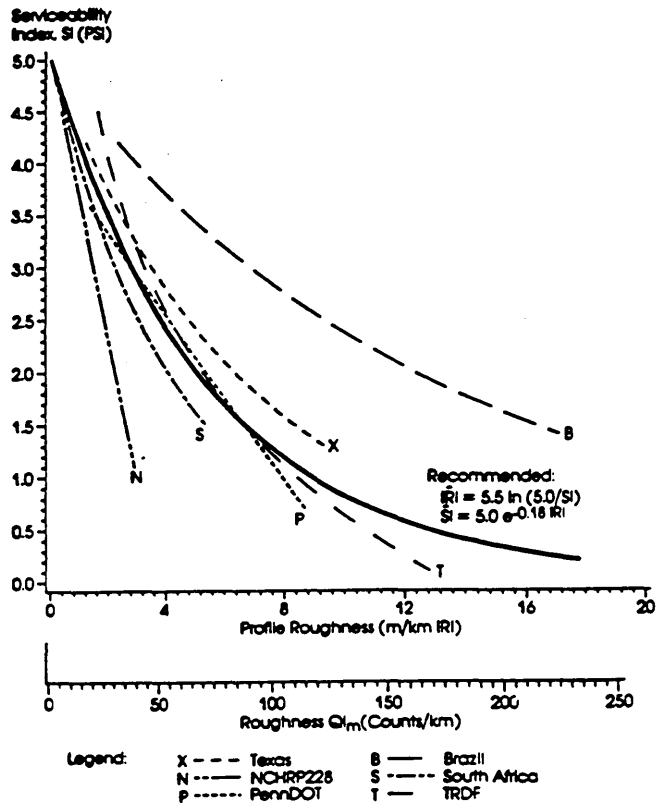

FIGURE 3 Weaver/AASHO scale used in NCHRP Project 1-23 to define PSR as mean panel rating.

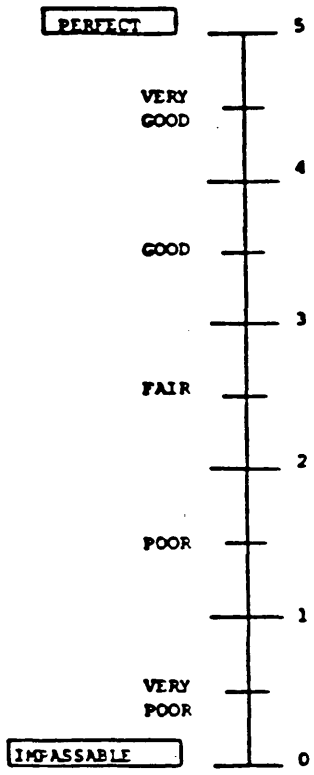

FIGURE 2 Approximate relationships between AASHO serviceability index, PSI, and QIm and IRI roughness scales, based on panel ratings from four sources (*5*).

RESEARCH APPROACH

A relationship is desired between IRI and the mean panel rating (PSR) over the range of conditions existing on freeways and expressways in urban areas and arterial highways in rural areas in the United States. After a comprehensive search of available data, the most comprehensive data were found in the NCHRP Project 1-23 data base (*1,6*) plus some additional similar data obtained from Indiana. The relationship between IRI and PSR (where PSR is defined as the mean highway user's panel rating) will be analyzed for five states obtained from the NCHRP Project 1-23 data base plus the sections in Indiana. The six states are Indiana (which did not separate COMP sections from AC sections), Louisiana,

Michigan, New Jersey, New Mexico, and Ohio. The number of sections in each pavement type category and state is as follows:

State	*AC*	*COMP*	*PCC*	*Total*
Indiana	42	–	24	66
Louisiana	13	13	22	48
Michigan	19	21	27	67
New Mexico	39	13	10	62
New Jersey	15	10	21	46
Ohio	34	32	23	89
Total	120	89	127	378

IRI was computed using the measured profile data. The program used to calculate IRI was written in Quick BASIC using the procedure recommended by Sayers et al. (*7*). The right wheelpath profile was used in calculating IRI because it was found that there was no significant difference if the left wheelpath or the average of right and left wheelpath profiles were considered. The IRI values were calculated from the original profile data for all states except Indiana, where the already calculated IRI values were provided by the Indiana Department of Transportation. The sample interval used for profile measurement was 6 in. The mean panel rating was used as the PSR, as defined by Figure 3.

Development of PSR Versus IRI Models

Data for all six states were entered into a Statistical Analysis System (SAS) data set. These data include IRI, PSR, and pavement type for every pavement section in each state. Several linear and nonlinear models with various types of transformations were considered. The following nonlinear model was found to best fit the boundary conditions and the actual data:

$$PSR = 5 * e^{(a * IRI)} \quad (4)$$

The logarithmic transformation was used in the actual regression:

$$\ln\left(\frac{PSR}{5}\right) = a * IRI \quad (5)$$

Regression analysis was conducted for all possible sets of data considering states and pavement types. The R^2 values obtained were very high (above 0.90) for all cases.

To provide a more realistic assessment of the accuracy of the relationship between PSR and IRI, the R^2 and standard error of the estimate (*SEE*) between the actual PSR values (dependent variable) and predicted PSR values (independent variable) were determined. These values are shown in Table 1 for each state and for each pavement type and in Table 2 for all states together for each pavement type.

As shown in Tables 1 and 2, most of the R^2 values are less than the 0.90 obtained for the transformed model. This occurs because the regression procedure works to minimize the error in the logarithm of PSR, not PSR directly.

In Figure 4 a plot of all state models shows that there is not much deviation between the predictions for each state, except the New Jersey model, which gives a somewhat higher prediction than the other states, especially for AC pavements.

Therefore, two analyses were conducted: one with and the other without the New Jersey sections, as shown in Table 2. The analysis without the New Jersey data gives higher R^2 values and lower *SEE* values than the analysis that includes the New Jersey sections (R^2 = 0.73 versus 0.68 for all pavement types).

Figure 5 shows the different models for each pavement type using combined data from all states. There is very little difference between these best-fit curves, indicating that for all practical purposes, the relationship between IRI and PSR is the same for all three pavement types. These results indicate that the model developed using all of the available data (excluding New Jersey

TABLE 1 Predictive Models for each State and Pavement Type

State	Pavement Type	Constant		R^2	SEE[2]
		a	SEE[1]		
IN	AC/COMP	-0.237800	0.005	0.92	0.244
	PCC	-0.327357	0.018	0.87	0.337
	ALL	-0.280107	0.010	0.88	0.329
LA	AC	-0.240457	0.015	0.80	0.337
	COMP	-0.296259	0.022	0.66	0.403
	PCC	-0.191240	0.007	0.84	0.221
	ALL	-0.224307	0.009	0.62	0.390
MI	AC	-0.258385	0.010	0.92	0.250
	COMP	-0.269314	0.012	0.86	0.337
	PCC	-0.273683	0.014	0.47	0.427
	ALL	-0.267337	0.007	0.79	0.356
NJ	AC	-0.146167	0.007	0.84	0.222
	COMP	-0.206388	0.011	0.65	0.259
	PCC	-0.194998	0.010	0.69	0.345
	ALL	-0.182296	0.007	0.64	0.336
NM	AC	-0.291208	0.010	0.81	0.370
	COMP	-0.368312	0.021	0.80	0.267
	PCC	-0.320090	0.018	0.67	0.134
	ALL	-0.301952	0.008	0.79	0.348
OH	AC	-0.196603	0.008	0.79	0.302
	COMP	-0.304379	0.015	0.54	0.415
	PCC	-0.227174	0.010	0.72	0.278
	ALL	-0.228277	0.008	0.58	0.388

[1] Standard error of the estimate (for the constant a).

[2] Standard error of the estimate in units of PSR.

Note: IRI in units of mm/m (1 mm/m = 1/63.36 in/mile)

TABLE 2 Predictive Models Developed for All States and for All States Except New Jersey

States	Pav. Type	Constant		R^2	SEE
		a	SEE		
All States	AC	-0.229945	0.005	0.76	0.383
	COMP	-0.276717	0.008	0.64	0.402
	PCC	-0.257445	0.008	0.62	0.442
	ALL	-0.248129	0.004	0.68	0.417
All States except NJ	AC	-0.239459	0.005	0.81	0.346
	COMP	-0.292981	0.008	0.70	0.383
	PCC	-0.271960	0.008	0.66	0.427
	ALL	-0.259708	0.004	0.73	0.393

Note: IRI in units of mm/m (1mm/m = 1/63.36 in/mile)

data) could be used for any of the pavement types without significant loss of accuracy for any pavement type. This equation is given in both metric and English units.

$$PSR = 5 * e^{(-0.26*IRI)} \quad (6)$$

where IRI is in millimeters per meter.

$$PSR = 5 * e^{(-0.0041*IRI)} \quad (7)$$

where IRI is in inches per mile.

For both Equations 6 and 7, $R^2 = 0.73$, $SEE = 0.39$ (units of PSR), $n = 332$ sections. A plot that shows this model with all the available data for PSR versus IRI is given in Figure 6.

These statistics compare favorably with those obtained from other studies, such as the AASHO Road Test where the R^2 values were 0.84 and 0.92 for AC and PCC pavements, respectively, and the *SEE* values were 0.38 and 0.32 units of PSR for AC and PCC pavements, respectively.

Most of the IRI/PSR data (especially for composite and PCC pavements) were observed over lower IRI and higher PSR ranges, as shown in Figure 6. This causes a weak definition of the relationship for higher IRI and lower PSR ranges, which results in a lower R^2 and higher *SEE* values for composite and PCC pavements.

CONCLUSIONS

The main conclusion of this research is that the mean panel rating of rideability can be predicted reasonably well from the IRI over a wide range of conditions across the United States for the three main types of existing pavements. Equation 7 or 8 is recommended for use in estimating PSR from IRI.

The following models may be used if it is desirable to consider each pavement type separately.

- *For AC pavements:*

$$PSR = 5 * e^{(-0.24*IRI)} \quad (8)$$

where IRI is in millimeters per meter,

$$PSR = 5 * e^{(-0.0038*IRI)} \quad (9)$$

where IRI is in inches per mile.

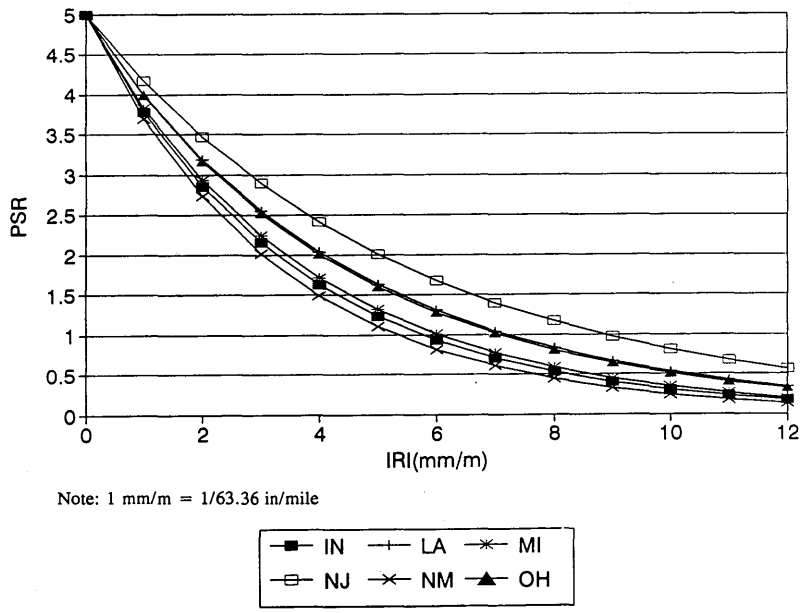

FIGURE 4 PSR versus IRI for all pavement types (models developed for each state).

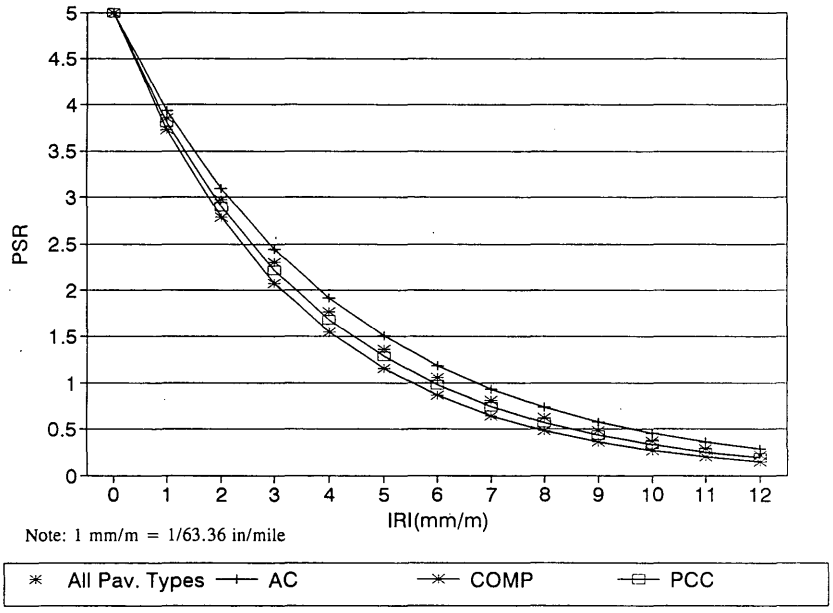

FIGURE 5 PSR versus IRI for each pavement type using data from all states.

- *For COMP pavements:*

$$PSR = 5 * e^{(-0.293*IRI)} \quad (10)$$

where IRI is in millimeters per meter, or

$$PSR = 5 * e^{(-.0046*IRI)} \quad (11)$$

where IRI is in inches per mile.

- *For PCC pavements:*

$$PSR = 5 * e^{(-0.272 * IRI)} \quad (12)$$

where IRI is in millimeters per meter, or

$$PSR = 5 * e^{(-0.0043 * IRI)} \quad (13)$$

where IRI is in inches per mile.

Because the maximum deviation of the predicted PSR value by any of these equations for each pavement type from that predicted by the overall model was not more than about 0.25 PSR units, it is recommended to use one model for all pavement types.

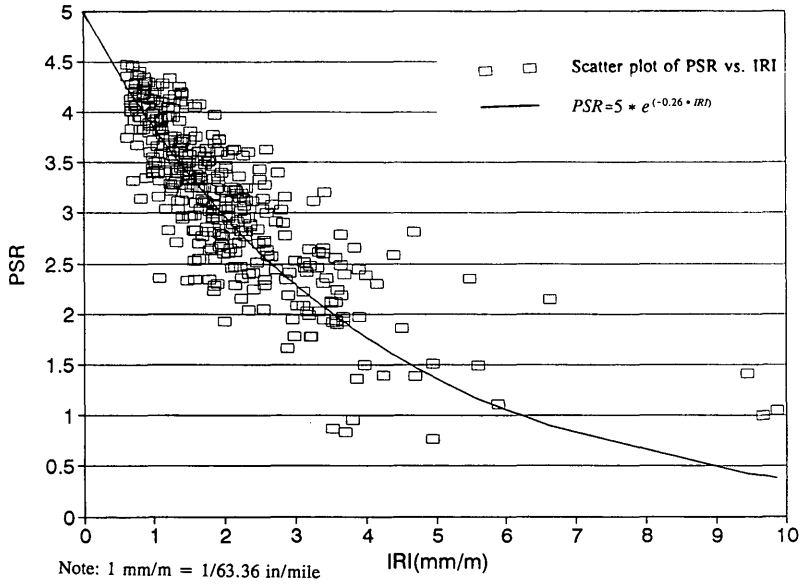

FIGURE 6 Plot showing recommended model with all data.

ACKNOWLEDGMENTS

This research was conducted for the Illinois Department of Transportation in cooperation with FHWA by the Department of Civil Engineering, University of Illinois. Gordon F. Hayhoe performed the analysis on the profile data from the states of Louisiana, Michigan, New Jersey, New Mexico, and Ohio, which were obtained from the NCHRP Project 1-23 data base. Additional data for Indiana were provided by Dave Waud, of the Indiana Department of Transportation.

REFERENCES

1. Janoff, M. S., J. B. Nick, P. S. Davit, and G. F. Hayhoe. *NCHRP Report 275: Pavement Roughness and Rideability.* TRB, National Research Council, Washington D.C., Sept. 1985.
2. Carey, W. N., and P. E. Irick. The Pavement Serviceability Performance Concept. *Bulletin 250*, HRB, National Research Council, Washington, D.C., 1960.
3. Yoder, E. J., and R. T. Milhous, *NCHRP Report 7: Comparison of Different Methods of Measuring Pavement Condition: Interim Report.* HRB, National Research Council, Washington, D.C., 1964.
4. Walker, R. S., W. R. Hudson, and F. L. Roberts. *Development of a System for High Speed Measurement of Pavement Roughness.* Research Report 73-5F. University of Texas, Austin, Nov. 1970.
5. Paterson, W. D. O. *Road Deterioration and Maintenance Effects.* The World Bank, Washington, D.C., 1987.
6. Janoff, M. S. *NCHRP Report 308: Pavement Roughness and Rideability Field Evaluation.* TRB, National Research Council, Washington, D.C., 1988.
7. Sayers, M. W., T. D. Gillespie, and W. D. O. Paterson. *Guidelines for Conducting and Calibrating Road Roughness Measurements.* World Bank Technical Paper 46. The World Bank, Washington, D.C., 1986.

Publication of this paper sponsored by Committee on Surface Properties–Vehicle Interaction.

Comparative Testing of Profilometers

ROHAN W. PERERA, STARR D. KOHN, AND CHERYL ALLEN RICHTER

A comparative testing experiment between the four K.J. Law profilometers that are used to collect data for the Long-Term Pavement Performance program was conducted in Ames, Iowa, in August 1992. The objectives of the comparison were to (a) determine whether the profilometers collect similar data, (b) determine whether the profilometers can collect repeatable data at a section, and (c) compare data collected by the profilometers with data collected by the Dipstick and the rod and level. Four asphalt concrete and four portland cement concrete sections were selected for testing. All profilometers obtained six replicate runs at 65 km/hr (40 mph) and 80 km/hr (50 mph) at all test sections. The international roughness index (IRI) computed from the profile data was used as the statistic to analyze profiles. An analysis of variance was separately conducted on the left and right wheelpath IRI. This analysis showed that similar profile data are being collected by the profilometers in both wheelpaths. All profilometers showed good repeatability in collecting data. Generally good agreement was obtained between the IRI computed from profiles measured by the Dipstick and the profilometers. A study of random measuring errors showed that they can have a considerable effect on IRI of smooth pavements. Generally, for pavements that had IRI values less than 1.6 m/km (100 in./mi), poor agreement was obtained between IRI computed from rod and level and profilometer profiles. This was attributed to random measuring errors during rod and level measurements. Better agreement was obtained between rod and level and profilometer IRI for profiles that had an IRI greater than 1.6 m/km (100 in./mi).

As a part of the Long-Term Pavement Performance (LTPP) program, pavement profile data are being collected annually at approximately 800 general pavement study and 100 specific pavement study sites in the United States and Canada. Profile data collection is a primary task of the LTPP program. These profile data will be used to develop pavement performance models. The profile data are being collected by regional contractors from four regions: North Central, Western, North Atlantic, and Southern. Each region employs its own K.J. Law profilometer to collect data within the region. Three of these profilometers are identical, with the distance between the sensors being 168 cm (66 in.). The fourth profilometer contains the same electromechanical equipment as the other profilometers, but the distance between the sensors in this unit is 137 cm (54 in.). This profilometer with the shorter distance between the sensors is being used by the North Central region. The profilometers record both the left and the right wheelpath profiles. The recorded profile data are used to compute the IRI of each wheelpath. Other statistical summaries such as root mean square vertical acceleration (RMSVA) and slope variance are also computed using the profile measurements. The profile data and computed indexes are stored in the LTPP information management system data base.

R. W. Perera and S. D. Kohn, Soil and Materials Engineers, 43980 Plymouth Oaks Boulevard, Plymouth, Mich. 48170. C.A. Richter, Long Term Pavement Performance Division, FHWA, Turner-Fairbank Highway Research Center, HNR-40, 6300 Georgetown Pike, McLean, Va. 22101-2296.

A comparative study between the profilometers from the four regions was conducted in August 1992 in Ames, Iowa. The objectives of this profilometer comparison were to

1. Determine whether the profilometers can collect similar data,
2. Determine whether repeatable data can be obtained by each profilometer at a given section,
3. Determine whether accurate data are being collected by the profilometers by comparing the IRI computed from profilometer data with IRI computed from Dipstick as well as rod and level data.

DESIGN OF EXPERIMENT

The following factors were identified as having a potential influence on the measurements collected by the profilometers: type of profilometer, speed of testing, surface type, and level of roughness. The experimental plan designed for this study is shown in Figure 1. Eight pavement sections were used for this study, with four of the pavement sections being asphalt concrete and the other four being portland cement concrete. For each pavement type, two levels of roughness were considered. A pavement was categorized as smooth if both wheelpath IRI values (average of right and left wheelpath IRI) were less than 2 m/km (125 in./mi) and as medium if both wheelpath IRI values were between 2 m/km (125 in./mi) and 4.7 m/km (300 in./mi). This experimental plan was intended to cover the range of conditions present in the LTPP test sections. At each section, all profilometers were scheduled to make six error-free runs at two test speeds of 65 km/hr (40 mph) and 80 km/hr (50 mph). The IRI computed from the profile data was used as the statistic in all analyses.

SELECTION OF TEST SECTIONS AND DATA COLLECTION

Selection of Test Sections

The test sections were selected such that they were similar to typical Strategic Highway Research Program test sections. Each test section was 152 m (500 ft) long with similar profile characteristics throughout its length, as well as immediately before and after the test section. The cross profile was uniform over the length of these sections, which were located on straight sections of roadway.

Profilometer Data Collection

A schedule was prepared for each profilometer giving the order in which they were to test the asphalt concrete pavements and the

portland cement concrete pavements. This schedule was prepared using a random number generating table. The portland cement concrete pavements were to be tested after 12:00 p.m. to minimize the effect of slab curling on profile measurements. Each test section was tested at two speeds, 65 km/hr (40 mph) and 80 km/hr (50 mph). All profilometer crews were instructed to align their vehicles along the wheelpaths when collecting data. Each crew was instructed to perform six error-free runs at both test speeds at all sections (for a total of 12 runs for a section).

Data Collection by Manual Devices

Profile measurements along the wheelpaths of the test sections using the Dipstick and the rod and level were completed in July 1992 before the profilometer comparison. In all sections, the left and right wheelpaths were marked by a chalk line, and markings were made along the wheelpaths at 0.3-m (1-ft) intervals. Profile measurements were performed using the Dipstick and the rod and level at 0.3-m (1-ft) intervals.

COMPARISON BETWEEN PROFILOMETERS

Computation of IRI

During a profilometer run, profile data on the left and right wheelpaths are collected. The IRI for each wheelpath was computed from the profile data using the Profscan program (*1*), which uses the algorithm given in a World Bank technical report (*2*). The average left wheelpath and right wheelpath IRI computed from the six profilometer runs at each section for both test speeds are shown in Table 1. As seen from these IRI values, the test sections did not completely satisfy the requirements for pavement roughness shown in the experimental design. This occurred because of difficulties in selecting suitable sites, which had to be close to each other so that the experimental testing could be completed in the shortest possible time.

Analysis of Variance

The main objective in this profilometer comparison experiment was to determine whether the IRI of the left and right wheelpaths computed from the measured profiles are similar between the profilometers. In addition, the effect of speed of testing on the computed IRI was also to be studied. The effect of the different profilometers and test speeds on the computed IRI can be determined by conducting a factorial analysis of variance (ANOVA) on the IRI.

The factors profilometer, speed, and sections were considered for the factorial ANOVA. In this design, the factors profilometer and speed are fixed whereas the factor section is random. Each cell in this design had six replicates. As the design consists of fixed and random factors, a mixed model analysis has to be performed (*3*). The SPSS program (*4*) was used to perform ANOVA. ANOVA was carried out separately for IRI of the left and right wheelpaths for the following profilometer combinations:

1. North Central, Western, North Atlantic, and Southern;
2. North Central, Western, and North Atlantic;
3. North Central, Western, and Southern;
4. North Central, North Atlantic, and Southern; and
5. Western, North Atlantic, and Southern.

The effects that were of importance in this study were type of profilometer, speed, and the interaction between profilometer and speed. The significance of each factor was tested at a significance level of 0.05. After performing ANOVA, the adequacy of the model was checked by plotting the residuals against the fitted values. An important assumption in ANOVA is the equality of variances. If this assumption is satisfied, the residuals should be structureless. Although the residual plot for the left wheelpath was structureless, the residual plot for the right wheelpath was not structureless, with a wide scatter in the residuals for the IRI values corresponding to Section 7. In Section 7, the right wheelpath area had severe cracking, which caused high variability between runs for all profilometers. Because the inclusion of Section 7 could influence the results of ANOVA in the right wheelpath, another series of ANOVA were conducted omitting Section 7. All procedures followed when conducting ANOVA were identical to those used in the earlier ANOVA. The residual plots from this analysis were structureless.

Results from ANOVA

Left Wheelpath IRI

The factors profilometer, speed, and the interaction between profilometer and speed were not significant for all profilometer com-

SURFACE TYPE / ROUGHNESS / SECTION / DEVICE		ASPHALT				CONCRETE			
		SMOOTH		MEDIUM		SMOOTH		MEDIUM	
SPEED (KMPH)		A	B	C	D	E	F	G	H
65	1								
	2								
	3								
	4								
80	1								
	2								
	3								
	4								

FIGURE 1 Experimental plan.

binations considered ($\alpha = 0.05$). These results show that there is no significant difference in the profiles measured in the left wheelpath by all profilometers. In addition, the results indicated that there was no difference in the profiles measured in the left wheelpath at test speeds of 65 km/hr (40 mph) and 80 km/hr (50 mph) for all profilometers.

Right Wheelpath IRI

Speed or the interaction between speed and profilometer were not significant for all profilometer combinations (significance level, 0.05). The factor profilometer was not significant ($\alpha = 0.05$) for the following profilometer combinations: (a) North Central, Western, and North Atlantic; and (b) North Central, Western, and Southern. However, the factor profilometer was significant ($\alpha = 0.05$) for the following profilometer combinations: (a) North Central, Western, North Atlantic, and Southern; (b) North Central, North Atlantic, and Southern; and (c) Western, North Atlantic, and Southern.

This analysis shows that the profiles measured by the four profilometers in the right wheelpath are not the same. But when the North Central and Western profilometers are combined separately with the North Atlantic and Southern Profilometers, the factor profilometer for the combination of the three profilometers is not significant. These results indicate that there is a difference in the IRI values computed from profiles measured by the North Atlantic and Southern profilometers.

At each section, the SPSS program (*4*) was used with the IRI values from the right wheelpath to perform a multiple comparison of the means using the Duncan procedure and to determine homogeneous subsets of data. The purpose of this analysis was to identify profilometers that are similar. A clear conclusion could not be obtained from this analysis. An examination of the average right wheelpath IRI values (see Table 1) showed that for most sections the IRI of the Southern profilometer was lower than the average for all profilometers, whereas the IRI of the North Atlantic profilometer was higher than the average for all profilometers. The cause for the factor profilometer to be significant for any profilometer combination that included the Southern profilometer and the North Atlantic profilometer can be attributed to this difference.

From this analysis it was not possible to clearly identify which profilometer was different. However, for all practical purposes the four profilometers can be assumed to be similar for two reasons. First, the factor profilometer was not significant for profilometer combinations of (a) North Central, Western, and North Atlantic and (b) North Central, Western, and Southern regions. Second, the right wheelpath IRI values shown in Table 1 for all four profilometers are close to each other for all sections, except for Section 7, which had cracking in the wheelpath.

REPEATABILITY OF PROFILOMETERS

Table 2 shows the standard deviations of the left wheelpath IRI for all test sections at both test speeds. The values shown in this table had the following distribution: 33 percent of the values were less than 0.015 m/km (1.0 in./mi); 30 percent of values were between 0.015 and 0.03 m/km (1.0 and 2.0 in./mi); 30 percent of the values were between 0.03 and 0.045 m/km (2.0 and 3.0 in./mi); and 7 percent of the values were greater than 0.045 m/km (3.0 in./mi). Generally in sections with low IRI values, the standard deviations were less when compared with sections with higher IRI values. Similar results were obtained for the standard

TABLE 1 Average Left and Right Wheelpath IRI

Wheel Path	Test Speed (kmph)	Profilometer	Average IRI (m/km) Asphalt Sections Section Number 3	5	6	7	Concrete Sections Section Number 1	2	4	8	Average IRI for all Sections (m/km)
Left	65	North Central	1.39	1.23	0.63	1.74	1.61	2.15	4.59	1.26	1.82
Left	65	Western	1.37	1.23	0.58	1.55	1.69	2.35	4.34	1.42	1.82
Left	65	North Atlantic	1.39	1.22	0.66	1.53	1.59	2.18	4.17	1.40	1.77
Left	65	Southern	1.37	1.23	0.60	1.53	1.70	2.38	4.34	1.44	1.82
Left	80	North Central	1.39	1.25	0.65	1.77	1.64	2.11	4.59	1.28	1.83
Left	80	Western	1.39	1.23	0.60	1.52	1.69	2.32	4.34	1.45	1.82
Left	80	North Atlantic	1.44	1.15	0.65	1.52	1.58	2.23	4.28	1.44	1.78
Left	80	Southern	1.39	1.22	0.60	1.56	1.77	2.34	4.40	1.48	1.84
Average Left Wheel Path IRI for Section			1.39	1.22	0.62	1.59	1.66	2.26	4.38	1.40	
Right	65	North Central	1.34	0.87	0.74	3.74	1.99	1.64	5.67	1.07	2.13
Right	65	Western	1.45	0.90	0.74	3.50	2.00	1.61	5.73	1.07	2.13
Right	65	North Atlantic	1.39	0.93	0.79	3.25	2.02	1.67	5.68	1.09	2.10
Right	65	Southern	1.31	0.90	0.74	3.06	1.97	1.66	5.62	1.07	2.04
Right	80	North Central	1.36	0.85	0.74	3.65	1.97	1.59	5.74	1.09	2.12
Right	80	Western	1.45	0.93	0.76	3.61	2.02	1.61	5.68	1.12	2.15
Right	80	North Atlantic	1.39	0.93	0.79	3.50	2.02	1.67	5.68	1.09	2.13
Right	80	Southern	1.33	0.88	0.74	3.08	1.97	1.59	5.56	1.09	2.03
Average Right Wheel Path IRI for Section			1.38	0.90	0.76	3.42	2.00	1.63	5.67	1.09	

Note: 1 m/km = 63 in/mile, 1 kmph = 0.62 mph

deviation of the right wheelpath IRI, except for Section 7. In Section 7, which had cracking along the right wheelpath, the standard deviation in IRI of the right wheelpath for the profilometers ranged from 0.06 to 0.22 m/km (4 to 14 in./mi). The following conclusions can be drawn from the analysis of standard deviations.

1. Because the standard deviation of IRI for the left and right wheelpaths in all sections was low for all profilometers, it can be concluded that the profilometers collect repeatable data.
2. There was no observed difference in the standard deviation of IRI for the left and right wheelpaths because of the difference in test speeds.
3. There was no observed difference in the standard deviation of IRI between the asphalt concrete and portland cement concrete pavements.

COMPARISON BETWEEN PROFILOMETERS AND MANUAL DEVICES

Manual Devices Used

Profile measurements were obtained using the Dipstick as well as the rod and level. The Dipstick measures the difference in elevation between two points that are 0.3 m (12 in.) apart. The Dipstick used was an autorecording device, which recorded elevations to the nearest 0.025 mm (0.001 in.). Rod and level measurements were performed at 0.3-m (1-ft) intervals using an autorecording Wild NA 2000 level. The elevations were measured using the feet option, which recorded each reading to the nearest 0.25 mm (0.01 in.). The rod was equipped with a circular bubble. For a single reading this instrument typically has a standard deviation of 0.3 mm (0.012 in.) at a distance of 50 m (164 ft) and a standard deviation of 0.5 mm (0.02 in.) at a distance of 100 m (328 ft) (*5*).

IRI from Manual Devices

The profile data obtained from the Dipstick and the rod and level were used to compute the IRI of the left and right wheelpaths. Dipstick measurements were available on both wheelpaths in all sections. Except for one section, two replicate runs of the Dipstick were available. Rod and level measurements were not performed in some sections. The IRI computed from the data collected by the manual devices are given in Table 3.

TABLE 3 IRI from Manual Devices

		IRI (m/km)		
Section	Wheel Path	Dipstick Run 1	Dipstick Run 2	Rod & Level
1	Left	1.82	–	–
2	Left	2.34	2.30	2.35
3	Left	1.45	1.47	–
4	Left	4.14	4.06	4.15
5	Left	1.31	1.45	1.45
6	Left	0.68	0.63	–
7	Left	1.89	1.78	–
8	Left	1.39	1.37	–
1	Right	2.13	–	–
2	Right	1.67	1.70	1.66
3	Right	1.39	1.34	–
4	Right	5.67	5.57	5.57
5	Right	0.93	0.93	–
6	Right	0.77	0.74	0.95
7	Right	3.60	3.42	–
8	Right	1.10	1.10	1.20

Note: – No tests performed
1 m/km = 63 in/mile

Comparison of IRI from Profilometers and Dipstick

The ratio between average profilometer IRI at 80 km/hr (50 mph) and average Dipstick IRI (profilometer IRI/Dipstick IRI) are shown in Table 4. The ratios shown in this table have the following distribution: 4 percent between 0.8 and 0.85, 9 percent between 0.85 and 0.9, 31 percent between 0.9 and 0.95, 27 percent between 0.95 and 1.00, 22 percent between 1.00 and 1.05, 6 percent between 1.05 and 1.10, and 1 percent between 1.10 and 1.15. These results indicate that in general there is good agreement between the Dipstick IRI and the profilometer IRI. A typical relationship between IRI computed from profilometer and Dipstick profiles is shown in Figure 2.

The differences between the IRI computed from profilometer and Dipstick profiles can be attributed to the following:

1. There are differences in the paths measured by the two devices.

TABLE 2 Standard Deviation of Left Wheelpath IRI

		Standard Deviation (m/km)							
Test Speed		Asphalt Sections Section Numbers				Concrete Sections Section Numbers			
(kmph)	Profilometer	3	5	6	7	1	2	4	8
65	North Central	0.030	0.009	0.013	0.021	0.041	0.038	0.071	0.036
65	Western	0.011	0.006	0.011	0.035	0.041	0.017	0.038	0.024
65	North Atlantic	0.043	0.051	0.013	0.036	0.027	0.038	0.017	0.039
65	Southern	0.014	0.016	0.011	0.032	0.044	0.032	0.011	0.011
80	North Central	0.016	0.024	0.016	0.036	0.038	0.016	0.106	0.025
80	Western	0.022	0.014	0.013	0.041	0.039	0.022	0.035	0.030
80	North Atlantic	0.052	0.022	0.022	0.047	0.054	0.033	0.028	0.025
80	Southern	0.014	0.011	0.009	0.036	0.017	0.017	0.016	0.008

Note: 1m/km = 63 in/mile, 1 kmph = 0.62 mph

2. The profilometers take measurements at every 2.5 cm (1 in.) and these data points are averaged over a 30-cm (12-in.) moving average and recorded as profile points every 15 cm (6 in.). The Dipstick records the elevation difference between two points that are 30 cm (12 in.) apart.

Figure 3 shows the relationship between the ratio profilometer IRI/Dipstick IRI with the IRI of the wheelpath. In this figure, the ratio profilometer IRI/Dipstick IRI is the average value of this ratio for all four profilometers for a wheelpath, whereas the IRI of a wheelpath corresponds to the average IRI obtained from all profilometer runs at 80 km/hr (50 mph) in that section. Results for the left and right wheelpaths of all sections are shown in this figure. This figure shows that most of the values fall within the range of 0.95 to 1.05.

Comparison of IRI from Profilometers and Rod and Level

The ratio between average profilometer IRI and rod and level IRI (profilometer IRI/rod and level IRI) is shown in Table 5. Figure 4 shows the relationship between the ratio profilometer IRI/rod and level IRI of a wheelpath and the IRI of that wheelpath. The ratio profilometer IRI/rod and level IRI in this figure is the average value of this ratio for all four profilometers for a wheelpath in a section. The IRI of a wheelpath corresponds to the average IRI obtained by considering all profilometer runs at 80 km/hr (50 mph) in a section for that wheelpath. Figure 4 includes data for both the left and right wheelpaths.

An examination of Figure 4 shows that poor agreement between the two devices was obtained at several wheelpaths, whereas good agreement was obtained at other wheelpaths. Poor agreement occurred in wheelpaths that had IRI values less than 1.6 m/km (100 in./mi). In all these instances the rod and level IRI values were greater than profilometer IRI values. Reasonable agreement between IRI computed from rod and level and profilometer profile data was generally obtained at IRI values greater than 1.6 m/km (100 in./mi).

ANALYSIS OF ROD AND LEVEL MEASUREMENTS

The resolution requirements for profile measurements given in an ASTM standard (E1364-90) are as follows:

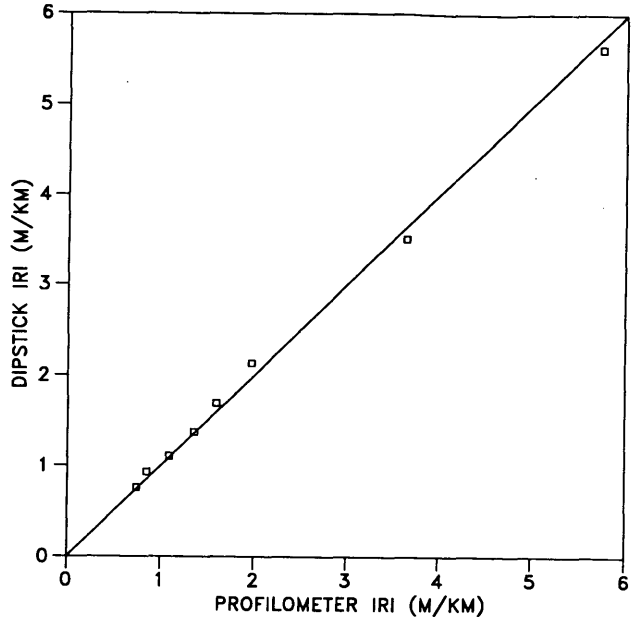

FIGURE 2 Comparison between Dipstick and North Central profilometer (right wheelpath).

1. IRI less than 0.5 m/km (32 in./mi); resolution = 0.125 mm (0.005 in.).
2. IRI between 0.5 and 1 m/km (30 and 63 in./mi); resolution = 0.25 mm (0.01 in.).
3. IRI between 1 and 3 m/km (63 and 190 in./mi); resolution = 0.5 mm (0.02 in.).
4. IRI between 3 and 5 m/km (190 and 317 in./mi); resolution = 1.0 mm (0.04 in.).

For the sections measured, the device used for rod and level measurements satisfied these resolution requirements. Errors that occur during rod and level measurements can be classified into the following categories:

1. Error caused by the rod not being truly vertical; and
2. Random error associated with each reading, which includes all errors except the error caused by the rod being not truly vertical

TABLE 4 Ratio Between Average Profilometer IRI and Average Dipstick IRI

		Average Profilometer IRI / Average Dipstick IRI							
		Asphalt Sections				Concrete Sections			
	Wheel	Section Number				Section Number			
Profilometer	Path	3	5	6	7	1	2	4	8
North Central	Left	0.95	0.95	0.98	0.95	0.90	0.92	1.11	0.92
Western	Left	0.95	0.94	0.90	0.83	0.93	1.01	1.05	1.03
North Atlantic	Left	0.97	0.90	1.00	0.83	0.88	0.95	1.03	1.02
Southern	Left	0.95	0.94	0.90	0.84	0.96	1.02	1.06	1.06
North Central	Right	0.99	0.92	0.98	1.04	0.93	0.94	1.02	0.99
Western	Right	1.06	1.00	1.00	1.03	0.95	0.95	1.01	1.01
North Atlantic	Right	1.01	1.00	1.04	1.00	0.95	0.99	1.01	0.99
Southern	Right	0.97	0.95	0.98	0.87	0.93	0.94	0.99	0.99

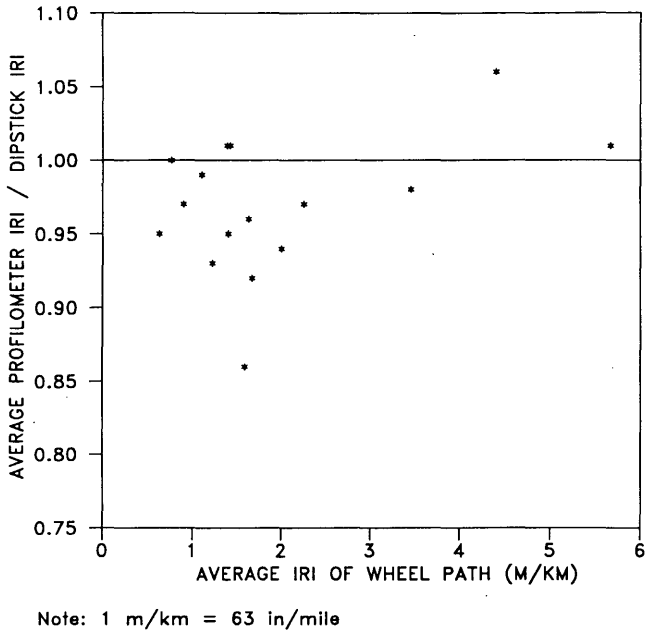

FIGURE 3 Ratio between profilometer and Dipstick IRI versus IRI of wheelpath.

For the autorecording level the standard deviation of a single measurement is typically 0.3 mm (0.012 in.) at a distance of 50 m (164 ft) and 0.5 mm (0.02 in.) at a distance of 100 m (328 ft) (*5*). Therefore, there is an error associated with each reading recorded by the instrument. During profile measurements, the maximum distance between the rod and the level was always less than 40 m (130 ft). Therefore, assuming that the readings at a point are normally distributed, there is a 68 percent probability for a reading to lie within the mean plus or minus a standard deviation and a 95 percent probability for the value to lie within the mean plus or minus two standard deviations (*6*).

Table 6 shows the error in reading the rod as a result of the deviation of the rod from the vertical when viewed along the line of sight of the level, for different rod reading heights. When compared with the ASTM resolution requirements of the level for profile measurements, a considerable error can occur when the rod is not truly vertical. The deviation of the rod from the vertical will always cause the value read to be greater than the true value.

The effect of random errors during leveling on the computer IRI was studied using the following scheme. A profilometer run was selected from one of the sections, and the IRI was computed for one wheelpath. Then a random error between −0.25 and 0.25 mm (−0.01 and +0.01 in.) was added to each point recorded by the profilometer. The random numbers between −0.25 and +0.25 mm (−0.01 and +0.01 in.) were generated using a random number generator. The IRI of this new profile containing the random error was then computed. The procedure was repeated using the original profilometer profile and random numbers between −0.5 and +0.5 mm (−0.02 and +0.02 in.), −0.75 and +0.75 mm (−0.03 and +0.03 in.), and −1 and + 1 mm (−0.04 in. and +0.04 in.), respectively. The results of these computations for five profiles are given in Table 7. This analysis shows that in general, a random error in a profile having a high IRI value does not have much effect on the computed IRI. However, for profiles that have relatively low IRI values, introduction of a random error can have a large effect on IRI, depending on the magnitude of the error.

The effect on IRI caused by the rod's not being held exactly vertical was studied using the same scheme outlined in the previous paragraph. The same wheelpaths that were used earlier were used for this study too. However, in this case the random numbers generated were all positive as an error because the rod is not vertical and thus is always positive. Random numbers between 0 and 0.25, 0 and 0.5, 0 and 0.75, and 0 and 1 were generated for this analysis. These numbers were added separately to the original profile recorded by the profilometer, and the IRI of each profile was computed. The results of this analysis are shown in Table 8. The conclusions arrived at in the earlier study described in the previous paragraph are true for this analysis too. A comparison of Tables 7 and 8 shows that the effect on IRI was greater because of random error associated with each reading than because of the error caused by the rod's being not exactly vertical. The reason for this is that an introduction of a random error that varies between positive and negative values will make a profile rougher than a random error that always is positive.

The error in a reading obtained by the level is a combination of random error associated with that reading and the error caused by the rod's not being vertical. For each reading obtained by the level, a combination of these two errors will cause an error in the recorded value. The results in Tables 7 and 8 show that errors during leveling can have an appreciable effect on the computed IRI of pavements having a low IRI value, whereas their effect is not very significant in pavement profiles having a high IRI.

TABLE 5 Ratio Between Average Profilometer IRI and Rod and Level IRI

		Average Profilometer IRI / Rod & Level IRI							
		Asphalt Sections				Concrete Sections			
	Wheel	Section Number				Section Number			
Profilometer	Path	3	5	6	7	1	2	4	8
North Central	Left	–	0.86	–	–	–	0.91	1.11	–
Western	Left	–	0.85	–	–	–	0.99	1.05	–
North Atlantic	Left	–	0.82	–	–	–	0.94	1.02	–
Southern	Left	–	0.85	–	–	–	1.01	1.05	–
North Central	Right	–	–	0.78	–	–	0.96	1.03	0.91
Western	Right	–	–	0.80	–	–	0.97	1.02	0.93
North Atlantic	Right	–	–	0.83	–	–	1.01	1.02	0.91
Southern	Right	–	–	0.78	–	–	0.96	1.00	0.91

Note: – Not measured by rod and level

The poor agreement between IRI computed from profiles measured with rod and level and profilometers on very smooth pavements can be explained by the effect of leveling errors on measured profiles. In addition, as described in the comparison between IRI values from the Dipstick and the profilometers, differences can also occur because of the differences in measured paths and the averaging of readings by the profilometers.

COMPARISON OF DISTANCE-MEASURING SYSTEMS OF PROFILOMETERS

An important factor in a profilometer comparison is to determine whether the distance-measuring systems of the profilometers are measuring the distance accurately so that measurements are obtained at specified intervals. This was investigated by placing a reflective tape at the beginning and the end of the test sections. This reflective tape is detected by the photo cell in the profilometer and is recorded as an event mark in the data file. The distance between the event marks in the data files was analyzed to determine the accuracy of the distance-measuring systems. The analysis showed that the distance-measuring systems of all profilometers were within the acceptable error.

CONCLUSIONS

The following conclusions are drawn from this analysis:

1. The profilometers are recording similar data in the left and right wheelpaths.
2. Profile measurements by the profilometers are independent of test speed at test speeds of 65 km/hr (40 mph) and 80 km/hr (50 mph).

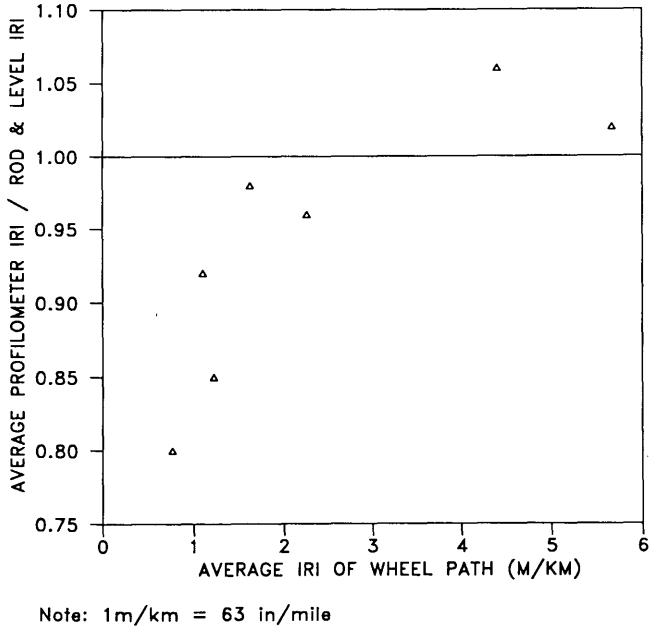

FIGURE 4 Ratio between profilometer and rod and level IRI versus IRI of wheelpath.

TABLE 6 Error Caused by Deviation of Rod from Vertical

Deviation of Rod from Vertical (Degrees)	Error in Rod Reading (mm) Rod Height 0.9 m	1.20 m	1.50 m
1	0.14	0.19	0.23
1.5	0.31	0.42	0.52
2	0.56	0.74	0.93
2.5	0.87	1.16	1.45
3	1.25	1.67	2.09
3.5	1.71	2.28	2.84
4	2.23	2.97	3.72
4.5	2.82	3.76	4.70
5	3.48	4.64	5.80

Note: 1 mm = 0.04 in

3. All profilometers generally showed excellent repeatability at a section in the left and the right wheelpaths. It was observed that the repeatability of the profilometers was not affected by speed of testing (65 km/hr versus 80 km/hr) or the surface type (asphalt concrete versus portland cement concrete).
4. Reasonable agreement was found between the IRI computed from Dipstick profile data and profilometer profile data for all four profilometers in the left and right wheelpath, for IRI values ranging from 0.8 to 5.6 m/km (50 to 360 in./mi). Exact agreement between IRI computed from Dipstick and profilometer data is unlikely because of the variations between the wheelpaths measured by the devices and because of different sampling and recording intervals of the two devices.
5. Random errors in a profile having a low IRI value can cause a considerable error on the computed IRI. The magnitude of the error depends on the magnitude of the random error. Random errors on a profile having a medium to high IRI value do not have much effect on the IRI.
6. The IRI computed from profiles measured using a level meeting the resolution requirements in ASTM E1364-90 for profile measurements generally showed good agreement with the IRI computed from the profilometer profiles for IRI values greater than 1.6 m/km (100 in./mi). There was generally poor agreement between the devices for profiles with IRI values less than 1.6 m/km (100 in./mi). Some difference in IRI between these two devices is expected because of the variations in wheelpath measured by the devices and because of the different sampling and recording interval of the two devices. However, it was seen that random errors in a rod and level survey can introduce considerable errors in the calculated IRI for pavements whose IRI value is generally less than 1.6 m/km (100 in./mi).
7. The following procedures should be followed when measuring profiles with the rod and level to minimize errors: (a) use a level having the resolution specified in ASTM E1364-90; (b) set up the instrument in such a way that only low readings are taken on the rod, which will minimize the error caused by deviations of the rod from the vertical; and (c) use a rod having a circular bubble and allow the rod person sufficient time to hold the rod vertical at a location before taking a reading.
8. IRI computed from rod and level measurements are generally taken as the "correct" measurement to validate other profile-measuring devices. This analysis indicates that on profiles having low IRI values leveling errors could influence the IRI considerably. Therefore, IRI from rod and level data of profiles having low IRI values should be examined with caution. When using the

TABLE 7 Effect on IRI Caused by Random Variations in Profile

IRI of Original Profile (m/km)	IRI of Profile with Random Variations (m/km) Range of Random Variation (mm)				Percentage Change in IRI Due to Random Variations Range of Random Variation (mm)			
	−0.25 to +0.25	−0.5 to +0.5	−0.75 to +0.75	−1 to +1	−0.25 to +0.25	−0.5 to +0.5	−0.75 to +0.75	−1 to +1
0.76	0.78	0.90	0.97	1.19	3.3	19.0	28.5	56.9
1.07	1.10	1.16	1.26	1.37	2.8	8.3	18.3	28.2
1.64	1.65	1.68	1.77	1.79	0.4	2.5	8.1	8.8
2.35	2.35	2.40	2.37	2.55	−0.2	1.9	0.8	8.2
4.43	4.43	4.44	4.44	4.51	−0.1	0.2	0.2	1.8

Note : 1 m/km = 63 in/mile, 1 mm = 0.04 in.

TABLE 8 Effect on IRI Caused by Positive Random Variations in Profile

IRI of Original Profile (m/km)	IRI of Profile with Random Variations (m/km) Range of Random Variation (mm)				Percentage Change in IRI Due to Random Variations Range of Random Variation (mm)			
	0 to +0.25	0 to +0.5	0 to +0.75	0 to +1	0 to +0.25	0 to +0.5	0 to +0.75	0 to +1
0.76	0.77	0.78	0.83	0.88	1.0	2.7	9.2	16.0
1.07	1.08	1.06	1.13	1.14	0.7	−0.6	5.5	6.9
1.64	1.64	1.66	1.67	1.82	−0.3	1.2	1.5	10.9
2.35	2.35	2.37	2.37	2.37	0.1	0.5	0.5	0.8
4.43	4.43	4.44	4.46	4.49	−0.1	0.1	0.5	1.2

Note: 1m/km = 63 in/mile, 1 mm = 0.04 mm

IRI computed from profiles measured with the rod and level for validating profile-measuring devices, it is recommended that pavements with a wide range of IRI be considered.

ACKNOWLEDGMENTS

The work described in this paper was sponsored by the LTPP Division of FHWA.

REFERENCES

1. *Profscan 1.3. User Documentation, Strategic Highway Research Program, Long Term Pavement Performance.* Pavement Management Systems, Amherst, N.Y., April 1991.
2. Sayers, M. W., T. D. Gillespie, and W. D. O. Paterson. *Guidelines for Conducting and Calibrating Road Roughness Measurements.* Technical Paper 46. World Bank, Washington, D.C., 1986.
3. Montgomery, D. C. *Design and Analysis of Experiments.* John Wiley & Sons, New York, 1984.
4. *SPSS/PC Advanced Statistics 4.0.* SPSS Inc., Chicago, 1990.
5. Ingensand, H. *Wild NA 2000, World's First Digital Level.* Technical Paper. Wild Leitz, Ltd., n.d.
6. Ott, L. *An Introduction to Statistical Methods and Data Analysis.* Duxbury Press, Boston, Mass., 1984.

The views expressed are those of the authors and do not reflect the official view of FHWA.

Publication of this paper sponsored by Committee on Surface Properties–Vehicle Interaction.

Side Friction Demanded and Margins of Safety on Horizontal Curves

J. F. MORRALL AND R. J. TALARICO

The findings of a research project that was conducted to determine the amount of side friction demanded and provided for a range of roadway curvatures, vehicle speeds and types, and pavement surface conditions are described. Seven horizontal curves located on rural two-lane highways in Alberta as well as curves at the Calgary Police Service's Driver Training Facility were used as test sites. A three-axis accelerometer and a ball bank indicator were installed in seven test vehicles, including passenger cars, a half-ton pick-up, and a tandem-axle gravel truck. Lateral accelerations and ball bank readings were taken as the vehicles traversed test curves at constant speeds. Speeds were increased in increments of 10 km/hr until impending side skid conditions were reached. Ball bank readings are regressed upon lateral accelerations for each vehicle type, and equations predicting the implied value of safe side friction, the safe speed of the curve, and the margin of safety provided by the safe speed are developed. Maximum values of side friction demanded on dry and icy roadways are determined and used to calculate the margin of safety provided at various speeds. It was found that the current design standards are quite conservative and provide a more-than-sufficient margin of safety for motorists.

As a vehicle corners, it is accelerated toward the center of the curve. According to Newton's Second Law, this acceleration must produce a force that is directed toward the center of the curve. This unbalanced force results in side thrust, which must be countered by the component of the vehicle's weight acting along the surface of the roadway, or by side friction between the tires and the pavement, or by some combination of the two. This is indicated by the following equation, commonly called the point-mass equation:

$$f_s + e = V^2/(127\ R) \quad (1)$$

where

f_s = side friction factor,
e = superelevation rate (m/m),
V = speed (km/hr), and
R = radius (m).

If a vehicle demands more side friction than the pavement/tire interface can provide the vehicle will skid off the roadway. AASHTO (*1*) notes that "the upper limit of this factor (f_s) is that at which the tire is skidding or at the point of impending skid." AASHTO (*1*) does not indicate the margin of safety against side-skid that the design factors provide. Although AASHTO notes that the f_s used for highway design should be substantially less than the f_s at impending skid, the agency (*1*) also notes that "in selecting maximum allowable side friction factors for use in design, one criterion is the point at which the centrifugal force is sufficient to cause the driver to experience a feeling of discomfort and cause him to react instinctively to avoid higher speed. The speed on a curve, at which discomfort due to centrifugal force is evident to the driver, can be accepted as a design control for the maximum allowable amount of side friction." AASHTO (*1*) also provides a caution that other factors, such as swerving and increased steering effort, are required and act to control driver speed at conditions of high friction demand. In addition, AASHTO (*1*) notes that when practical, "the maximum factors selected should be conservative for dry pavements and provide a margin of safety for operating on pavements that are wet as well as ice or snow covered." This paper describes the findings of a research project that was conducted to determine the amount of side friction demanded and provided for a range of roadway curvatures, vehicle speeds and types, and pavement surface conditions.

J. F. Morrall, Department of Civil Engineering, University of Calgary, 3500 University Drive, N.W., Calgary, Alberta, Canada T2N 1N4. R. J. Talarico, Reid Crowther and Partners, Ltd., Suite 300, 4243 Glanford Avenue, Victoria, British Columbia, Canada V8Z 4B9.

RECENT RESEARCH

Surprisingly little research has been done in the area of side friction and margins of safety since the late 1940s. In fact, very few full-scale road tests have been conducted, and only a small number of these have been conducted on icy pavement surfaces. Instead of conducting full-scale tests, some researchers (*2–4*) used an assumed value of side friction provided to calculate the margin of safety a vehicle has when cornering.

Other researchers have used skid trailers to determine how much side friction a tire can provide (ANSI/ASTM E670–79; *5*). The skid trailer is connected to a tow vehicle so that the longitudinal axis of the trailer is at an angle to the line of motion of the two vehicle. As the tow vehicle moves, the trailer moves forward, with the wheels rolling forward with a side skid motion. Because of the lack of a driving force on the trailer tires, combined with the absence of the vehicle roll that occurs during cornering, skid trailers do not provide a realistic model of a side-skidding vehicle.

Others (*6*) have observed vehicle speeds on curves and used the point-mass equation to calculate the amount of friction demanded. Relationships between curve geometry and friction factor were then established. Lamm et al. (*6*) found that motorists demand more friction on curves sharper than 2 degrees/100 m and at operating speeds lower than 80 km/hr. By observing driver behavior on curves, McLean (*7*) also found that drivers tend to demand more side friction on tighter, highly superelevated curves.

Research into side friction on icy pavement surfaces is extremely sparse. The research that has been conducted on this type of surface typically consisted of driving a vehicle around a circular

path with a known radius until the driver felt that impending skid conditions were reached (*8,9*). By recording the time required to drive the vehicle through a number of laps, the point-mass equation was used to determine the side friction factor.

Most researchers note that the friction factors used for design should not use all of a tire's available friction for cornering (*2,3,10*); the tire must be able to provide braking friction as well. By limiting the allowable side friction factor used for design to a certain percentage of the maximum side friction factor, designers can ensure that enough friction remains for other maneuvers.

Because the side friction factor is essentially an acceleration, measured in *g*-units, in the plane of the road, one can use an accelerometer to measure the friction factor directly. This method was used in a research project conducted by the Department of Civil Engineering at the University of Calgary for Alberta Transportation and Utilities (*11*).

DATA COLLECTION PROCEDURE

To measure the amount of side friction demanded by traffic and supplied by pavement, tests were conducted on rural two-lane highway curves within the province of Alberta and on the Calgary Police Service's Driver Training Facility. Curvatures ranged from 290 to 3490 m, whereas maximum superelevation rates ranged from 2 to 8 percent. Because all sites are located on relatively flat terrain, most of the available friction is available for cornering.

Site selection was based on the following factors (*6,11*):

1. Circular curves with no spiral transitions,
2. Paved sections with paved shoulders,
3. No changes in lane or shoulder widths,
4. Gentle sideslopes and removal of roadside hazards and other physical features that may create a dangerous environment,
5. Grades less than 5 percent,
6. Location away from the zone of influence of intersections, towns, and so on, and
7. Relatively low traffic volumes.

A wide range of test vehicles, typical of those found on rural two-lane highways in Alberta, was used for this project. These test vehicles included two late model sports cars, a sports sedan, a compact car, a half-ton pick-up truck, and a tandem-axle gravel truck; a Calgary Police service cruiser was also used for high-speed tests. All vehicles were tested unloaded, with the fuel tank approximately half full, and tire pressures equal to those recommended by the tire manufacturer.

A ball bank indicator and a commercial accelerometer (the G-Analyst) were used to measure ball bank readings and corresponding lateral accelerations on the test curves. During vehicle roll, the ball bank reading is the sum of the centrifugal force angle and the body roll angle, minus the superelevation angle, and therefore provides a measure of the centrifugal force acting on the occupants of a vehicle (*12*). Since the G-Analyst can be calibrated for a vehicle's roll and pitch angles, the side friction factor in the plane of the roadway can be measured. A radar speedometer was used to collect traffic speed data at the test sites, and to substantiate the calculated test vehicle speeds.

As test vehicles traversed a curve at constant speed (ranging from 60 to 120 km/hr), a passenger took ball bank readings and placed flags in the G-Analyst's memory at predetermined sections of the roadway.

RELATIONSHIP BETWEEN SPEED AND CURVATURE

Vehicle speeds on horizontal curves are a function of many variables, including site, traffic, and motorist characteristics along with other variable factors (*13*). Because each test site is located on fairly level terrain and has good sight distance, uniform lane and shoulder widths, and design speeds, the effects that these parameters have on operating speeds cannot be determined. Since superelevation is strongly correlated with curvature, it was not considered as an independent variable in any of the regression models. The following criteria were used to determine the most appropriate model:

- The selected regression equation must have a multiple regression coefficient that is significant at the 95 percent level.
- The coefficient estimator for each of the independent variables included in the regression equation must be significantly different from zero at the 95 percent level.

On the basis of field observations on nine curves in Alberta, regression analysis was used to obtain estimates of the effect on operating speed produced by degree of curvature. Linear, multiplicative, exponential, and reciprocal regression models were developed. The model given here was found to best satisfy the given criteria:

$$V_{85} = e^{[4.561 - 0.00586(DC)]} \text{ km/hr} \quad (2)$$

where

V_{85} = 85th-percentile speed (km/hr),
DC = degree of curve (degrees/100 m),
r^2 = coefficient of determination, and
S.E. = standard error of estimate (km/hr).

For this relationship, $r^2 = 0.631$ and S.E. = 0.0326, which suggest that the relationship given here is moderately strong.

SIDE FRICTION FACTORS AND BALL BANK ANGLES

Regression analysis was used to obtain models of the relationship between ball bank angle and side friction factor (determined by using the acceleration data collected with the G-Analyst). Because the ball bank indicator can be accurately read only to the nearest degree, it is possible that small lateral acceleration values may be assigned to ball bank angles that equal zero. Therefore, these regression models were not forced through the origin. Ball bank angles were found to vary linearly with side friction factors. Coefficients of determination between ball bank angle and side friction factor for the highway sites range from 0.976 to 0.645. Some of this variation may be a result of vehicle characteristics because these relationships were determined using data collected for all vehicle types. In general, the correlation coefficients between ball bank angle and side friction factor are lower for flatter curves than for sharper curves. This difference may be because of the small range of ball bank angles developed on these sites. No ball bank readings greater than 6.5 degrees were developed on the flatter curves, whereas ball bank readings greater than 15 degrees were commonly developed on the sharper curves. Therefore, small er-

rors in ball bank readings have a greater effect on the flatter curves than they do on the sharper curves. In addition, because the flat curves are longer than the sharp curves, drivers have more opportunities to make steering inputs on the flatter curves. AASHTO (*1*) defines the safe speed of a curve as that which produces a ball bank angle of ± 10 degrees for speeds greater than 55 km/hr. The relationships developed between ball bank angle and side friction factor were used to determine the amount of side friction that corresponds to the safe speed. Using these "safe side friction" values combined with the radius of curvature and the as-built maximum superelevation rate, the safe speed for each curve was calculated. It was found that, based on AASHTO (*1*) design criteria for horizontal curves, curves flatter than 1000 m provide a very high margin of safety. For the tighter curves, speeds greater than 90 km/hr can be achieved before driver discomfort is noticed. This indicates that the margins of safety provided on these curves by design guidelines (*1*) are lower than those provided on the flatter curves.

Regression models relating ball bank angle and side friction factor on icy pavement surfaces also were developed. Coefficients of determination for ball bank angle and side friction factor for the icy curves range from 0.85 to 0.70—substantially lower than those obtained for dry pavements. The main source of variation is caused by differences in ice temperature and ice surface condition. Because climatic conditions could not be controlled, the data analyzed were collected under temperatures ranging from −20°C to −5°C. Furthermore, the ice surfaces of the 30- and 50-m curves were very smooth, whereas that of the 70-m curve was noticeably rougher. Finally, variation also may have been introduced by repeated wheel loads heating the ice cover.

Safe side friction factors for icy surfaces were determined using the regression equations developed for icy pavement. These values, combined with the point mass curve equation, were then used to calculate safe speeds of 25, 31, and 38 km/hr for the 30-, 50-, and 70-m icy curves, respectively.

SIDE FRICTION FACTORS AND BALL BANK ANGLES FOR TEST VEHICLES

Regression models relating ball bank angles to side friction factors (determined by using the acceleration data collected with the G-Analyst) for each test vehicle were also developed. Because of data limitations and marginal differences in side friction factors between vehicle types, along with the fact that design guidelines (*1*) are based on all classes of vehicles, data for all vehicle types were grouped together. The resulting relationship is shown in Figure 1. The high coefficient of determination and low standard error indicated that the relationship is strong between ball bank angle and side friction factor.

Using Figure 1, safe side friction factors for the inside and outside of a given curve were found to be 0.1588 and 0.1790. These factors are slightly higher than those found by previous researchers (*14–16*).

A similar regression model was developed for the icy curves. The regression model for these curves has a lower coefficient of determination ($r^2 = 0.78$) than that of the highway curves. This is mainly a result of variations in ice temperature and surface condition. The safe side friction factors for all the vehicles on the icy curves was determined to be 0.187. However, because side skid occurred at ball bank angles of less than 10 degrees, this safe side friction factor is unrealistic. In fact, side skid occurred at substantially lower ball bank angles than those at which discomfort is noticed. Therefore, basing design side friction factors on driver comfort levels in jurisdictions where freezing temperatures routinely occur during the winter months is clearly not a conservative approach to highway design.

PEAK SIDE FRICTION DEMANDED

It is widely known that drivers tend to drive a spiral when traversing a horizontal curve (*17*), which means that side friction demands do not increase instantaneously to their peak value as a vehicle enters a curve. Instead, the amount of side friction demanded varies with the distance along the curve, as Figure 2 shows, and increases with speed. On dry pavement surfaces, it was found that peak side friction demanded can occur anywhere along a curve. On icy pavement surfaces it was found that the amount of side friction demanded increases gradually as a vehicle enters a curve and gradually decreases as the vehicle exits the curve. This suggests that drivers steer a spiral when traversing a curve and may be because, compared with the highway curves, icy curves had very smooth surfaces, thereby negating the effects of surface roughness on lateral acceleration readings. In addition, because these curves are very short compared with the highway curves and because drivers can devote much more of their attention to the driving task, fewer steering inputs are required.

To investigate whether side friction factors given in current design guidelines provide an adequate margin of safety, the peak amount of side friction demanded by all vehicle types under a range of speeds on each test curve was determined. Because the amount of peak side friction demanded (fs_p) varies with the radius of curvature, peak values obtained on the inside and the outside of each highway curve were determined. Linear regression models were found to fit the data points the best and are shown in Table

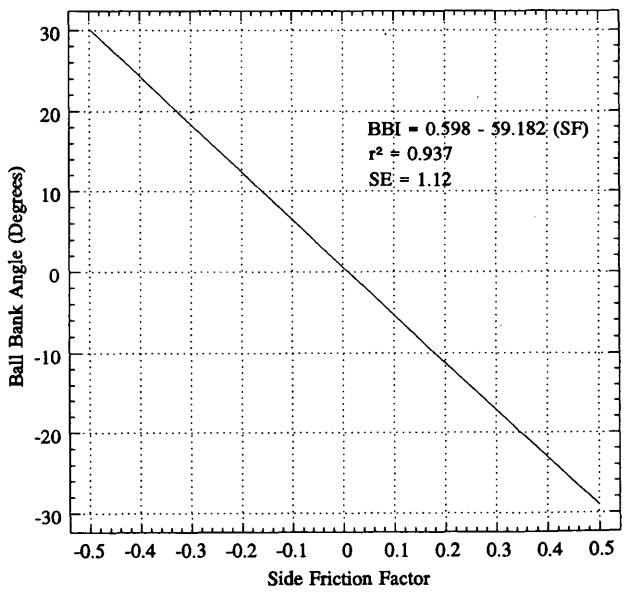

FIGURE 1 Regression of ball bank angle on side friction factor for all vehicles on highway test curves.

1 for the inside and outside of each highway curve as well as for the icy curves.

For the highway curves, Table 1 indicates that the correlation between peak side friction factor and speed decreases as the radius of curvature increases. In fact, the coefficients of determination between speed and peak side friction factor for the 3000- and 3490-m radius curves are so low that no significant relationship exists. This is largely because the peak friction demanded on the flatter curves is small, which means that factors that have minor influences on the peak friction demanded on sharper curves now play a larger role. In addition, because the flatter curves are longer than the sharper curves, there are more opportunities for factors such as steering inputs and pavement surface irregularities to affect the amount of peak friction required.

At speeds between 65 and 90 km/hr, the side friction factors suggested by AASHTO (*1*) for design are exceeded on the 290- and 435-m radius curves. This indicates that more side friction is being used at these speeds than the design guidelines recommend.

The relationships between peak friction demanded and speed for the icy curves along with the side friction factors recommended for design (*1*) are given in Table 1 and also are shown graphically in Figure 3. The moderately low coefficient of determination for the 30-m curve is because only a narrow range of speeds could be investigated. Furthermore, because the air temperature increased from approximately −14°C to slightly below freezing during the time in which these data were collected and because the ice layer had started to melt, the tests had to be discontinued and completed on another day. Therefore, the ice temperature and surface condition introduced variation in the data for which the regression model does not take into account.

As Figure 3 indicates, peak side friction demanded increases with speed and radius of curvature. Figure 3 also shows that more side friction is demanded than design guidelines (*1*) provide for speeds greater than 25, 29, and 34 km/hr for 30-, 50-, and 70-m curves, respectively. Therefore, the margin of safety that the design side friction factors provide appears to be inadequate for icy surfaces.

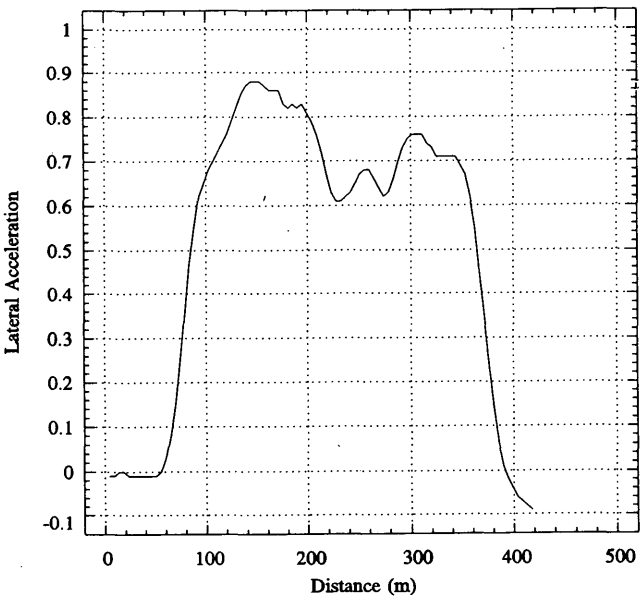

FIGURE 2 Side friction demanded by 1991 Caprice police cruiser on 435-m radius curve.

MARGIN OF SAFETY AGAINST SKIDDING

To estimate the margin of safety a curve provides against skidding, the side friction at impending skid conditions and the peak side friction demanded must be known. Once these values are known, the margin of safety can be defined as

$$MS_{\text{skid}} = f_{s\ \text{skid}} - f_{s\ \text{peak}} \tag{3}$$

where

MS_{skid} = margin of safety against skidding,
$f_{s\ \text{skid}}$ = side friction factor at impending skid condition at a given speed, and
$f_{s\ \text{peak}}$ = peak side friction demanded at a given speed.

Because the side friction at impending skid depends on the pavement surface condition, different margins of safety exist on dry, wet, and icy pavements.

Margin of Safety on Dry Pavements

Because impending skid conditions were reached at two test sites with the higher-powered vehicles only, limited data on side friction factors at impending skid were obtained. However, the data collected suggest that the maximum amount of side friction provided is approximately 0.90. This value agrees well with the findings of other researchers, (*4,17,18*). Using these data, combined with the margin of safety definition given in Equation 3, margins of safety against skidding on dry pavement for each highway site were calculated. These margins of safety, along with those for wet and icy pavements, are shown in Table 2.

Table 2 indicates that on dry pavement the margin of safety decreases with speed and decreases at a faster rate on tighter curves than on flatter curves. For example, the margin of safety provided on the 3500-m radius curve varies from 0.93 to 0.85 for all speeds. This suggests that drivers are using a minimal amount of friction for cornering, which leaves the bulk of the total available friction for changes in deceleration, acceleration, or direction. Therefore, these curves provide a high level of driving dynamic safety on dry pavement. Furthermore, these values indicate that very little superelevation is needed on these types of curves. Because the manner in which margin of safety against skidding was defined does not account for the superelevation provided on a curve, the provision of superelevation will increase the frictional supply of a curve and increase further the margin of safety. By providing superelevation equal to reverse crown, not only would an adequate margin of safety on dry pavements be provided, but construction costs would also decrease.

For the 290- and 435-m radius curves, the margin of safety decreases with speed at approximately 14 times the rate of the flatter curves. This rapid decrease suggests that there may not be enough friction available for drivers to perform evasive maneuvers under normal operating speeds. In addition, the coefficients of determination between speed and margin of safety of the linear regression models for the flatter curves are low. This indicates that a large portion of the variance in margin of safety cannot be ex-

plained by speed for these sites and is mainly the result of the poor relationship between peak side friction demanded and speed that exists for these sites.

Margin of Safety on Wet Pavements

Impending skid tests on wet pavement were not conducted for two reasons. First, there is no standard method for measuring water layer thickness on pavements. Second, the relatively high superelevation rates provided on these curves prohibited a uniform water thickness layer from being formed. Other researchers (*4*) have found that the maximum side friction provided by wet pavements is 0.58 at 30 km/hr, decreasing to 0.41 at 113 km/hr. For this study, side friction factors of 0.54 at 30 km/hr, decreasing to 0.315 at 200 km/hr, were used.

Regression equations to relate margins of safety to speed were developed for each highway site; coefficients of determination ranged from 0.55 to 0.99. These equations were then used to calculate the margin of safety against skidding at various speeds for each site and are given in Table 2.

Once again, sharper curves appear to provide a lower margin of safety against skidding than do flatter curves. In fact, at speeds of 110 km/hr or greater, no margin of safety against skidding exists on the three sharpest curves. For vehicles traveling at the 85th-percentile speeds on these curves, margins of safety range from approximately 0.06 to 0.13. Therefore, sharp curves do not provide a sufficient margin of safety against skidding under wet pavement conditions for vehicles traveling at the normal operating speed of the curve. Moreover, very little friction is available for motorists to perform evasive maneuvers if required. Therefore, the provision of adequate superelevation on these types of curves is critical. In fact, if drivers are surprised on these sites during rainy weather on curves with adequate superelevation, it is possible that they may lose control of their vehicle and skid off the roadway.

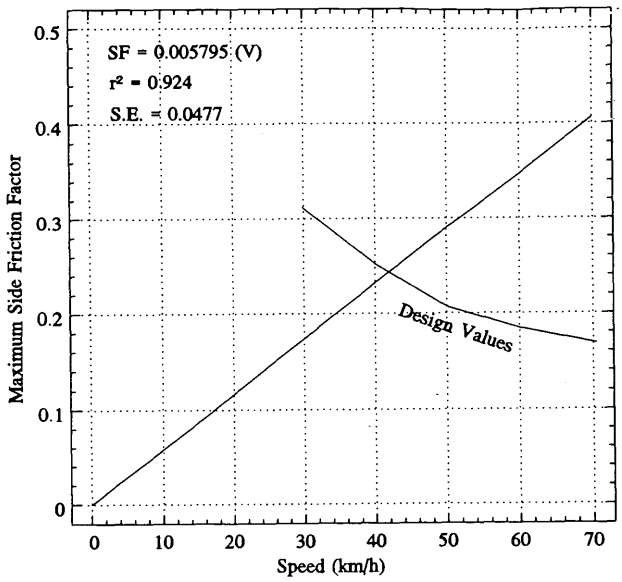

FIGURE 3 Variation of maximum side friction factor on ice with speed.

For the four flatter curves tested, margins of safety against skidding of approximately 0.38 can be expected at the normal operating speeds of vehicles on these highways. These frictional reserve levels appear to be adequate to provide enough braking

TABLE 1 Relationship Between Peak Side Friction, Radius of Curve, and Speed

Radius (m)	Direction of Travel	Regression Equation	R^2 (%)	S.E.
30*	Inside	fs_p = -0.0629 + 0.0926(V)	62.12	0.0420
50*	Inside	fs_p = -0.143 + 0.0106(V)	88.73	0.0217
70*	Inside	fs_p = -0.906 + 0.0073(V)	82.32	0.0295
290	Inside	fs_p = -0.385 + 0.00683(V)	96.94	0.0421
	Outside	fs_p = 0.451 - 0.00670(V)	91.55	0.0405
435	Inside	fs_p = -0.405 + 0.00745(V)	97.98	0.0382
	Outside	fs_p = 0.337 - 0.00645(V)	96.34	0.0233
580	Inside	fs_p = -0.391 + 0.00570(V)	93.42	0.0490
	Outside	fs_p = 0.322 - 0.00466(V)	92.92	0.0254
1164	Inside	fs_p = -0.158 + 0.00220(V)	79.79	0.0200
	Outside	fs_p = 0.188 - 0.00218(V)	83.2	0.0200
1164	Inside	fs_p = -0.184 + 0.00253(V)	84.17	0.0208
	Outside	fs_p = 0.235 - 0.00260(V)	77.24	0.0265
3000	Inside	fs_p = 0.000606(V)	22.74	0.0248
3490	Inside	fs_p = 0.000458(V)	13.1	0.0226
	Outside	fs_p = -0.000360(V)	32.7	0.0103

* icy curves

TABLE 2 Margin of Safety Against Skidding on Dry, Wet, and Icy Pavement

Speed (km/h)	Pavement Condition	Margin of Safety for Different Degrees of Curve								
		DC= 191	DC= 115	DC= 82	DC= 20	DC= 13	DC= 10	DC= 5	DC = 2*	DC = 1.6*
30	Dry	-	-	-	1.08	1.08	1.12	0.99	0.88	0.89
	Wet	-	-	-	0.72	0.72	0.76	0.63	0.52	0.53
	Icy	-0.08	-0.12	-0.16	-	-	-	-	-	-
40	Dry	-	-	-	1.01	1.01	1.06	0.97	0.88	0.88
	Wet	-	-	-	0.62	0.61	0.67	0.58	0.48	0.49
	Icy	0.02	0.01	-0.05	-	-	-	-	-	-
60	Dry	-	-	-	0.88	0.86	0.95	0.93	0.86	0.87
	Wet	-	-	-	0.41	0.39	0.48	0.46	0.40	0.41
80	Dry	-	-	-	0.74	0.71	0.84	0.88	0.85	0.86
	Wet	-	-	-	0.24	0.21	0.34	0.38	0.35	0.36
100	Dry	-	-	-	0.60	0.56	0.72	0.84	0.84	0.85
	Wet	-	-	-	0.08	0.04	0.20	0.31	0.31	0.33
150	Dry	-	-	-	0.26	0.19	0.44	0.73	0.81	0.83
	Wet	-	-	-	-0.29	-0.37	-0.12	0.17	0.26	0.28
200	Dry	-	-	-	-.08	-0.19	0.15	0.62	0.78	0.81
	Wet	-	-	-	-0.67	-0.77	-0.43	0.03	0.19	0.22

* r^2 of regression model is less than 0.45.
- no data available

friction for drivers to stop safely, even if superelevation rates equal to reverse crown are provided on these types of curves.

It was also evident that the margin of safety decreases at a higher rate with speed on wet pavements than on dry pavements. In addition, wet pavements provide a margin of safety of approximately 0.50 less than dry pavements for any given speed and radius of curvature. This significant reduction in available side friction clearly indicates that water on pavement dramatically decreases the margin of safety against skidding.

Margin of Safety on Icy Pavements

Lateral acceleration and speed data at impending skid conditions were collected on icy pavement surfaces. These data were then used to develop regression models relating side friction factors to speed, as given in Table 2. A linear regression model was found to best fit the data points and is shown in Figure 3. Figure 3 is based on over 130 lateral acceleration and speed readings; the speeds ranged from approximately 20 to 50 km/hr. The moderate correlation coefficient indicates that the relationship between margin of safety and speed is moderately strong.

Knowing the maximum friction provided at impending skid, along with the design side friction factors, the margin of safety against skidding provided by the design factors can be defined as

$$MS_{\text{design}} = f_{s\ \text{skid}} - f_{s\ \text{design}} \quad (4)$$

where $f_{s\ \text{design}}$ is the side friction factor assumed for design.

A negative margin of safety, as presented in Table 2, means that design guidelines are using more side friction than the tire-pavement interface can provide. Therefore, a negative margin of safety is clearly undesirable. Because design friction factors are not specified for speeds less than 30 km/hr (*1,19*), a side friction factor of 0.31 was assumed for a design speed of 29 km/hr. This approach is conservative because side friction factors increase with decreasing speed.

Table 2 indicates that the margin of safety against skidding on the icy curves increases with increasing radius and speed. This increase is because substantially higher side friction factors are assumed for lower speeds than for slightly higher speeds. Because the side friction provided at impending skid conditions varies marginally with speed, the large change in design friction factors with speed causes the margin of safety to increase with speed. Therefore, lower design side friction factors for speeds of less than 40 km/hr would increase the margin of safety for curves with low design speeds.

It was found that the side friction factors suggested by design guidelines (*1,19*) do not provide any margin of safety against skidding for speeds less than 37 to 44 km/hr for radii of 30 and 70 m, respectively. In addition, only a small margin of safety exists for speeds greater than 48 km/hr. This margin of safety does not appear to be adequate to accommodate emergency braking or other evasive maneuvers. Therefore, it appears that the side friction factors suggested by design guidelines do not provide adequate margins of safety for vehicles traveling on icy pavements, especially on curves with lower design standards.

SUMMARY

The findings of this research project can be summarized as follows:

1. Ball bank angles of ±10 degrees yield side friction factors of 0.16 to 0.17 for the test vehicles used; these values correspond well to those suggested for design (*1*). In addition, safe side friction factors appear to be relatively constant across the vehicle types investigated, which suggests that most drivers will experience the same level of comfort on horizontal curves regardless of the type of vehicle they are driving. Basing horizontal curve guidelines on ball bank angles may not be a conservative approach to highway design, because skid may occur at low speeds before discomfort is perceived, especially on icy pavement surfaces, or in vehicles with high centers of gravity. Under these circumstances, motorists do not have any warning that they are approaching the limit of stability. Therefore, basing design side friction factors on the amount of friction demanded and supplied would seem to be a more conservative approach to horizontal curve design.

2. Because drivers tend to steer a spiral when entering and exiting a horizontal curve, the amount of side friction drivers demand is not constant. However, models can be created to predict peak friction demands as a function of vehicle speed for different curvatures on dry and icy pavement surfaces. These relationships provide a more accurate representation of actual driving behavior and could be used instead of the point mass equation to estimate the frictional demands drivers place on horizontal curves.

3. Curvatures flatter than 500 m provide high levels of driving dynamic safety on both dry and wet pavements. Motorists would be able to brake safely from the operating speed on these types of curves without exceeding the frictional supply. For curves with radii greater than 1000 m, the margins of safety are so high that these curves could be constructed with maximum superelevation equal to reverse or normal crown and would still provide frictional reserve levels large enough to allow vehicles traveling at normal operating speeds to brake safely without skidding. This suggests that the minimum radii for maximum superelevation equal to normal crown used for design (*1*) are very conservative. Decreasing the maximum superelevation rate on these types of curves would provide the following benefits:

–Minimize the operational problems associated with intersections on curves.

–Decrease the probability of vehicles with high centers of gravity overturning.

–Decrease the probability of a slow-moving vehicle sliding toward the center of an ice-covered curve. In fact, by using the point-mass equation, it can be determined that a vehicle traveling slower than 15 km/hr on a curve with a maximum superelevation rate of 8 percent and a radius of curvature greater than 300 m will slide down the superelevation, toward the center of the curve. As noted previously (*20*), Alberta Transportation and Utilities' most recent design standards have decreased the maximum superelevation rate from 8 to 6 percent.

4. The margin of safety against skidding decreases with increasing curvature and speed. On dry pavements, the margin of safety that exists on curves sharper than 500 m appears to provide adequate frictional reserve levels to allow vehicles traveling at normal highway operating speeds to brake safely. On wet pavement, these curves provide no margin of safety for operating speeds of 110 km/hr or greater. Because it is not uncommon for Alberta drivers to travel at these speeds, these types of curves appear to be underdesigned.

5. The margins of safety provided by design guidelines appear to provide adequate margins of safety against skidding. The problem appears to lie with the speeds at which vehicles in Alberta are operated. By tuning design speeds with operating speeds, the amount of side friction supplied would increase, whereas frictional demands would remain relatively constant. The overall effect would be an increase in the margin of safety provided on sharp curves, along with fewer overdesigned flat curves.

6. The side friction provided by icy pavements at impending skid conditions shows slight but significant variation with speed. The side friction factors used for low-speed urban design appear to be too high for speeds less than 40 km/hr and do not provide any margin of safety against skidding on icy pavements. Therefore comfort levels may not result in conservative curve designs in regions where icy pavement conditions routinely occur. Therefore, lower friction factors than those recommended by current design guidelines (*1,19*) should be considered. Because basing guidelines solely on icy pavement conditions is not economical and the consequences of an accident at such low speeds are minimal, the side friction factors should be a compromise between wet pavement conditions and icy pavement conditions.

ACKNOWLEDGMENTS

This research project was sponsored by the Research and Development Branch of Alberta Transportation and Utilities. The assistance of Roy Jurgens, Allan Lo, and Bill Kenny is greatly appreciated.

REFERENCES

1. *A Policy on Geometric Design of Rural Roads.* AASHTO, Washington, D.C., 1990.
2. Dunlap, D. F., P. S. Fancher, R. E. Scott, C. C. MacAdam, and L. Segel. *NCHRP Report 184: Influence of Combined Highway Grade and Horizontal Alignment on Skidding.* HRB, National Research Council, Washington, D.C., 1978.
3. Zuk, W. Instability Analysis of A Vehicle Negotiating a Curve with Downgrade Superelevation. In *Highway Research Record 390*, HRB, National Research Council, Washington, D.C., 1972, pp. 40–44.
4. Harwood, D. W., J. M. Mason, W. D. Glauz, B. T. Kulakowski, and K. Fitzpatrick. *Truck Characteristics for use in Highway Design and Operation.* Final Report, Project 8932-S. Midwest Research Institute, Kansas City, Mo., 1989.
5. Salt, G. F. Research on Skid-Resistance at the Transport and Road Research Laboratory (1927–1977). In *Transportation Research Record 622*, TRB, National Research Council, Washington, D.C., 1976, pp. 26–38.
6. Lamm, R., E. M. Choueiri, and T. Mailaender. Side Friction Demand Versus Side Friction Assumed for Curve Design on Two-Lane Rural Highways. In *Transportation Research Record 1303*, TRB, National Research Council, Washington, D.C., 1991, pp. 11–21.
7. McLean, J. R. Driver Behaviour on Curves—A Review. *Proc., Australian Road Research Board*, Vol. 7, Part 5, 1974, pp. 129–143.
8. Paustian, R. G. Tractive Resistance as Related to Roadway Surfaces and Motor Vehicle Operation. *Iowa State College of Agriculture and Mechanic Arts Official Publication*, Vol. 33, No. 9, 1934, pp. 87–108.
9. Whitehurst, E. A. *STP 456: The Cornering Capacity of Studded Tires, in Highway Skid Resistance.* American Society for Testing and Materials, 1969, pp. 144–153.
10. Lamm, R., E. M. Choueiri, and T. Mailaender. Accident Rates on Curves as Influenced by Highway Design Elements—An International Review and In-Depth Study. *Proc., Road Safety in Europe*, Gothenburg, Sweden, VTI Rapport 344A, Swedish Road and Traffic Research Institute, Linköping, Sweden, 1989, pp. 33–54.

11. Morrall, J. F. and R. J. Talarico. *Side Friction Factors for Horizontal Curve Design*. Department of Civil Engineering, University of Calgary, Alberta, Canada, 1993.
12. Merritt, D. R. Safe Speeds on Curves: A Historical Perspective of the Ball Bank Indicator. *ITE Journal*, Sept. 1988, pp. 15–19.
13. Oppenlander, J. C. *Special Report 89: Variables Influencing Spot Speed Characteristics*. HRB, National Research Council, Washington, D.C., 1966.
14. Barnett, J. Safe Side Friction Factors and Superelevation Design. *Proc., Highway Research Board*, Vol. 16, 1936, pp. 69–80.
15. Moyer, R. A. and D. S. Berry. Marking Highway Curves with Safe Speed Indicators. *Proc., 20th Annual Meeting of the Highway Research Board*, Washington, D.C., 1940, pp. 399–428.
16. Stonex, K. A. and C. M. Noble. Curve Design and Tests on the Pennsylvania Turnpike, *Proc., Annual Meeting of the Highway Research Board*, Vol. 20, 1940, pp. 419–451.
17. Harwood, D. W. and J. M. Mason. Horizontal Curve Design for Passenger Cars and Trucks. Presented at 72nd Annual Meeting of the Transportation Research Board, Washington, D.C., 1993.
18. Gegenbach, W. *Das Verhalten von Kraft-Fahrzeugreifen auf trockener und nasser Fahrbahn*. Dissertation, Institute for Transport Studies, University of Karlsruhe, Germany, 1967.
19. *Manual of Geometric Design Standards for Canadian Roads*. Transportation Association of Canada, Ottawa, Ontario, 1986.
20. Kenny, W. *Superelevation Policy for Rural Roads in Alberta*. Alberta Transportation and Utilities, Canada, 1990.

The views expressed in this paper are those of the authors and not necessarily those of the sponsoring agency.

Publication of this paper sponsored by Committee on Surface Properties–Vehicle Interaction.

Findings from Five Years of Operating Oregon's Automated Woodburn Port of Entry

MILAN KRUKAR AND KEN EVERT

In 1987 the Oregon Department of Transportation automated the new Woodburn port of entry (POE), located on Interstate Highway 5 southbound at milepost 274.40. The reasons were to minimize weighmaster and public utility commission tasks; improve weight, size, and safety enforcement; provide more data for planning and design purposes; maximize Weighmaster resources; improve tax collection and audit capabilities; and save time for the trucking industry. Automation of the Woodburn southbound POE interfaced six components: (a) weigh-in-motion sorter scales, (b) automatic vehicle identification system, (c) electronic static scales, (d) supervisory computer, (e) various software interfaces, and (f) motor carrier data base. The findings from this automation on the basis of 5 years of operation show improvements and cost savings in (a) weighmaster functions, (b) performance measures, (c) POE operations and functions, (d) human resources deployment, (e) data collection, (f) tax audit trails, (g) tax collection, and (h) the private motor carrier industry.

In 1987 the Oregon Department of Transportation (ODOT) automated the new Woodburn port of entry (POE), located on Interstate 5 southbound at Milepost 274.40. The reasons were to minimize weighmaster and public utility commission (PUC) tasks, improve weight, size, and safety enforcement, provide more data for planning and design purposes, maximize weighmaster resources, improve tax collection and audit capabilities, and save time for the trucking industry.

This was a demonstration project jointly funded by ODOT and FHWA. In addition, this project is part of the HELP Crescent demonstration. Funding of the latest automatic vehicle identification (AVI) equipment was through HELP. This paper presents the findings from this automation on the basis of 5 years of operation, 1988 to 1993.

BACKGROUND

Present-day heavy vehicle enforcement has evolved from monitoring heavy vehicles carrying Oregon's basic commodities, such as timber and agricultural products, to one of service to help the truckers operate safely and efficiently within Oregon's laws (*1*). This service concept has evolved into "one-stop shopping" where the facilities are built to weigh heavy vehicles, provide PUC services, and conduct truck safety inspections. PUC and weighmaster personnel are now located in the same building and there is a truck inspection facility with two bays. Delays are minimized as much as possible.

M. Krukar, Transportation Development Branch; K. Evert, Driver and Motor Vehicle Services Branch, Oregon Department of Transportation, 325 13th Street, N.E., Room 605, Salem, Oreg. 97310.

ODOT, through the weighmasters, operates six POEs besides 65 weigh stations and 19 mobile enforcement sites and conducts statewide portable scale operations. These six ports are located at Woodburn I-5 southbound (SB), Ashland I-5 northbound (NB), Cascade Locks I-84 eastbound, Farewell Bend I-84 westbound, Umatilla I-82 SB, and Klamath Falls Highway 97 NB. These ports principally monitor Interstate traffic entering Oregon.

Three of these ports were built between 1975 and 1982. The initial design for the Woodburn POE began in 1982. Before the Woodburn SB POE was built, the three existing ports did not entirely meet the one-step shopping concept. The weighmasters and PUC decided in this initial design phase to consider the idea of combining weight and size enforcement, PUC permits, and truck safety inspection at one location.

In late 1983 the Oregon State Highway Division started a weigh-in-motion (WIM) and AVI demonstration project, testing a medium speed WIM data collection system with AVI on I-5 NB at Jefferson. The results have been reported by Krukar (*2*).

In late 1984, on the basis of the initial success of the WIM/AVI Demonstration Project, the idea of interfacing WIM/AVI with the static scale and installing a supervisory computer (SC) with appropriate software to monitor, store, modify, hold the PUC data base, and transfer weight data was discussed. This concept developed into the Woodburn SB POE Automation Demonstration Project as described by Krukar (*3*). Construction on the Woodburn POE started in 1985.

AUTOMATION OF WOODBURN POE

Need for Automation

The Woodburn POE is the busiest port in the state. All POEs are operated around the clock, 7 days a week. A minimum of 2,000 trucks pass through this facility during a 24-hr period. During peak periods, more than 4,000 trucks per day pass through the POE. As many as 150 to 200 trucks may pass through during a peak hour.

When this POE was designed, it was estimated that the port would handle an average of 1,700 vehicles per day with peak days of 2,200 to 2,300. These estimates have been exceeded, and there was a need to lessen this workload increase on the weighmasters. POEs are labor intensive for the weighmasters, requiring 60 percent of the field staff to be dedicated to POE operation.

The automation of the port was an answer to this need. Automating the system would provide long-term increases in productivity, resulting in reduced manpower requirements, better data

collection, more efficient truck weight, size, and safety enforcement, improved weight-mile tax collection and audits, and time savings to POE users.

Components

The automation of the Woodburn SB POE consists of six elements: (a) the WIM sorter, (b) the AVI system, (c) the electronic static scales, (d) the supervisory computer, (e) various software interfaces, and (f) the Motor Carrier data base. Table 1 presents the components used in this project.

POE FUNCTIONS

Operations Functions

The purpose of a POE is to monitor and regulate trucks using state highways with respect to weight, size, safety, and weight-distance taxation. These various functions are divided or shared between the weighmasters and the PUC.

The purpose of the weighmasters is to protect Oregon's highways from overloaded and oversized trucks and to monitor truck safety and the transport of hazardous materials. Their functions are tied to their purpose. Weighmasters' functions are to weigh trucks to ensure that they are legal with respect to gross, axle, and tandem-axle weight, height, width, and length and to comply with federal bridge formula. Weighmasters have statutory authority to control weight, size, and safety and cite violators. They, along with PUC, monitor trucks for safety and the transport of hazardous materials. The weight information is used by PUC for weight-distance tax audits.

PUC has both regulatory and tax collection functions. The Motor Carrier Division's functions at POEs are to collect weight-distance taxes from those vehicles that are not already registered, ensure authority compliance, enforce truck equipment safety standards, and monitor the transport of hazardous materials. The latter two functions are shared with weighmasters although PUC has statutory responsibility and lead agency status in safety compliance.

At present, a weighmaster takes 20 to 40 sec to weigh a truck at a static scale, depending on the truck type. More time is needed if the truck is found to be in violation. The weighmaster manually records the truck identification, commodity, number of axles, gross weight, and axle weights. Thirteen manual tasks are required to complete the previously given procedure. This information is sent to the PUC Motor Carrier Division, where it is manually entered into the ODOT mainframe computer. This information is used for tax audit purposes.

About 85 percent of the trucks passing through the POE have appropriate PUC papers and are within legal weight. The remaining 15 percent either are cited for some kind of weight or size violation or need an extended weight permit or a PUC permit for

TABLE 1 Equipment and Software Used in POE Automation

Type	Manufacturer	Model	Amount
WIM Sorter	CMI-Dynamics	SS 200-IDC (R)	1
AVI Transponders	General Railway Signal	01320-30	350
Reader-Activator	General Railway Signal	41795	1
Antennas	General Railway Signal	59656-12/13	1
Static Scales			
Readout	Weightronix	WW110	2
Load Cells	Mastron		2
Deck	Contractor		2
Supervisory Computer			
Computer	Motorola	8400 E, 161 MB Hard Disk	1
Processor	Motorola	68020	1
Streaming Tape	Motorola	60 MB	1
D.R.A.M.	Motorola	8 MB	1
CRTs	Motorola	TM 228	3
Printers	IBM	4224	2
Software			
Relational Database Software	Informix	Informix SQL	
Mainframe Communications	Motorola	SNA 3270/3770	1
Rational Database Custom Software	Informix/Motorola*	4th Generation Language for Customware Programming	1

* Motorola is no longer in the business of supplying this type of software.

weight registration, or both. These trucks will have to go to the legalizing loop and park. Truck drivers will have to make a stop that may vary from 5 to 25 min longer if their load is weight illegal and has to be adjusted or removed. Extra time is needed by the weighmaster to write citations.

Automated Functions

The automated system at the Woodburn POE allows trucks with transponders to bypass the static scales and the PUC office. A total of 85 percent of the transponder-equipped trucks will be able to take advantage of this, minimizing their productivity losses. A truck with a transponder has its identification number read by the AVI reader and is also weighed and height monitored by the WIM scale and height detector. These data are transmitted to the SC where they are stored for future transfer to the ODOT mainframe computer. The SC has data on 250,000 vehicles, which includes information about whether any given PUC plate is suspended or for some other reason is invalid. This allows the weighmaster to take immediate action in cases of suspended plates. In the past this information was not readily available to provide timely action at the POE. The SC also has name and address files on 40,000 carriers. If the transpondered truck meets both the weight and height limits and registration requirements, then it is automatically permitted to bypass the static scales and the PUC office, minimizing time loss.

If the WIM scale shows that the truck does not meet gross or axle weight limits or bridge formula or oversize criteria, or both, and the SC shows that it meets PUC requirements or safety inspection validation, or both, then the truck has to go only to the static scales to be weighed. If in violation, the driver receives a citation, which is printed automatically. If the WIM scale shows that the weights are legal but the SC shows that the PUC registration requirements are not met, then the truck can bypass the static scales but still has to go to the PUC office to have its credentials reviewed and obtain the necessary papers. If the truck violates both the legal weight limits and size limits and the PUC requirements, then the truck goes to both the static scales and the PUC office. This automated system reduces the number of vehicles going to the static scales by almost 50 percent. All WIM data are stored and telemetered daily. The WIM data on trucks that are allowed to bypass the static scales and PUC office are transferred and stored on the SC computer.

The linking of the Weightronix static scales to the SC allows the automatic recording and storing of the static weights. The weighmaster directly enters the truck identification (PUC number) with the commodity data number into the SC. This automated system improves weighmaster productivity by reducing the present 13 manual tasks to 4. PUC saves on keypunch operator time and keypunching errors. The system also allows the audit staff to have near real-time data available during carrier audits, thus improving the effectiveness of the audit.

Safety inspection information is also in the SC files. Weighmasters can tell when a truck was inspected. If the truck has not been inspected recently, the system can automatically send it to the safety inspection bay. The SC also has available the necessary programs to utilize the Federal Motor Carrier Safety Class Rating Code.

The static weight information, along with the WIM information on trucks bypassing the static scales, is stored and transferred to the ODOT mainframe computer. The SC provides the weighmaster a daily summary of the number and types of vehicles weighed at the static scales and the number of violations by type. PUC is able to update the vehicle files to the SC on a near real-time basis. This is currently done on a 3-hr basis because of the necessity to control batch size.

The combination of AVI, SC, and WIM permits trucks to bypass the static scales and the PUC office, provided they meet both PUC and weight limit requirements and regulations. A POE with a WIM sorter scale, but without AVI and SC, will not permit trucks to bypass the PUC station—only the static scale. Therefore, an AVI and SC system are needed to make the POE automation demonstration work properly.

Originally, only 350 trucks were equipped with transponders. This has now been increased to 1,100. Approximately 100 trucks with transponders pass through the Woodburn POE daily. This limited system demonstrates the feasibility of the fully automated POE and demonstrates even more forcefully the improved productivity of the weighmasters.

Figure 1 shows the location of the various aspects of the automation system.

FIVE YEARS OF OPERATION

General Comments

The port with the WIM sorter system and AVI opened in January 1987. In December 1987 the automation software, the SC, and accessory electronic equipment were put in place and tested. Full operation started in January 1988. The system and operation have been described in detail by Krukar and Evert (*4*).

The system has worked beyond expectations. The weighmasters have completely accepted the system and so have the trucking firms and drivers. The system has allowed for successful operation of the port despite the fact that the vehicle traffic has almost doubled and has exceeded the design capacity.

Some modifications have been made to the original port layout and facilities design. The portland cement concrete (PCC) entry pavement has been extended an additional 100 ft by replacing some of the asphalt concrete (AC) pavement in the entrance lane. This was done because the AC was rutting very badly at the junction with the PCC pavement. The truck inspection building was extended by 40 ft so that triple trailers could be inspected under cover during inclement weather.

WIM Sorter System

This system, similar to the one installed at the NB Woodburn weigh station on I-5 NB, has worked very well with minimum down time. The scales, axle sensor, loops, overheight detector, and directional signal lights have worked very well. Scale accuracy for 5-axle tractor-semitrailers has been within 3 percent for axles and 2 percent for gross weight. The only weak link has been the Dynax axle sensor, which fails in 12 to 24 months. The axle sensors cost $500, excluding installation.

Automation System

Krukar and Evert have described this system in general. The software programming and functions have been described by Rytter

(5). The electronic hardware, the accompanying software, and software interfaces have worked very well. The system was accepted by the field users. One of the reasons is that the programmers and weighmaster staff worked directly with the operators. The second was that field weighmasters were represented on the Technical Advisory Committee and given input in the initial design. The third reason was that their tasks were simplified from 13 to 4 steps. Fourth, the weighmasters and managers had instant information, menus, and tables (see Figure 2) that provide opportunities to increase efficiency and develop useful information for facilities operation.

Some software upgrades have been made. The custom code has been revised four times. Software modifications have been made to simplify some tables, add additional information, and comply with changes to the citation format mandated by the State Supreme Court.

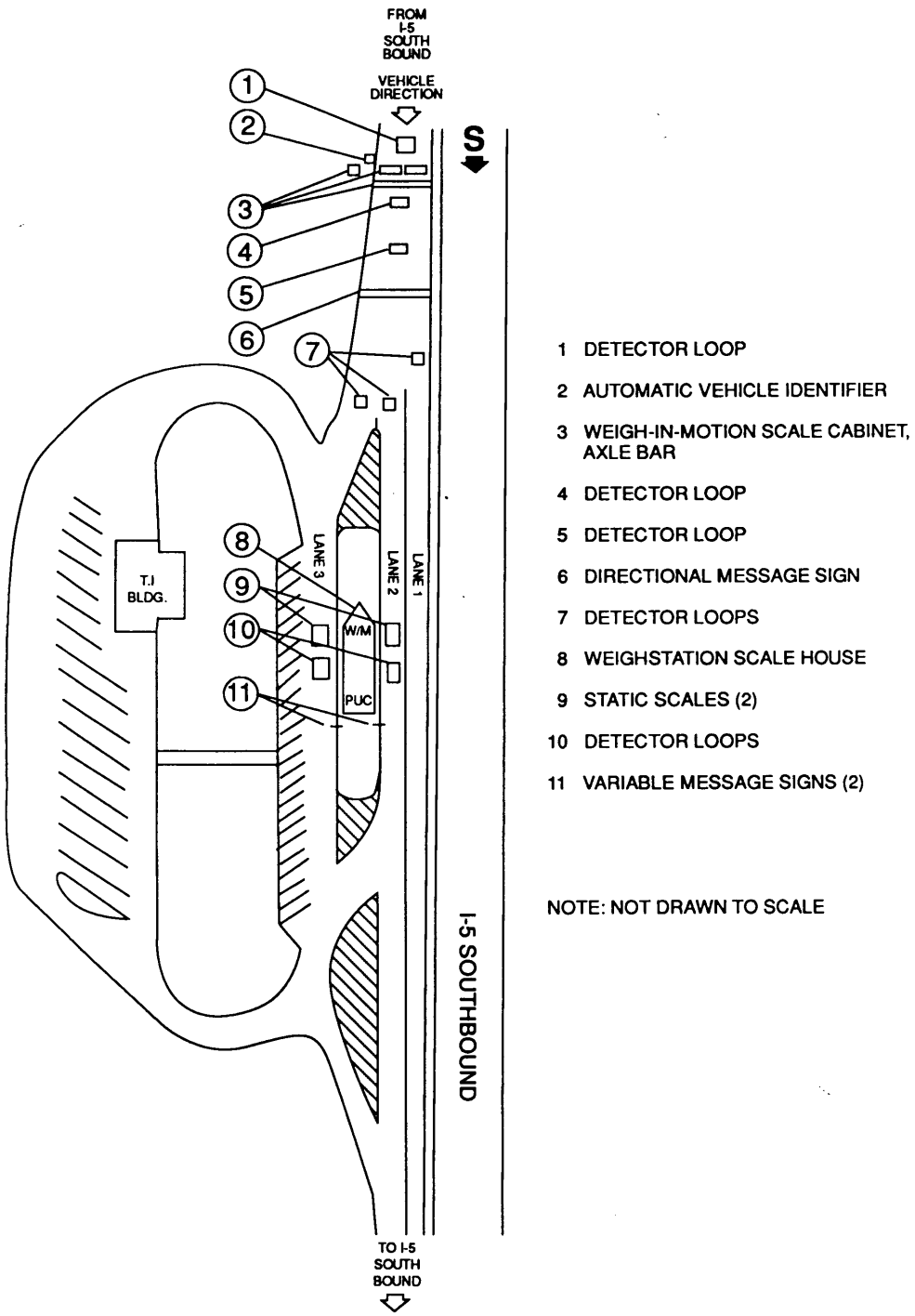

FIGURE 1 Woodburn SB POE.

The SC storage capacity needs to be upgraded, and faster response is needed. The additional information and growth of traffic has slowed average data processing time from 125 to 147 msec (maximum processing time has exceeded 600 msec during peak periods). In other words, the present electronic system is becoming obsolete.

AVI System

The original AVI system was the General Railway Signal system, originally tested in 1984 to 1985 at three sites (*2,3*). This was in place in 1986 with about 350 trucks carrying the transponders. Because Oregon is part of the HELP Crescent Demonstration Project, the recommended AVI system with readers and transponders was installed. Some 1,100 Oregon registered trucks carry this transponder. These AVI systems are operating satisfactorily.

MAIN MENU
Supervisory Weighmaster Applications Menu
Weighmaster Applications Menu
Report Generation Applications Menu
Record Maintenance Application
Weigh Station Parameters Application
  SUPERVISORY WEIGHMASTER APPLICATIONS MENU
  Configure Weigh Station Application Parameters
  Configure Weigh Station System Parameters
  Configure User Application Access Privileges
  Start WIM Interface
  Terminate WIM Interface
  Display Shared Memory
  WEIGHMASTER APPLICATIONS MENU
  Static Scale Weigh
  Citation Writing
  PUC Plate Number Assignment
  Chronic Offender Review
  Citation Modification
  Vehicle Statistics Modification
  Vehicle Statistics Display and Print
  REPORT GENERATION APPLICATIONS MENU
  Daily Reports
    PUC Daily Weight Report
    Daily Summary Reports
    Temporary Plate Number Report
  Monthly Reports
    Monthly/Quarterly Triples Activity Report
    Monthly/Quarterly Operation Summary
    Monthly/Quarterly Statistics Modification Report
    Monthly/Quarterly Citation Modification Report
    Monthly/Quarterly Productivity Progress Summary
    Monthly/Quarterly Chronic Offender Report
  Extract Functions
    Manual Statistic Extract Function
    Manual Citation Extract Function
    Manual Percent Weight Changes Extract
    Manual WIM/Statistic Raw Data Extract
    Manual Daily Statistic Collection Function
  Review Functions
    Review Statistic Extract Tracking
    Review Citation Extract Tracking
    Review Percent Weight Changes Tracking
    Review WIM/Statistic Raw Data Tracking
    Review Update Batch Tracking
    Review Daily Statistic Collection Tracking
  Record Maintenance Application
  Weigh Station Parameters Application

FIGURE 2 Hierarchical Menus Used in Application System.

Downtime and Maintenance Costs

Monthly records from Woodburn show that downtime for all the automation components averaged 4 hr/month or 48 hr/year. Maintenance costs, including parts and labor, averaged $2,500/year or about $208/month. In a maintenance contract with Motorola, monthly SC electronics and software maintenance charges were $472, or $5,664 yearly.

Costs of Systems

The POE costs for land, buildings, and pavement came to $2,200,000. The additional work cost $100,000, so the total was $2,300,000. Automation cost $412,000. Total costs were $2,712,000. Table 2 presents the costs by item.

FINDINGS

POE Functions

Tables 3 and 4 indicate that the vehicle traffic has exceeded design estimates. Empties are not weighed at the static scales; all other vehicles are weighed unless they are allowed to bypass. The WIM sorter system gross weight threshold was initially set at 30,000 lb, meaning that legal vehicles under 30,000 lb were allowed to bypass the static scales. The increase in traffic has forced this gross weight threshold to be set to 50,000 lb. About 50 percent of the vehicles weighed by the WIM sorter are allowed to bypass.

If the WIM sorter system had not been in place, the system would have been clogged with time delays for trucks because of queuing and potential safety problems. By 1992 the weighmasters would have had to install another static scale, scale house, and lane. The estimated cost for a third scale and accessories is $175,000.

Weighmaster Functions

Crew Size

The original crew size was 18. The WIM/AVI automation system has allowed the crew to be reduced by 2 to a total of 16. This has resulted in monthly fully loaded salary savings of $3,260/person or $39,120/year. For two people, annual salary savings are $78,200, totaling $391,000 for the 5 years.

If a third scale had to be installed, three more weighmasters would have had to be hired in 1993. Their annual fully loaded salaries would have totaled $117,360. In addition, two crew members would have been needed during the four operations before the third scale was opened. The annual salary savings for two persons are $78,200 and $391,000 for the 5-year period.

Daily staffing requirements have been reduced from six to five persons from Monday through Friday. On Saturday and Sunday shifts, staffing requirements have been reduced from four to three persons. Total salary savings are $273,800 annually and $599,400 for the 5-year period (Table 5).

Productivity Gains

Originally, the Woodburn port crew also was in charge of four outlying stations located at Woodburn I-5 NB, Hubbard Highway

TABLE 2 Costs for Woodburn POE and WIM/AVI/Automation

Item	Cost - $
Port-of-Entry: land, construction, buildings and additions	2,300,000
WIM/AVI	200,000
WIM/AVI/SC Communications Software Interface	10,000
SC and Accessory Electronics Hardware	55,000
SC Software (custom/database)	45,000
Functional Specification	12,000
Variable Upgrade #1 Variable Upgrade #2	30,000 10,000
Variable Message Signs	50,000
TOTAL	2,712,000

TABLE 3 Comparison of Number of Vehicles Weighed by Day of Week: Woodburn SB POE

Year:	1988	1993	Growth in Weighings	
Week:	9/26 - 10/3	6/28 - 7/4		
Day:	Weighings*	Weighings*	Difference	% Change
Monday	3,204	3,723	+ 519	+ 16.2
Tuesday	3,293	3,835	+ 543	+ 16.5
Wednesday	3,194	3,972	+ 778	+ 24.7
Thursday	3,061	3,583	+ 522	+ 17.1
Friday	2,912	3,347	+ 435	+ 14.9
Saturday	1,348	1,059	- 289	- 21.4
Sunday	1,032	804	- 228	- 12.6
TOTAL	18,044	20,323	2,280	+ 12.6

* Weigh-in-Motion Sorter System

99E NB and SB, and Tillamook. This responsibility has been increased by two more additional stations located at Molalla and Dayton. The crew is weighing more vehicles with fewer people. Weighmasters normally had to perform 13 manual tasks to weigh trucks and record data. The system has reduced this to four. The result has been to improve morale and reduce stress and fatigue, as demonstrated by a significant reduction in sick leave usage.

The SC system has allowed the weighmasters to spot potential violators immediately, thus improving weight enforcement and tax collection. In addition, the files in the SC let the weighmasters know if the truck has a valid safety inspection sticker and, if expired, automatically flag it for safety inspection. This improves safety inspection and benefits the public by providing safer highways.

The summary tables automatically prepared by the SC allows the POE supervisors time for other duties. Past information can now be located, where before mountains of paperwork needed to be sorted.

The ability to set the SC override of the legal WIM gross weight threshold to 50,000 lb has reduced the number of non-transpondered trucks needing weighing in a 24-hr period, from 3,000 to 4,000 trucks per day to 2,000 to 2,600 per day (Tables 3 and 4). This enabled the weighmasters to bypass small light trucks and focus closer attention on heavier vehicles for size, weight, and safety inspection.

Performance Measures

ODOT is developing performance measures for all units. The Woodburn POE, because of all the data, was one of the first crews to put on the productivity incentive matrix. In 1992, the crews earned an additional $5,200 in cash bonuses each for the year.

Crew Deployment

The Woodburn POE supervisor also is in charge of six outlying weigh stations and portable scale operations in the area. The SC has allowed for more efficient scheduling of manpower for additional weigh station operations on other highways. This has increased the number of weighings on those routes, thus enhancing weight and size enforcement.

PUC Functions

Weight-Mile Tax Collection

The automated system at this POE has increased the collection of truck weight-mile taxes through improved truck weight information. PUC estimates this increase at $11,500 annually or $57,500 during the 5-year period.

Trucking firms behind in their tax payments are now identified at the POE, although tax audits would have caught them eventually, since they are supposed to be audited every 2 years. The automation system allows auditing to happen in a more timely manner. One large trucking firm was apprehended owing $41,000. These delinquent taxes and reinstatement fines were collected before the vehicle was allowed to leave the port. Thus, PUC was alerted to audit this carrier more closely and was able to reduce the loss of interest in this account.

TABLE 4 Percentage of Vehicles Screened by Woodburn POE Sorter System

Day	Number of Vehicles				Percentage of Vehicles Screened by WIM
	Recorded by WIM		Weighed by		
	Total	Empty	WIM	Static Scale	
Monday	3,723	1,032	2,691	1,020	62.1
Tuesday	3,835	1,108	2,727	1,414	48.1
Wednesday	3,972	1,051	2,921	1,573	46.1
Thursday	3,583	1,006	2,577	1,296	49.7
Friday	3,347	936	2,411	1,221	49.3
Saturday	1,059	248	811	523	35.5
Sunday	804	182	622	505	18.8
TOTAL	20,323	5,563	14,760	7,552	48.8

* This does not include empty vehicles with scale manipulated errors. Therefore, on some days the number of vehicles easily exceeds 4,000 per day.

Tax Audit Productivity

Productivity gains have come from more efficient and immediate truck weight information, resulting in improved tax audits. Automation eliminates the keypunch errors made by PUC operators. The data are now more reliable, up-to-date, and current, thus helping with tax audits, all of which results in more efficient truck weight-mile tax collection.

Personnel Productivity

The automatic storing of truck data in the SC from the WIM and static scales and automatically transferring these data daily to the ODOT mainframe has reduced the need for manual data entry. This reduction has freed the use of this person for other duties. PUC estimates monetary savings to be $10,000/year.

Safety Enforcement Enhancement

The vehicle safety files contain information on truck safety inspection. This enables the weighmasters and PUC safety personnel to know whether the truck's safety inspection is current and whether the carrier has a high or low safety profile. This system has improved and increased truck vehicle safety inspections. These data are also used by safety auditors when performing on-premise investigations of a carrier's log books and after-the-fact safety audits.

Data Collection

Various ODOT functions have been and will be benefiting from improved truck weight data. Data from the WIM and static scales are now available on the ODOT mainframe for planning purposes, pavement design, research, traffic, and cost responsibility. In the past, these data were available but had to be processed manually and were costly to collect and access. Now they are available immediately on a daily and weekly basis. Also, data bases are being set up on truck freight commodities and weight.

Truck Productivity

The automated POE allows 50 percent of the trucks to bypass the static scales and PUC office, which minimizes time losses. Time

TABLE 5 Summary of Savings from Automation to State and Private Industry

Beneficiary	Source	Function	Annually $	5-Year Total $
A. STATE	Weighmaster	a. Automotation Crew Reduction (2)	78,200	391,000
		b. No Automation POE Expansion Postponement*	175,000	175,000
		Additonal Crew Need (3 for 1 yr)**	117,400	117,400
		Normal Crew (2 for 5 yrs)***	78,200	391,000
Subtotal			$448,800	$1,074,400
	PUC Motor Carrier Services	a. Data Entry	10,000	50,000
		b. Tax Collection	11,500	57,500
Subtotal			$21,500	$107,500
STATE TOTAL			$470,300	$1,181,900
B. PRIVATE INDUSTRY	Trucking	a. Time Savings****	286,300	1,431,500
PRIVATE INDUSTRY TOTAL			$286,300	$1,431,500
C. TOTAL SAVINGS			$756,600	$2,613,400
D. AVERAGE ANNUAL SAVINGS OVER 5-YEAR PERIOD a. State b. Private Industry c. Total				$236,380 $286,300 $522,680

* Third scale and house, equipment, and lane installed in 1992 and in operation during 1993.

** Three additional crew members would be needed to run the third scale.

*** If there was no automation, the normal crew size would be 18, two more than for automation.

**** Truck operating costs are estimated to be $44 per hour. Only 50 percent of trucks would report to static scales.

savings are on the order of 60 to 120 sec/vehicle, which results in savings in operating costs of $286,260 to $572,130 annually.

If all trucks had transponders, as much as 85 percent of the vehicles would bypass the static scales. If mainline sorting could be installed at Woodburn, estimated time savings per vehicle would be about 5 min.

The improved enforcement of weight limits and safety helps the legitimate trucking firms and improves their competitive situation by reducing illegal or unethical operations.

SUMMARY OF SAVINGS AND COSTS

Savings

The savings to the state and private industry from the WIM/AVI/SC automation system have been summarized in Table 5. Savings to the state are $470,300 annually and $1,181,900 for the 5 years of operation. Private industry savings are $286,300 annually, amounting to $1,431,500 during the 5-year period. Total annual savings, that is, state and private industry, amounted to $757,000 and $2,613,400 during the 5-year period. Average annual savings for the state, for private industry, and for both are $236,380, $286,300, and $522,680, respectively.

Costs

The costs for POE facilities and the automation system are given in Table 2. Table 6 presents the total costs of WIM/AVI/SC hardware and software (amounting to $362,000). Annual maintenance costs for WIM, hardware, and software are $8,200, amounting to $80,500 for the 5-year period. Average annual costs over the 5-year period amounted to $88,500.

LIMITS OF AUTOMATION

The system is incapable of measuring truck width or overall vehicle length. At present, no equipment that will measure these two parameters is available, which is a serious limitation of the automated system. Weighmasters need the ability to enforce these two important parameters. There is a need to get manufacturers interested in developing such equipment.

CONCLUSIONS

The present WIM/AVI/SC automation system at the Woodburn POE has been amazingly successful, despite the fact that very few trucks have transponders. There have been both monetary and nonquantifiable benefits to ODOT, PUC, and the trucking industry. The result of this success has led to the automation of other ports, excluding the WIM sorter system.

On the basis of ODOT experiences with Woodburn, mainline sorting has been installed at the new Umatilla POE on I-82 SB and at the Wilbur and Booth Ranch weigh stations near Roseburg on I-5 SB and NB, respectively. These systems currently use variable message signs. The system at the Ashland POE on I-5 NB will use mainline sorting with a two-way communication AVI system to screen vehicles 5 mi from the port.

The success of the Woodburn port project has resulted in the development by the weighmasters of an integrated tactical enforcement network plan (*6*) using the electronic hardware and software principles. In addition, a strategic/business plan for a statewide IVHS-CVO system is in the making (*7*).

The complete success of the automation system at Woodburn SB POE and other ports will depend on all trucks carrying some kind of identification that can be automatically read. The limited number of transponders in the demonstration has shown that this system can work successfully. The WIM sorting system by itself has shown that

TABLE 6 Summary of Costs from Automation

Beneficiary	Source	Annually $	5-Year Total $
WIM/AVI	Hardware	200,000	200,000
	Software Interface	10,000	10,000
Total		$210,000	$210,000
WIM/AVI/SC	Hardware	55,000	55,000
	Functional Specifications	12,000	12,000
	Software	85,000	85,000
Total		$152,000	$152,000
Maintenance	WIM Sorter	2,500	12,500
	Hardware/Software	5,700	68,000
Total		$8,200	$80,500
TOTAL COSTS		$370,200	$442,500
Average Costs annual Over 5-Year Period			$88,500

*Costs for port-of-entry are excluded (see Table 2).

it can successfully reduce truck volumes and improve POE truck movement as well as provide significant economic enhancements.

FUTURE RESEARCH NEEDS

Research needs to make these systems more effective and usable under mainline sorting conditions are the following:

1. Automated vehicle width, length, and height measurements. This would allow extra legal movements to be checked for compliance with state-issued variance permits.
2. WIM systems capable of self-calibration/correlation with static scales. This will allow a reduction in legal vehicles being brought into the station and a reduction in overloaded vehicles being allowed to bypass as reported by Krukar and Evert (*8*).
3. Driver identification. A means is needed to identify drivers of vehicles to ascertain compliance with driver qualifications and hour-of-service requirements.

REFERENCES

1. Krukar, M., and K. Evert. Weight Enforcement Strategies in Oregon from 1921 to 1990 and Beyond. *Proc., 40th Annual Road Builders' Clinic*, Moscow, Idaho, 1989.
2. Krukar, M. *The Oregon Weight-in-Motion/Automatic Vehicle Identification Demonstration Project. Final Report.* Highway Division, Oregon Department of Transportation, Salem, Sept. 1986.
3. Krukar, M. *Woodburn Southbound Port-of-Entry Automation Experimental Project. White Paper.* Planning Section, Highway Division, Oregon Department of Transportation, Salem, March 1986.
4. Krukar, M., and K. Evert. The Automation of the Woodburn Southbound Port-of-Entry on Interstate 5. *Proc., 3rd National Conference on Weigh-in-Motion: Applications and Future Directions.* St. Paul, Minn., Oct. 1988.
5. Rytter, D. A. *Functional Specifications for Woodburn Port-of-Entry Project.* Motorola Computer Systems, Inc., April 1987.
6. Krukar, M., and K. Evert. Integrated Tactical Enforcement Network (Automated Enforcement Facilities in Oregon). *Proc., National Traffic Data Acquisition Technologies Conference*, Austin, Tex., Aug. 1990.
7. *Strategic Plan for IVHS/CVO in Oregon.* Oregon Department of Transportation and Oregon Public Utilities Commission, July 1993.
8. Krukar, M., and K. Evert. Mainline Screening for Enforcement. *Proc., National Traffic Data Acquisition Conference*, Sacramento, Calif., Oct. 1992.

Publication of this paper sponsored by Committee on Vehicle Counting, Classification, and Weigh-in-Motion Systems.

Comparison of Weight Data Collected at Weigh-in-Motion Systems on the Same Route

CURTIS DAHLIN AND MARK NOVAK

An analysis has been made of weigh-in-motion (WIM) data that were collected by continuously operating systems at three different sites on the same route. The analysis examined the gross weight distribution of 5-axle tractor-semitrailers. Each direction had its own unique pattern. The eastbound 5-axle tractor-semitrailers were predominantly loaded and showed a similar pattern at all three WIM stations. The westbound 5-axle tractor-semitrailers were predominantly empty and showed the same pattern at the three WIM stations. One result of these consistent patterns at the three WIM stations is that, as a minimum, on selected routes where long-haul loading characteristics (origin-destination, commodities hauled, etc.) are known, data users, such as forecasters, can confidently use weight data collected at one location and apply it to another location on that route. A second result is that these repeating patterns make it possible to monitor the calibration of WIM systems. When a shift in the weight distribution takes place at one site while remaining constant at the other two, it indicates a possible change in calibration. These changes in calibration are readily observable. The techniques demonstrated here can also be used to analyze data collected at WIM sites that may be distant from other WIM sites.

In recent years, there has been a dramatic increase in the number of weigh-in-motion (WIM) sites in many states. The Minnesota Department of Transportation (Mn/DOT) also has increased its sites, primarily to meet the needs of the Strategic Highway Research Program (SHRP). The installation of continuously operating WIM systems at an increasing number of sites provides the analyst with the opportunity to look for patterns that repeat at a number of sites. This report looks at data that are repeated on a given route.

The weight data studied were those collected for 5-axle tractor-semitrailers. They are the principal trucks carrying cargo long distances in Minnesota. They typically contribute 70 to 90 percent of the equivalent single-axe loads (ESALs) to Minnesota's pavements.

Weight data from three sites located on one route, Trunk Highway 2 (TH-2), were selected for study. TH-2 is an east-west route in the northern part of the state. The sites, listed from west to east, are located as follows:

1. East of TH-32,
2. On the Bemidji Bypass, and
3. East of Deer River.

They are numbered Sites 1 through 3, respectively. It is about 110 km (70 mi) between Sites 1 and 2 and 90 km (55 mi) between Sites 2 and 3. All three sites are on a four-lane highway. Sites 1 and 3 have bending plate scales, whereas Site 2 has hydraulic load cell. The data used in this report are from the right lane only. That is where most of the 5-axle tractor-semitrailers travel, and it is also the design lane.

The weight pattern on TH-2 is characterized by the presence of primarily loaded 5-axle tractor-semitrailers eastbound and empty 5-axle tractor-semitrailers westbound. The principal commodity moved here is grain from North Dakota to the Great Lake ports at Duluth-Superior. Grain also moves eastbound (hence the loaded trucks), but fewer loads of various types move westbound (hence the unloaded trucks). Pulpwood is also moved at Sites 2 and 3, and general cargo is moved at all three sites.

The number of 5-axle tractor-semitrailers per week increases during the move from Site 1 to Site 3. Site 1 has about 750, Site 2 has about 1,600, and Site 3 has about 1,700 vehicles per week. There are no large 5-axle tractor-semitrailer generators or major intersecting routes between Sites 1 and 3, but there are smaller feeders that account for the change in volume. Consequently, given the long-haul nature of 5-axle tractor-semitrailer operations, it is likely that many of the 5-axle tractor-semitrailers monitored at Site 1 also pass through Sites 2 and 3. Also, the increase in 5-axle tractor-semitrailer traffic between Sites 1 and 2 have the same loading characteristics as those shown at both of those sites, so the weight loading pattern is the same. In analyzing weight data using the distribution of gross weight of 5-axle tractor-semitrailers, a minimum sample of 150 vehicles is recommended.

METHODOLOGY

The study and interpretation of WIM data and the methods used to determine its validity are still in the formative years. One issue that is open for discussion is the calibration of scales and the resulting validity of the weight data that is collected over an extended period—a topic that was discussed in an earlier report (*1*). The reintroduction of one of the key indicators used in that report is useful in interpreting the TH-2 data under examination here. That indicator is the distribution of the gross weight of 5-axle tractor-semitrailers. Of specific concern is the placement of the peaks for the empty and loaded trucks. The empty trucks should peak at about 12.7 to 14.5 Mg (28 to 32 kips), whereas the loaded trucks generally should peak at between 31.7 to 36.3 Mg (70 to 80 kips) on those routes where 36.3 Mg (80 kips) is the legal limit.

Minnesota Department of Transportation, Transportation Building, Mail Stop 450, 395 John Ireland Boulevard, St. Paul, Minn. 55155.

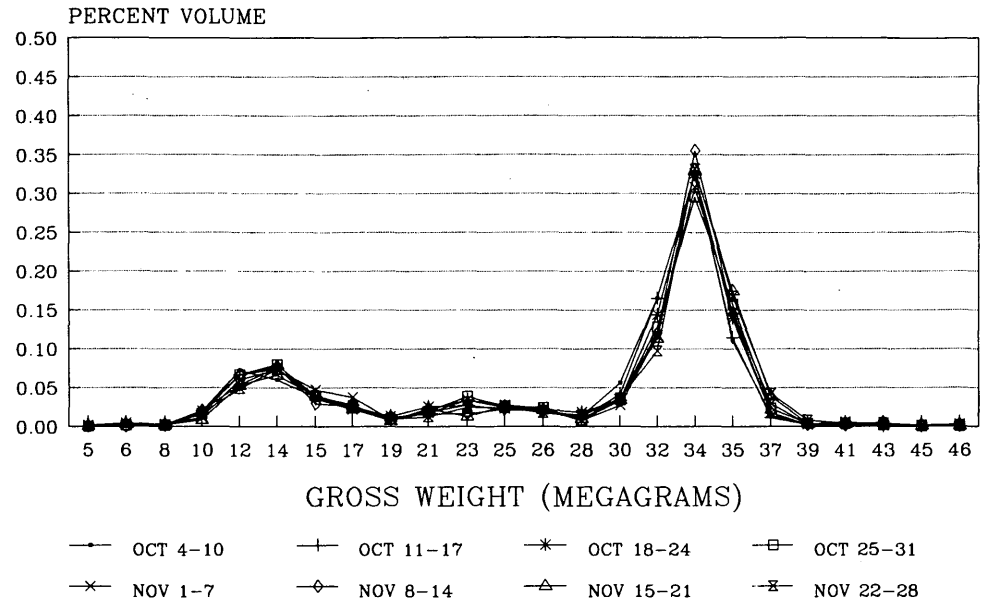

EASTBOUND, RIGHT LANE

FIGURE 1 Distribution of gross weight of 5-axle tractor-semitrailers for Site 2.

DATA REPEATABILITY AT A SITE

The first step in the analysis of these data is to determine whether weights at a given site repeat week after week. Figure 1 shows the distribution of gross weight of 5-axle tractor-semitrailers at Site 2. This shows weight data from the eastbound lane for 8 consecutive weeks, beginning October 4, 1992. The gross weight is shown in megagrams, and the values shown represent the bottom of the range. For example, 12 represents 12 to 14 Mg (26 to 30 kips). This work was originally done in English and then soft-converted to metrics. Consequently, the weights on the *x*-axis for these figures do not progress smoothly. There are between 1,600 and 1,800 5-axle trucks in each of these weeks. This consistent pattern means that generally the same trucks are traveling this route each week and that they are carrying the same approximate load each week. That is the general nature of cargo movement on

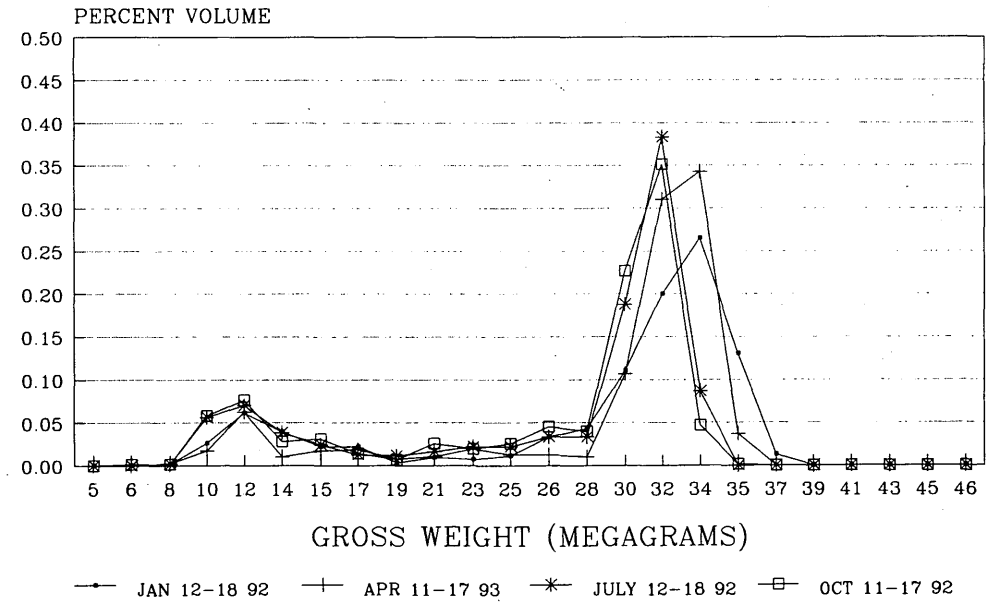

EASTBOUND, RIGHT LANE

FIGURE 2 Distribution of gross weight of 5-axle tractor-semitrailers for Site 1.

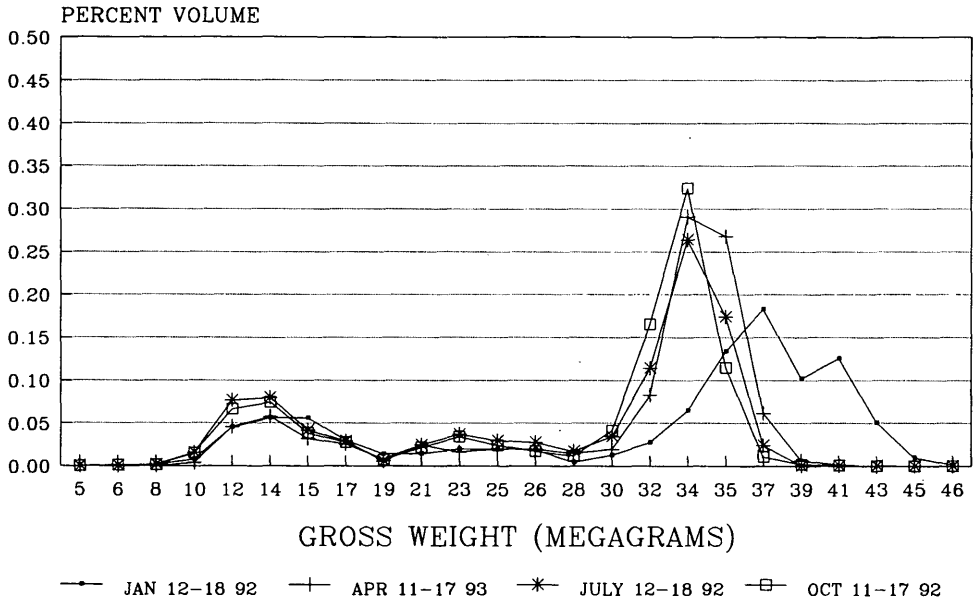

EASTBOUND, RIGHT LANE

FIGURE 3 Distribution of gross weight of 5-axle tractor-semitrailers for Site 2.

moderate- to high-volume truck routes. There is a strong tendency toward repeatability.

DATA REPEATABILITY BETWEEN SITES

Now that the repetitiveness of weight patterns at a specific site has been demonstrated, the next step is to analyze what is happening at the three sites over a period of time. For purposes of analysis in this report, 1 week was selected from each season of the year at each of the sites. This ensures that the data are as comparable as possible from site to site. Figures 2 through 4 show distributions for eastbound traffic for Sites 1 through 3, respectively, whereas Figures 5 through 7 show distributions for westbound traffic for those same respective sites. Three of the weeks are from 1992 and the other is from 1993. The week from 1993

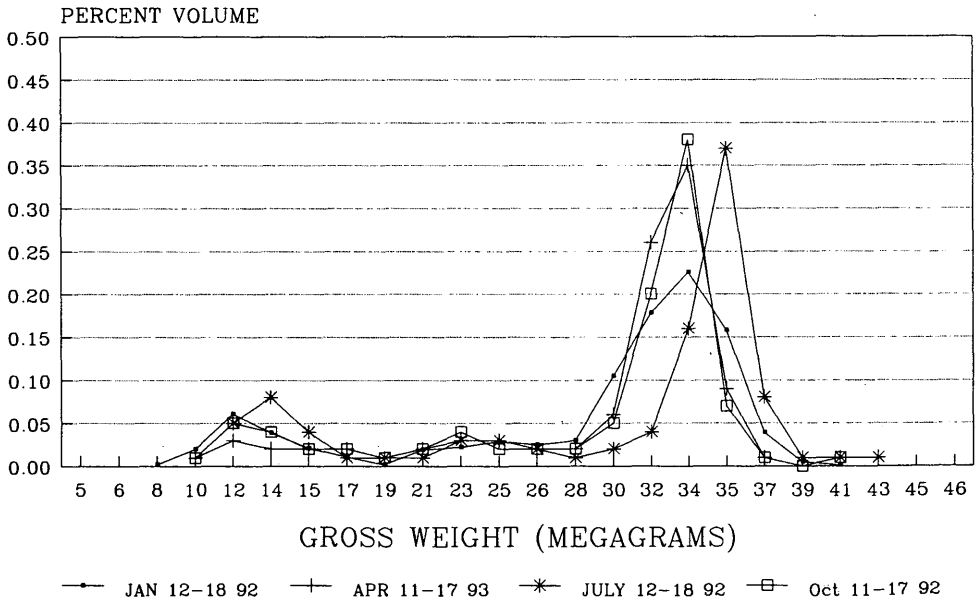

EASTBOUND, RIGHT LANE

FIGURE 4 Distribution of gross weight of 5-axle tractor-semitrailers for Site 3.

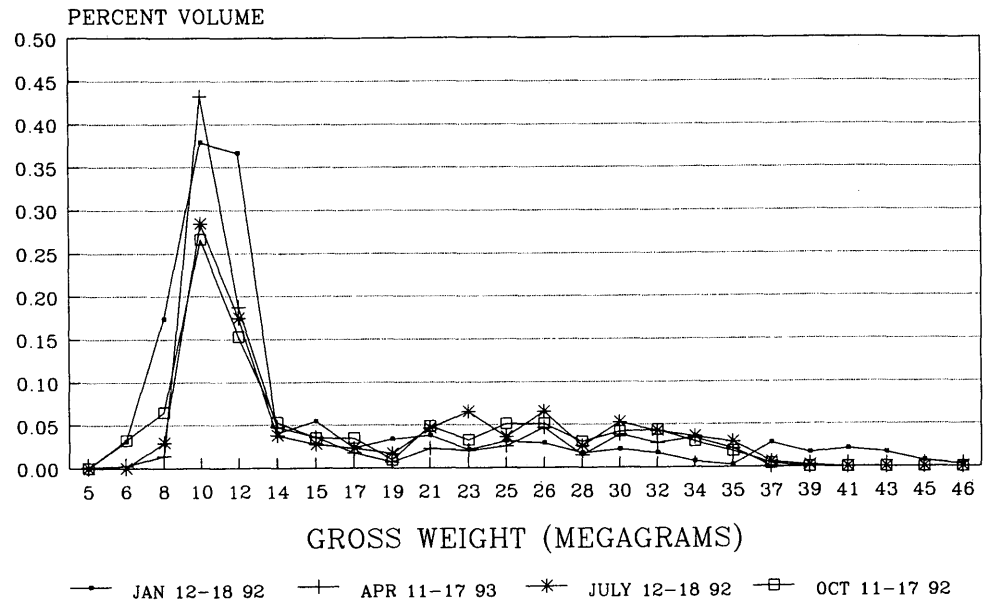

FIGURE 5 Distribution of gross weight of 5-axle tractor-semitrailers for Site 1.

(April 11–18) was included because not all three sites were operating in April 1992. Generally, these plots demonstrate that the same pattern exists over both time and space. They exist over time in that for each specific site throughout a year the same general pattern is repeated. They exist over space in that this same pattern repeats from site to site, spanning the 200 km (125 mi) between Sites 1 and 3. A more detailed examination of the data shown in these figures helps to interpret some of the seeming apparent inconsistencies in the data. In Figures 2 through 4, one of the larger observed differences occurs in Figure 3 during the week of January 12 through 18. The peak for the loaded trucks has shifted quite sharply to the right. There is a slight shift for that week in Figure 2 and no shift for that week in Figure 4. Although Minnesota allows trucks to haul an additional 10 percent during the winter, it is not clear if that additional hauling was taking place during that week in January because the data are inconsistent.

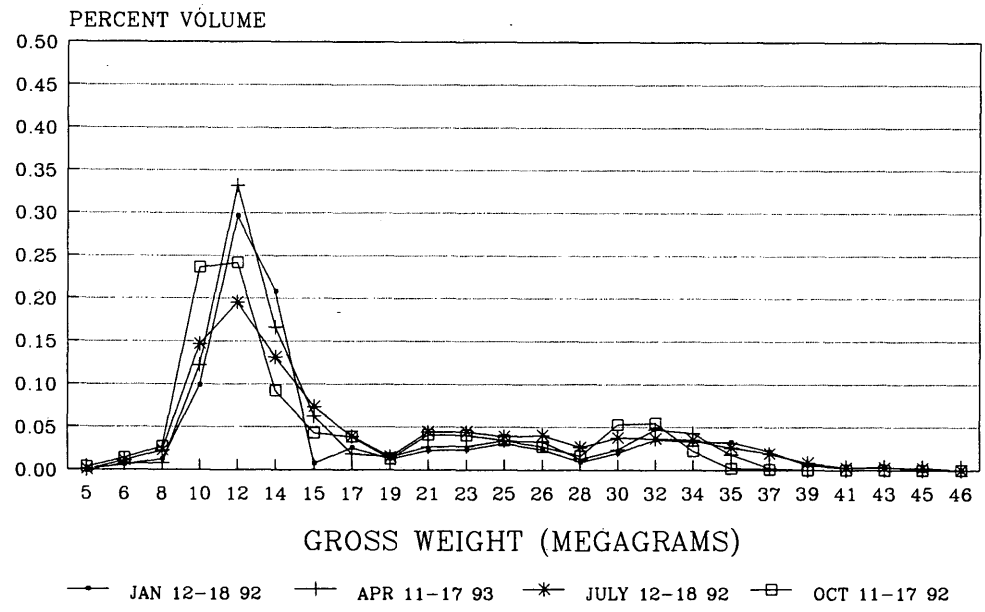

FIGURE 6 Distribution of gross weight of 5-axle tractor-semitrailers for Site 2.

A look at the peak for the empties for that week in Figure 3 shows a shift to the right, as was previously observed for the loaded trucks. Because both peaks for the January data in Figure 3 shifted and since there was no corresponding appreciable shift at the other sites, one can conclude that there was likely a drift in calibration that took place at Site 2 during that week.

A shift in the same direction for both peaks at a site likely means that there was a change in the calibration. Given that condition, if there is, for example, a 1.8-Mg (4-kip) shift for the empties, there will be about a 4.5-Mg (10-kip) shift in the peak for the loaded trucks. The percentage shift will be about the same for both peaks. A shift in one peak and not the other could be interpreted to mean that the data were valid. Although it is less pronounced, the same phenomenon occurs in Figure 4 during the week of July 12 through 18. The peaks for the empty and loaded both shifted to the right, whereas the other two sites did not show a shift in either peak.

In Figures 5 through 7, the most striking inconsistency is the week in October in Figure 7. The peak for the empty vehicles for that week differs from that of the other 3 weeks at that site. The peak for the loaded vehicles is also slightly different. Both peaks shifted in the same direction. The data appear to indicate a problem with calibration.

SHIFTS IN CALIBRATION

As already noted earlier, the calibration probably has been off for some of the lanes in this data set. By focusing on the peak for the weights of the empty vehicle, some differences are observable from one figure to another. Intuitive judgment supported by static weight data indicates that the peaks for empty 5-axle tractor-semitrailers should be in the range of 12.7 to 14.5 Mg (28 to 32 kips) (*1*). Using this criterion, Figures 2–4, 6, and 7 are properly calibrated, with the exceptions of the weeks previously discussed. Figure 5 is off quite sharply for 3 of the 4 weeks, with the weights peaking between 10 and 12 Mg (22 and 26 kips).

To simplify the issue as much as possible, the patterns in only two of the weeks (April and July) for Figures 5 through 7 will be examined. As has been pointed out earlier, because the scales are probably monitoring many of the same 5-axle tractor-semitrailers at these three sites, it is not surprising that the patterns are the same. Consequently, the empty vehicle peaks for April and July in Figure 5 should be the same in Figures 6 and 7. They are not. The former peaks between 10 and 12 Mg (22 and 26 kips), whereas the latter peak between 12 and 14 Mg (26 and 30 kips). To accept the weights from those 2 weeks as being valid at all three sites (Figures 5–7), it would have been necessary for the empty vehicles to secure 1.8-Mg (4-kip) loads between Sites 1 and 2 and for those loads to remain constant between Sites 2 and 3. The probability of there being 1.8-Mg (4-kip) loads available for most of those empty trucks between Sites 1 and 2 during those 2 weeks is highly unlikely. This difference has to be attributed to a drift in calibration.

Figure 8 illustrates another example of drifts in calibration. This figure shows 3 weeks of eastbound traffic at Site 3 in late 1991. Both the peaks for the empty and loaded vehicles shifted, and the shifts were all in the same direction. In this example, the peaks for November 3–10 were to the left, for December 15–22, in the middle, and for November 10–17, to the right. Loads carried by trucks can and do change. However, what typically takes place is that loaded trucks take on even larger loads, whereas empty trucks locate small loads. The weight of empty vehicles should not change appreciably. This means that there was a drift in calibration.

CONCLUSIONS

Two important observations can be made about the data examined here. The first is that in certain cases weight data collected at one

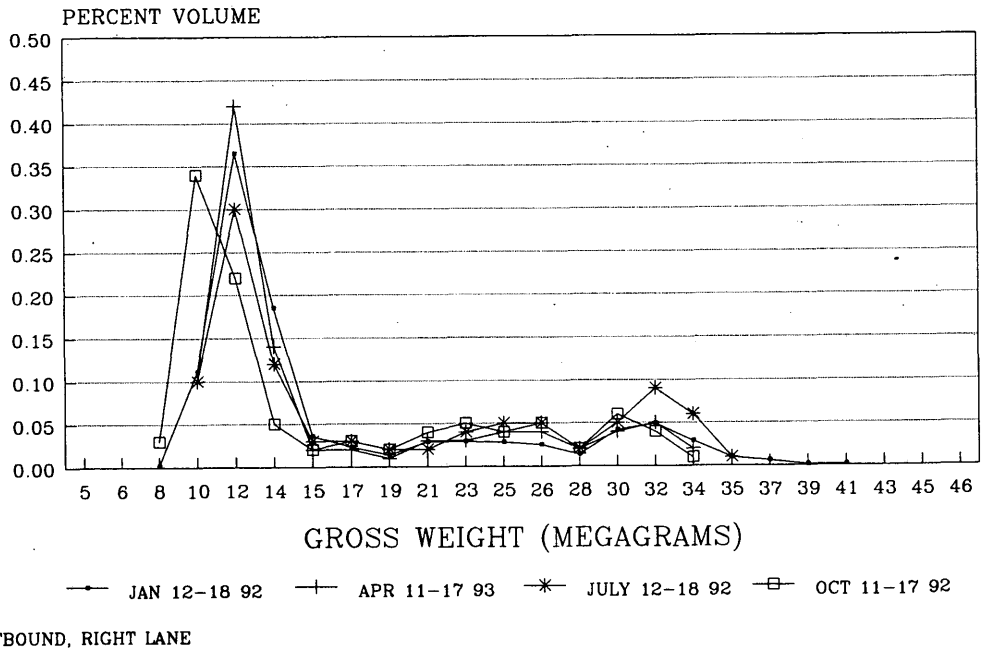

FIGURE 7 Distribution of gross weight of 5-axle tractor-semitrailers for Site 3.

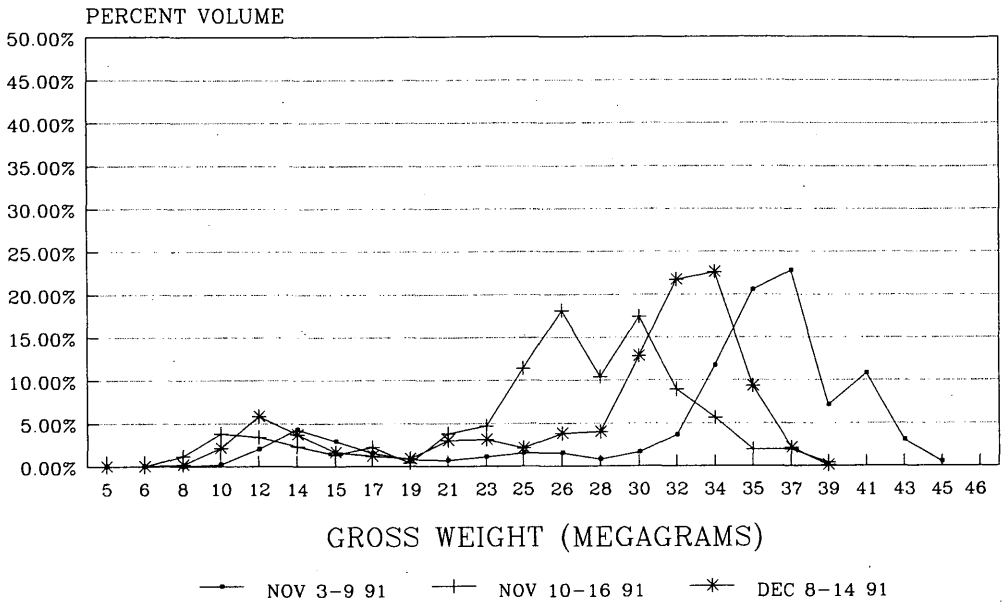

FIGURE 8 Distribution of gross weight of 5-axle tractor-semitrailers for Site 3.

site on a given route could quite confidently be used, perhaps by a traffic forecaster, at the other sites on that route. The directional patterns observed at these three sites were all similar. In fact, given some knowledge of the commodities hauled on the route and the origins and destinations of those commodities, the forecaster can probably apply those weight data to the entire length of TH-2 in Minnesota. Furthermore, it probably could be applied to other parallel routes in the area that have the same loading characteristics. For some projects, where it is known that the vehicle loading characteristics discussed earlier are similar, forecasters will be able to quite confidently use weight data collected at sites other than the specific location where they are stationed.

The second point is that by observing weight data in the format used here, it is possible to determine when there are probable drifts in the calibration. Even seemingly small drifts in calibration are significant because of the fourth-power relationship between weight and ESALs. This analysis can be done by comparing data from one site with those from another and also by looking at data from one site over time. Data that were collected during a drift in calibration should be set aside and not processed. A considerable amount of data should be collected and analyzed before a judgment is made about validity. Otherwise, any conclusions drawn may be erroneous. The exception would be in those instances where the system kept on collecting data during a major malfunction (*1*). The analyst needs to be as certain as possible that data that are in fact valid are not labeled as being invalid and vice versa. Experience in dealing with the data will be essential in eventually making the proper judgments.

Examination of data from three sites on the same route has shown that drifts in calibration do occur and that they are observable. Because this trend has been established, the analyst can apply the same techniques used here to data collected at other individual sites. There is no need for multiple sites on the same route to make this application. A sufficient amount of data collected at one site over a period of time plus time for analysis and consideration of the possible explanations for variations in the patterns provides what is needed.

REFERENCE

1. Dahlin, C. A. Proposed Method for Calibrating Weigh-in-Motion Systems and for Monitoring That Calibration Over Time. In *Transportation Research Record 1364*, TRB, National Research Council, Washington, D.C., 1992, pp. 161–168.

Publication of this paper sponsored by Committee on Vehicle Counting, Classification, and Weigh-in-Motion Systems.

Getting Better Truck Flows and Loads: Truck Weight Case Study

PHILIP I. HAZEN, RICHARD REEL, AMBE NJOH, AND GORDAN MORGAN

Florida has 20 years of experience in running continuous weigh-in-motion (WIM) stations and currently has 13 continuous WIM stations in operation. Therefore, an exhaustive investigation of the WIM data with the purpose of determining the optimum number of WIM sites to address the needs of pavement management systems was conducted by the Florida Department of Transportation for FHWA. The study was organized according to results of specific tasks (1 through 5). Under the early tasks the WIM data were examined for seasonal patterns or other patterns for allocating a continuous WIM station to a pattern group. Florida found little or no seasonal patterns. However, Florida has decided to divide the state into seven geographic areas for WIM data collection and analysis. The basic unit of analysis was the average equivalent single-axle load (ESAL) value per truck for a day at a site. Daily ESAL values are more variable than was originally thought. Florida found that 1 week (7 days) of data collection at stable sites, two 1-week collections at moderately stable sites at semiannual intervals and four 1-week collections at unstable sites spread over the quarters of a year were recommended. The last task investigated how many WIM sites should be conducted within Florida. These results should be helpful to other states conducting a WIM program.

FHWA's Traffic Monitoring Guide (TMG) (*1*) recommends randomly collecting truck volumes and classes at 300 sites and truck weight data at 90 sites over a 3-year period. This is 100 and 30 sites, respectively, per year. A state that follows the TMG recommendations will obtain systemwide averages for four systems: (a) Interstate rural, (b) Interstate urban, (c) total non-Interstate rural, and (d) total non-Interstate urban.

Pavement management systems (PMS) and other management systems, on the other hand, need site-specific data or at least data for one site for each "long" section of highway. For example, a long section existing between the major intersections on the National Highway System would be perhaps 10 to 50 mi in rural areas and 1 to 10 mi in cities.

FHWA initiated research in late 1991 to address this problem. Hallenbeck (*2*) of the Transportation Research Center, University of Washington, Seattle, was selected to analyze truck classification data from over 20 continuous vehicle classification stations conducted by the state of Washington. Hallenbeck reported on the preliminary results at the 1993 TRB Annual Meeting (*2*). A report on the analysis of vehicle classification has been completed (*3*). In addition, a final report has been completed on how a state transportation agency would develop a data collection framework for truck volumes and truck weights for their PMS (*4*); this report will be distributed by FHWA in mid-1994.

P. I. Hazen, Office of Environmental Planning, FHWA, U.S. Department of Transportation, 400 Seventh Street, S.W., Washington, D.C. 20590. R. Reel, A. Njoh, and G. Morgan, Transportation Statistics Office, Florida Department of Transportation, 605 Suwannee Street, MS 27, Tallahassee, Fla. 32399.

In late 1991, Florida Department of Transportation (FDOT) was selected to analyze truck weight data from more than 13 continuous weigh-in-motion (WIM) stations. A draft final report has been completed (*5*). This paper reports FDOT's analysis of their voluminous WIM data. The goal of truck WIM data collection and analysis is to support the estimation of 18,000-lb (8172-kg) equivalent single-axle loads (ESAL) yearly on the highways in a state's PMS.

This report is organized according to the five research subtasks as follows: (a) establishing combination truck use patterns by highway functional classification and seasonal pattern, (b) developing preliminary vehicle classification and WIM statistics, (c) investigating the short count program using both classification and WIM data, (d) determining the difference in accuracy of the annual average ESAL factor for 3S2 or combination trucks resulting from application of monthly and day-of-week factors instead of directly estimating from short counts, and (e) analyzing WIM count locations to determine the number of short counts needed for a PMS.

ESTABLISH COMBINATION TRUCK USE PATTERNS

Investigation of Strata of WIM sites

One objective of this study was to investigate a cost-effective combination of permanent and short-count WIM stations. Differences in loadings of trucks by season were explored to determine ways of using WIM data collection to account for seasonality. In addition to rural/urban and functional classification designations, a state's highways were investigated in terms of two truck use patterns: intercity and seasonal. Intercity were those routes with fairly uniform annual patterns typical of routes serving a large city. Highly Seasonal were those routes serving such areas as agriculture and forestry and connecting to shipping or processing centers. Loading differences should include the analysis of classification (volume) differences and also load (ESAL) differences.

Florida's seasonal variation is rather small and heavily influenced by less predictable factors, such as variations in the expected weather and the economic climate. Because of this probable lack of pronounced seasonality, it was determined that assignment of the state's entire network of highways to strata based on seasonality would be difficult and not useful. Other states, particularly those with severe winter weather, should have much more pronounced seasonality in their truck load factors.

Characteristics of WIM Stations in Florida

FDOT's continuous WIM (CWIM) program has been in operation for 17 years. The original Radian CWIM equipment was replaced

with PAT CWIM equipment beginning in the fall of 1988. There are 13 active Florida CWIM sites whose characteristics are shown in Table 1. Florida has substantial data from seven of these sites beginning in 1991, as shown in Figure 1.

Station 9926 had incomplete data for 1991 and was eliminated. The remaining six sites were grouped into strata: (a) rural Interstate Site 9901 on I-10; (b) other rural principal arterials such as Site 9909 on US-19/98, Site 9917 on US-41, and Site 9925 on US-92; and urban Interstate Sites 9922 on I-275 and 9924 on I-110.

For each WIM site, the day-to-day variation was considerably greater than any seasonal variation. This indicates that seasonal factors are not needed by Florida to expand short counts to an annual average but that daily or 48-hr counts may need day-of-week factors to produce annual averages.

Figure 2 shows the variation over the 365 days of the year for Site 17. Note that Saturday has higher but Sunday has lower daily load factors than the weekdays. This is typical of highways used for hauling agriculture products. Other sites had different patterns.

In summary, Florida determined that there was adequate data for six of the Florida DOT CWIM sites in 1991 to use in the analyses of the remaining tasks. These six stations did not display any meaningful grouping.

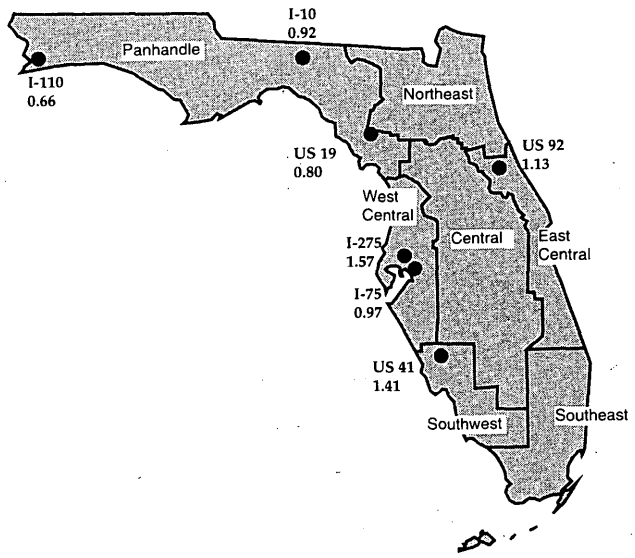

FIGURE 1 Florida stations, average load factors.

DEVELOP PRELIMINARY VEHICLE CLASSIFICATION AND WIM STATISTICS

As part of developing preliminary vehicle classification the vehicle classification data collected by WIM sites were analyzed for average daily volumes, coefficient of variance (CV), and standard deviation over the year. Individual Classes 4 through 13 of the TMG and the combined classes 1-3, 4-7, 8-10, 11-13, and 4-13 were analyzed.

The first three columns of Table 2 display this information for combined Sites 01, 09, 17, 22, and 25 for 1991. There are less than 365 days because the five major holidays were taken out so as to not bias the average daily characteristic. Further, equipment failures and other incidents that resulted in bad days were taken out. However, to be included, a station had to have data for 2 days for each weekday or 14 days minimum per month and a minimum of 2 months per quarter over the four quarters of the year. The full report contains further details on the editing. As seen in the table, the Class 9 or 5-axle tractor and single trailer was 63.9 percent of all trucks with a CV of 41.6 percent in the daily volume.

TABLE 1 Damage Factor Mean, Standard Deviation, and Coefficient of Variation by WIM Station

Station	Mean	Std. Dev.	Coef. Var.
9901	0.92209	0.08821	0.09566
9908	1.75369	1.03356	0.58937
9909	0.80457	0.10059	0.12502
9917	1.40501	0.26807	0.19080
9918	1.27461	0.28976	0.22733
9922	1.56912	0.23702	0.15105
9923	1.25626	0.24289	0.19334
9924	0.65787	0.10111	0.15370
9926	0.97530	0.12286	0.12598
9927	1.41328	0.14927	0.10562
9929	0.64974	0.23544	0.36236
9930	0.95220	0.29060	0.30519

The differences in the CV of the ESAL factor per individual truck and the CV of the average daily ESAL factor per truck class were calculated over various periods as follows. First, Florida calculated the ESAL factor per truck and the CV for each of Classes 4 through 13 of the TMG and the following combined classes: single unit, single trailers, and multitrailers. (Because of the bimodal distribution of weights around empty and loaded vehicles, the CV is expected to be large.) This was true; for example, for Class 9 trucks the mean ESAL factor for individual trucks for a day was 1.159 with a CV of 110.9 percent (see Table 2, Column 6).

Second, Florida calculated the average daily ESAL factor for each truck Class 4 through 13 of the TMG and the following combined classes: single unit, single trailer, and multitrailer. The CV of the average daily ESAL factors was calculated over the days of the year. Third, Florida compared the CV of the ESAL factor from the individual trucks within a class with the CV of the average daily ESAL factor of that class over days of the year. (The average daily ESAL factor no longer has a bimodal distribution and is expected to have a low CV.) This was true; for example, for Class 9 trucks the average daily ESAL factor compared over 360 days of the year had a CV of only 17.5 percent. Further, truck combinations with single trailers represented 73 percent of total trucks and had a CV of only 16.1 percent. Because sampling is based on the time of day, the CV of 17.5 and 16.1 percent is important (see Table 2, Column 7).

INVESTIGATE SHORT-COUNT PROGRAM

Investigation of the short-count program analyzed the vehicle classification and weight data to determine an appropriate and effective short-count duration. The first step was to determine the optimum duration and frequency of short counts to provide vehicle classification counts using six durations (1, 2, 3, and 7 days, and 2 and 3 weekdays plus a 2-day weekend) and five-count frequencies (once every 3 years and 2 years, and once, twice, and four times per year) in all possible combinations. The second step was to repeat the first step to develop the average daily damage

(ESAL) factors. The analysis was performed by randomly sampling the year's data and drawing up to 30 sample periods for each period length and frequency per year. The 2-day, 2- or 3-weekday and 2-weekend days, and 7-day periods at various frequencies during the year are of special interest. The mean and CV were calculated for each period. The CV was plotted against the cost in a figure similar to that of the TMG (*1*, p. 3-3-3).

Florida based the average annual damage factor on the mean of all days. Florida found that for both truck volumes and weights, the CV decreases as sample duration and frequency increases. There are three conclusions relevant just to truck weights. First, for highways with more than 200 trucks per day in the critical lane, to obtain truck damage factors with a 95 percent probability of being accurate to within 10 percent of the true mean, 7-day surveys twice a year, approximately 6 months apart, are necessary. Second, for highways with less than 200 loads (or trucks) per day in the critical lane, to obtain truck damage factors with a 95 percent probability of being accurate to within 10 percent of the true mean, 7-day surveys four times a year, approximately 3 months apart, are necessary. If a state can accept an 85 percent probability of being within 10 percent, 7-day surveys twice a year at 6-month intervals will suffice. Third, for highways with less than 100 loads (or trucks) a day in the critical lane, FDOT minimum designs exceed the expected loadings. See Figure 3 for partial results.

A conclusion relevant to truck volumes only is that truck volumes are more variable than truck damage factors. The only sampling plan that allows a 95 percent probability of estimating truck volumes within 10 percent of the annual average is 7-day surveys four times a year at 3-month intervals. See Figure 4 for partial results.

DETERMINE ACCURACY IMPROVEMENT

The purpose of this next task was to determine whether ESAL accuracy can be improved by applying monthly or day-of-week adjustment factors to collected data. This task was accomplished in three steps: (a) estimate annual average ESAL factors directly from short counts (i.e., use the results of Task 4); (b) determine accuracy improvement from using monthly and day-of-week factors for ESALs; and (c) compare the results between the unfactored and factored data.

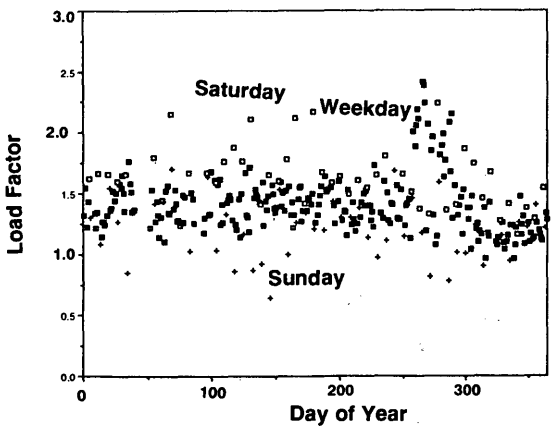

FIGURE 2 Daily load factors over 1991: Site 17, US-41.

Florida found some differences between factored and unfactored data, but the differences are not statistically significant. Since applying adjustment factors requires significant additional time and work and has not been shown to provide significant improvement in accuracy, Florida had decided that no adjustment factors (monthly or day-of-week) would be applied to the weight data. [The opposite was true in Washington, as discussed by Hallensbeck and O'Brien (*4*).]

Generally Florida found a lack of seasonality or other monthly patterns to the ESAL (weight) data. This diminishes the argument for continuous WIM stations. However, Florida's recommended data collection over 7 days covers the variability over the days of a week, and data collection two to four times a year covers the large general variability and some of the seasonal variability.

ANALYZE AVAILABLE WIM COUNT LOCATIONS

Analyzing WIM count locations develops a rationale and a sampling framework to predict ESALs on any individual section for a PMS. State highway agencies do not find it cost-effective to conduct WIM measurements on all highway sections, making it desirable to use average values from a substratum of the highway system. The procedures for determining sample size for truck weight (ESAL per truck) are discussed in the TMG; however, the data used were limited and collected before the 1982 legislation that authorized twin trailer trucks nationally. This research was to define the number of sample sites needed, especially for a PMS.

The task involves analyzing WIM data, calculating the CV of ESALs per truck per day for the Class 9 or single trailer combination trucks and the optimum sample size. Heavy volumes and routes having a high proportion of trucks in one season should be emphasized in allocating samples. The premise was that CWIM stations will provide monthly and day of week factors. The factors can be used to factor the sample site data to annual average day and also can be used with special data collection sites for project development or special analysis.

The data comprised the mean, standard deviation, and CV for damage factors at 13 stations. The data for all except Station 9925 are contained in Table 1. The mean damage factors for these sites ranged from a low of 0.64974 for Site 9929 to a high of 1.56912 for Site 9922. The CV for the factors ranged from a low of 9.6 percent for Site 9901 to a high of 59 percent for Site 9908.

Cluster Analysis

Clustering in its purest scientific form was presented in the TMG and a recent paper by Arizona DOT (*6*). A dendrogram or scatter plot of data was inspected and suggested three major clusters. The first was only one station, Station 9908, that stands apart from the others with the highest CV in damage factor values (approximately 59 percent). The second cluster contains Stations 9917, 9918, 9922, 9923, 9925, and 9927. The third cluster contains Stations 9901, 9909, 9924, 9926, 9929, and 9930.

The grouping scheme that emerged from the clustering analysis brought together under the same umbrella urban Interstate, rural non-Interstate and rural Interstate roadways. This scheme deviates significantly from what conventional wisdom on roadway classi-

TABLE 2 Daily Volumes and Load Factors for Sites 01, 09, 17, 22, and 25 Combined

Class of Trucks	Description of Trucks	Days *	Total No. of Trucks	Classification			Truck Weight			Cumulative		
				Ave. Daily Vol.			Daily Load			Ave. Daily L.F.		
				No.	C.V.	S.D.	No.	C.V.	S.D.	No.	C.V.	S.D.
04	Buses	360	21,672 (1.3%)	60	37.2	22.4	0.354	75.3	0.27	0.355	15.0	0.05
05	2-axle single unit	360	277,524 (16.9%)	771	43.8	337.4	0.392	191.6	0.75	0.372	17.6	0.07
06	3-axle single unit	360	82,110 (5.0%)	228	47.4	108.1	1.002	158.3	1.59	0.931	33.4	0.31
07	4-axle single unit	306	14,458 (0.9%)	47	67.1	31.7	2.914	55.0	1.60	2.720	25.1	0.68
08	<4-axle single trailer	360	151,758 (9.2%)	422	50.6	213.5	1.284	166.2	2.13	1.158	30.9	0.36
09	5-axle single trailer	360	1,051,737 (63.9%)	2,992	41.6	1,214	1.159	110.9	1.29	1.214	17.5	0.21
10	6+-axle single trailer	352	5,367 (0.3%)	15	58.2	8.9	0.942	108.0	0.02	0.908	44.0	0.40
11	5-axle multi-trailer	356	33,862 (2.1%)	95	40.8	38.9	1.587	82.9	1.32	1.641	17.2	0.28
12	6-axle multi-trailer	354	6,850 (0.4%)	19	54.3	10.5	0.646	107.7	0.70	0.672	39.2	0.26
13	7+ multi-trailer	272	749 (0.0%)	3	62.0	1.7	1.933	79.5	1.54	1.931	62.8	1.21
04-07	Single Units	360	395,764 (24.0%)	1,099	43.6	479.7	0.609	185.7	1.13	1.031	96.7	1.00
08-10	Single trailers	360	1,208,862 (73.4%)	3,358	41.9	1,406	1.174	120.9	1.42	1.213	16.1	0.20
11-13	Multi-trailers	356	41,461 (2.5%)	117	41.7	48.8	1.438	89.6	1.29	1.494	18.5	0.28
04-13	All classes	360	1,646,087 (100%)	4,573	40.8	1,864	1,045	131.6	1.38	1.148	71.5	0.82

*Equipment failures result in missing days. The full report discusses editing procedures.

fication dictates. As implied above, the analyses are a necessary, but not sufficient, determinant of WIM station grouping. Hence Florida concluded that the final grouping schedule must depend on other than purely scientific criteria including, but not limited to, "expert" judgment, particularly knowledge of the various stations.

Recommended Grouping Scheme

Next, Florida investigated a pseudoscientific clustering procedure based mainly on geography and the knowledge of the damage factor distribution within the state. These two factors played a pivotal role in Florida's efforts to group the WIM stations once the number necessary for each cluster had been determined.

Geographical Differences

Different parts of a state have different types of agriculture, industry, mining, or other activities and have related differences in

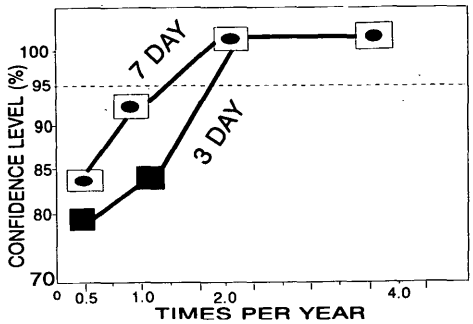

FIGURE 3 Truck ESALs, Station 01.

truck weights. In the case of Florida, there are differences in population characteristics that may be reflected in geographic differences in truck weights. For example, the northern end of the state tends to be less populated, and it also was on the way to the more populous southern end of the state. Thus North Florida may have more long-haul trucking than local trucking, compared with South Florida. The key question in this regard is whether the region involved is sufficiently large and uniform to make truck weight measurements at any one part of an area representative of the entire area.

For tourism purposes, the state of Florida was divided into seven main regions. A cursory inspection of damage factors registered at existing weighing sites revealed the presence of homogeneous configurations of damage factor values, which can be grouped by regions approximating those established for tourism purposes. Florida's efforts resulted in seven clusters of seven geographic regions and an eighth cluster composed of the four major Interstate highway systems. The regions and the Interstate highway systems are as follows. Region 1 (Northwest Panhandle) includes Station 9924 on I-110, SHRP 4100 on SR-85, SHRP 4108 on US-98, SHRP 4096 on SR-20, and 9908 on US-319.

Region 2 (northeast) includes SHRP 4105 on SR-9A and SHRP 3997 on US-17.

Region 3 (east) includes SHRP 4138/4000 on US-92, SHRP 4059/4109 on US-1, SHRP 1370 on SR-407, SHRP 4102/4101 on SR-528, SHRP 4107 on SR-70, and, SHRP 1030 on US-1.

Region 4 (central) includes only Station 9918 on US-27.

Region 5 (west) includes SHRP 3996 on US-19 and Station 9927 on US-92.

Region 6 (southwest) includes Station 9917 on US-41 and SHRP 4099 on SR-884.

Region 7 (southeast) includes Station 9930 on US-1, SHRP 1060 on SR-878, and SHRP 4103 on SR-836.

This grouping includes some stations that are greatly different. For example, WIM 9908 in Region 1 at 1.7537 and SHRP 4059/4109 at 0.6997 in Region 3 have damage factors that are greatly different from those of the other stations in their group. As time permits, these stations should be investigated with respect to the reason for the large difference.

Interstate highways are known to differ from other highway types in both the amount and the kind of traffic they carry and to have relatively uniform characteristics along their lengths. Therefore, each of the four major Interstate highways in the state is placed into a separate category for the purpose of this study. The first is I-4, a highway that runs east to west connecting I-95 at Daytona to I-75 at Tampa. No WIM station is located on this highway. The closest WIM station is on SR-546 (Memorial Boulevard in Lakeland). This station registered a mean damage factor of 1.4133 with a CV of 10.6 percent. This damage factor is associated with I-4 for the purpose of the analysis in this report. The second Interstate highway is I-10. Three weighing stations, with mean damage factor values ranging from 0.8805 to 0.9221, are located on this highway. The third highway is I-75, which has four weighing stations having mean damage factors ranging from 0.9753 to 1.5691. The last highway is I-95, which has three weighing stations having mean damage factors of 0.9424, 1.0069, and 1.2563, respectively.

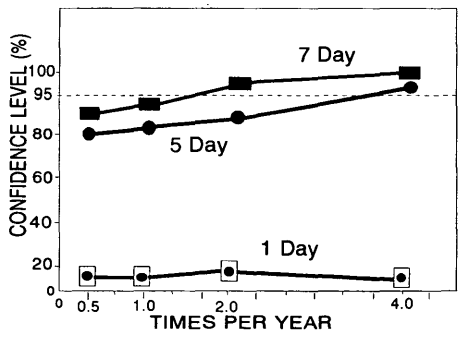

FIGURE 4 Truck volume, Station 01.

Separating principal arterial and minor arterial highways by region is both logical and intuitively appealing to Florida, where experience reveals that principal arterial highways mainly handle the intercity movement of goods, whereas the minor arterials mostly handle farm-to-market traffic. For example, in the northern part of the state, the minor arterial highways are used mostly by trucks transporting timber from the forests to wood processing mills, whereas the principal arterial highways handle mostly traffic that carries non-raw material from one city to another.

The following 16 groups include the regional, Interstate, and functional classification categories and provide a reasonable framework for possible regional damage factor differences for the study:

1. Panhandle principal arterial,
2. Panhandle minor arterial,
3. Northeast principal arterial,
4. Northeast minor arterial,
5. East central principal arterial,
6. East central minor arterial,
7. Central principal arterial,
8. Central minor arterial,
9. West central principal arterial,
10. West central minor arterial,
11. Southeast principal arterial,
12. Southeast minor arterial,
13. Interstate 4,
14. Interstate 10,
15. Interstate 75, and
16. Interstate 95.

Grouping Analysis Using TMG-Based Method

Essentially the TMG bases the number of permanent annual traffic recorders (ATRs) on the number of groups of highways and the CV of the data within each group. The TMG estimates that, provided the data in question exhibit a CV of from 10 to 15 percent, five to eight ATRs were required for each group. As shown below, the higher the CV, the larger the number of required number of ATRs. The following equation, which can be used to estimate the number of permanent counters, is provided in TMG (p. 3-2-7).

$$D = Ts \times \mathrm{CV}/\sqrt{n} \quad (1)$$

where

D = precision interval expressed as a decimal,
Ts = value of Student's T-distribution with $1 - d/2$ level of confidence and $n - 1$ degrees of freedom, and
CV = coefficient of variation.

Solving for the number of degrees of freedom, the equation becomes

$$n = (Ts \times CV/D) \quad (2)$$

This equation is indeterminate because the value n occurs on both sides of the equation; the value of Student's T is dependent on n. To use this equation additional data were required. Since Task 3 showed that two weighing surveys of 1-week duration taken approximately 6 months apart should provide sufficient accuracy and precision, the data from the seven WIM stations not used in the previous analysis (because of insufficient data coverage for the entire year) were processed to provide damage factors.

Truck weight data collected in 1991 for the Strategic Highway Research Program General Pavement Study sections in Florida were examined for use in this task. Twenty locations had 1 week of weight data collected during December 1991. The TMG model was applied to these data. It showed that 157 WIM stations were required to attain the 95-10 precision level to be distributed as given in Table 3.

Although the number of WIM stations (157) is statistically and mathematically sound, that number is expensive. It was necessary to seek a strategy that is capable of generating fewer, yet adequate, WIM stations for Florida.

Alternative Methods Based on Measures of Central Tendency

TMG page 3-2-8 specifies that samples be selected in compliance with a precision level of 10 percent and a 95 percent confidence (95-10) "for each individual seasonal group excluding recreational groups where no precision requirement is specified." On the basis of this compliance level, the following model, which incorporates this precision level and has as its core an important measure of central tendency, namely standard deviation, was developed:

$$n = \left[\frac{(Z)(\sigma)}{\delta}\right]^2 \quad (3)$$

where

n = optimum sample size,
Z = Z-score associated with desired confidence level,
σ = population standard deviation, and
δ = desired precision or allowable error.

The following values were given:

Population mean = 1.0728,
Z = 1.96,
σ = 0.28004, and
δ = 10 percent of population mean, or $0.1 \times 1.07281 = 0.1073$

Substituting in Equation 3 presented above:

$$n = \{(1.96 \times 0.28004)/0.1073\}^2 = 26.127, \text{ or } 26 \text{ sites} \quad (4)$$

Upon arriving at 26 as the optimum sampling size, it was necessary to determine the number of sites required for each of the seven regions by roadway classification (principal versus minor arterial) and the four Interstate highways. This problem was resolved by testing two stratified sample-based methods.

One method uses truck daily vehicle miles of travel (TDVMT) comprising the following three steps. (a) Existing sites were grouped by region. (b) Then the TDVMT for each group were computed. (c) Finally, the number of sites necessary for each category was calculated. The proportion of the optimum number of sites assigned to any given region was equivalent to that region's total TDVMT as a proportion of the total TDVMT for all sites combined. This process ensured that roadways or segments thereof experiencing high truck activity were adequately represented in the sample. After rounding to the closest whole number where fractions of a site were computed, the total number of sites required was found to be 32 subdivided as follows: Interstate highways, 15; principal arterial, 10; and minor arterial, 7. To understand how these sites were subdivided by region it is necessary to see the full report.

The other is a damage factor-based method that also has three steps: (a) existing sites were grouped by functional class of high-

TABLE 3 WIM Site Distribution Based on TMG Model

Cluster or Group	C.V.	Ts	n
I-4	0.000	*	5
I-10	0.070	2.920	4
I-75	0.098	2.353	5
I-95	0.133	1.943	7
Panhandle Principal Arterial	0.222	1.761	15
Panhandle Minor Arterial	0.178	1.833	11
North Florida Principal Arterial	0.167	1.860	10
North Florida Minor Arterial	0.125	2.015	6
East Central Florida Principal Arterial	0.282	1.717	23
East Central Florida Minor Arterial	0.125	2.015	6
Central Florida Principal Arterial	0.167	1.860	10
Central Florida Minor Arterial	0.000	*	6
West Central Florida Principal Arterial	0.156	1.895	9
West Central Florida Minor Arterial	0.000	*	6
Southeast Florida Principal Arterial	0.182	1.812	11
Southeast Florida Minor Arterial	0.000	*	6
Southwest Florida Principal Arterial	0.191	1.796	12
Southwest Florida Minor Arterial	0.091	2.353	5
TOTAL			157

* indicates that no Ts value was available and that the n is of an adjacent region.

way; (b) the damage factors for each group were computed; and (c) the number of sites necessary for each category was calculated as a proportion of the extent to which its mean damage factor deviates on the average from the population mean. It also came up with an optimum of 26 sites. In evaluating 26 stations, no WIM station was required for minor arterial roads in the north or east region, or for principal arterial roads in the north, west, or southeast region. This made no sense, according to FDOT. Thus, where this was the case, the region was automatically awarded one station. For this reason the total number of sites required is again 32 instead of 26.

Whereas the number 32 may be statistically logical, it is not intuitively appealing. Certainly not even the most innovative sampling design will guarantee the fair representation of the entire state by only 32 sites. More directly, Florida believes that 32 WIM stations are far too few for a state as large as Florida. Thus, Florida deemed it necessary to seek more reasonable strategies. Two closely related strategies were considered.

Separate Groups for Interstate, Principal Arterial, and Minor Arterial Highways

The relevant highways were divided into three distinct groups, namely, minor arterial (MA), principal arterial (PA), and major Interstate (MIS). Then, Equation 3 was modified such that σ equals the strata standard deviation instead of the overall population standard deviation.

Finally, Equation 3 was applied to the damage factor data contained in each of the three groups. As an example, Florida determined the adequate sample size for all minor arterial highways. The following data are given:

$$Z = 1.96$$

$$\sigma = 0.27250$$

$$\delta = 10 \text{ percent of population mean} = 0.1 \times 1.07281 \quad (5)$$

Therefore,

$$n = \{(1.96 \times 0.2750)/0.1 \times 1.07281)\}^{**}2 = 24.99 \quad (6)$$

On the basis of the formula, the optimum number of WIM stations required for MA highways is 25. Likewise, the number of stations required for PA and MIS highways was calculated to be 33 and 20, respectively. The total number of sites required therefore is 78 (i.e., 25 + 33 + 20).

The number of sites required for each subgroup or stratum was computed with the aid of the following equation:

$$AD = \frac{1}{N} \sum |\bar{X}_i - \bar{X}_p| \quad (7)$$

where

AD = average deviation,
X_p = population mean, and
X_i = mean of strata 1, 2, . . ., n.

Florida found that some strata contain two sites or less. In this case, especially where the stratum contains only a single site or two sites with identical values, average deviation results are meaningless. This problem was dealt with by employing the average deviation values for adjacent strata. This was the case, for instance, with MA roads in the north and east regions and PA roads in the west. The adjustments resulted in 18 more sites being added to the 78. Thus, on the basis of this strategy, the recommended sample size is 96. Table 4 shows the distribution of the 96 sites. Figure 1 shows how Florida is divided into seven regions.

Reflecting on Alternative Sampling Methods

The first sampling strategy was based on the TMG and generated 6 to 8 WIM sites in each of the 18 strata, resulting in 157 sites. Florida rejected 157 sites because it was too costly for the available resources. The second sampling strategy combined the 18 strata into one statewide stratum and found that only 32 sites are necessary. Although 32 sites could be a fallback position, Florida believes that 32 sites do not adequately cover the state, that is, fulfill the need for data by region and functional class of highway. The last sampling method was based on the three highway classes (MIS, PA, and MA) and determined that 96 WIM sites would provide the 95-10 precision level for the three highway classes and could be allocated to the 18 strata, resulting in more than one site per strata.

An examination of the data reveals little statistically significant difference between the functional groups, but the damage factors differ significantly by region. Thus, an alternative strategy was to select samples on the basis of the regional distribution of damage factors. The steps involved in the sample selection process are the same as those discussed above, except that intraregional differences (e.g., minor versus principal arterial roads) are ignored. When adjustments were made for regions with only one observation, the adjusted sample size was found to be 59. Another strategy resulted in 77 sites.

Reflecting on Central Tendency-Based Strategy

A fundamental objective of the study reported here was to devise strategies capable of improving cost-effectiveness and precision in WIM programs. Cost-effectiveness is essentially the principal rationale for suggesting that samples of highway segments instead of entire highway segments be surveyed. Ideally, optimal precision can be attained by recording damage factors and related data for entire highway segments within the state. Such a stratagem is, however, unrealistic given its enormous cost vis-à-vis the fact that resources (financial and otherwise) are finite. Further, Florida contends that 157 sites are too many given the resources that are available to the state.

However, if cost-effectiveness constituted the only concern, Florida would have settled for the lowest number of samples (32) which was arrived at earlier. Certainly cost-effectiveness was not the only concern. Florida contends that 32 sites cannot adequately cover a state as large as Florida, which has 67 counties. To ensure that precision was not sacrificed for the sake of cost-effectiveness, precision was built as a principal component into the sampling model presented above. In so doing, a delicate balance was struck between cost-effectiveness and precision, which were important objectives of the task.

The TMG does not specifically endorse or recommend any particular method for determining the number and locations of ATRs. This is because decisions generally are based on local conditions. Hence, a method that may be deemed suitable for Florida may not necessarily be suitable for another state. The main reason for walking through the various procedures and methods that were explored before arriving at what Florida considers to be an appropriate method for determining the number and location of WIM sites in Florida is to provide the reader with a wide array of methods to choose from should the need arise. As implied earlier, some of the methods that may be considered inappropriate for Florida may be useful elsewhere.

In arriving at the decision to utilize the damage factor by functional class sampling strategy and hence 96 sites, a number of factors—some of which were other than mathematical and statistical—were taken into account. Florida noted for instance that, based on local data, the TMG model failed to provide the 95-10 condition stipulated in the TMG. Florida also noted that a cluster analysis in its purest mathematical form is of little or no use in grouping the state's CWIM and portable WIM sites and associated damage factor values. Florida further observed that the utility of other more rigorous methods tailored along the lines of the TMG model was significantly diminished by their inability to generate a sizable number of locations. These observed phenomena are plausibly attributable to the rather small sample size dealt with in the study. It is possible that where a larger sample size is available or for other possible reasons, some of the strategies considered and rejected in the case of Florida may find utility elsewhere.

CONCLUSION

The 96 WIM sites appear to be the best choice in being affordable and meeting the stipulated precision level. On the basis of known truck travel behavior, truck weights, and the resulting pavement damage factors, Florida believes 96 sites can be reasonably distributed throughout the state and are adequate to generate sample damage factors for the 18 groupings by region and functional class of highway in accordance with the 95-10 precision level recommended by the TMG. Florida does not contemplate adding more than a few more continuous WIM stations to the 13 continuous WIM stations now available. Therefore, it is likely that most of the 96 stations would be operated 1, 2, or 4 weeks per year depending on the importance and stability of the truck flows at the station. In one aspect this would be similar to the 90 WIM sites recommended by the TMG over a 3-year period. In another aspect

TABLE 4 Projected Number of WIM/SHRP Sites by Region and Highway Class

Region	Class.	Dam. Fact.	AD	AD/ADtot	Stations		
					M.A.	P.A.	HWYS
Panhandle	M.A.	0.6512					
		0.6657	0.4143	0.1285	7		
	P.A	0.6579					
		0.6809					
		1.7537					
		0.6579	0.1352	0.0419		5	
North	M.A.	0.9935	0.0793	0.0246	4		
	P.A.	0.9560					
		0.9642	0.1127	0.0350		4	
East	M.A.	1.1203					
		1.0652	0.0199	0.0062	4		
	P.A.	1.1349					
		0.6997					
		1.3581					
		1.1455	0.0118	0.0036		5	
Central	M.A.	1.2986	0.2258	0.0700	4		
	P.A.	1.2746	0.2018	0.0626		7	
West	M.A.	1.4133	0.3405	0.1056	6		
	P.A.	0.9300	0.1429	0.0443		5	
S.W.	M.A.	1.2986	0.2258	0.0700	4		
	P.A.	1.4050	0.3322	0.1031		11	
S.E.	M.A.	0.8961	0.1767	0.0548	3		
	P.A.	0.9522					
		1.0986	0.0474	0.0001		2	
I-4		1.4133	0.3405	0.1056			9
I-10		0.8845					
		0.8540					
		0.9221	0.1860	0.0577			5
I-95		0.9424					
		1.0069					
		1.2563	0.0043	0.0013			5
I-75		1.3139					
		0.9753					
		1.3391					
		1.5691	0.2265	0.0703			6
Mean:		1.0728			32	39	25
Std. Dev.:		0.2800					
ADtot:		3.2235					
				Opt. Size	78	TOTAL:	96

it is different because of the length of data collection, i.e., 1 to 4 weeks instead of 2 days per year.

RECOMMENDATIONS

In future work, assuming that stratification by region and functional class is able to group highways with similar damage factors and reduce the number of samples required, then the overall population mean damage factor of 1.0728 should not be used in Equation 3, but the mean damage factor for each stratum will be used in determining the sample size of the stratum. Further, the size of the TDVMT reflects the importance of a highway and should be used to allocate the 96 sites in a manner similar to that done earlier for the 32 sites.

Because of the large variability in damage factors among sites and those adjacent to each other, it is recommended that project WIM data be collected for the design of a major improvement.

Ultimately, the decision on how to group WIM stations in any state or locale falls under the purview of professionals who should use their experience and judgment. In this case, geographic region is the underlying common attribute by which the sites are grouped. Although Florida finds a purely scientific clustering procedure unsuitable, it is possible that another state may find it otherwise.

REFERENCES

1. *Traffic Monitoring Guide.* Publication FHWA-PL-017. FHWA, U.S. Department of Transportation, 1992.
2. Hallenbeck, M. Seasonal Truck Volume Patterns in Washington State. Presented at 72nd Annual Meeting of the Transportation Research Board, Washington, D.C., 1993.
3. Hallenbeck, M. and S. G. Kim. *Final Technical Report for Task A: Truck Loads and Flows.* Transportation Research Center, University of Washington, Seattle, June 1993.
4. Hallenbeck, M. and A. O'Brien. *Truck Flows and Loads for Pavement Management.* Transportation Research Center, University of Washington, Seattle, Oct. 1993.
5. *Getting Better Truck Flows and Loads for Pavement Management: Draft Task B: Truck Weight Case Study.* Florida Department of Transportation, Tallahassee, Aug. 1993.
6. Flaherty, J. Cluster Analysis of Arizona Automatic Traffic Recorder Data. Presented at 72nd Annual Meeting of the Transportation Research Board, Washington, D.C., 1993.

Publication of this paper sponsored by Committee on Vehicle Counting, Classification, and Weigh-in-Motion Systems.

Objectives and Content of AASHTO *Guide to Metric Conversion*

DANIEL S. TURNER AND JAY K. LINDLY

In response to congressional action and an executive order AASHTO formed a task force to investigate metrication. In its report, the task force recommended development of the AASHTO *Guide to Metric Conversion*. The guide, a document prepared to help steer the American highway industry through metric conversion, was prepared by the University of Alabama, through a contract with NCHRP. Chapters in the guide introduce the reasons for conversion, give examples of conversions by other nations, outline the steps in forming an agency conversion plan, give hints and suggestions, and provide checklists of suggested activities. Appendexes provide tables of metric conversion factors, critical geometric design criteria expressed in metric units, and case studies that list conversion activities and estimated costs for two branches of highway agencies. Example materials taken from the guide are discussed to illustrate the content of the document, which was published by AASHTO in 1993.

The United States is converting to the metric system of weights and measures. Metrication was mandated by congressional legislation and by an executive order. This change reflects two significant factors: the move toward a global economy and the fact that the world's measurement system is now metric.

As of 1991, the United States was the only industrialized nation in the world that had not converted to metric (*1*). Congress, in adopting the Omnibus Trade and Competitiveness Act of 1988, amended the Metric Conversion Act of 1975 to require the federal government to convert to metric. Executive Order 12770 was issued on July 25, 1991. It required federal agencies to convert to metric under the leadership of the Secretary of Commerce within a fixed period of time.

In response to the congressional legislation and the executive order, FHWA formed a metric conversion plan that was approved on October 31, 1991. The plan called for an orderly series of conversion activities, terminating with a requirement that, after September 30, 1996, all direct federal and federal-aid construction contracts must be in metric.

PURPOSE OF PAPER

This paper was written to chronicle AASHTO's response to the federal metrication initiative and to introduce the AASHTO *Guide to Metric Conversion*. The objectives and content of the guide are covered in the remainder of this paper.

AASHTO ACTIONS

AASHTO's Standing Committee on Highways selected a metrication task force in 1991 that was chaired by Robert L. Clevenger, of the Colorado Department of Transportation. The task force was asked to work with FHWA to address the effects of converting to the metric system.

The task force identified three primary issues for early attention: (a) timing—meeting the conversion schedule adopted by FHWA; (b) cost—looking for cost-effective approaches; and (c) public relations—having a public awareness/information program. After assessing the overall situation, the task force obtained a budget from AASHTO that allowed it to take several decisive actions:

1. A resolution was prepared (and sent to the AASHTO policy committee) requesting the U.S. Department of Commerce to develop and implement a public awareness program.
2. A consultant was engaged to review the Canadian conversion experience and to prepare a summary report. The consultant also arranged a meeting between the task force and members of the Ontario Ministry of Transportation.
3. Requests were sent to all AASHTO subcommittees requesting that hard and soft conversions be reviewed and that conversion factors be developed in each subcommittee's area of expertise.
4. A second consultant was engaged to prepare a comprehensive metric conversion guide report.

The task force continued to function throughout 1992, periodically reviewing the work of its consultants and otherwise helping position AASHTO and the American highway industry to move smoothly forward with metrication. The metrication guide was approved by the task force in early November 1992 and forwarded to AASHTO for review and printing.

DEVELOPMENT OF AASHTO GUIDE

In March 1991 NCHRP issued a contract to the Civil Engineering Department of the University of Alabama to develop the AASHTO *Guide to Metric Conversion*.

The objective of the project was to develop a comprehensive guide document on metric conversion that could be considered for adoption by AASHTO. It would provide guidance to AASHTO and to national, state, and local transportation agencies on the planning, procedures, and actions necessary for conversion to metric. Materials were to be included to emphasize aspects of cost minimization—that is, methods by which unit costs and total costs could be reduced and possibly absorbed into the existing budgets of transportation agencies.

Under the guidance of the NCHRP Project Panel, the university developed a draft outline of the proposed guide. It included a main report text providing an overview of factors to be considered, the planning to be accomplished by the various departments within

Civil Engineering Department, University of Alabama, P.O. Box 870205, Tuscaloosa, Ala. 35487-0205.

agencies, and the sequential steps necessary for a smooth conversion. The planned report was also to summarize previous studies on metric conversion, to include several case studies on the conversion of branches of modern state highway agencies, to include flow charts or critical path method (CPM) charts, and to transmit any of AASHTO's new metric criteria that might be adopted by the time the guide was published.

Preparation of the guide was accomplished under the guidance of the NCHRP panel using the following work steps:

1. A literature review was conducted, using automated and traditional search procedures, telephone calls to knowledgeable experts, and interviews.
2. An outline was developed for the proposed report. It was annotated to show important topics and subtopics, and where possible it identified materials that could serve as source documents for preparation of each portion of the guide.
3. The NCHRP project panel reviewed the draft outline and offered suggestions and improvements.
4. The university prepared a list of key items for consideration for conversion. This list was organized by level of government, type of agency, highway functional area, and type of activity. The purpose was to begin developing categories of information for the guide.
5. The university developed the first draft of the guide using the list of key considerations, the annotated outline, and the literature review.
6. The NCHRP panel circulated the draft widely, gathered review comments, and offered constructive criticisms.
7. The university modified the draft document and provided a manuscript in a format suitable for publication by AASHTO.
8. The NCHRP panel balloted and approved the manuscript. Likewise, AASHTO balloted and approved the manuscript. Finally, the guide was published and assimilated by AASHTO in the spring of 1993.

The timetable for production of the guide was extremely compressed. The contract was issued in March 1992. The goal of the university was to have a first draft ready in time for review before the AASHTO annual meeting in October 1992. This meant that the majority of the project work had to be completed within 6 months. This somewhat constrained the number of activities that could be conducted and the amount of materials that could be placed within the guide. For example, the case studies were limited to states already deeply involved in metric conversion, and those within reasonable travel distance from the university. It also made it very difficult to collect and publish new metric criteria adopted by AASHTO. Most of the committees and task forces that were charged to develop metric criteria could not finish the experience and submit their results for balloting before publication of the guide.

CONTENT OF GUIDE

The guide is organized to make key pieces of information easy to find. The material is arranged topically, with each chapter devoted to a separate subject. The broad topic areas include reasons for making the change, procedures for forming a plan, hints and suggestions, and extensive checklists.

Chapter 1 contains an introduction to metrication and enough historical and background information so the user can understand why conversion is necessary. Important legislative and government activities are also introduced. Chapter 2 outlines the metric conversion experiences of other nations. The successful conversion of Canada in the mid-1970s provided a good example for the United States.

Chapter 3 lists the major steps in forming a metric conversion plan. Each step in the process is discussed sufficiently to guide agencies in forming their own plans. Practical hints and suggestions have been grouped into Chapter 4. These are useful in choosing strategies to enhance cost-effectiveness, improve timeliness, and avoid pitfalls. Chapter 5 contains extensive checklists of possible conversion activities. These are grouped by general process and by highway functional area.

The appendexes include a list of state highway agency metric coordinators; a review of metric units, terms, symbols, and conversion factors; example flow charts for conversion activities; interim AASHTO metric criteria for geometric design; two cases studies of conversion plans for branches of state highway agencies; and a bibliography of metric references.

Chapter 1: Introduction

Chapter 1 provides background information for metrication of the United States highway industry. It starts with an historical overview. The metric system started in France at about the time of the French Revolution (*2*). Over time it was improved and standardized, and in 1960 the General Conference on Weights and Measures adopted the International System of Units. This version of metric is known by its abbreviation SI and is now the most-used measurement system in the world.

Chapter 1 goes on to explain the necessity for conversion. With all of the world's other nations working in metric, U.S. businesses are at a distinct competitive disadvantage. This disadvantage will grow larger over time if the United States does not convert.

Several benefits of metric conversion are discussed in this chapter. These include international acceptance of metric, conversions already under way in the private sector, simplicity of use and calculations, and the opportunity to "rationalize" or redesign operations during the conversion process.

The majority of this chapter is spent outlining the legal basis for highway conversion. The Metric Conversion Act of 1975, the Omnibus Trade and Competitiveness Act of 1988, and Executive Order 12770 are explained. Department of Transportation (DOT) metric conversion planning guidelines and FHWA conversion activities are also reviewed.

Chapter 2: Conversion Experiences of Other Nations

Chapter 2 draws from the conversion experiences of other nations to illustrate some of the aspects of metrication. A large number of nations made the conversion in the 1960s and 1970s. America's neighbor Canada had a conversion experience that was almost uniformly positive. The Roads and Transportation Association of Canada (the equivalent of AASHTO) let this change. The Canadian experience provided many positive examples for America, including the following:

- Architectural and engineering firms found that it took less than 1 week for staff members to learn to think and produce in metric. Most tradespeople were able to adapt within hours.

- The changeover of highway signs turned out to be the biggest "non-event" in the entire conversion experience (*3*), thanks to a thorough public awareness program.
- The highest cost area was conversion of signs, followed by conversion of computer programs, then staff training, and public information.
- Thorough planning and a good public awareness campaign improved the success of the metrication program.

This chapter of the guide concludes by emphasizing three primary lessons found in the metrication of other nations: (a) metrication was not difficult once the decision was made to proceed, (b) the process should begin early because there is never too much time, and (c) strong leadership must be established at the top.

Chapter 3: Forming a Metric Conversion Plan

Chapter 3 establishes the broad general steps that are used to form metric conversion plans for individual agencies. Whether an agency is large or small, the same general steps are used, including the following:

- The agency leadership demonstrates metric support.
- A metric coordinator is named.
- A metric committee or work group is formed.
- A study is undertaken to identify activities and programs subject to conversion.
- An agency conversion plan and timetable are formulated.
- Conversion responsibilities are assigned to individuals and sections of the agency.
- Metric standards are established.
- A public awareness program is planned and conducted.
- Laws and statutes are revised to reflect metric units and to encourage the conversion process.
- Coordination efforts are conducted with other government agencies, units of local government, industry, contractors, materials and equipment suppliers, professional organizations, utility firms, and others.
- Metric training activities are conducted.
- The plan is monitored and modified as necessary to ensure implementation.

The chapter goes on to explain each of these basic steps. For example, qualifications and responsibilities of the metric coordinator are discussed. This job probably will be a full-time responsibility for at least the first portion of the conversion program. This individual should have the authority to make most metric decisions and may need a separate budget and staff members. This person should have a sound knowledge of the overall operation of the agency, a good working relationship with people, and a personal interest in the metric system (*4*). The primary job of the metric coordinator will be organizing and leading the conversion. However, training and dispensing metric information will occupy large portions of this person's time.

The remainder of this chapter amplifies the other steps in forming and implementing the plan. For example, metric standards and criteria must be adopted during the early portion of the process. Otherwise, it is impossible to revise agency publications, specifications, and other documents to conduct the conversion. Likewise, changes to laws and regulations must begin early because these are normally time-consuming, lengthy experiences.

An important part of the overall conversion is continuous and close coordination and liaison activities within each agency. The metric coordinator must be kept informed of each step during plan development and implementation by each section of the agency. The coordinator must ensure that every work unit is aware of the conversion plans and current status of every other unit, and of the agency as a whole.

It is very important for each agency to develop information networks to provide coordination with affected groups. Other units of government (environmental organizations, policy organizations, permitting organizations, etc.) must be kept informed. Likewise, contractors' organizations, utility firms, consulting engineers, and many others must be aware of the conversion timetable so that they can plan their own conversions. It would not be realistic to expect contractors to suddenly begin building roads in metric without prior knowledge of the desired timetable. Other topics discussed in the chapter include methods for educating and training employees on metric issues and monitoring the conversion implementation program.

Chapter 4: Hints and Suggestion

Chapter 3 outlined the major steps in a typical metric conversion plan. Application of any step to a particular highway agency is a matter of preference and degree of emphasis necessary to fit the needs of that agency. Chapter 4 was written to provide helpful hints and suggestions to help agencies tailor and fine tune the contents of their conversion plans.

This chapter contains a sampling of ideas from countries that already have converted and suggestions taken from current publications. A total of 15 major topics are discussed:

- Computer programs and data bases,
- Costs,
- Conversion of historical data,
- Discouraging use of dual units,
- Equipment modifications and purchases,
- Granting exceptions,
- Flexibility of the plan,
- Hard and soft criteria,
- Materials,
- Metric pilot projects,
- Conversion of publications,
- Rationalization,
- Screening for errors,
- Metric highway signs, and
- Timing.

For each of these topics, enough discussion is included to provide a rationale for forming a strategy. Reasons are often given why one type of conversion activity might be preferred over another type.

An example is the discussion on discouraging the use of dual units. The natural tendency for people is to prefer that dual (both U.S. and metric) units be used whenever possible. Unfortunately, as long as U.S. units are used (even in dual listings) people read only the numbers given in U.S. units. They will not convert. It is best to discourage dual listings. The FHWA plan indicates that

dual measurements are to be avoided after fiscal year 1993 unless it is determined to be beneficial in specific instances. (*5*).

Chapter 5: Checklists

Chapters contains a series of checklists that are provided as convenient reminders to those agencies preparing conversion plans. Two broad categories of checklists are presented: (a) general processes and (b) highway agency functional areas. Highway agencies of any size or any level of government may use the checklists to identify appropriate activities for their conversion plans.

This chapter is the largest in the guide. This allows agencies ample opportunities to pick and choose from the suggested activities. The following general processes are covered:

- Awareness and training;
- Contracts;
- Equipment;
- Formats and forms;
- Legislation and regulations;
- Machinery;
- Manuals and references;
- Materials and supplies;
- Output, communications, and publications;
- Conversion management;
- Standard specifications and policies;
- Storage; and
- Tools, jigs, and templates.

In addition to the general topics, additional checklists are provided for the following highway functional areas:

- Computer services;
- Construction;
- Environmental concerns;
- Location, surveys, and photogrammetry;
- Maintenance;
- Materials;
- Management systems;
- Planning and coordination;
- Preconstruction or design;
- Research;
- Right of way; and
- Traffic engineering.

These lists are not exhaustive, but they do include most of the functions and activities performed in a normal highway agency. These checklists should be considered only as starting points or reminders for the agency during preparation of its own unique plan.

Appendix A: State Highway Agency Metric Coordinators

Appendix A contains a list of the persons appointed as metric coordinators for the various state highway agencies. It also includes as resource persons three Canadian managers familiar with that country's conversion experience. The authors recognize that this list will rapidly become out of date. However, it provides names, addresses, and telephone numbers that will be of great use during the early stages of conversion. It allows the state-level coordinators to telephone each other. It also provides local governments and others possessing copies of the guide access to the appropriate state highway agency coordinators. This should provide timely access to information about ongoing conversion activities.

Appendix B: Metric Units, Term, Symbols, and Conversion Factors

FHWA has adopted the SI version of metric and has adopted the provisions of ASTM E380 Standards of Metric Practice as the authoritative reference to proper use of SI. This appendix contains extremely useful references to types of units, symbols, prefixes, pronunciations, and rules for writing metric symbols and names. It also contains useful tables of conversion factors from U.S. units to metric units.

Appendix C: Example Flow Charts

To assist in preparing conversion plans, Appendix C contains several typical flow charts. Examples include two flow charts from the FHWA metrication plan. Several flow charts developed during the Canadian conversion are also displayed. These range from very simple overviews to complex CPM charts showing the earliest and latest possible start dates for each conversion activity to complete all activities within the allotted time frame.

Appendix D: AASHTO Metric Criteria and Controls

Each AASHTO committee and task force was asked to recommend metric criteria for its appropriate area. This appendix contains the interim recommendations of the Subcommittee on Design. These criteria have been approved by AASHTO and are tentatively scheduled for inclusion in the next version of the Green Book.

Over time, virtually all AASHTO controls and criteria will be converted to metric. This will be a lengthy process requiring balloting of the states. Some interim criteria might change as the states gain experience in using them. Although some of the new criteria are contained within the guide, readers are reminded to check with AASHTO for the most up-to-date criteria before initiating a design.

Appendexes E and F: Case Studies

Two cases studies are included in the guide. The first study documents the preparation of a metrication plan by the Maintenance Bureau of the Alabama Highway Department. The second case study involves development of a metrication plan for the Design Section of the North Carolina Department of Transportation. Each case study is presented in abbreviated form.

For both states, a general description is included of the highway agency and the roadway system. Information is presented on the size and function of the bureau or section under study. This allows the reader to make comparisons with his or her own highway

agency. The steps undertaken during the studies and the resulting plans are summarized in these appendexes, and both include conversion cost estimates. Of particular interest is the Alabama presentation of typical sign conversion costs.

Appendix G: Partial Bibliography of Metric References

The authors developed a limited bibliography of metric references. It is organized into categories on professional and technical societies, government publications, training information, general publications, and international publications. Overall, there are more than 100 references in this appendix.

SUMMARY

The metrication of the American highway industry will not be simple. It will require substantial commitments of time, resources, and management efforts. This paper introduces the AASHTO *Guide to Metric Conversion*, which has been prepared to facilitate the conversion. The guide is intended for highway agencies at all levels of government, for the private sector, and for affiliated organizations. Its publication will provide an excellent starting place for conversion activities.

ACKNOWLEDGMENTS

This work was sponsored by AASHTO, in cooperation with FHWA, and was conducted in NCHRP, which is administered by TRB.

REFERENCES

1. *Metric Reporter*, Vol. 21, No. 4. American National Metric Council, Arlington, Va., April 1992.
2. *Metrication Report*. AASHTO, Washington, D.C., June 1974.
3. Gleeson, J. E. Conversion of Metric Traffic Control Devices in Ontario. *ITE Journal*, pp. 35–38, Aug. 1979.
4. *Guide to Metric Conversion of Highway Engineering*. Roads and Transportation Association of Canada, Ottawa, Ontario, 1976.
5. *Federal Register*, Vol. 57, No. 113, Washington, D.C., June 11, 1992.

Publication of this paper sponsored by Committee on Section B—Pavement Management.

Can the Highway Community Be Ready for Metric By 1996?

JAY K. LINDLY, DANIEL S. TURNER, AND DAVID R. GEIGER

Recent actions by Congress and the President are redirecting the United States transportation industry to design and construct metric highways in 1996. All federal lands highway and federal-aid construction projects advertised for bids after September 30, 1996, will be in metric units. The reasons for making metric conversions, the federal timetable for conversion, and a general conversion plan that can be used by highway agencies of all sizes are described. It is recommended that readers obtain a copy of the AASHTO *Guide to Metric Conversion*, which was published in 1993. A public awareness campaign by all levels of government is advocated to ensure that a public backlash to metrication does not occur.

Recent actions by Congress and the President are redirecting the U.S. transportation industry to design and construct metric highways in 1996. All federal lands highway and federal-aid construction projects advertised for bid after September 30, 1996, will be in metric units. Highway agencies presumably will wish to avoid the confusion of working in two separate systems, so it is assumed that by that date almost all highway projects will be designed and constructed in metric units. This paper will describe the reasons for making the metric conversion, the timetable for conversion, and the general plan that AASHTO and FHWA urge highway agencies to use in their conversion processes.

NCHRP and AASHTO are aware of the confusion that may be generated by the metric conversion announcement. Those organizations worked on the AASHTO *Guide to Metric Conversion*, which was published in 1993. The guide contains background information, conversion tables, a conversion plan that can be followed by highway agencies of any size, case studies, and cost estimates for important conversion steps.

CAN IT BE DONE?

Great Britain, Canada, South Africa, Australia, and New Zealand all converted to the metric system in the 1960s and 1970s. Their experiences contained many positive aspects and proved that conversion can be accomplished at relatively low cost. The *Metric Guide for Federal Construction* highlights some of these findings (*1*).

- There was no appreciable increase in either building design or construction cost, and conversion costs for most construction industry sectors were minimal or offset by later savings. (This comment applies to all industries, not just highway design construction.)
- The architecture/engineering community liked metric dimensioning because it was less prone to error and easier to use than feet and inches. Engineering calculations were also faster and more accurate because there were no unit conversions and no fractions.
- Metric offered a one-time chance to reduce the many product sizes and shapes that have accumulated over the years but are no longer useful, thus saving production, inventory, and procurement costs.
- Architecture/engineering firms in these countries found that it took a week or less for staff members to learn to think and produce in metric, and most tradespeople took only a few hours to adapt.

Those nations have pointed the way to metrication in the United States. To paraphrase Canadian officials (*2*): metrication was easier than anticipated; it was primarily a matter of making the decision to do it, then following through in a systematic manner.

WHY SWITCH?

The United States was the center of world commerce after World War II. Since that time, the European Community (EC) has overtaken the United States as the world's largest market, Japan and other Pacific rim nations have emerged as fierce economic competitors, and America's largest trading partners—Canada and Mexico—are predominantly metric countries. The share of the world's product types manufactured in the United States has shrunk from 75 to 25 percent since World War II (*3*), and metricating its industries is essential to maintaining economic leadership. A number of benefits that the United States can gain by converting to the metric system are discussed below.

International Competitiveness

The EC has indicated that it will not import nonmetric products after 1992. Japan has identified the nonmetric nature of U.S. products as a major impediment to their sale in Japan. All in all, it has become increasingly difficult for United States' products to compete in the international arena.

Conversion by Private Sector Companies

U.S. industries such as IBM and General Motors (GM) already have converted. GM was pleasantly surprised to find that conversion costs were less than 1 percent of original estimates. The elim-

J. K. Lindly and D. S. Turner, Civil Engineering Department, University of Alabama, Box 870205, Tuscaloosa, Ala. 35487-0205. D. R. Geiger, FHWA, U.S. Department of Transportation, 400 Seventh Street, S.W., Washington, D.C. 20590.

ination of dual fastener sizes during metric conversion allowed IBM to reduce its total number of fasteners from 30,000 to 4,000. When the liquor industry converted, the number of container sizes dropped from 53 to 7 (*1*).

System Simplicity

Design and construction tasks eventually will be performed more efficiently because the metric system is simpler to use than the customary system. The metric system is decimally based, and there is no need to convert from one measurement unit to a different measurement unit. For example, the area of a billboard does not have to be obtained by multiplying 17 ft $4^{3}/_{16}$ in. by 21 ft $8^{11}/_{16}$ in.

BACKGROUND

Government and industry leaders have been urging America to switch to the metric system for almost 200 years. For example, Thomas Jefferson and John Quincy Adams were among the founding fathers who unsuccessfully lobbied the nation to convert. More unsuccessful attempts were made over the years, with the most recent failed effort taking place in 1975. The current push for the metric system started with congressional legislation in 1988.

Metric Conversion Act of 1975

Congress passed legislation in 1975 (15 U.S.C. 2056) declaring a national policy to encourage and coordinate a shift to the metric system. Conformance with the plan was voluntary, and few industries made this important change. Additionally, the public vocally expressed its desire not to convert. As a result, no significant move to metrication took place, and the experience left a bad taste in the mouths of those public agencies that had attempted conversion and met public rejection.

Omnibus Trade and Competitiveness Act of 1988

The current move to the metric system was launched in 1988 with the amendment of the Metric Conversion Act of 1975 (the Act) by Section 5164(b) of the Trade and Competitiveness Act (Public Law 100-418). As amended, the Act now designates the metric system as the preferred system of weights and measurements for U.S. trade and commerce. It requires each federal agency to use the metric system in its procurements, grants, and other business-related activities to the extent economically feasible by the end of 1992. However, conversion is not required when it is impracticable, likely to cause significant inefficiencies, or likely to cause loss of markets by U.S. firms, such as when foreign manufacturers are producing competing products in nonmetric units.

The Controller General was named to review the implementation of the Act at the end of fiscal year 1992 and report to Congress. The report would include recommendations for any further legislation.

The obvious objective of the Metric Conversion Act as now amended is to convert the United States to the metric system. The buying power of the federal government will be the impetus for the change. Because it conducts extensive grant activities, the U.S. Department of Transportation (DOT) is included under the provisions of the Act.

Executive Order 12770

The President's Executive Order 12770, Metric Usage in Federal Government Programs, was signed July 25, 1991 (*4*). It required all federal agencies to formulate metric transition plans by November 30, 1991, to accomplish the metrication aims of the 1988 legislative amendment.

Further, each federal agency is directed to seek the cooperation of federal, state, and local agencies to implement metric construction. Thus, state and local highway agencies will be affected through U.S. DOT and FHWA. As pointed out earlier, all federal-aid projects must be advertised in metric units after September 30, 1996.

The Department of Commerce was given the task of coordinating the effort. It was authorized to charter an interagency council on metric policy; to issue guidelines, promulgate rules, and take other actions to implement the policy; and to report annually to the President about implementation status. On October 1, 1992, the Department of Commerce recommended additional measures and legislation to achieve the full economic benefits of metric usage.

FEDERAL CONVERSION PLANS

The 1988 legislation and Executive Order 12770 set September 30, 1992, as the deadline for each federal government agency to begin using the metric system in procurements, grants, and other business-related activities. The Department of Commerce interpreted the 1992 deadline to mean that a schedule for conversion should be in place at that time, and some metric conversion activities should be under way.

The U.S. DOT is a federal agency and was thus required to adopt a metric conversion plan. FHWA is one of nine agencies of the U.S. DOT, and each one was required to create comprehensive conversion plans.

FHWA Plan

FHWA's Metric Transition Plan was approved by the Secretary of Transportation on October 31, 1991. It is a 5-year plan to convert FHWA activities and business operations to the metic system. FHWA has four major programs, including the federal-aid highway program. It is through this program that most of the impacts of metric conversion will be felt by state and local highway agencies. It is FHWA's intent that all federal lands highways and federal-aid construction contracts advertised for bids after September 30, 1996, will contain only metric measurements. Thus, federal-aid projects let after that date at the state, county, and city level will all be affected.

FHWA Timetable

Table 1 presents a paraphrased version of FHWA's metric transition timetable as published in the *Federal Register* (*5*). The

timetable has been criticized by several state and local highway agencies that totally objected to metric conversion. They indicated a belief that conversion would be "impractical" or likely to cause "significant inefficiencies" in the highway industry. They also object that if conversion must take place, the timetable does not give them enough time to complete the job. FHWA counters these arguments by stating its belief that the loss of inefficiencies will not be long term, significant, or compromising to public safety. As for timetable length, FHWA states that neither the Department of Commerce nor Executive Order 12770 permits a longer time frame (5).

Conversion Costs

The *Federal Register* (5) makes reference to several studies of the cost of metric conversion. An ad hoc AASHTO Metrication Task Force in 1974 estimated the cost of metrication to federal, state, and local highway agencies at $200 million. The task force further predicted that signing changes would compose approximately 30 percent of total conversion costs and would constitute the largest single requirement of funds. Creating and converting existing computer programs to metric was estimated to be 25 percent of total conversion costs. Training was estimated to consume 10 percent of conversion monies. Revising and reprinting existing manuals, specifications, and standard plans were estimated at an additional 10 percent.

Two states provided more current cost estimates. One state highway agency from a slightly smaller-than-average state estimated its total direct conversion costs at $9 million. Another state highway agency from an average-sized state estimated that converting speed limit and distance signs would cost between $1 million and $4 million.

FHWA Participation

Although Congress has not authorized FHWA or any other federal agency special funding to provide reimbursement to states and local highway agencies for metric conversion costs, FHWA can participate in project-specific right of way, design, and construction costs. Therefore, FHWA will participate at the appropriate pro rata share for costs that state and local highway agencies incur while changing highway signs to metric units under existing federal-aid categorical programs. As noted earlier, this is anticipated to be the most costly activity.

Other Emphases

The FHWA Metric Conversion Plan emphasizes several other guidelines, including the following:

- ASTM-E380 is designated the authoritative reference for applying metric units and conversions.
- Each FHWA region and division office has designated an individual to cooperate with state and local governments during their metric conversions.
- FHWA intends to avoid the dual use of standard and metric measurements during the conversion process.
- FHWA intends to convert historic records and data to metric units only when necessary for ongoing operations and future projections.
- FHWA advises using "hard" metric conversions when appropriate and to the extent practical. Hard conversion involves converting a customary measurement to its exact metric equivalent, then rounding the metric equivalent to a convenient value for actual use. For example, the exact or "soft" conversion of a 12-ft lane width is 3.658 m. This is an odd number that is difficult to remember. A better idea is to round this to 3.50 or 3.75 m, which is a "hard" conversion.
- FHWA believes that a campaign to make the public aware of metrication is imperative to allow it to become a part of the process and to avoid a public backlash.

CONVERSION DIFFICULTIES

Because of the involvement of both Congress and the President and the buying power of federal agencies, the most recent U.S. conversion effort is far more likely to succeed than the 1975 attempt. However, there are certain stumbling blocks to the conversion effort. The following list is provided not as reasons to avoid participating in the metric conversion but as items highway agency administrators should be aware of when making genuine efforts to implement the policy:

TABLE 1 FHWA Metric Transition Timetable

Program Elements/Activities	Target Dates (Completed)
FHWA metric conversion plan.	(Approved 10/31/91)
Initiate revision of pertinent laws and regulations that serve as barriers to metric conversion.	(1991)
Full metric conversion of FHWA manuals, documents, and publications.	1994
Full metric conversion of FHWA data collection and reporting.	1995
Newly authorized Federal Lands Highway and Federal-aid construction contracts in metric units only.	September 30, 1996

- There is lack of a national awareness of metrication and national will to metricate. Public awareness campaigns and programs of public involvement will be required to interest the public in the conversion process.
- Highway agency personnel still seem unsure that conversion will actually take place and may therefore not give their conversion activities a high priority.
- Highway agency personnel are concerned about a public backlash to conversion, the predictable negative reaction by the trucking industry, and the cost of conversion.
- There appear to be few benefits to state and local highway agencies, whereas all benefits seem to go to those involved in international trade.

As the preceding list indicates, there are many potential objections to highway metric conversion. All of them are extensions of the natural human resistance to change. A thoughtful, comprehensive conversion plan by state and local highway agencies will be required to ensure metrication's success.

FORMING A METRIC CONVERSION PLAN

Each state, county, and city highway agency is unique in terms of its size, personnel, and the amount and type of roadway projects its constructs. For these reasons, plans may be expected to differ from agency to agency. Each agency's plan must meet its own unique needs. However, any agency must start its conversion plan the same way, by instilling a will to convert—a determination by both administrators and field personnel—to make the conversion a success. Once the importance of the conversion process is understood, the ease of making the conversion will be greatly enhanced.

AASHTO's *Guide to Metric Conversion* will present a conversion sequence that can be used by highway agencies of any size. Small agencies may not use all the steps; larger agencies may enlarge the steps or add further activities. An abbreviated list of the sequence found in the AASHTO guide follows:

- The agency CEO demonstrates metric support.
- A metric coordinator is named.
- A metric committee or work group is formed.
- A study identifies activities and programs to be converted.
- An agency conversion plan and timetable are formulated.
- Conversion responsibilities are assigned to individuals.
- Metric standards are established.
- A public awareness program is planned and conducted.
- Laws and statutes are revised to reflect metric units and to encourage the conversion process.
- Coordination efforts are conducted with other government agencies, industry, contractors, material and equipment suppliers, professional organizations, and others.
- Metric training activities are conducted.
- The plan is monitored and modified as necessary to ensure implementation.
- Follow-up activities are conducted.

Several state highway agencies already have recognized that significant time and effort will be required to make the conversion. They have learned from Canada (*6*) that it may take over 4 years to convert existing manuals, computer programs, and so forth. To meet the October 1996 deadline, several states have already begun their efforts, two of which are used here as examples. The Indiana Department of Transportation (IDOT) already has taken several steps. Topographic surveys are being performed already in metric units, and IDOT is rewriting their nine-volume design manual in metric units. IDOT intends to start their first metric design in November 1992.

The North Carolina Department of Transportation (NCDOT) is another agency that has positioned itself well for metric conversion. One of its first actions was to request the Institute for Transportation and Education (ITRE) at the University of North Carolina to evaluate the impacts of the metrication legislation and to recommend compliance approaches. NCDOT has appointed a metric coordinator, formed a metric committee, and expanded materials from the ITRE study to complete an agency conversion plan and a timetable that meets FHWA target dates.

SUMMARY

This paper has posed the question, "Can the highway community be ready for metric by 1996?" The answer to this question is transparent: the highway community must be ready!

The experiences of other nations, particularly the recent experience of Canada, have demonstrated that a large, industrialized nation can convert its highways from customary to metric units. U.S. DOT and FHWA have established schedules for completion of the federal highway metrication in the United States. FHWA is working with national organizations to convert the needed standards and computer programs to metric, and they will be working with state and local agencies to help them make their conversions.

Although that framework has been established, strong leadership from the Department of Commerce will be required to coordinate metrication in various industries and to provide a much needed national public awareness campaign of metrication. State and local highway agencies must be convinced that metrication will happen and that federal agencies already have begun to lead the way. Highway agencies must encourage legislators to change or repeal existing laws and regulations written in the customary system of units. The task of changing legislation may be quite large, encompassing such areas as motor fuel tax units, speed limit signs, allowable axle weights, and commercial licenses.

Everyone must be given time to become accustomed to the idea of metric highways. The public must feel that it has been given a choice in the matter or at least has been well informed of metrication before it takes place. Contractors, equipment, and material suppliers, and others directly related to the highway industry must be given time to make their adjustments. Even hotel and restaurant associations must be informed so that member establishments that are located on Interstate highways can modify their printed literature to identify their location at the new exit number. In short, education both within and outside the highway construction business must begin now.

The experience of other nations has shown that there is never enough lead time during the conversion to metrics. The time for U.S. highway agencies to start planning their conversion is now because 1996 is just around the corner.

ACKNOWLEDGMENTS

This work was sponsored by AASHTO officials, in cooperation with FHWA, and was conducted in NCHRP, which is administered

by TRB. The contributions of the AASHTO Task Force on Metrication and its Chairman, Robert Clevenger of the Colorado DOT, are also greatly appreciated.

REFERENCES

1. *Metric Guide for Federal Construction.* National Institute of Building Sciences, Washington, D.C., 1991.
2. *Trip Report to Canada May 1–4, 1991.* U.S. Metrication Operating Committee, Construction Subcommittee, Washington, D.C., 1991.
3. Fohs, D. G. Transportation Metrication. *Stone Review*, Feb. 1992.
4. Executive Order 12770: Metric Usage in Federal Government Programs. *Federal Register* (Presidential Documents), Vol. 58, No. 145, pp. 35801–35803, July 29, 1991.
5. FHWA Metric Conversion Policy. *Federal Register* (Notices), Vol. 57, No. 113, pp. 24843–24846, June 11, 1992.
6. Smith, P. NCHRP Project 20-7 Task 54. Draft of *Precepts for Highway Metric Conversion*, 1992.

Publication of this paper sponsored by Committee on Section B—Pavement Management.